ABERRANT MACROPHAGE AND MONOCYTE FUNCTION IN LUNG FIBROSIS

INVESTIGATING MACROPHAGES AND MONOCYTES AS PROFIBROTIC IMMUNOPATHOGENIC CONTRIBUTORS TO PULMONARY FIBROSIS

By MEGAN VIERHOUT, M.Sc, B.Sc. (Honours)

A Thesis Submitted to the School of Graduate Studies in Partial Fulfillment of the Requirements for the Degree Doctor of Philosophy

DOCTOR OF PHILOSOPHY (2024) McMaster University

Medical Sciences Hamilton, Ontario, Canada

TITLE: Investigating Macrophages and Monocytes as Profibrotic Immunopathogenic Contributors to Pulmonary Fibrosis

AUTHOR: Megan Vierhout, M.Sc, B.Sc. (Honours)

SUPERVISOR: Dr. Martin Kolb

NUMBER OF PAGES: 289

LAY ABSTRACT

Idiopathic pulmonary fibrosis is a disease of unknown cause (*idiopathic*) that affects the lungs (*pulmonary)* and leads to abnormal and excessive scar tissue formation (*fibrosis*). This causes serious breathing difficulties for IPF patients, and progressive damage in the lungs eventually leads to fatal respiratory failure. Currently, there is no cure for IPF. Treatment options are limited, with only two approved anti-fibrotic drugs that can slow down disease progression but cannot halt or reverse it. Thus, there is a need to further investigate the underlying processes driving the disease and new potential ways to treat it. Macrophages are a type of white blood cell and the most common immune cells in the lung. It is believed that they play a key role in IPF and contribute to the process of "scarring gone wrong" by interacting with other cells and possibly even transforming into other disease-related cell types. However, macrophages can be challenging to study and their exact mode of action remains to be deciphered. Monocytes, another type of white blood cell, exist mainly in the blood and are pre-cursor cells for macrophages. In IPF, it is believed that monocytes leave the bloodstream and enter the lung tissue, where they differentiate into macrophages that contribute to disease processes. Despite being increased in the blood of IPF patients, very little is known about monocytes in IPF. This PhD thesis begins by exploring the evidence for profibrotic processes in macrophages from human IPF lung tissue, and their potential ability to transform into scar-producing cells. As little is known about this process in lung fibrosis, we also formally glean evidence from other forms of fibrosis, including kidney and cardiac. Next, we establish and validate a novel, biologically-relevant system to study profibrotic macrophages using precision-cut lung slices, which

addresses the challenges of studying macrophages in a way that translates to lung disease. Finally, we investigate monocytes collected from the blood of IPF patients to better understand the attributes and processes of these cells, their link to macrophages, and future potential ways to target them.

ABSTRACT

Idiopathic pulmonary fibrosis (IPF) is a fatal and relentless form of interstitial lung disease, characterized by excessive deposition of extracellular matrix in the lung tissue, declining lung function, and ultimately, respiratory failure. The prognosis of IPF is relatively poor and comparable to some aggressive forms of cancer, with a median survival of just 3 to 5 years after diagnosis. Etiology of IPF remains widely unknown and anti-fibrotic interventions options are limited, with just two drugs, nintedanib and pirfenidone, being approved for treatment of the disease. Although these medications slow disease progression and may extend survival, they are not curative and cannot halt or reverse fibrogenesis. Thus, there is a critical need to investigate the mechanisms that drive disease and strategies to target them. It is believed that macrophages are vital contributors implicated in the pathogenesis of IPF. Through secretion of profibrotic mediators, interaction with various cell types, and mediation of wound healing responses, multiple studies have shown that macrophages drive profibrotic processes. The quantities of both alternatively activated macrophages in the lung and circulating monocytes in the blood have been found to be increased in IPF patients. Additionally, depletion of these cells in animal models of pulmonary fibrosis have shown that they are fundamental for development of the fibrotic response. However, the detailed attributes and mechanisms of these cells remain to be elucidated. Recently, there has been growing interest in the mechanism of macrophage-myofibroblast transition (MMT), where macrophages transform into myofibroblast-like cells that are key effectors in fibrosis. We begin by exploring the evidence for MMT in lung tissue from IPF patients, to gain further insight into the profibrotic mechanisms of

macrophages present in the disease. Through mining of a single cell RNAseq dataset of lung tissue explants from IPF patients and controls, and using our curated biobank of IPF surgical lung biopsies for various tissue-based assessments, we demonstrate findings supporting myeloid origin of ACTA2/α-SMA positive cells in IPF. Next, we establish and validate a novel, translational approach for investigation of macrophage profibrotic programming in the lung. Given the interactive and dynamic nature of macrophages, as well as their high degree of phenotypic plasticity, traditional *in vitro* systems present major limitations in the translation of research findings to true macrophage behaviour in disease. Precision-cut lung slices (PCLS) are living tissue slices derived from the full organ which bypass the limitation of artificially recreating the lung architecture and recapitulating the sophisticated microenvironment. Using our polarization cocktail and PCLS, we develop a moderate-throughput, biologically-relevant system for profibrotic macrophage programming in the lung. We also demonstrate induction of overall features of fibrosis in our system, which we show may be attributable to MMT, as described previously. Complementing our novel platform, we also describe the implementation of high-content imaging using Iterative Bleaching Extends Multiplexity (IBEX) to explore cellular phenotype and spatial characteristics in PCLS, which has potential for expansion to other cultured organ slice systems. Lastly, we investigate the attributes and mechanisms of circulating monocytes isolated from the blood of IPF patients. We confirm their increased quantity in IPF and uncover an aberrant metabolic phenotype. We show that gatekeeper enzyme PDK4 may function as a potential associated target that is also implicated in macrophage polarization, and further explore the mechanistic involvement of aberrant

metabolism using our developed PCLS system. Overall, the findings presented in this thesis support the pursuit of knowledge to better understand the profibrotic contribution of macrophages and monocytes in IPF, and offer insights for the development of novel therapeutic interventions in fibrosis.

ACKNOWLEDGEMENTS

A PhD is a journey best travelled in the company of others, and I am so fortunate to have had the support of exceptional scientists and leaders during my degree. Firstly, I would like to extend my utmost gratitude to my supervisor, Dr. Martin Kolb. Thank you for warmly welcoming me into the Kolb Lab family and equipping me with a toolkit for success. Thank you for supporting my endeavours, both at and beyond the lab bench, and consistently cheering me on with great enthusiasm. Your guidance and insights have been incredibly valuable during my scientific journey and have inspired me to think in terms of translational impact. Thank you for your kindness and always ensuring that us trainees have what we need to thrive. I am extremely grateful for your mentorship and the remarkably supportive and encouraging learning environment you provided, in which I was able grow as a scientist, critical thinker, and leader. It has been an honour to train under your mentorship.

I would like to also extend my profound appreciation to Dr. Kjetil Ask. Thank you for initially taking a chance on me as an undergraduate student as my original supervisor. You have taught me to fearlessly face challenges and become a resilient, versatile scientist. You have inspired me to become a curious and creative thinker with an unwavering drive for scientific discovery. Thank you for trusting me with scientific autonomy and always being available to discuss new results and provide invaluable advice. You have exemplified what it means to be a tenacious scientist, while also being a kind and compassionate person. Thank you for always believing in me and supporting me to reach my full potential.

I would also like to deeply thank my supervisory committee members, Dr. Nathan Hambly. Dr. Anthony Rullo, and Dr. Maggie Larché. Your guidance, feedback, and perspectives

have been instrumental during my PhD journey. I truly appreciate your generosity in sharing your expertise and knowledge to help me shape my projects. I also thank you for your trust in providing me with additional project opportunities to collaborate and gain further insight working in your areas of expertise, which have enriched my graduate studies (the viral study, cell-specific targeting in the lung review, and the scleroderma biobanking project – just to name a few)!

To Dr. Joshua Koenig and Dr. Manel Jordana, words cannot describe how grateful I am that you invited me into the high-content imaging space. Not only have I learned so much and gained invaluable perspectives, but I also gained two additional mentors in the process. Thank you for welcoming me to lab meeting, letting me work at your lab bench, and always finding time to look at my microscopy images. You have challenged and encouraged me to think in new ways, bolstering my growth as a scientist and microscopist. I am forever thankful for your exceptional mentorship, generosity, and kindness.

To Dr. Carl Richards, Dr. Jeremy Hirota, and Dr. John McDonough, thank you for always having an open door to talk fibrosis and respiratory research. It has been a privilege to discuss ideas with you, listen to your thoughtful advice, and gain new perspectives. Thank you for your constant enthusiasm and willingness to support my scientific training.

To my internship supervisor and mentor, Dr. Stephan Klee. Thank you for providing me with the opportunity to learn science halfway across the world. I am extremely grateful for the vast amount of learning and scientific growth I achieved in just three short months in Germany. Thank you for your guidance, insightful discussions, and providing me with a laboratory home away from home.

To Joanna Kasinska and Fuqin Duan, I deeply thank you for your expert technical assistance during my degree. Thank you for teaching me new techniques, always being willing to lend a hand, and taking care of all of us in the lab. I'm so fortunate to have had your assistance and companionship during long experiments. It has been a privilege to work alongside such talented, knowledgeable and kind individuals.

To Dr. Anna Dvorkin-Gheva, your bioinformatic knowledge and expertise is simply unmatched. Thank you for your analytical proficiency, fruitful discussions, and always being willing to answer all of my questions. It has been an utmost privilege to work with you and learn from you.

To Mary Jo Smith, Mary Bruni, and Xiaoxing Ma of the McMaster Core Histology Facility. For many years you have provided nothing but high-quality work and expert input, and for this I deeply thank you. Your attention to detail and expertise in histology were instrumental in my PhD work.

To Dr. Joao Bronze de Firmino and Dr. Mouhanad Babi of the McMaster Centre for Advanced Light Microscopy (CALM). I am beyond thankful for your training and support in microscopy. Thanks to the supportive and positive atmosphere you provided, CALM quickly became one of my favourite places on campus where I spent hundreds of hours imaging. I am incredibly fortunate to have had the opportunity to learn from you as world-class microscopists and such phenomenal people.

To the amazing Ask and Kolb lab members: Anmar, Alex, Safaa, Tran, and Albina, as well as Rosa from the McDonough lab; and alumni: Takuma, Kohei, Toyoshi, Sonia, Soumeya, Olivia, Spencer, Aaron, Pareesa, Vaishna, Pari, Colin, and Amir. Thank you for being my

colleagues, mentors and friends during this journey. I have learned so much from you and grown alongside you as scientists. Thank you for your support, companionship, and inspiration. To the most talented undergraduate students, Vitoria (Koenig Lab) and Henry (University of Bath). You are incredibly skilled researchers who were already operating at PhD-caliber during your undergraduate studies. I thank you immensely for everything you have both taught me.

To the members of the Firestone Institute for Respiratory Health Society of Trainees (FIRHst), thank you for the opportunity to work alongside such incredible student leaders. To my fellow FIRHst Co-Presidents, Sudeshna Dhar and Jenny Nguyen, I am so fortunate to have worked with you both as such amazing leaders and friends. It was an honour to build FIRHst with you and I could not have dreamed of better teammates. To Dr. Dawn Bowdish and Dr. Martin Kolb, thank you for always advocating for the trainee community and making sure FIRHst had everything we needed. You are exceptional leaders who have led our community by example.

To my McMaster Medical Science Student Association (MMSSA) colleagues, it was a blast working with you throughout the years to bring the MedSci student community together. Emily and Rida, I am beyond confident that the future of MMSSA is in amazing hands.

Lastly, to my family; my mother Nagat, my father Wayne, my brother Jeremy, and our family dog Ozzie. Your unwavering support throughput my PhD has been meaningful beyond words, and you have helped me achieve my dreams. To my partner Antek, thank you for your extraordinary support, understanding, and patience throughout this journey. To my in-laws Beata and Andrzej, thank you for supporting me in every way possible. And

to my incredible friend network, especially Carla, Milena, Alyssa, and Nicole, thank you for always being so enthusiastic, encouraging, and excited for me. Thank you for keeping me grounded.

TABLE OF CONTENTS

LIST OF FIGURES

LIST OF TABLES

LIST OF ABBREVIATIONS

α-SMA: alpha-smooth muscle actin

AM: alveolar macrophage

ARDS: acute-respiratory distress syndrome

Arg-1: Arginase 1

BSC: biological safety cabinet

BMDM: bone marrow derived macrophages

CC: control cocktail

CCAC: Canadian Council on Animal Care

CCL17: cc-chemokine ligand 17

CCL18: cc-chemokine ligand 18

CCR2: cc-chemokine receptor 2

CD: cluster of differentiation

COL1A1: collagen type 1 alpha 1

DCA: dichloroacetate

DE: differentially expressed

DLCO: diffusing capacity for carbon monoxide

ECM: extracellular matrix

FAP: fibroblast activation protein

FC: fibrotic cocktail

FFPE: formalin-fixed paraffin-embedded

FSP1: fibroblast-specific protein 1

FVC: forced vital capacity

GFP: green fluorescent protein

GO: gene ontology

GSEA: gene set enrichment analysis

H_2O_2: hydrogen peroxide

H&E: hematoxylin and eosin

HBSS: Hanks' Balanced Salt Solution

IBEX: iterative bleaching extends multiplexity

IHC: immunohistochemistry

IL: interleukin

ILD: interstitial lung disease

IM: interstitial macrophages

IPF: idiopathic pulmonary fibrosis

IR: ischemia-reperfusion

$LiBH_4$: lithium borohydride

MMT: macrophage-myofibroblast transition

MPS: Mononuclear Phagocytic System

OCT: optimal cutting temperature compound

OXPHOS: oxidative phosphorylation

PBMC: peripheral blood mononuclear cells

PBS: phosphate-buffered saline

PC: polarization cocktail

PCLS: precision-cut lung slices

PDAC: pancreatic ductal adenocarcinoma

PDH: pyruvate dehydrogenase

PDK: pyruvate dehydrogenase kinase

PMA: phorbol 12-myristate 13-acetate

RES: Reticuloendothelial System

scRNAseq: single-cell RNA sequencing

SGK-1: serum- and glucocorticoid-inducible kinase 1

TCA: tricarboxylic acid

TCF: T-cell factor

TGF-β: transforming growth factor beta

UUO: unilateral ureter obstruction

WST-1: water-soluble tetrazolium 1

YFP: yellow fluorescent protein

DECLARATION OF ACADEMIC ACHIEVEMENT AND PREFACE

Comprehensive Exam Pass with Distinction (2022)

Graduate Courses

MS 742: Applied Topics in Respiratory Physiology	Grade: A+
MS 707: Statistical Methods in Health Research	Grade: A+
MS 771: Research Methodology in Health Sciences	Grade: A+

I am the main contributor and primary author of all chapters included in this thesis. Chapter 1 is an overall introduction and overview of the literature on the key topics related to the projects in the thesis. It includes pertinent background information to provide context and understanding of the rationale for each of the chapters, as well as an explanation of the central aim and objectives of the thesis. Chapter 2 is a published manuscript in *Wound Repair and Regeneration* entitled "Monocyte And Macrophage Derived Myfibroblasts: Is It Fate?" which contains results supporting evidence for monocyte/macrophage myofibroblast transition (MMT) in IPF. Through mining of a single cell RNAseq dataset of lung tissue explants from IPF patients and controls, and using our curated biobank of IPF surgical lung biopsies for various tissue-based assessments, we demonstrate findings supporting myeloid origin of ACTA2/α-SMA positive cells in IPF. Additionally, we provide a comprehensive systematic analysis examining the known evidence for MMT in other organ systems. The work in Chapter 2 was conducted from 2020-2021. Chapter 3 is submitted for peer review to *Biochemical and Biophysical Research Communications* and is also uploaded as a preprint to *bioRxiv*. This manuscript is entitled "A Novel *Ex Vivo* Approach for Investigating Profibrotic Macrophage Polarization Using Murine Precision-Cut Lung Slices". The work in this chapter outlines the establishment and validation of a

novel biologically-translational approach to study profibrotic macrophage programming in precision-cut lung slices (PCLS). In addition to demonstrating features of profibrotic macrophage polarization and fibrosis, our PCLS system also contains potential evidence of MMT, building on the concept of Chapter 2. Chapter 3 was conducted from 2021-2024. Chapter 4 is prepared for submission to *STAR* (invited submission), entitled "Highly Multiplexed Imaging for Cellular Phenotyping in Murine Precision-Cut Lung Slices Using Iterative Bleaching Extends Multiplexity (IBEX)." This directly builds on the work of our established PCLS system in Chapter 3, and describes in detail how to conduct high-content staining and imaging on PCLS using IBEX for the elucidation of cellular phenotype, which to our knowledge has not been previously reported in any *ex vivo* cultured organ slice system. The work in Chapter 4 was conducted from 2023-2024. Chapter 5 is entitled "Identification of Aberrant Metabolic Phenotype in Circulating Monocytes in Idiopathic Pulmonary Fibrosis Through Transcriptomic Profiling and Implications on Profibrotic Macrophage Polarization" and is to be submitted. This chapter combines two projects I worked on during my PhD into one larger manuscript. First, we investigate the characteristics of monocytes in IPF, and confirm the presence of monocyte-derived profibrotic macrophages in the lungs of IPF patients. Through a transcriptomic study on $CD14^+$ monocytes isolated from the blood of IPF patients, we uncover a phenotype associated with aberrant metabolism, and identify PDK4 as a potential target. In the subsequent study, we explore the effects of modulating metabolism and the PDK axis on profibrotic macrophage polarization. We also employ the use of our PCLS system, as described in Chapter 3, for intervention studies. The work in Chapter 5 was conducted from

2020-2024. Each chapter includes a preface that contains an overview of the importance and novelty of the work, as well as a detailed breakdown of author contributions. Chapter 6 then discusses a critical analysis of the research findings in the conducted projects as well their interrelatedness. It highlights the overall significance and implications of the results, and how these contribute novel knowledge to the field.

CHAPTER 1

INTRODUCTION

Thesis Graphical Abstract

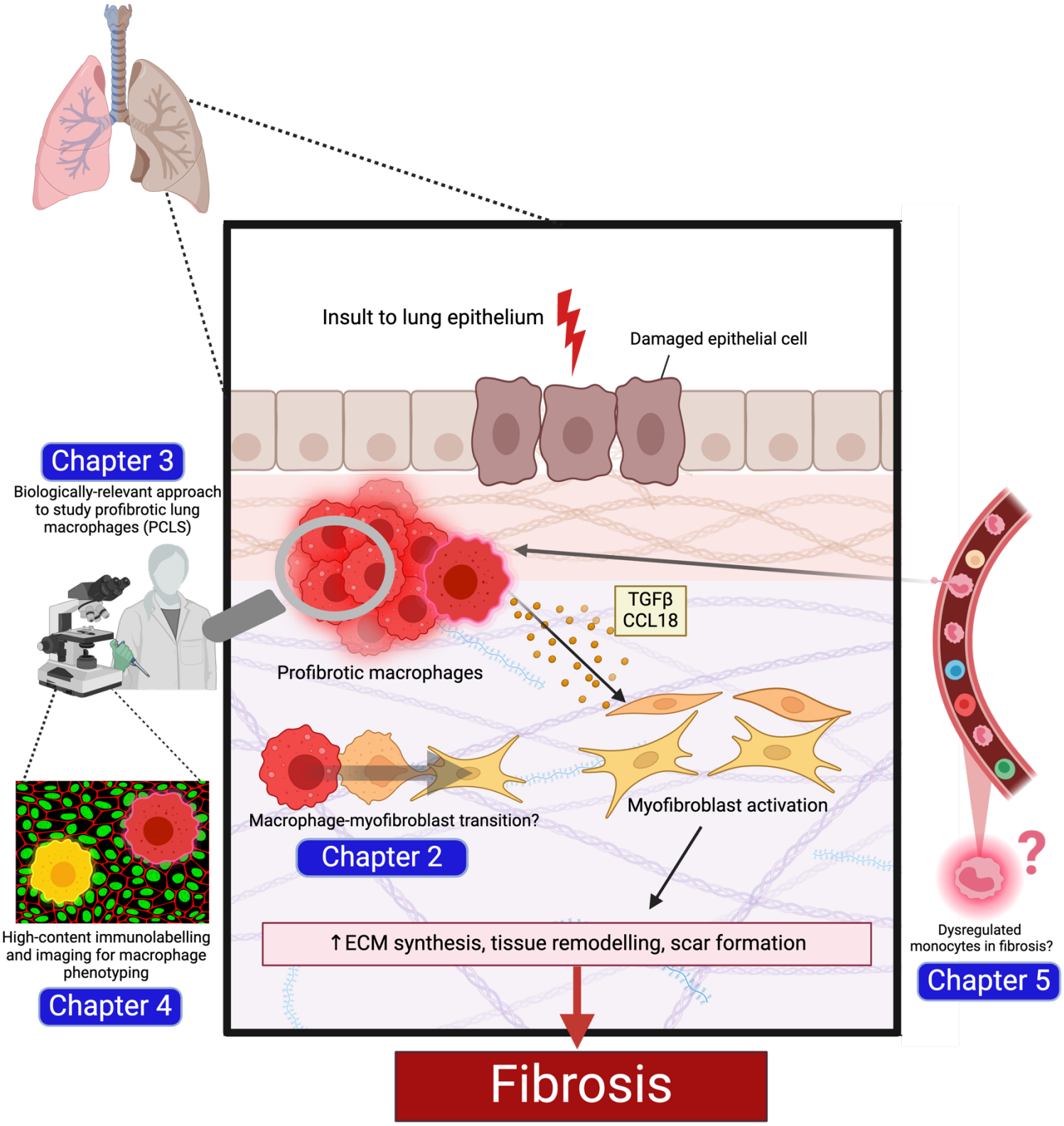

Thesis Graphical Abstract:

This figure depicts the overall accepted pathobiology for idiopathic pulmonary fibrosis (IPF). In summary, disease-related processes are thought to initiate with epithelial insult, which then cascades into recruitment of macrophages to the site of injury. Macrophages secrete profibrotic mediators including CCL18 and TGF-β, which lead to hallmark functions of fibrosis including fibroblast recruitment and proliferation, fibroblast to myofibroblast differentiation, and deposition of extracellular matrix (ECM) in the lung. Macrophages may also directly contribute to myofibroblast populations through macrophage-myofibroblast transition (MMT). Additionally, circulating monocytes in the blood have been shown to be increased in IPF, and are believed to contribute to profibrotic macrophage populations in the lung. However, very little is known about the overall characteristics and potential disease-driving features of these monocytes.

The chapters of this thesis are depicted throughout this figure by blue boxes, which are laid out in relation to the according IPF pathobiological factors each chapter investigates. Chapter 2 focuses on the process of MMT in IPF and fibrosis overall. Chapter 3 entails the development of a biologically relevant approach to study profibrotic macrophage polarization in the lung, which also involves aspects related to MMT. Chapter 4 directly builds on Chapter 3 with the establishment of a detailed methodology for visual and quantitative comprehensive phenotyping of macrophages in precision-cut lung slices (PCLS) using high-content immunolabelling. Lastly, Chapter 5 focuses on the investigation of the potential dysregulated properties of

circulating monocytes in IPF, as precursor cells for pulmonary macrophages. Figure created using BioRender.com.

Fibrotic Lung Disease and Idiopathic Pulmonary Fibrosis

Epidemiologic data has shown that 45% of all deaths in the developed world are linked to chronic fibroproliferative disease [1]. Fibrotic disorders comprise a range of pathologies and can impact various organs in the human body, largely being classified by extensive tissue remodelling and accumulation of excessive extracellular matrix (ECM) components in affected tissues [2]. This aberrant scarring and pathologic tissue remodelling can significantly compromise organ function, potentially cascading into failure and, in severe cases, death [1]. With the recent emergence and ongoing infections of the COVID-19 pandemic, fibrosis, especially in the lung, has been increasingly on the global radar [3,4].

Interstitial lung diseases (ILD) are classified by deleterious wound healing processes which produce chronic inflammation and fibrosis in the lung tissue. Among ILDs, idiopathic pulmonary fibrosis (IPF) is one of the most prevalent subtypes and the most lethal [5]. Common symptoms of IPF include dyspnea, persistent dry cough, chronic fatigue, and declining lung function [6], with disease progression ultimately leading to respiratory failure. The prognosis of IPF is poor and similar to some forms of aggressive cancer, with a median patient survival of 3 to 5 years after diagnosis [7]. Although the cause and pathogenesis of IPF remain widely unknown, it has been shown that smoking, certain environmental exposures, and genetic polymorphisms constitute disease risk factors [8,9]. In attempt to better understand indicators of progression in IPF and fibrotic ILD, there has been a strong interest in biomarker studies in fibrosis patients [10–14], with an increasing focus on the circulatory

compartment [12,15,16]. Currently, there are two approved antifibrotic therapies for IPF: nintedanib and pirfenidone. Both medications slow progression and can extend survival time in IPF [17]. However, neither drug is curative nor able to reverse fibrogenesis, and so there is a critical need to develop new treatment options. Overall, IPF remains an etiologically complex, poorly understood, and aggressive form of fibrosis, warranting further investigation and elucidation of its disease-driving factors.

Key Cellular Players of Interest in Pathophysiology of IPF

Macrophages and Fibrotic Lung Disease

Macrophages are the most common immune cells in the lung [18]. They are remarkably plastic, heterogenous cells with a broad range of effector functions as key orchestrators of immunomodulation in the lung. Pulmonary macrophages are stratified into the two broad categories of alveolar (AM) and interstitial (IM) macrophages, based on their localization in the lung [19]. AM are understood to arise from the yolk sac during embryonic development, and during a healthy state are primarily a self-sustaining population with minimal contribution from the circulation [19]. They are responsible for various homeostatic roles in the lung, including catabolizing surfactant and clearing pathogens and debris. However, in settings of lung injury there is recruitment of circulating monocytes from the blood to the tissue, where they then differentiation into monocyte-derived AM [19]. IM are smaller than AM and are believed to play a role in immunoregulation and barrier immunity [19]. Generally, IM are widely understudied in the setting of disease, however they are known to play a role in tissue remodelling [19], which supports their fibrotic potential. The

classification of macrophages further branches into polarization states, which is a highly debated area of research. Historically, it was believed that macrophage polarization was a dichotomy, consisting of opposite "M1 pro-inflammatory" and "M2 anti-inflammatory" macrophages. This was widely based on *in vitro* classification, and it is now accepted that macrophage polarization exists along a spectrum with dynamically shifting activation states [20].

Although the pathogenesis of IPF is widely unknown, it is predominantly agreed upon that epithelial injury initiates the cascade of fibrogenic processes in the lung [8]. Macrophages are then recruited to the site of injury and release of a combination of profibrotic mediators, including cc-chemokine ligand 18 (CCL18) and transforming growth factor beta (TGF-β) [21], fuelling a multifaceted sequence of fibrogenesis in the lung. Specifically, macrophage-mediated signalling stimulates migration and proliferation of fibroblasts, as well as their differentiation into myofibroblasts, overall resulting in the deposition of ECM components in the lung [21]. While it is believed that AM are the primary source of TGF-β in lung fibrosis, both AM and IM are implicated in profibrotic processes in the lung, with ongoing investigation to clarify their differential roles [19,22]. Additionally, various markers associated with "M2-like" programming, including CCL18, TGF-β, cluster of differentiation (CD) 206, interleukin (IL) 10, and arginase 1 are expressed by macrophages involved in fibrosis [23,24]. Notably, levels of both CD206 and CD163, were significantly increased in serum of IPF patients [25]. CD206 levels were also linked to increase mortality risk [25], which is in line with previous studies reporting the association of serum CCL18

levels with disease progression in IPF [26]. Furthermore, supporting their multifaceted functionality, recent studies unveiled a mixed activation state of macrophages in IPF that involves both pro-inflammatory and pro-fibrotic characteristics [27]. It has also been shown that macrophages are essential for the development of lung fibrosis. In bleomycin-induced murine models of pulmonary fibrosis, that macrophage depletion led to amelioration of the fibrotic response, centralizing the functional role of macrophages in fibrogenesis [28]. Undoubtedly, macrophages play a dynamic role in the development of fibrosis and are highly adaptable mediators. Further investigation is needed to elucidate a comprehensive understanding of these dynamics and how they can be targeted or modulated in the context of therapeutics for fibrosis.

Circulating Monocytes and Fibrotic Lung Disease

Monocytes are circulating cells derived from the bone marrow, which are involved in innate and adaptive immunity. Although monocytes are much less understood in IPF than macrophages, it is believed that as precursors of macrophages, monocytes may play an impactful role in mediating fibrogenesis. In response to epithelial injury and dysregulated immune signalling, monocytes are recruited to the lung where they differentiate into profibrotic macrophages and contribute to the aberrant wound healing milieu [29]. Lineage-tracing experiments in animal models of lung fibrosis have demonstrated contribution of monocytes to both IM and AM populations in the lung [19]. Additionally, in an *in vivo* murine lung fibrosis study, deletion of CCR2, a critical receptor for monocyte recruitment, protected mice from developing fibrosis, thus demonstrating the important role of recruited monocytes in orchestrating fibrotic

responses [30]. In the human three main subsets of monocytes exist, being classical ($CD14^{+}CD16^{-}$), intermediate ($CD14^{+}CD16^{+}$), and non-classical ($CD14^{dim}CD16^{+}$). Classical monocytes are the most common subset, followed by non-classical and then intermediate. Classical monocytes are also believed to have the highest inflammatory activity and entry into the tissue, while intermediate monocytes are inflammatory but do not actively patrol the bloodstream, and non-classical are generally considered anti-inflammatory.

Importantly, multiple studies have shown that circulating monocyte number is increased in IPF and predictive of poor disease outcomes [31–34], suggesting a potential association between these cells and disease progression. Given the ongoing challenge of prediction of mortality in IPF, this is of potential clinical relevance. Additionally, in a published IPF biomarker study reporting a 52-gene signature for prediction of transplant-free survival using peripheral blood mononuclear cells (PBMC), cellular deconvolution revealed that monocytes were the main contributors to the high-risk profile [12]. However, very little is known about the properties of monocytes in IPF. Further investigation is required to elucidate potential targetable aspects of monocyte behaviour in IPF and their relationship to profibrotic macrophage polarization.

Avenues of Interest: Dysregulated Mechanisms in IPF

Macrophage to Myofibroblast Transition

Monocytes are highly plastic cells that have been shown to have diverse transformation options including monocyte to endothelial cell transition, monocyte to

dendritic cell transition, monocyte to macrophage transition, and ultimately, macrophage–myofibroblast transition (MMT). This was a term introduced by Nikolic-Paterson et al. in 2014 to describe the transition of bone marrow-derived monocytes into myofibroblasts in the kidney [35]. Evidence for MMT likely existed before this time, and it was reported almost a decade earlier that blood monocytes in culture transformed into fibroblast-like cells with spindle-shaped morphology [36].

Studies directly reporting evidence for MMT have been mainly conducted in the kidney [37]. Overall, studies demonstrating evidence of MMT in lung fibrosis are especially limited. DiCampli et al. 2021 exhibited that cells of monocytic origin contribute to the mesenchymal cell population, which then differentiate into myofibroblasts in a murine model of bronchiolitis obliterans [38]. This was shown in via CX3CR1 lineage tracing. More recently, the role of MMT in a rodent lung silicosis model was also exhibited [39]. The importance of circulating fibrocytes, defined as CD45-collagen-1 copositive cells, in IPF patients has been previously reported, substantiating the involvement of hybrid monocytic mesenchymal cells in human biology in IPF [40]. However, more evidence in patients is needed to explore this notion further.

Cellular Metabolism in IPF

Metabolic dysfunction is implicated in the pathophysiology of lung disease [41]. In IPF lung cells, mainly fibroblasts and epithelial cells, these perturbations contribute to a decreased ability to adapt to cellular stress, overall increasing vulnerability to injury and subsequent fibrogenesis [42]. As the main metabolic organelle, mitochondria are

responsible for generation of ATP from glucose. In normal conditions, 70% of the cell's metabolic needs are supplied by oxidative phosphorylation (OXPHOS) – a highly efficient energy production pipeline [43]. However, under certain conditions, cells may switch from OXPHOS to glycolysis as their primary source of energy production. While metabolic flexibility can be beneficial and allow cells to adapt to various stimuli, such as low oxygen levels or increased demands for energy production, the shift from OXPHOS to glycolysis may also be pathologic. The metabolic preference for glycolysis, even in the presence of adequate oxygen levels, is termed the Warburg effect. The Warburg effect has historically been a hallmark characteristic of many cancers, giving cells a survival advantage and allowing them to evade apoptosis [44]. OXPHOS downregulation has been linked to poor clinical outcomes across all cancer types [45]. Although glycolysis is a faster process for energy production than OXPHOS, it is significantly less efficient and yields lactate as a by-product.

The Warburg effect and diminished capacity for OXPHOS have been linked to the pathogenesis of IPF [46,47]. Lung myofibroblasts adopt an enhanced glycolytic program in IPF [47]. It is believed that this contributes to the fibrotic landscape and perpetually sustains the disease state, as lactic acid levels were found to be increased in the lungs of IPF patients which in turn led to activation of TGF-β and further myofibroblast differentiation [48,49]. The Warburg effect has also been observed in epithelial cells and macrophages in pulmonary fibrosis [50]. It has been found that alveolar macrophages in IPF have reduced OXPHOS-related gene expression and

damaged mitochondria [27]. Additionally, inhibition of glycolysis in alveolar macrophages from a murine pulmonary fibrosis model led to a decrease of "M2-like" markers [51].

In healthy individuals, monocytes are one of the most energetic cell types and function with high levels of both OXPHOS and glycolysis [41]. Therefore, shifts in this balance may be characteristic of disease. Dysregulated metabolism and OXPHOS have been found in monocytes from sarcoidosis patients, as well as circulating cells in COPD [41,52]. Recent work has demonstrated that targeting the mitochondria in human monocytes with treatment of hydrogen sulfide augmented monocyte phenotype, shifted cellular metabolism, and reduced expression of profibrotic markers CD206 and CD163 [53]. Overall, modulation of monocyte metabolism and phenotype may have therapeutic potential in fibrotic lung disease but requires further investigation in patient-derived samples.

Pyruvate Dehydrogenase Kinase 4 and Disease

Pyruvate dehydrogenase (PDH) is an enzyme that catalyzes the conversion of pyruvate into Acetyl-CoA. The PDH complex connects glycolysis with the citric acid cycle and OXPHOS, and overall mediates the transition from anerobic metabolism in the cytosol to aerobic metabolism in the mitochondria [54]. Pyruvate dehydrogenase kinase (PDK) inhibits the activation of the PDH complex, thus signifying it as a gatekeeper kinase between glycolysis and OXPHOS, and master regulator of metabolic shifts. Among the four isoforms of PDK, PDK4 is invariably upregulated in mitochondrial dysfunction-related metabolic diseases, rendering it a strong indicator of metabolic

pathology [58]. A schematic displaying PDK's involvement in cellular metabolism can be found in **Figure 1.**

PDK4 expression has been shown to be implicated in multiple diseases, with the majority of published research being in the cancer field. Studies have demonstrated that PDK4 plays a role in the promotion of malignancy in acute myeloid leukemia, ovarian cancer, and bladder cancer [44,59]. As an indicator of poor prognosis in various patient settings, increased PDK4 expression has been found in breast cancer, gastric cancer, pulmonary arterial hypertension, and sepsis-induced cardiomyopathy [44,60–62]. Monocytic-specific increases in PDK4 expression have also been reported in disease, with significantly increased PDK4 mRNA levels found in $CD14^+$ monocytes from patients with acute-respiratory distress syndrome (ARDS) and coronary artery disease [63,64]. PDK has also been shown to be related to lung fibrosis. In animal models of pulmonary fibrosis, PDK was shown to be significantly upregulated in lung myofibroblasts [50,65].

Dichloroacetate (DCA) is a well-established PDK inhibitor that has passed phase I and II toxicity testing in humans [66]. DCA has traditionally been used for the treatment of lactic acidosis, however it is also being explored as an alternative cancer therapy. Clinical trials with DCA for brain and colon cancer were shown to have favorable outcomes [67,68]. Its utility as a potential antifibrotic and restorer of mitochondrial function through the promotion of OXPHOS has been demonstrated in animal models. Specifically, treatment with DCA administered through drinking water led to suppression of bleomycin-induced lung fibrosis, and effectively regulated PDK-

mediated glycolytic reprogramming [65]. Furthermore, in human and murine fibroblasts treated with TGF-β, PDK inhibition decreased α-SMA expression in a dose-dependent manner [65]. These *in vivo* and *in vitro* studies were largely fibroblast-focused, and the specific effects of DCA-mediated PDK inhibition on macrophages and other cells in the context of lung fibrosis remains to be investigated.

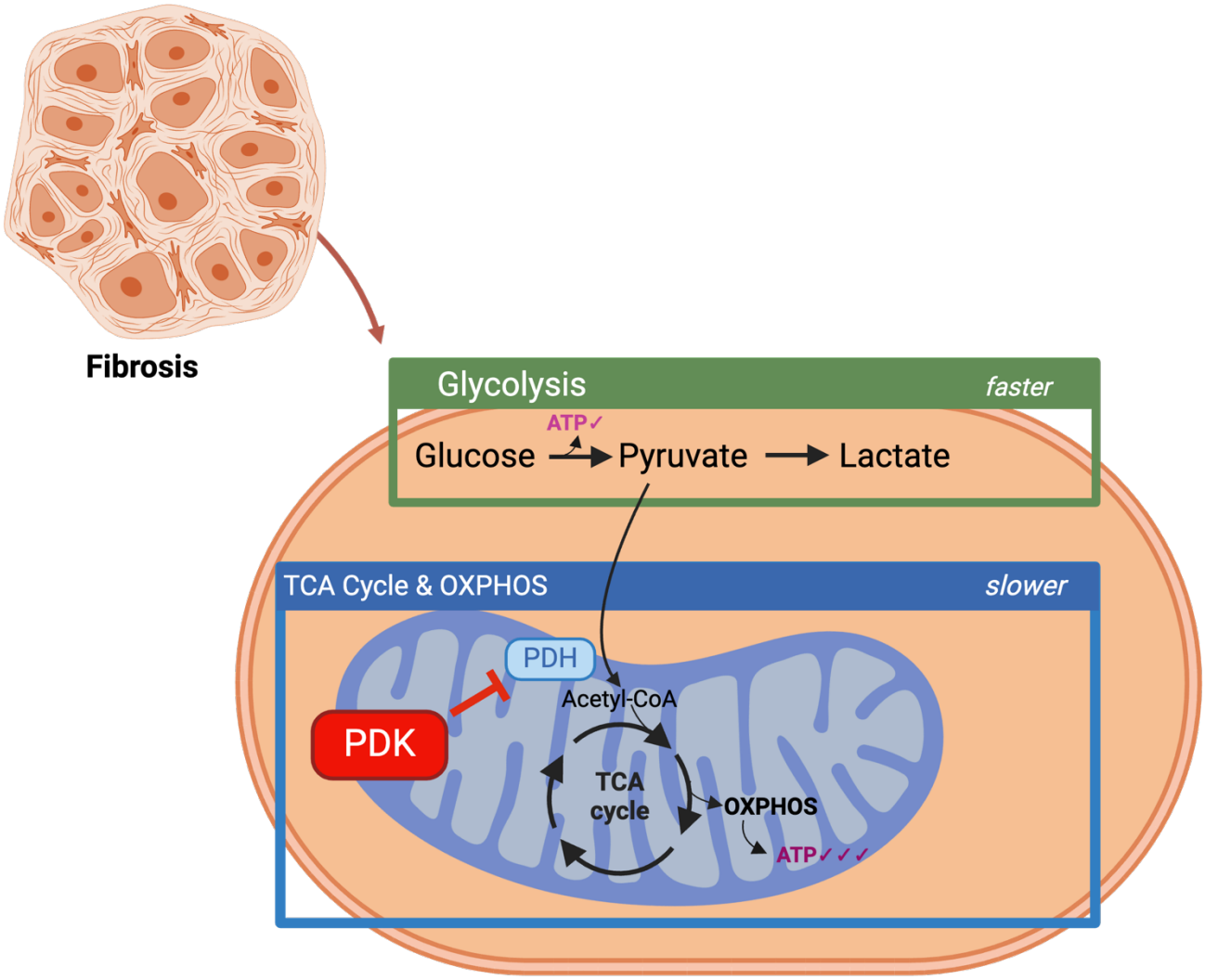

Figure 1: Pyruvate dehydrogenase kinase in cellular metabolism

In cellular metabolism, the connection between glycolysis and the TCA cycle + OXPHOS is mediated by PDH (light blue), which converts pyruvate into Acetyl-CoA. PDK (red) is a kinase that inhibits PDH, and thus serves as a gatekeeper kinase for OXPHOS. Figure created using BioRender.com.

Modelling Lung Research in a Translation Manner: Precision-Cut Lung Slices

Precision-cut lung slices (PCLS) are living tissue slices generated from the whole lung that are cultivated *ex vivo*. The lung is one of the body's most complex organs, with a highly unique architecture and cellular composition [69]. Compared to traditional *in vitro* cell and organoid culture systems, PCLS offer the benefit of naturally containing all cells, structures, and cell-matrix interactions found in the lung. This eliminates the need for scientist-made recreation and thus bypasses limits related to biological accuracy and translation. This is especially pertinent for highly plastic, interactive cells like macrophages, whose complex phenotypes cannot be fully understood in two-dimensional *in vitro* systems. Studies have demonstrated the ability to model features of fibrosis in PCLS [70], as well confirmed the presence of immune cells in PCLS including macrophages [71]. However, studies specifically examining profibrotic programming of macrophages using a PCLS system have not yet been reported.

OVERARCHING AIM AND CORE OBJECTIVES OF THESIS

The overarching aim of this PhD thesis is to investigate and ultimately interfere with profibrotic macrophage programming contributing to the pathogenesis of pulmonary fibrosis. This is fundamentally connected to the central hypothesis of the thesis, which is that modulating aberrant mechanisms governing macrophage activation status will hamper fibrogenesis in the lung. To address this from multifaceted angles, we developed the following constellation of interrelated key objectives: 1: Assess the presence of novel profibrotic mechanism MMT in the IPF lung, which has shown to be implicated in other forms of fibrosis (Chapter 2). 2: Establish a biologically-relevant, translational system to investigate macrophage profibrotic programming in the lung (Chapter 3). The established system will also include features related to the process of MMT. 3: Further building on the system developed in chapter 3, solidify means to perform comprehensive visual and quantitative phenotypic analysis of lung macrophages, and determine this in the established system (Chapter 4). 4: Uncover the profibrotic features of monocytes in IPF and examine their relationship with disease progression (Chapter 5). 5: Investigate the mechanistic implications of the identified dysregulated features on lung macrophage profibrotic polarization, also using the translational system developed in chapter 3. Overall, the findings from these investigations fed into the central knowledge paradigm for understanding the contribution of macrophages to the pathogenic landscape of IPF. A detailed depiction of the multi-component pathobiology for IPF, as well as the relationship to each of the

chapters in this thesis to the overall landscape of lung fibrosis, can be found in the **Thesis Graphical Abstract.**

CHAPTER 2

MONOCYTE AND MACROPHAGE DERIVED MYFIBROBLASTS: IS IT FATE?

Megan Vierhout, Anmar Ayoub, Safaa Naiel, Parichehr Yazdanshenas, Spencer D Revill, Amir Reihani, Anna Dvorkin-Gheva, Wei Shi MD and Kjetil Ask

This chapter contains a perspective article which includes original data and results as well as a comprehensive systematic approach examining the evidence for MMT. This work offers new insights on the concept of MMT across a range of organ systems and fibrotic disorders, including IPF. Through mining of a scRNAseq dataset of lung tissue explants from IPF patients and controls, we show that a subset of cells in the lung that have myofibroblast features co-express markers of monocytic origin ($ACTA2^{+}MAFB^{+}$). Using our curated biobank of lung tissue from IPF patients, consisting of FFPE surgical lung biopsies, we performed various histological staining assessments with histochemical, immunohistochemical, and FISH techniques to examine macrophage and myofibroblast expression pattern in the IPF lung. We observed coexpression of MAFB, ACTA2, and CD68 transcripts, as well as localization of α-SMA and CD68 proteins in similar areas, suggesting that ACTA2/α-SMA positive cells in lungs of IPF patients could stem from the myeloid lineage. Exploring evidence for MMT across a range of fibrotic disorders uncovered involvement of this process in several diseases, including kidney fibrosis, cardiac fibrosis, and pancreatic malignancy. Concordant with the evidence we examined in IPF, multi-organ MMT involvement was substantiated by coexpression of macrophage markers (such as CD68 and F4/80) and myofibroblasts (α-SMA). Overall, the work outlined in this chapter provides mechanistic insights for the role monocytes and macrophages in fibrogenesis, as well as their complex interplay with myofibroblasts, supporting these cells as driving profibrotic contributors in the landscape of multi-organ fibrosis, including IPF.

Author Contributions:
MV: methodology, formal analysis, investigation, writing – original draft, writing – review & editing, visualization; **AA**: investigation, writing – review & editing; **SN:** investigation, writing – review & editing; **PY:** investigation, writing – review & editing; **SDR:** investigation, writing – review & editing; **AR:** investigation, writing – review & editing; **ADG:** formal analysis, investigation, data curation, writing – review & editing; **WS:** conceptualization, writing – review & editing; **KA:** conceptualization, resources, writing – review & editing, supervision, project administration, funding acquisition

Citation: M. Vierhout, A. Ayoub, S. Naiel, P. Yazdanshenas, S.D. Revill, A. Reihani, A. Dvorkin-Gheva, W. Shi, K. Ask, Monocyte and macrophage derived myofibroblasts: Is it fate? A review of the current evidence, Wound Repair and Regeneration 29 (2021) 548–562. https://doi.org/10.1111/wrr.12946.

Published in *Wound Repair and Regeneration* (2021)

Monocyte and Macrophage Derived Myofibroblasts: Is it Fate?

A Review of the Current Evidence

Megan Vierhout MSc[1], Anmar Ayoub MD[1], Safaa Naiel MSc[1], Parichehr Yazdanshenas BSc[1], Spencer D Revill BTech[1], Amir Reihani BSc[1], Anna Dvorkin-Gheva PhD[2], Wei Shi MD/PhD[3] and Kjetil Ask PhD[1,2]

Affiliations:

[1] Department of Medicine, McMaster University and The Research Institute of St. Joe's Hamilton, Firestone Institute for Respiratory Health, Hamilton, ON, Canada.

[2] Department of Pathology and Molecular Medicine, McMaster Immunology Research Centre, McMaster University, Hamilton, ON, Canada

[3] Department of Surgery, Children's Hospital Los Angeles, Keck School of Medicine, University of Southern California, Los Angeles, CA 90027, USA

Short Running Title: Monocyte/Macrophage Derived Myofibroblasts

Corresponding Author. Kjetil Ask, 50 Charlton Ave East, Hamilton, ON, Canada L8N 4A6, Phone: (905) 522 1155 ext. 33694; Fax: (905) 521 6183; E-mail: askkj@mcmaster.ca

Key words: Macrophage to Myofibroblast Transition, Monocyte to Myofibroblast Transition, Fibrosis

LIST OF ABBREVIATIONS

a-SMA: a-smooth muscle actin

BMDM: bone marrow derived macrophages

CD: cluster of differentiation

COL1A1: collagen type 1 alpha 1

ECM: extracellular matrix

FAP: fibroblast activation protein

FFPE: formalin-fixed paraffin-embedded

FSP1: fibroblast-specific protein 1

GFP: green fluorescent protein

H_2O_2: hydrogen peroxide

H&E: hematoxylin and eosin

ILD: interstitial lung disease

IPF: idiopathic pulmonary fibrosis

IR: ischemia-reperfusion

MMT: macrophage-myofibroblast transition

MPS: Mononuclear Phagocytic System

M2: alternatively activated macrophage phenotype

PDAC: pancreatic ductal adenocarcinoma

PMA: phorbol 12-myristate 13-acetate

RES: Reticuloendothelial System

SGK-1: serum- and glucocorticoid-inducible kinase 1

TCF: T-cell factor

TGF-β: transforming growth factor beta

UUO: unilateral ureter obstruction

YFP: yellow fluorescent protein

ABSTRACT

Since the discovery of the myofibroblast over 50 years ago, much has been learned about its role in wound healing and fibrosis. Its origin, however, remains controversial, with a number of progenitor cells being proposed. Macrophage-myofibroblast transition, or MMT, is a recent term coined in 2014 that describes the mechanism through which macrophages, derived from circulating monocytes originating in the bone marrow, transformed into myofibroblasts and contributed to kidney fibrosis. Over the past years, several studies have confirmed the existence of MMT in various systems, suggesting that MMT could potentially occur in all fibrotic conditions and constitute a reasonable therapeutic target to prevent progressive fibrotic disease. In this perspective, we examined recent evidence supporting the notion of MMT in both human disease and experimental models across organ systems. Mechanistic insight from these studies and information from *in vitro* studies is provided. The findings substantiating plausible MMT showcased the co-expression of macrophage and myofibroblast markers, including CD68 or F4/80 (macrophage) and a-SMA (myofibroblast), in fibroblast-like cells. Furthermore, fate-mapping experiments in murine models exhibiting myeloid-derived myofibroblasts in the tissue further provide direct evidence for MMT. Additionally, we provide some evidence from single cell RNA sequencing experiments confirmed by fluorescent *in situ* hybridization studies, showing monocyte/macrophage and myofibroblast markers co-expressed in lung tissue from patients with fibrotic lung disease. In conclusion, MMT is likely a significant contributor to myofibroblast formation in wound healing and fibrotic disease across organ systems. Circulating precursors including monocytes and the

molecular mechanisms governing MMT could constitute valid targets and provide insight for the development of novel antifibrotic therapies, however further understanding of these processes is warranted.

INTRODUCTION

Myofibroblasts were first introduced by Gabbiani *et al.* in 1971 for their role in wound healing and tissue granulation[1]. Since their discovery, many have studied the mechanisms of collagen deposition and the characteristics of myofibroblasts in fibrotic conditions[2–5]. Myofibroblasts have been distinguished by the expression of alpha-smooth muscle actin (α-SMA), a marker not expressed by quiescent fibroblasts[6–8], making it unique to differentiated myofibroblasts.

Although the origin of these cells remains unclear and controversial, a number of pathways to their emergence have been proposed. The main contributing precursor is local recruitment from connective tissue fibroblasts[9]. Local mesenchymal stem cells and bone marrow-derived stem cells constitute other possible origins[9]. Alternatively, polarized epithelial and endothelial cells can differentiate into cells of mesenchymal phenotype and myofibroblasts through the epithelial-mesenchymal transition and endothelial-mesenchymal transition, respectively[10].

The concept of bone marrow-derived circulatory myofibroblast progenitors was first published in 1994 by Bucala *et al*. with the observation of circulating fibrocytes at the site of tissue injury[11]. These novel cells were characterized by the co-expression of bone marrow marker CD (cluster of differentiation) 34, and fibroblast markers collagen and vimentin[11]. Fibrocytes have been identified to be increased in fibrotic disease and associated with severity, where fibrocyte numbers were correlated with early mortality[12]. Additional studies have demonstrated that these fibrocytes had markers associated with monocytic origin and labeled them as “profibrotic monocytes”[13]. These circulating cells

are thought to extravasate from the circulation into injured and inflammatory areas where they can differentiate into myofibroblasts and contribute to extracellular matrix (ECM) deposition[14]. These ideas are consistent with recent findings whereby circulating monocytes have been identified to be increased and associated with lower survival in a variety of fibrotic diseases[15–17], however, the differences between monocytes and fibrocytes have not been clearly delineated.

Monocytes, a natural precursor for macrophages, are highly plastic bone-marrow derived circulating cells that are most commonly classified by the expression of CD14[18]. The monocyte's capacity to be a precursor cell for diverse transformation options can be appreciated through the monocyte to endothelial cell transition[19], monocyte to dendritic cell transition[20], monocyte to macrophage transition[20], and ultimately, the macrophage-myofibroblast transition (MMT), which is a term coined by Nikolic-Paterson *et al*. in 2014 to describe the transition of bone marrow-derived monocytes into myofibroblasts in the kidney[21]. However, plausible evidence for MMT prevailed before this time. In 1991, Labat *et al.* discovered that blood monocytes in culture transformed into fibroblast-like cells and coined these cells "neo-fibroblasts"[22]. Monocyte-derived mesenchymal cells were also denominated by Kuwana *et al*., who found that spindle-shaped cells emerged from cultured CD14 monocytes[23]. Despite scientific efforts, uncovering progenitor phenotypes and the regulatory components of the MMT mechanisms has been challenging[24]. Due to the heterogenous nature of macrophages and fibroblasts, there is a lack of consensus in characterizing their behaviours and phenotypes[25,26]. Since Metchnikoff's discovery of the macrophage system in the late 1880s, there has been a debate on whether

fibrocytes/fibroblasts should be included in the Reticuloendothelial System (RES) or in the updated classification of the Mononuclear Phagocytic System (MPS), mostly due to the lower phagocytic capacity of fibroblasts[27]. Therefore, we are proposing here that fibrocytes and monocytes can contribute to the pool of myofibroblasts, however the exact relationship between fibrocytes and MMT is not understood. It has been suggested that the RES and MPS systems need to be revisited and updated classifications may be required[28–31].

Although it has been shown that circulating precursors are able to transform into myofibroblast-like cells in several *in vitro* systems and *in situ,* evidence of MMT remains scarce. In this perspective review, we used a systematic approach to curate the current evidence accumulated since the term MMT was coined by Nikolic-Paterson *et al.* in 2014[21], supporting the notion that myofibroblasts share monocyte or macrophage markers to provide a perspective on MMT across organ systems in humans and experimental models. We further address the need for additional studies to confirm that MMT acts as a significant contributor to myofibroblast accumulation and progressive fibrotic disease, and constitutes a valid therapeutic target. The 13 reviewed articles highlight various clinical, *in vivo*, and *in vitro* designs utilized to assess MMT. Of the 13 studies, nine (69%) were focused on kidney fibrosis, two (15%) on lung disease (fibrosis and tuberculosis), one (7%) on cardiac fibrosis, and one (7%) on pancreatic cancer. The main outcomes to evaluate MMT were co-expression of monocyte/macrophage (CD68 and F4/80) and fibroblast/myofibroblast [α-SMA, Collagen I, fibroblast-specific protein 1 (FSP1), fibroblast activation protein (FAP)], cell morphology, gene expression, and protein expression. Inhibitors and drugs targeting pathways of interest were often used to determine if mechanisms were critical for

MMT. While reviews (n=12) were excluded, nine addressed MMT, specifically in kidney[14,32–36], liver[37], and fibrosis overall[38]. A summary of the included studies and their results can be found in Table 1.

EVIDENCE OF MMT IN KIDNEY DISEASE

Kidney Fibrosis

Kidney fibrosis is characterized by a substantial accumulation of myofibroblasts in the interstitial space[39]. These myofibroblasts create and deposit fibrillar matrix, which leads to deterioration of the architecture of the tissue[39]. This results in increased stiffness, disrupted blood flow, and decreased nephron function[39]. It has been shown that myofibroblasts also act as inflammatory cells, releasing cytokines and chemokines that can lead to kidney tissue damage[39].

Human

MMT cells, which express both monocyte/macrophage and fibroblast/myofibroblast markers, were seen to be largely present and elevated in investigations of kidney fibrosis in human chronic allograft disease, where over 60% of α-SMA$^+$ cells were CD68$^+$ [40]. The dual positive cell quantity was significantly higher in diseases that did not have active fibrosis, including diabetic kidney disease and end-stage renal disease[40]. This was correlated with clinical measures in biopsies from chronic renal allograft rejection patients, where more than 50% of myofibroblasts were CD68$^+$$\alpha$-SMA$^+$, and the quantity of these cells was correlated with severity of fibrosis and renal allograft function[41]. MMT macrophages in kidney disease also have a predominant alternatively activated (M2)

phenotype, which was supported by $CD68^+\alpha\text{-}SMA^+CD206^+$ cells in a fibrotic region of crescentic glomerulonephritis tissue[42].

Mouse

The unilateral ureter obstruction (UUO) and ischemia-reperfusion (IR) injury murine models were mainly used to study kidney fibrosis. In multiple studies, evidence for MMT in fibrotic kidney tissue from mice with UUO was observed by the co-expression of F4/80 and α-SMA via immunofluorescence and flow cytometry[40–45]. In the IR injury model, the accumulation of $F4/80^+\alpha\text{-}SMA^+$ cells was also observed, in addition to $CD206^+\alpha\text{-}SMA^+$ cells[40,46].

Various fate mapping/lineage tracing studies with green fluorescent protein (GFP) or Tomato-marked bone marrow-derived cells have demonstrated that myofibroblasts in the kidney were derived from the bone marrow. In these studies, over 90% of macrophage-myofibroblast double positive cells in the UUO model were determined to be of myeloid lineage[44], and were demonstrated to express collagen I in addition to F4/80 and α-SMA[42,44,47], supporting the notion that a significant portion of myofibroblasts is derived from the circulatory pool.

Rat

In a glomerulosclerosis model of diabetic rats, intraglomerular MMT was observed. The presence of $CD68^+\alpha\text{-}SMA^+$ cells was detected by immunofluorescence and flow cytometry, demonstrating the involvement of MMT in diabetic nephropathy[48].

In the above studies, the most commonly identified mechanism was the Smad3 pathway, where Smad3 knockout mice had decreased MMT and fibrosis[40,41,45,47]. Other critical

targets in kidney fibrosis include CXCL10[43], Pou4f1[40], A_{2B} adenosine receptor[48], β-catenin[44], Rac1[46], and Src[45], which were shown to be required for MMT through silencing or treatment with inhibitors.

EVIDENCE OF MMT IN LUNG DISEASE

Lung Fibrosis

In lung fibrosis, myofibroblasts possess a pathologic phenotype defined by augmented proliferation and survival[49]. The lung interstitium is riddled with myofibroblast accumulations and deposition of collagen and ECM[49]. Myofibroblasts assemble in fibroblastic foci and as these regions expand, they eventually dismantle the alveolar basement membrane[49].

Rat

MMT was studied in UUO-induced pulmonary fibrosis, where approximately 30% of myofibroblasts in the lung were derived from MMT. Cells co-expressing CD68 and α-SMA were characterized as double positive cells ($CD68^+\alpha$-SMA^+)[50]. $F4/80^+\alpha$-SMA^+ cells were also present, and triple co-expression showed collagen I staining in the majority of these cells, further supporting the MMT phenotype[50]. Lastly, approximately 35% of the myofibroblasts were co-positive for M2 macrophage marker, CD206, in the fibrotic lung tissue, demonstrating that cells likely transitioned through an M2 state prior to myofibroblast transition[50]. This study also demonstrated that inhibiting mineralocorticoid receptor reduced MMT[50].

While the UUO model was successfully used to model pulmonary fibrosis in this study, it should be noted that this is not a conventional model for interstitial lung disease (ILD).

This model may result in a smaller proportion of invading monocytes as compared to primary pulmonary fibrosis models. Although there have been a number of studies using primary pulmonary fibrosis models where macrophage depletion resulted in a reduction of myofibroblasts and fibrosis[51,52], this does not provide direct evidence for MMT. Additionally, the UUO model involves an acute inflammatory response that is not typical of progressive ILD. Future studies are needed to investigate MMT in primary pulmonary fibrosis models.

Human

To our knowledge, there are currently no studies claiming that MMT occurs in human lung fibrosis. To investigate MMT in human lung tissue, we recently examined dual expression of CD68 and ACTA2 in publicly available single cell RNA sequencing (scRNAseq) datasets containing samples from donors and IPF patients and found that approximately 50% of $ACTA2^{+}$ (α-SMA gene) cells were $CD68^{+}$[31]. In order to better characterize MMT cells, additional markers and multiplex analysis, both *in vitro* and *in vivo* are required. These potential targets can be studied with various methods to explore their expression and involvement in human disease. In order to trace cells from myeloid origin, markers that remain consistently expressed after entering the tissue are required. An example is the monocytic marker MafB, which was earlier proposed to be a suitable marker to follow myeloid cells *in vivo*[53]. MafB is a transcription factor that regulates the differentiation and activity of monocytes and macrophages[54]. It has been shown to be lineage specific, and is specifically expressed in $CD14^{+}$ monocytes[54] and not in other hematopoietic lineages[55]. This specificity differentiates MafB from other myeloid transcription factors[55]. To

determine a potential suitability to identify myeloid-derived parenchymal myofibroblasts, we examined MafB expression in a publicly available scRNAseq dataset from IPF patients and controls (**Figure 1**). Overall, 27 cell populations were defined in the dataset (**Figure 1A. i.**). As expected, MafB was found to be significantly upregulated in the monocyte (fold change = 2.07) and macrophage (fold change = 2.01) cell populations, with the addition of conventional dendritic cells (fold change = 1.46) (**Figure 1A. ii-iv.**). We then looked at the expression of ACTA2 and found that the majority of cells that appear to have a relatively high expression belong to the fibroblast, myofibroblast, and smooth muscle cell populations (**Figure 1B. i.)** When we examined co-expression of MafB and ACTA2, we found that 26.9% of $ACTA2^+$ cells expressed MafB (**Figure 1B. ii.**). Interestingly, this proportion was similar to the proportion (30%) of $CD68^+\alpha\text{-}SMA^+$ cells seen in the myofibroblast population in the lung fibrosis paper included in this review[50]. We then further examined potential colocalization of mRNA using fluorescent *in situ* hybridization on archived formalin-fixed paraffin-embedded (FFPE) surgical lung biopsies from an IPF patient. In **Figure 2**, we show three separate regions in a section of IPF lung tissue. Plausible colocalization of MafB, ACTA2, and CD68 RNA transcripts can be seen in the tissue. Tissues were also stained with hematoxylin and eosin (H&E), and α-SMA and CD68 immunohistochemistry. Serial sections stained with α-SMA and CD68 show localization of these proteins in similar areas. This could suggest that ACTA2/α-SMA positive cells in lungs of IPF patients could stem from the myeloid lineage, however further investigation is required to determine if these cells are specific to MMT. Overall, these types of strategies may assist in future exploration of MMT.

Tuberculosis

Granulomas are present in tuberculosis as a barrier against the infection, which differs from other lung fibrosis where wound healing occurs to restore damaged tissue architecture[56]. Fibroblasts have been found to be present in granuloma-associated fibrosis in tuberculosis, however their purpose and stimulating factors remain unclear[56].

Non-Human Primate (Macaque)

A study focusing on tuberculosis-related granulomas, and specifically in granuloma-associated fibrosis, used a systems biology approach to show that MMT can play an important role in the dynamics of granuloma-associated fibrosis in tuberculosis lungs. The results were confirmed in the non-human primate model, where $CD11^{+}\alpha\text{-}SMA^{+}$ cells were present in the fibrotic regions of granulomas from tuberculosis-infected macaque lung tissue[57]. This study also reported that STAT1 and STAT3 signaling must occur in a concerted manner for macrophages to undergo MMT, as predicted by computational simulations[57]. It should be noted that the tuberculosis model also involves an acute inflammatory response that is atypical in progressive ILD.

EVIDENCE OF MMT IN HEART DISEASE

Cardiac Fibrosis

In cardiac fibrosis, myofibroblasts arise from cardiac fibroblasts activated by various stressors including stretch, inflammation, and cytokines[58]. Cardiac myofibroblasts are characterized by increased ECM production and the ability to contract[58]. These cells can also secrete growth factors that lead to hypertrophy of cardiomyocytes[59].

Mouse

A myocardial infarction and heart failure model in transgenic mice was utilized to study myocardial remodeling and fibrosis. Yellow fluorescent protein expression restricted to the myeloid lineage allowed for fate mapping experiments. Evidence for MMT in the heart included the co-expression of fibroblast markers collagen I, prolyl-4-hydroxylase, FSP1, and FAP in yellow fluorescent protein positive cells in the heart tissue[60]. According to these findings, macrophages adopt a fibroblast-like phenotype, allowing the neo-expression of the aforementioned markers at the site of myocardial healing.

EVIDENCE OF MMT IN CANCER

Pancreatic Ductal Adenocarcinoma

Pancreatic ductal adenocarcinoma (PDAC) is characterized by a fibrotic response that involves cancer-associated fibroblasts, tumor-associated macrophages, and ECM[61]. Cancer-associated fibroblasts are believed to play a role in cancer initiation and progression[61]. These cells may also secrete ECM and chemokines, leading to chemoresistance and hindrance of the delivery of therapeutics[61].

Human

$CD68^+\alpha$-SMA^+ and $CD68^+FSP1^+$ cells were detected in FFPE pancreas tissue from PDAC patients[61], demonstrating proof of MMT in this disease. $CD14^+$ monocytes isolated from PDAC patients co-expressed α-SMA and CD68 when cultured without other stimuli[61]. Some of these cells also acquired a spindle-shaped morphology[61]. Additionally, transcriptomic analysis of PDAC tissue found that monocytes cultured in the presence of hydrogen peroxide (H_2O_2) exhibited upregulation of the p53 pathway, indicating that macrophage-to-myofibroblast transition is induced by stabilizing p53 through reactive

oxygen species generation[61]. *In vitro* studies showed that oxidative stress can activate the p38-MAPK pathway and promote MMT[61].

EVIDENCE OF MMT *IN VITRO*

Multiple *in vitro* studies with bone marrow-derived macrophages demonstrated the ability of these cells to transition into myofibroblasts. A schematic summary of these studies can be seen in **Figure 3**. Bone marrow-derived macrophages (BMDM) from mice were commonly used to test the effects of various compounds on MMT. MMT in these cells was exhibited by colocalization of macrophage markers (F4/80 or CD68) and α-SMA in several studies, after stimulation with transforming growth factor beta (TGF-β)[40,43–45,47]. The morphology of these cells also evolved to be spindle-shaped with cytoplasmic extensions[43,45]. Treatment of BMDM with IL-4 also stimulated expression of ECM and α-SMA at the protein level. In human macrophages derived from $CD14^+$ monocytes, *in vitro* assessments demonstrated a time-dependent increase of multiple fibroblast markers, including α-SMA, collagen type 1 alpha 1 (COL1A1), FSP1, and collagen secretion, after treatment with phorbol 12-myristate 13-acetate (PMA)[60]. The co-expression of these markers *in vitro* suggests a likely mechanism that links macrophages and myofibroblasts and contributes to disease progression.

MECHANISMS INVOLVED IN MMT

Kidney

Limited information is available on how the MMT process occurs. In the reviewed studies, a wide range of interventions were used to test the involvement of pathways and mechanisms in MMT. The most commonly studied mechanism was Smad3, which was

investigated in four kidney fibrosis studies[40,41,45,47]. Overall, Smad3 is required for MMT, as exhibited by decreased MMT and fibrosis in Smad3 knockout mice[40,41,45,47]. Smad3 is a mediator of TGF-β signalling, suggesting that MMT occurs through a TGF-β dependent pathway. This is also further supported by the multiple *in vitro* studies that induced MMT with TGF-β stimulation[40,43–45,47]. As a transcription factor, Smad3 is translocated to the nucleus after TGF-β binds to its receptor. One study identified transcription factor Pou4f1 as a Smad3 target in kidney fibrosis, and demonstrated it to be a crucial downstream regulator of MMT[40]. Pou4f1 was also found to be present in MMT macrophages in fibrotic sites, as indicated by α-SMA colocalization[40]. Another identified target of the Smad3 pathway in kidney fibrosis is proto-oncogene tyrosine protein kinase Src[45]. Src was shown to be required for MMT both *in vivo* and *in vitro*[45]. It is a Smad3 target gene and is upregulated in MMT macrophages[45]. The Smad3/TGF-β pathway has been implicated in fibrotic disease[62–64], and its relevance in MMT may also suggest that this process is critical for fibrogenesis.

Related to the Smad3 pathway are β-catenin and T-cell factor (TCF). It has previously been demonstrated that Wnt/β-catenin signaling is required for the differentiation of mesenchymal stem cells into myofibroblasts[65]. TGF-β/Smad signalling participates in crosstalk with the Wnt/β-catenin pathway, with the convergance of the pathways occuring at the activation of β-catenin via β-catenin/TCF, making β-catenin/TCF key to profibrotic processes[44]. In kidney fibrosis, it was shown that inhibition of β-catenin interaction with TCF reduced MMT, as this redirected the TGF-β pathway to β-catenin binding to Foxo1

instead of TCF[44]. A summary of the Smad3/TGF-β and β-catenin MMT mechanisms can be seen in **Figure 4A**.

A_{2B} adenosine receptor has also been shown to play a role in renal fibrosis[48]. When diabetic rats were treated with an A_{2B} adenosine receptor antagonist, reduced glomerulosclerosis as well as decreased macrophage infiltration and MMT were observed[48]. Activation of this receptor in the glomeruli has previously been seen to release TGF-β[66], and treatment with antagonists has resulted in decreased collagen and α-SMA levels in the kidney[67,68].

Another MMT mechanism that has been observed in kidney fibrosis is dependent on CXCL10[43]. When CXCL10 was knocked down or targeted with pterostilbene, a bioactive compound found in blueberries, in a murine model of kidney fibrosis, MMT was decreased[43]. CXCL10 protein was also shown to be increased in UUO mice[43]. CXCL10 has overall played a controversial role in fibrosis, with studies indicating that it has both profibrotic[69] and antifibrotic[70,71] functions.

The final MMT mechanism in the kidney involves Rac1, a member of the Rho family GTPase, that was also shown to play a significant role in kidney fibrosis[46]. Rac has previously been identified as a potential therapeutic target in fibrosis, and has been shown to play a role in the fibrotic phenotype of fibroblasts[72,73]. Rac1 was seen to be activated in the kidneys after IR, and treating mice with a Rac1 inhibitor led to a reduction in α-SMA levels and ECM proteins, and impaired accumulation of M2 macrophages and MMT[46].

Lung

In the UUO-induced lung fibrosis model highlighted in this review, the mineralocorticoid receptor was seen to play a key role in MMT. Aldosterone, a mineralocorticoid steroid

hormone, binds to the mineralocorticoid receptor in the cytosol[50]. Mineralocorticoid receptor then transfers to the nucleus[50]. This receptor has been involved in various animal models of fibrosis[50], and antagonists have been demonstrated to attenuate pulmonary fibrosis in bleomycin rodent models[74]. Mineralocorticoid-sensitive inflammation and fibrosis involves serum- and glucocorticoid-inducible kinase 1 (SGK-1), which upregulates NF-κB and leads to the expression of inflammatory mediators[50]. Increased expression of SGK-1 has been linked to lung fibrosis[50]. In this rat UUO model of lung fibrosis, blocking mineralocorticoid receptor with eplerenone was seen to reduce the quantity of MMT cells[50]. This study exhibited increased quantity of mineralocorticoid receptor in UUO lungs, however it was not specific to a certain cell type.

Additionally, in the computational simulations conducted to study tuberculosis-related granuloma-associated fibrosis in the lung, it was predicted that macrophages undergoing MMT must experience a concerted signalling process involving transcription factors STAT1 and STAT3[57]. STAT1 stimulation promotes an inflammatory phenotype, while STAT3 provides an anti-inflammatory signal[57], and inflammatory macrophage transition into myofibroblasts has previously been demonstrated in fibrosis[42]. According to the model, STAT1 signalling must be initiated first, followed by initiation of STAT3 signaling approximately 7 days later[57]. These mechanisms are outlined in **Figure 4B.**

Pancreas

In PDAC studies, *in vitro* experiments demonstrated that oxidative stress through exposure to H_2O_2 induced MMT[61]. Oxidative stress can activate the p38-MAPK pathway, which can induce α-SMA expression in monocytes/macrophages[61]. In the pancreas, p38-MAPK has

been linked to pancreatitis and inhibition studies have shown alleviation of the inflammatory response[75]. p38-MAPK is also a downstream target of TGF-β, and blocking this pathway has been shown to be associated with decreased ECM production[76]. This supports that the p38-MAPK axis, governed by oxidative stress stimulation, may be important in MMT. This mechanism is illustrated in **Figure 4C.**

FUTURE DIRECTIONS

The current evidence is from a collection of organ systems in human, mouse, rat, and non-human primate experimental models. A schematic representation of the MMT process highlighted in this review can be seen in **Figure 5**. Given the direct proof, as demonstrated through lineage tracing, co-expression of known markers of both cell types and inhibition of key MMT mechanisms, the literature suggests that there is accumulating evidence that MMT is a contributor to fibrotic processes. Previous studies have depleted the monocyte and macrophage population *in vivo* with clodronate treatment and other strategies and showed decreased quantities of myofibroblasts and resulting fibrosis[51,52,77]. The explanation for this was attributed to the belief that macrophages are indirectly required for differentiation and recruitment of myofibroblasts in the tissue. However, eliminating these cells may also deplete progenitor populations and therefore have a direct effect on myofibroblast quantities. With MMT evidence in mind, a shift in interpretation of the conclusions of previous macrophage depletion studies may be considered.

To our knowledge, there are four substantial limitations that need to be considered in MMT investigations. The first is surrounding the effect of the microenvironment on the MMT process. It is clear that circulating cells are not the only contributor to fibrogenesis and the

progression of fibrotic disease. If fibrosis developed only from contributions of the circulatory component, multiple organ systems would be impacted in a single patient. Therefore, the microenvironment may also play a key role in causing these cells to transition, and there is likely a complex interplay between circulating cells and the microenvironment in the tissue. Circulating monocytes and resident macrophages are dynamic components of the immune system. This entails that they can specialize in a tissue-specific fashion to control the homeostasis of several organs. Monocytes are known to give rise to most tissue-resident macrophages[78]. However, Gordon & Taylor[79] proposed that under normal conditions, macrophage proliferation occurs locally to regenerate tissue-resident cells, with the circulating progenitors having little role in this process. Furthermore, monocyte-derived macrophages emerge in response to local trauma, infection, or inflammation[79]. This suggests that the tissue microenvironment controls the plasticity of circulating monocytes[78,79], which, in turn, regulates MMT and the fibrotic crosstalk. Although evidence suggests the important role of circulatory cells in myofibroblast differentiation, in absence of favorable tissue landscape, these progenitors are insufficient for the initiation and progression of MMT. Further studies are required to investigate the fibrotic microenvironment in disease.

Another limitation is associated with morphology of MMT cells. Spindle-like morphology is characteristic of myofibroblasts, and cells undergoing MMT were shown to attain this morphology. M2 macrophages have been reported to acquire a spindle-shape morphology that could be considered fibroblast-like[80,81]. A number of the MMT studies in this review showed a predominant M2 macrophage phenotype or colocalization with M2 macrophage

marker CD206[40,42,46,50]. This may demonstrate that the cells transitioned through an M2 state before becoming myofibroblasts. M2 macrophages can also release TGF-β[82], which may play a role in the MMT process. However, studies that identified M2 macrophages to have a spindle shape did not investigate if they were in a transitional state, and whether they would ultimately become myofibroblast-like cells. Therefore, these results require further consideration. This point overall also raises caution that the observation of cells acquiring a spindle-like morphology is not solely indicative of MMT, and needs to be combined with other assessments, such as staining.

While the studies included in this review provide adequate data for characterization of cells resulting from MMT, there is limited evidence in the literature regarding their functionality. A distinguishing feature of myofibroblasts is their contractile nature[6,7], however this has not yet been directly demonstrated in MMT studies. Further investigation of the contractile and functional properties of MMT myofibroblasts, both *in vitro* and *in vivo* are required. Additionally, the current MMT literature mainly focuses on colocalization of α-SMA with monocyte/macrophage markers. A principal characteristic of myofibroblasts is the presence of α-SMA in their stress fibres, which plays a large role in the function and contractile nature of these cells[7]. In some of the literature examined in this review, α-SMA$^+$ macrophages were shown to express α-SMA in the cell membrane[45,61] or dispersed throughout the cell[41,43,44,47,47,48,50,60] via high resolution imaging of immunofluorescence staining. This is a limitation of the evidence supporting MMT, and further studies are required to examine stress fibres in MMT cells.

Lastly, there is little mechanistic insight currently available to support potential MMT processes, especially in cardiac fibrosis. Further mechanistic studies are required to better understand the role of MMT *in vitro* and *in vivo.* It is not clear whether there is crosstalk between the mechanisms explored in this review, and further research is required to elucidate this. Linked to the deficit of information regarding mechanisms, the information on the extent of MMT and role of myofibroblasts in fibrotic disease progression is very limited. The clinical observation, based on examination of fibrotic tissues, is that myofibroblasts reside in the fibrotic areas and are responsible for the deposition of ECM. These observations are almost exclusively based on cross-sectional observations as serial surgical biopsies are usually not performed in the clinical setting. The progressive nature of fibrosis is variable and little information or biomarkers exist in any fibrotic system indicative of progressive disease. Most animal models recapitulate fibrotic processes but are usually not progressive in nature and not suited to study progressive disease. The key observation in the cited literature is that myofibroblasts, seen as α-SMA$^+$ cells, often share markers of myeloid nature, seen as CD68 or F4/80 positive cells, and could be derived from circulating cells. Once mechanistic insights are gained from experimental studies, it is crucial to also explore targets of interest in samples of human disease.

Further investigations are required to elucidate the properties and functions of cells undergoing MMT. More complex systems, and potentially *ex vivo* studies, can be used to study the role of the microenvironment and gain mechanistic insight in MMT. Studies to provide evidence of cells to contract in *in vitro* and *in vivo* systems are also warranted, as well as investigations to further examine stress fibres in these cells. Other circulatory cells,

such as the closely related fibrocyte, also warrant additional exploration as a potential contributor to the myofibroblast pool. Additionally, development of scRNAseq platforms allows examination of RNA abundance with high accuracy and sensitivity, in addition to very high throughput[83]. This opens opportunities to define and study various cell populations, which may have great utility in MMT. Various methods are being developed for characterization of dynamics between these populations, among them are calculations of trajectories[84], and of RNA velocity[85]. While building trajectories is a non-directional approach and therefore requires a prior assumption and knowledge of directionality between the examined cells, the RNA velocity method allows researchers to find directionality of change, by yielding a high-dimensional vector, which predicts a future state of individual cells. Such a method has extraordinary potential for revealing the dynamics between monocytes, macrophages and myofibroblasts. In addition, new technology, such as scRNAseq in combination with genetic barcoding allows simultaneous identification of lineage histories and transcriptomic profile for single cells in mice, which will accurately define the ancestry of monocytes, distribution and mobilization of the progeny, and their tissue destination and fate in either physiological or pathological conditions[86].

In conclusion, there is accumulating evidence that MMT may occur in multiple organ systems, including the kidneys, lung, heart and pancreas. It is important to highlight that conclusions supporting the presence of MMT were linked to the co-existence of monocyte/macrophage and myofibroblast attributes in cells and tissue, lineage tracing and fate mapping strategies, and severity of disease in the studied models. We propose that

further studies and molecular phenotyping techniques are required to better characterize the features of these MMT cells.

ACKNOWLEDGEMENTS

We sincerely thank the McMaster Immunology Research Centre's Core Histology Facility (Mary Jo Smith and Mary Bruni) and the Molecular Imaging and Phenotyping Core facility (www.mpic-facility.ca) for outstanding service. This work was funded in part by the Canadian Lung Association (K. Ask). M. Vierhout is funded by the Canadian Institutes of Health Research (CIHR) Doctoral Award: Frederick Banting and Charles Best Canada Graduate Scholarships (Grant No. 170793). S. Naiel is funded by the Government of Ontario under the Ontario Graduate Scholarship (OGS) Program.

CONFLICT OF INTEREST

K. Ask reports grants from Alkermes, Prometic, GSK, Canadian Institute for Health Research, Pharmaxis, Indalo, Unity Biotechnology, Canadian Pulmonary Fibrosis Association, Collaborative Health Research Projects, Pieris Pharmaceuticals, Bold Therapeutics, Pliant, CSL Behring and grants and personal fees from Boehringer Ingelheim outside of the submitted work. All authors declared no potential conflicts of interest.

FIGURES

A.

i.

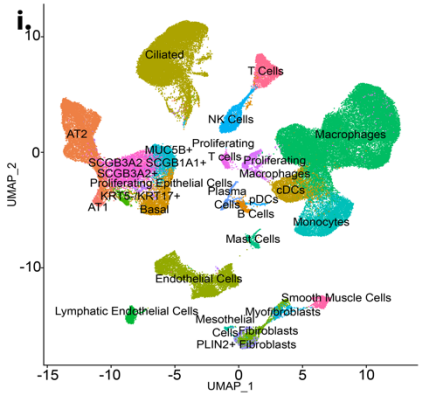

ii.

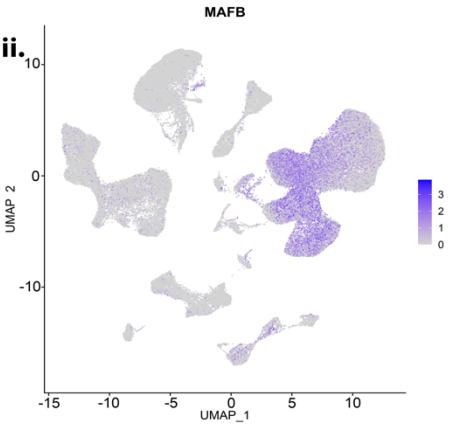

iii.

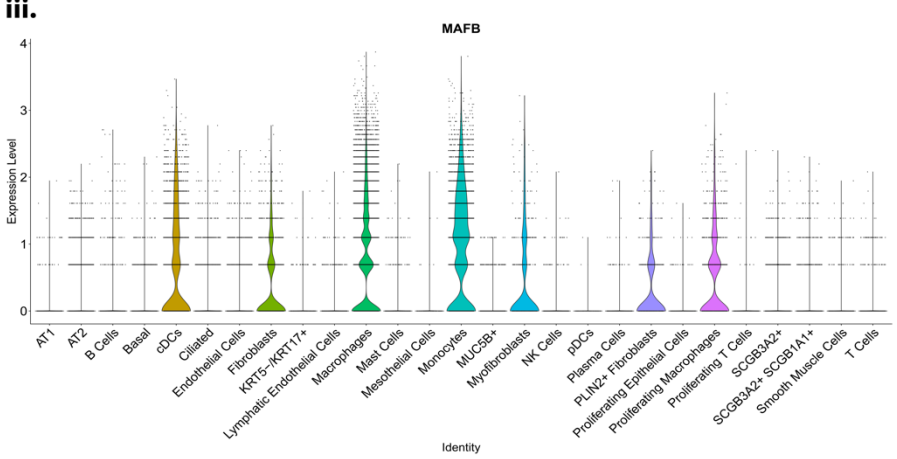

iv. **Cell population markers**

cluster	avg_logFC	FC	p_val	p_val_adj
Monocytes	0.73	2.07	0	0
Macrophages	0.70	2.01	0	0
Conventional Dendritic Cells	0.38	1.46	1.86E-119	4.83E-115

B.

i.

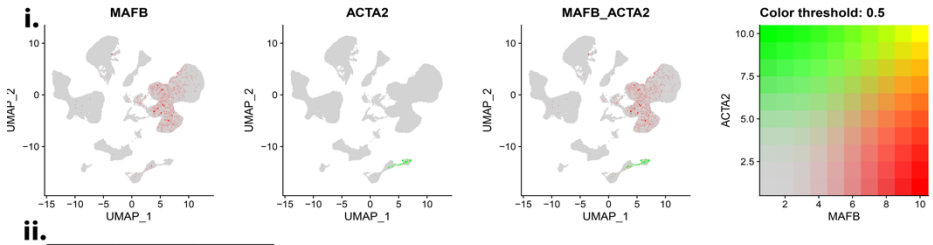

ii.

	MAFB-	MAFB+
ACTA2-	54,277	23,192
ACTA2+	5,199	1,915

26.9%

p-value = 1.041E-07

Figure 1: scRNAseq dataset comprised of samples obtained from peripheral lung tissue removed at the time of lung transplant surgery from patients with IPF (n = 12) and from nonfibrotic controls (n = 10).

Data were obtained from a publicly available dataset containing samples from donors and IPF patients (GSE135893). The dataset contained samples obtained from peripheral lung tissue removed at the time of lung transplant surgery from 12 patients with IPF and from 10 non-fibrotic donors. Processing, analysis, and visualizations were performed using Seurat package[87] in R. Cell populations were defined using the markers from the source paper related to the dataset. After examination of the expression level distributions for MafB and ACTA2 genes, all cells showing levels of expression > 0 were defined as "positive" for that gene.

A:

i. UMAP plot of cell populations. Overall, 27 cell populations were defined in the dataset.

ii. UMAP plot showing levels of expression of MafB. The majority of cells that appear to have a relatively high expression of MafB (purple) belong to the monocyte, macrophage, and conventional dendritic cell populations.

iii. Violin plot of MafB expression across various cell populations. Several cell populations exhibited various extents of elevated expression of MafB.

iv. Cell populations in which MafB was found to be significantly upregulated: monocytes (fold change = 2.07), macrophages (fold change = 2.01) and conventional dendritic cells (fold change = 1.46) (adjusted $p<0.05$).

B:

i. UMAP plots showing expression of MafB and ACTA2 separately and superimposed together. As seen in panel A. ii., the majority of cells that appear to have a relatively high expression of MafB (red) are in the monocyte, macrophage, and conventional dendritic cell populations. The majority of cells that appear to have a relatively high expression of ACTA2 (green) are in the fibroblast, myofibroblast, and smooth muscle cell populations. Co-expression of the two markers is also shown. The colour legend reflecting the levels of expression is included on the right.

ii. Number of cells selected based on their levels of MafB and ACTA2 expression (expression level of 0 was considered as negative). Out of all ACTA2 positive cells, 26.9% were positive for MafB (red arrow).

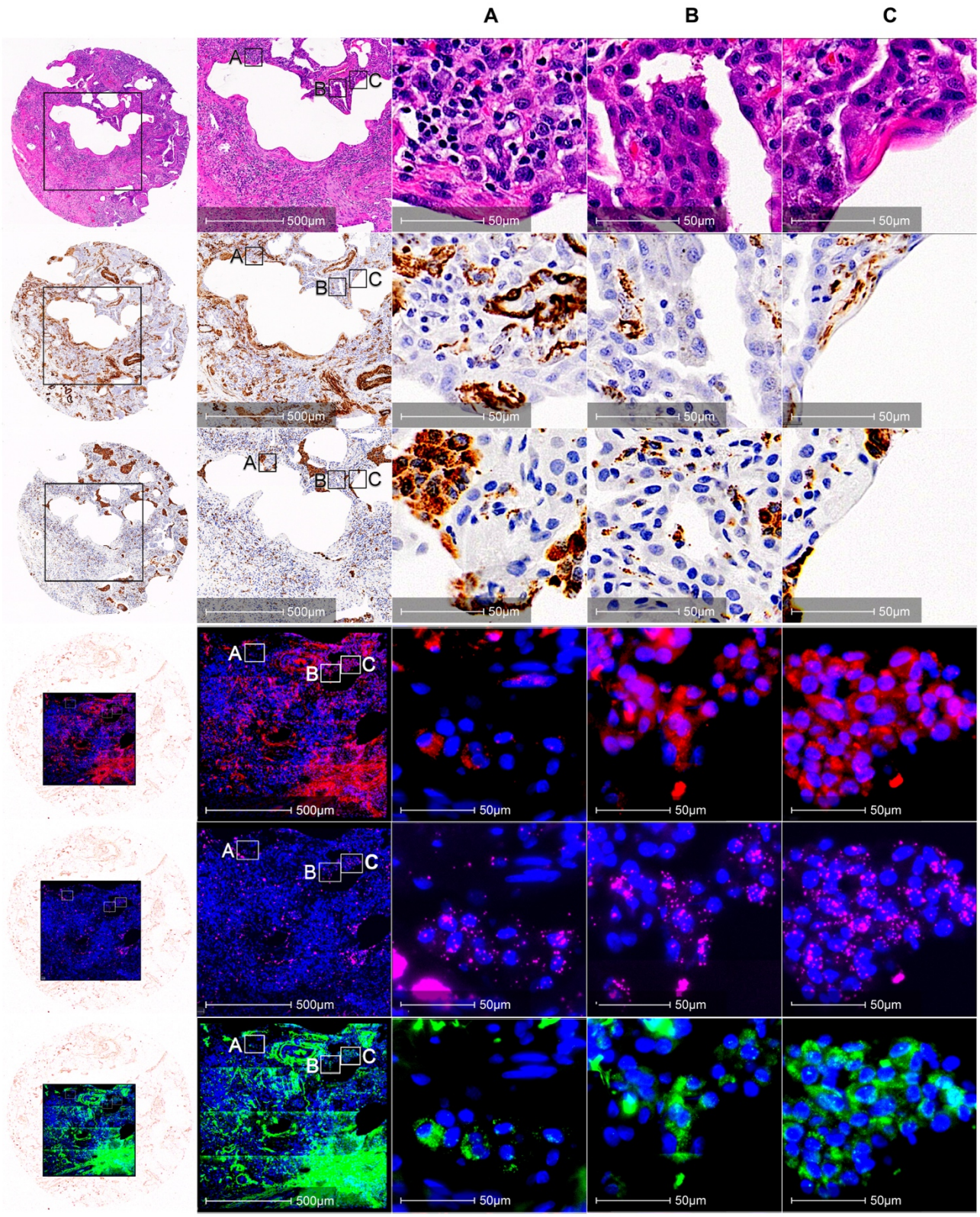
A
B
C
H&E
α-Smooth Muscle Actin (αSMA) (IHC)
CD68 (IHC)
ACTA2 (FISH)
MAFB (FISH)
CD68 (FISH)
500μm
50μm

Figure 2: Staining of FFPE lung tissue from an IPF patient. Three separate regions (A,B, and C) from IPF lung tissue are shown together and separately. Sections were stained with H&E, α-SMA (IHC), CD68 (IHC) and triple positive MafB+ACTA2+CD68 fluorescent *in situ* hybridization (FISH). Serial sections stained with α-SMA and CD68 IHC show localization of these proteins in similar areas. As can be seen in the MafB, ACTA2 and CD68 channels, colocalization of MafB (pink), ACTA2 (red) and CD68 (green) RNA transcripts are present in cells in the lung tissue.

Work completed using human lung tissues was as previously described[88]. In short, procedures using human tissues were approved by the Hamilton Integrated Research Ethics Board (11-3559 and 13-523-C). FFPE IPF lung tissue samples were acquired from the biobank for lung diseases at St. Joseph's Hospital in Hamilton, Ontario, and selected based on the evaluation of trained molecular pathologists and radiologists. IHC staining was completed with Agilent Dako CD68 (M0876) and α-SMA (M0851) antibodies. Commercially available RNAscope® (ACD Bio) fluorescent *in situ* hybridization assay was used for staining of MafB (400808), ACTA2 (311818), and CD68 (560598) stained with a Leica BondRX. Slides were digitized using an Olympus VS120 slide scanner at 20X (histological and immunohistochemical stains) and 40X magnifications (fluorescent *in situ* hybridization) and visualized with HALO image analysis software (Indica Labs, v3.2.1851.229).

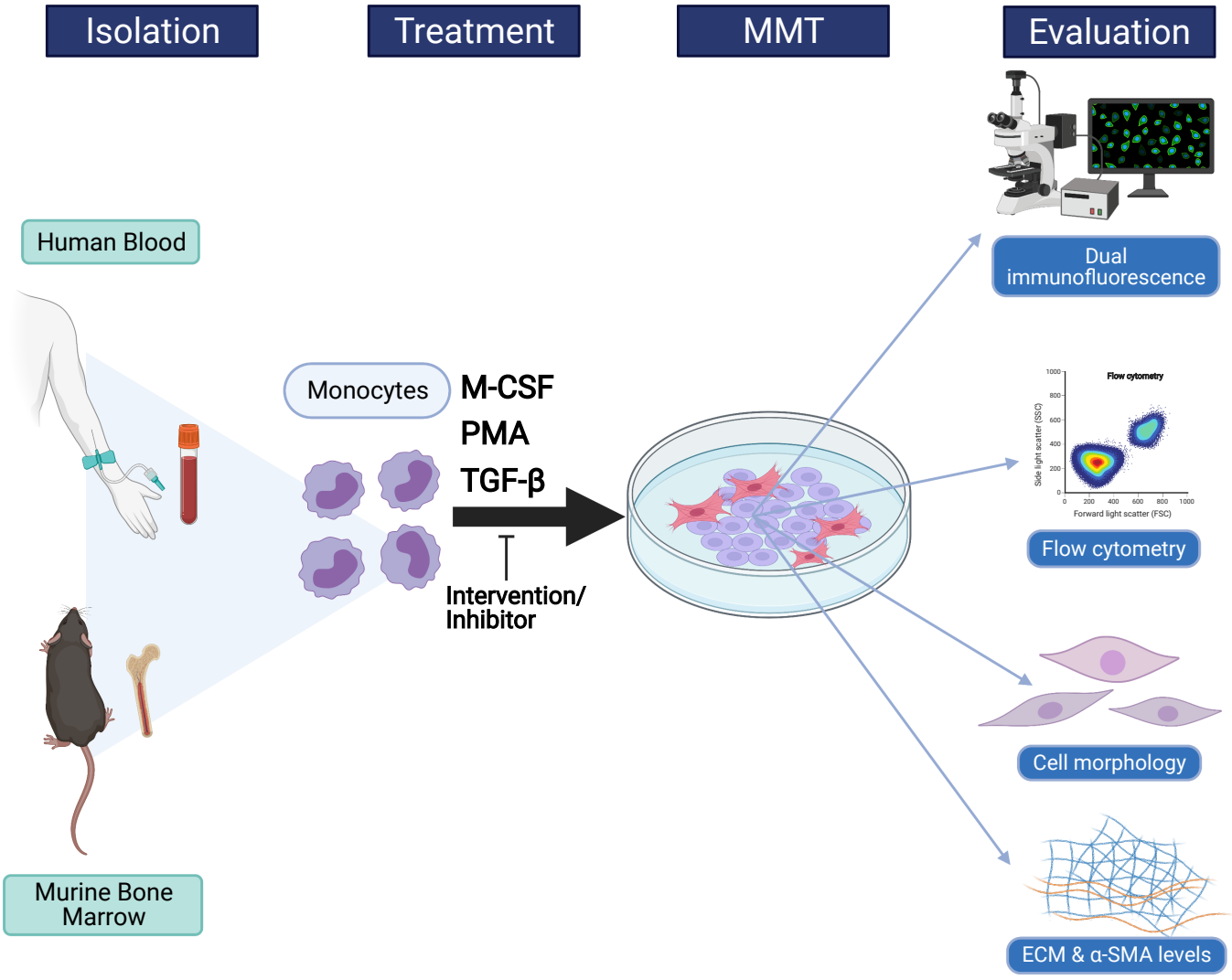

Figure 3: Schematic representation of *in vitro* MMT studies. Macrophages were derived from monocytes from human blood or murine BMDM. Cells were treated with M-CSF or PMA, TGF-β, and inhibitors of mechanisms under investigation. Several outcomes were measured to assess MMT, including dual immunofluorescence, flow cytometry, morphology changes, and ECM and α-SMA protein assessments. Created with BioRender.com

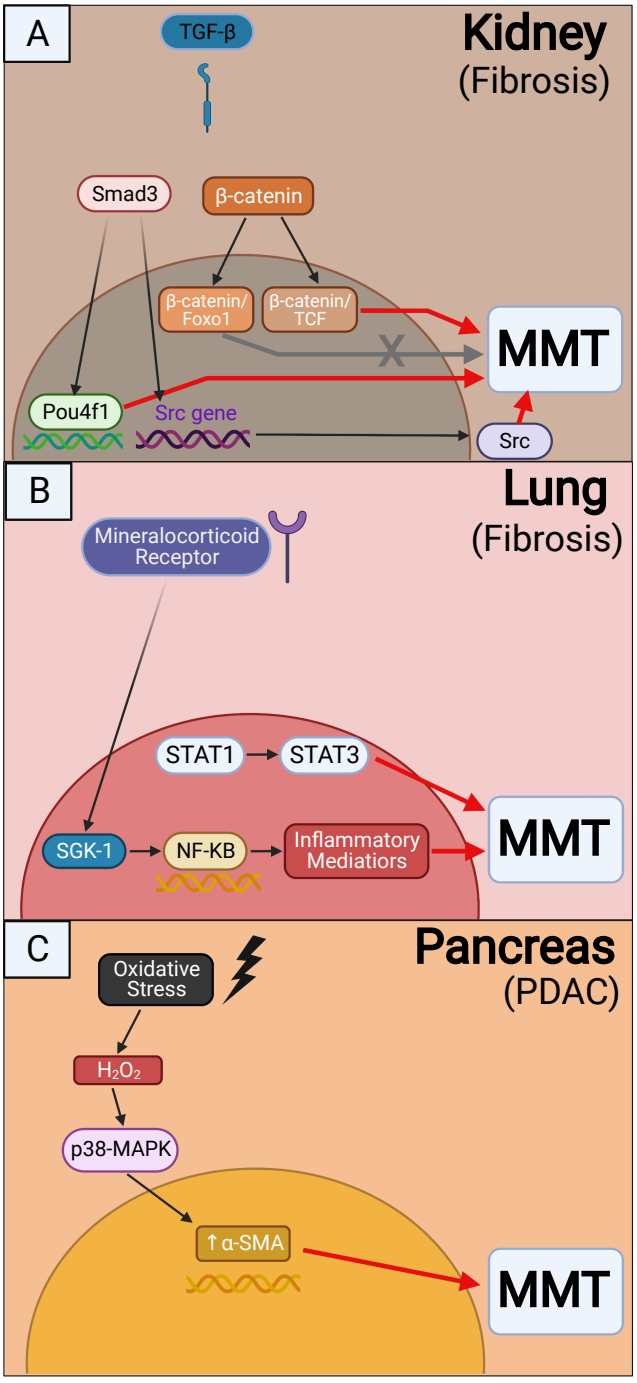
A
TGF-β
Kidney
(Fibrosis)
Smad3
β-catenin
β-catenin/
Foxo1
β-catenin/
TCF
MMT
Pou4f1
Src gene
Src
B
Mineralocorticoid
Receptor
Lung
(Fibrosis)
STAT1
STAT3
SGK-1
NF-KB
Inflammatory
Mediators
MMT
C
Oxidative
Stress
Pancreas
(PDAC)
H2O2
p38-MAPK
↑ α-SMA
MMT

Figure 4: Mechanisms for MMT highlighted in this review.

A: In the kidney, transcription factor Smad3 is translocated to the nucleus after TGF-β binds to its receptor. Pou4f1 and Src have been identified as targets of Smad3 target in kidney fibrosis, and involved downstream in MMT. β-catenin also plays a role in MMT, and its binding to TCF promotes MMT. β-catenin/Foxo1 binding, however, reduces MMT.

B: In the lung, mineralocorticoid receptor has been seen to interact with SGK-1, which upregulates NF-κB and leads to the expression of inflammatory mediators. Although the mechanism is not fully elucidated, mineralocorticoid receptor has been claimed to be necessary for MMT in a lung fibrosis model, as blocking it reduces MMT. It should also be noted that exhibited increased quantity of mineralocorticoid receptor was seen in a UUO-induced lung fibrosis model[50], however it was not specific to a certain cell type. STAT1 and STAT3 signalling have also been seen to be required for MMT in granuloma-associated fibrosis in tuberculosis.

C: In the pancreas, it has been proposed that oxidative stress via H_2O_2 can induce MMT in PDAC. Oxidative stress activates p38-MAPK, which can induce α-SMA expression in monocytes/macrophages. Created with BioRender.com

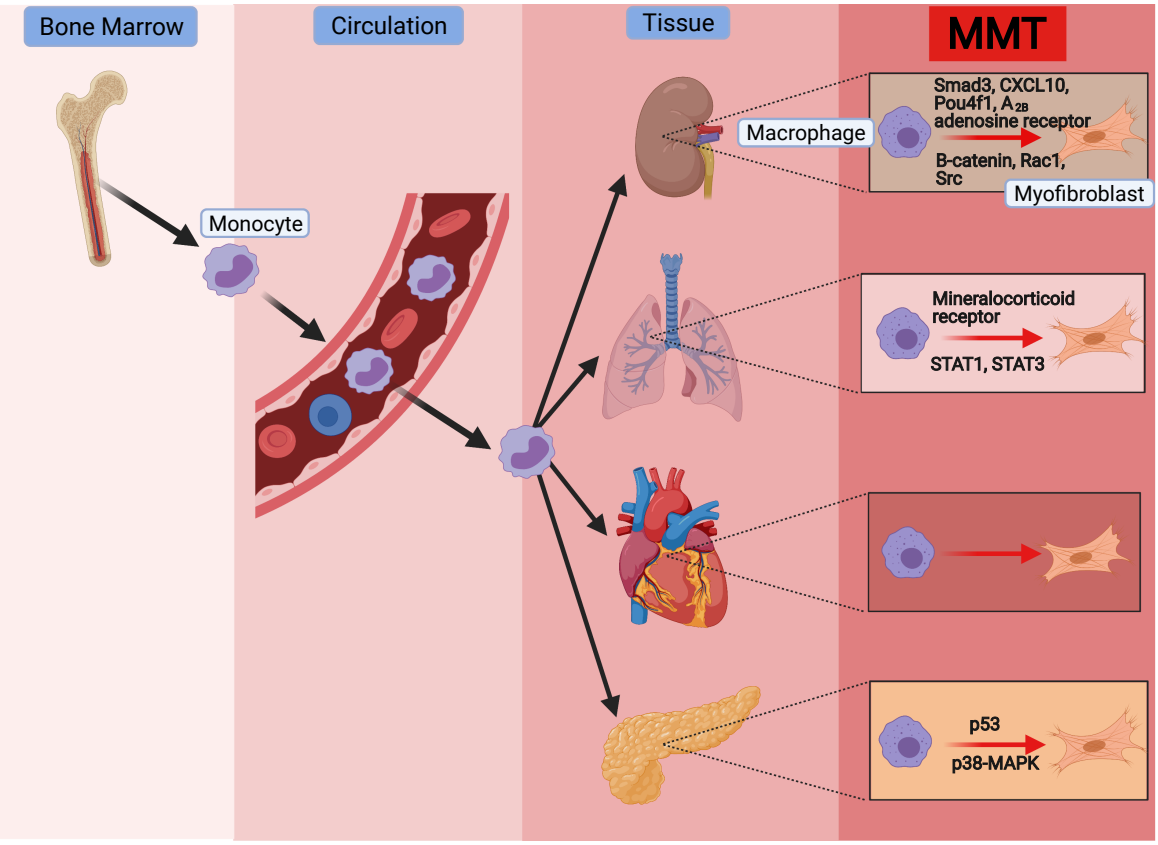

Figure 5: **Schematic representation of MMT process highlighted in this review.** Monocytes leave the bone marrow and enter the circulation. From there, they extravasate and enter various tissues in the body, where they can transform into macrophages and then myofibroblasts. Several key mechanisms have been identified for transition into myofibroblasts, including Smad3, CXCL10, Pou4f1, A_{2B} adenosine receptor, β-catenin, Rac1, and Src in the kidney, mineralocorticoid receptor, STAT1 and STAT3 in the lung, and p53 and p38-MAPK in the pancreas. Created with BioRender.com

TABLES

Table 1: Summary of Included Studies

Disease(s)	Organ	Intervention	Clinical	In vivo	In vitro	Computational model	Co-localisation markers	Methods used to determine co-localisation	Mechanism of action	Reference
Lung fibrosis	Lung	X		X			1) $CD68^+/\alpha\text{-}SMA^+$ 2) $F4/80^+/\alpha\text{-}SMA^+/COL1A1$	Immunofluorescence, α-SMA/collagen expression	RAAS and mineralocorticoid receptor	Yang et al. (2021)[39]
Tuberculosis	Lung					X	$CD11^+/\alpha\text{-}SMA^+$	Computational analysis, immunofluorescence, cell morphology	STAT1/STAT3	Evans et al. (2020)[40]
PDAC	Pancreas	X	X		X		1) $CD68^+/\alpha\text{-}SMA^+$ 2) $CD68^+/FSP1^+$	Immunofluorescence, cell morphology, α-SMA/ECM expression	p53 through Reactive Oxygen Species generation, p38/MAPK pathway	Huang et al. (2020)[41]
Cardiac fibrosis	Heart			X	X		1) $CD90^+/F4/80^+$ 2) $YFP/COL1A1^+/FSP1^+/FAP^+$ 3) $FSP1^+/COL1A1^+/\alpha\text{-}SMA^+$	Immunofluorescence, flow cytometry, cell morphology	N/A	Haider et al. (2019)[42]
Diabetic neuropathy, kidney fibrosis	Kidney	X		X	X		1) $CD68^+/Nephren^+$ 2) $CD68^+/\alpha\text{-}SMA^+$	Immunofluorescence, flow cytometry, cell morphology, α-SMA/collagen expression	A_{2B} adenosine receptor	Torres et al. (2020)[43]
Chronic kidney allograft rejection, kidney fibrosis	Kidney		X	X			1) $CD68^+/\alpha\text{-}SMA^+$ 2) $F4/80^+/CD68^+/\alpha\text{-}SMA^+$	Immunofluorescence, flow cytometry, cell morphology, α-SMA/collagen expression	Smad3	Wang et al. (2017)[44]
Kidney fibrosis	Kidney	X		X	X		$F4/80^+/\alpha\text{-}SMA^+$	Immunofluorescence, flow cytometry, cell morphology, α-SMA/collagen expression	CXCL10	Feng et al. (2020)[45]
		X	X	X	X		$F4/80^+/Pou4fl^+/\alpha\text{-}SMA^+$	Immunofluorescence, flow cytometry, cell morphology, α-SMA/collagen expression	Pou4fl, Smad3	Tang et al. (2020)[46]
		X		X	X		1) $F4/80^+/\alpha\text{-}SMA^+$ 2) GFP+/F4/80 +/α-SMA+	Immunofluorescence, flow cytometry, α-SMA/collagen expression	β-catenin, TCF, Foxo1	Yang et al. (2019)[47]
		X		X	X		1) $CD206^+/CD45^+$ 2) $CD206^+/\alpha\text{-}SMA^+$	Immunofluorescence, flow cytometry, α-SMA/collagen expression	Rac1	Liang et al. (2018)[48]
		X		X	X		CD68+/α-SMA+	Immunofluorescence, flow cytometry, cell morphology, α-SMA/collagen expression	Src, Smad3	Tang et al. (2018)[49]
			X	X			$CD68^+/\alpha\text{-}SMA^+$	Immunofluorescence, flow cytometry, α-SMA/collagen expression	N/A	Meng et al. (2016)[50]
				X	X		$GFP^+/F4/80^+/\alpha\text{-}SMA^+$	Immunofluorescence, flow cytometry, α-SMA/collagen expression	TGF-β, Smad3	Wang et al. (2016)[51]

Table 1: To systematically identify the scientific literature providing plausible evidence for MMT, the following PubMed search string was established: '(monocyte/fibroblast transition) OR (monocyte/myofibroblast transition) OR (monocyte-fibroblast transition) OR (macrophage-fibroblast transition) OR (macrophage-myofibroblast transition) OR (fibrocyte-fibroblast transition) OR (MMT AND fibroblast AND macrophage)'. The publication date was filtered from 2014 to 2021. This yielded a total of 41 results. The search was last updated on 5 February 2021. Primary research articles in the English language that included evidence of direct MMT through co-expression of monocyte/macrophage and fibroblast/myofibroblast markers were included. Manuscripts that did not demonstrate a direct link to MMT, including studies showing cells indirectly required for fibroblast differentiation, were excluded. All articles were screened by at least two independent reviewers. Based on the selection criteria, a total of 13 studies (out of 41) were included in this review. Abbreviations: CD, cluster of differentiation; COL1A1, collagen type 1 alpha 1; ECM, extracellular matrix; FAP, fibroblast activation protein; FSP1, fibroblast specific protein 1; GFP, green fluorescence protein; PDAC, pancreatic ductal adenocarcinoma; RAAS, renin-angiotensin-aldosterone system; TGF-β, transforming growth factor beta; YFP, yellow fluorescent protein; α-SMA, alpha-smooth muscle actin.

REFERENCES

1. Gabbiani G, Ryan GB, Majno G. Presence of modified fibroblasts in granulation tissue and their possible role in wound contraction. Experientia. 1971;27(5):549-550
2. Naiel S, Tat V, Padwal M, et al. Protein misfolding and ER stress in chronic lung disease: will cell-specific targeting be the key to the cure? Chest. 2020;157(5):1207-1220.
3. Hinz B, Phan SH, Thannickal VJ, Galli A, Bochaton-Piallat M-L, Gabbiani G. The myofibroblast: one function, multiple origins. Am J Pathol. 2007;170(6):1807-18164.
4. LeBleu VS, Taduri G, O'Connell J, et al. Origin and function of myofibroblasts in kidney fibrosis. Nat Med. 2013;19(8):1047-1053.
5. Masterson R, Hewitson TD, Kelynack K, et al. Relaxin down-regulates renal fibroblast function and promotes matrix remodelling in vitro. Nephrol Dial Transplant. 2004;19(3):544-552.
6. Tomasek JJ, Gabbiani G, Hinz B, Chaponnier C, Brown RA. Myofibroblasts and mechano-regulation of connective tissue remodelling. Nat Rev Mol Cell Biol. 2002;3(5):349-363.
7. Hinz B. Myofibroblasts. Exp Eye Res. 2016;142:56-70.
8. Skalli O, Ropraz P, Trzeciak A, Benzonana G, Gillessen D, Gabbiani G. A monoclonal antibody against alpha-smooth muscle actin: a new probe for smooth muscle differentiation. J Cell Biol. 1986;103(6): 2787-2796.
9. Micallef L, Vedrenne N, Billet F, Coulomb B, Darby IA, Desmoulière A. The myofibroblast, multiple origins for major roles in normal and pathological tissue repair. Fibrogenesis Tissue Repair. 2012;5(1):S5.

10. Kalluri R, Weinberg RA. The basics of epithelial-mesenchymal transition. J Clin Invest. 2009;119(6):1420-1428.
11. Bucala R, Spiegel LA, Chesney J, Hogan M, Cerami A. Circulating fibrocytes define a new leukocyte subpopulation that mediates tissue repair. Mol Med. 1994;1(1):71-81.
12. Moeller A, Gilpin SE, Ask K, et al. Circulating fibrocytes are an indicator of poor prognosis in idiopathic pulmonary fibrosis. Am J Respir Crit Care Med. 2009;179(7):588-59413.
13. Mathai SK, Gulati M, Peng X, et al. Circulating monocytes from systemic sclerosis patients with interstitial lung disease show an enhanced Profibrotic phenotype. Lab Investig J Tech Methods Pathol. 2010;90(6):812-823.
14. Tang PM-K, Nikolic-Paterson DJ, Lan H-Y. Macrophages: versatile players in renal inflammation and fibrosis. Nat Rev Nephrol. 2019;15 (3):144-158.
15. Scott MKD, Quinn K, Li Q, et al. Increased monocyte count as a cellular biomarker for poor outcomes in fibrotic diseases: a retrospective, multicentre cohort study. Lancet Respir Med. 2019;7(6):497-508.
16. Teoh AKY, Jo HE, Chambers DC, et al. Blood monocyte counts as a potential prognostic marker for idiopathic pulmonary fibrosis: analysis from the Australian IPF registry. Eur Respir J. 2020;55(4):1901855.
17. Kreuter M, Lee JS, Tzouvelekis AE, et al. Monocyte count as a prognostic biomarker in patients with idiopathic pulmonary fibrosis (IPF): a retrospective, pooled analysis from ascend, capacity, and inspire. Paper presented at: D13 ILD PROGNOSIS AND BIOMARKERS II [Internet]. American Thoracic Society International Conference

Abstracts; 2020: A6207-A6207. https://www.atsjournals.org/doi/ abs/10.1164/ajrccm-conference.2020.201.1_MeetingAbstracts. A6207

18. Yang J, Zhang L, Yu C, Yang X-F, Wang H. Monocyte and macrophage differentiation: circulation inflammatory monocyte as biomarker for inflammatory diseases. Biomark Res. 2014;2:1.
19. Lopes-Coelho F, Silva F, Gouveia-Fernandes S, et al. Monocytes as endothelial progenitor cells (EPCs), another brick in the wall to disentangle tumor angiogenesis. Cell. 2020;9(1):107.
20. Coillard A, Segura E. In vivo differentiation of human monocytes. Front Immunol. 2019;10:1907. https://www.frontiersin.org/articles/ 10.3389/fimmu.2019.01907/full
21. Nikolic-Paterson DJ, Wang S, Lan HY. Macrophages promote renal fibrosis through direct and indirect mechanisms. Kidney Int Suppl. 2014;4(1):34-38.
22. Labat M, Bringuier A, Seebold-Choqueux C, et al. Cystic fibrosis: production of high levels of uromodulin-like protein by HLA-DR blood monocytes differentiating towards a fibroblastic phenotype. Biomed Pharmacother. 1991;45(9):387-401.
23. Kuwana M, Okazaki Y, Kodama H, et al. Human circulating CD14+ monocytes as a source of progenitors that exhibit mesenchymal cell differentiation. J Leukoc Biol. 2003;74(5):833-845.
24. Witherel CE, Abebayehu D, Barker TH, Spiller KL. Macrophage and fibroblast interactions in biomaterial-mediated fibrosis. Adv Healthc Mater. 2019;8(4):1801451.
25. Lynch MD, Watt FM. Fibroblast heterogeneity: implications for human disease. J Clin Invest. 2018;128(1):26-35.

26. Hannan RT, Peirce SM, Barker TH. Fibroblasts: diverse cells critical to biomaterials integration. ACS Biomater Sci Eng. 2018;4(4):1223-1232.

27. Yona S, Gordon S. From the reticuloendothelial to mononuclear phagocyte system - the unaccounted years. Front Immunol. 2015; 6:328.

28. Hume DA, Ross IL, Himes SR, Sasmono RT, Wells CA, Ravasi T. The mononuclear phagocyte system revisited. J Leukoc Biol. 2002;72(4): 621-627.

29. Hume DA. The mononuclear phagocyte system. Curr Opin Immunol. 2006;18(1):49-53.

30. Hume DA. Differentiation and heterogeneity in the mononuclear phagocyte system. Mucosal Immunol. 2008;1(6):432-441.

31. Ask K, Vierhout M, Dvorkin-Gheva A, Shi W. Mononuclear phagocytic system and fibrosis: back to the future? Eur Respir J. 2021;57(3): 2004466. https://erj-ersjournals-com.libaccess.lib.mcmaster.ca/ content/57/3/2004466

32. Tang PC-T, Zhang Y-Y, Chan MK-K, et al. The emerging role of innate immunity in chronic kidney diseases. Int J Mol Sci. 2020;21(11):4018.

33. Srivastava SP, Hedayat AF, Kanasaki K, Goodwin JE. microRNA crosstalk influences epithelial-to-mesenchymal, endothelial-to-mesenchymal, and macrophage-to-mesenchymal transitions in the kidney. Front Pharmacol. 2019;10:904.

34. An C, Jia L, Wen J, Wang Y. Targeting bone marrow-derived fibroblasts for renal fibrosis. In: Liu B-C, Lan H-Y, Lv L-L, eds. Renal Fibrosis: Mechanisms and Therapies. Advances in Experimental Medicine and Biology. Singapore: Springer; 2019:305-322. https://doi.org/10. 1007/978-981-13-8871-2_14

35. Meng X-M, Mak TS-K, Lan H-Y. Macrophages in renal fibrosis. In: Liu B-C, Lan H-Y, Lv L-L, eds. Renal Fibrosis: Mechanisms and Therapies. Advances in Experimental Medicine and Biology. Singapore: Springer; 2019:285-303. https://doi.org/10.1007/978-981-13- 8871-2_13

36. Yan J, Zhang Z, Jia L, Wang Y. Role of bone marrow-derived fibroblasts in renal fibrosis. Front Physiol. 2016;7:61.

37. Gressner OA, Gao C. Monitoring fibrogenic progression in the liver. Clin Chim Acta. 2014;433:111-122.

38. Miao H, Wu X-Q, Zhang D-D, et al. Deciphering the cellular mechanisms underlying fibrosis-associated diseases and therapeutic avenues. Pharmacol Res. 2021;163:105316.

39. Yang F, Chang Y, Zhang C, et al. UUO induces lung fibrosis with macrophage-myofibroblast transition in rats. Int Immunopharmacol. 2021;93:107396.

40. Evans S, Butler JR, Mattila JT, Kirschner DE. Systems biology predicts that fibrosis in tuberculous granulomas may arise through macrophage-to-myofibroblast transformation. PLoS Comput Biol. 2020;16(12):e1008520.

41. Huang X, He C, Hua X, et al. Oxidative stress induces monocyte-tomyofibroblast transdifferentiation through p38 in pancreatic ductal adenocarcinoma. Clin Transl Med. 2020;10(2):e41.

42. Haider N, Bosca L, Zandbergen HR, et al. Transition of macrophages to fibroblast-like cells in healing myocardial infarction. J Am Coll Cardiol. 2019;74(25):3124-3135.

43. Torres A, Muñoz K, Nahuelp an YR, et al. Intraglomerular monocyte/macrophage infiltration and macrophage–myofibroblast transition during diabetic nephropathy is regulated by the A2B adenosine receptor. Cells. 2020;9(4):1051.

44. Wang Y-Y, Jiang H, Pan J, et al. Macrophage-to-myofibroblast transition contributes to interstitial fibrosis in chronic renal allograft injury. J Am Soc Nephrol. 2017;28(7):2053-2067.

45. Feng Y, Guo F, Mai H, et al. Pterostilbene, a bioactive component of blueberries, alleviates renal interstitial fibrosis by inhibiting macrophage-myofibroblast transition. Am J Chin Med. 2020;48(07): 1715-1729.

46. Tang PM-K, Zhang Y, Xiao J, et al. Neural transcription factor Pou4f1 promotes renal fibrosis via macrophage–myofibroblast transition. Proc Natl Acad Sci. 2020;117(34):20741-20752.

47. Yang Y, Feng X, Liu X, et al. Fate alteration of bone marrow-derived macrophages ameliorates kidney fibrosis in murine model of unilateral ureteral obstruction. Nephrol Dial Transplant. 2019;34(10):1657- 1668.

48. Liang H, Huang J, Huang Q, Xie YC, Liu HZ, Wang H. bing. Pharmacological inhibition of Rac1 exerts a protective role in ischemia/reperfusion-induced renal fibrosis. Biochem Biophys res Commun. 2018;503(4):2517-2523.

49. Tang PM-K, Zhou S, Li C-J, et al. The proto-oncogene tyrosine protein kinase Src is essential for macrophage-myofibroblast transition during renal scarring. Kidney Int. 2018;93(1):173-187.

50. Meng X-M, Wang S, Huang X-R, et al. Inflammatory macrophages can transdifferentiate into myofibroblasts during renal fibrosis. Cell Death Dis. 2016;7(12):e2495.

51. Wang S, Meng X-M, Ng Y-Y, et al. TGF-β/Smad3 signalling regulates the transition of bone marrow-derived macrophages into myofibroblasts during tissue fibrosis. Oncotarget. 2016;7(8):8809- 8822.

52. Campanholle G, Ligresti G, Gharib SA, Duffield JS. Cellular mechanisms of tissue fibrosis. 3. Novel mechanisms of kidney fibrosis. Am J Physiol - Cell Physiol. 2013;304(7):C591-C603.

53. Moore MW, Herzog EL. Regulation and relevance of myofibroblast responses in idiopathic pulmonary fibrosis. Curr Pathobiol Rep. 2013;1 (3):199-208.

54. Zhou Y, Peng H, Sun H, et al. Chitinase 3-like 1 suppresses injury and promotes fibroproliferative responses in mammalian lung fibrosis. Sci Transl Med. 2014;6(240):240ra76.

55. Gibbons MA, MacKinnon AC, Ramachandran P, et al. Ly6Chi monocytes direct alternatively activated profibrotic macrophage regulation of lung fibrosis. Am J Respir Crit Care Med. 2011;184(5):569-581.

56. Aziz A, Vanhille L, Mohideen P, et al. Development of macrophages with altered Actin organization in the absence of MafB. Mol Cell Biol. 2006;26(18):6808-6818.

57. Liu T-M, Wang H, Zhang D-N, Zhu G-Z. Transcription factor MafB suppresses type I interferon production by CD14+ monocytes in patients with chronic hepatitis C. Front Microbiol. 2019;10:1814. https://www.ncbi.nlm.nih.gov/pmc/articles/PMC6692491/

58. Moriguchi T, Hamada M, Morito N, et al. MafB is essential for renal development and F4/80 expression in macrophages. Mol Cell Biol. 2006;26(15):5715-5727.

59. Butler A, Hoffman P, Smibert P, Papalexi E, Satija R. Integrating single-cell transcriptomic data across different conditions, technologies, and species. Nat Biotechnol. 2018;36(5):411-420.

60. Tat V, Ayaub EA, Ayoub A, et al. FK506-binding protein 13 expression is upregulated in interstitial lung disease and correlated with clinical severity. A potentially protective role. Am J Respir Cell Mol Biol. 2020; 64(2):235-246.

61. Warsinske HC, DiFazio RM, Linderman JJ, Flynn JL, Kirschner DE. Identifying mechanisms driving formation of granuloma-associated fibrosis during Mycobacterium tuberculosis infection. J Theor Biol. 2017;429:1-17.

62. Czubryt MP. Cardiac fibroblast to myofibroblast phenotype conversion— an unexploited therapeutic target. J Cardiovasc Dev Dis. 2019;6(3):28. https://www.ncbi.nlm.nih.gov/pmc/articles/PMC6787657/

63. Ma Z-G, Yuan Y-P, Wu H-M, Zhang X, Tang Q-Z. Cardiac fibrosis: new insights into the pathogenesis. Int J Biol Sci. 2018;14(12):1645-1657.

64. Flanders KC. Smad3 as a mediator of the fibrotic response. Int J Exp Pathol. 2004;85(2):47-64.

65. Meng X-M, Tang PM-K, Li J, Lan HY. TGF-β/Smad signaling in renal fibrosis. Front Physiol. 2015;6:82. https://www.frontiersin.org/ articles/10.3389/fphys.2015.00082/full

66. Gauldie J, Kolb M, Ask K, Martin G, Bonniaud P, Warburton D. Smad3 signaling involved in pulmonary fibrosis and emphysema. Proc Am Thorac Soc. 2006;3(8):696-702.

67. Cao H, Wang C, Chen X, et al. Inhibition of Wnt/β-catenin signaling suppresses myofibroblast differentiation of lung resident mesenchymal stem cells and pulmonary fibrosis. Sci Rep. 2018;8(1):13644.

68. Roa H, Gajardo C, Troncoso E, et al. Adenosine mediates transforming growth factor-beta 1 release in kidney glomeruli of diabetic rats. FEBS Lett. 2009;583(19):3192-3198.

69. Xie T, Li G, Yang H, Wang X, Li J, Zhang W. Abstract 17075: inhibition of adenosine A2B receptor ameliorates renal fibrosis by regulating macrophage infiltration and polarization. Circulation. 2017;136 (suppl_1):A17075.

70. Cardenas A, Toledo C, Oyarzún C, et al. Adenosine a 2B receptormediated VEGF induction promotes diabetic glomerulopathy. Lab Invest. 2013;93(1):135-144.

71. Singh KP, Zerbato JM, Zhao W, et al. Intrahepatic CXCL10 is strongly associated with liver fibrosis in HIV-hepatitis B co-infection. PLoS Pathog. 2020;16(9):e1008744.

72. Tager AM, Kradin RL, LaCamera P, et al. Inhibition of pulmonary fibrosis by the chemokine IP-10/CXCL10. Am J Respir Cell Mol Biol. 2004;31(4):395-404.

73. Roman J, Mutsaers SE. Epigenetic control of CXCL10: regulating the counterregulator in idiopathic pulmonary fibrosis. Am J Respir Cell Mol Biol. 2018;58(4):419-420.

74. Choi SS, Sicklick JK, Ma Q, et al. Sustained activation of Rac1 in hepatic stellate cells promotes liver injury and fibrosis in mice. Hepatol Baltim Md. 2006;44(5):1267-1277.

75. Shi-wen X, Liu S, Eastwood M, et al. Rac inhibition reverses the phenotype of fibrotic fibroblasts. PLoS One. 2009;4(10):e7438.

76. Lieber GB, Fernandez X, Mingo GG, et al. Mineralocorticoid receptor antagonists attenuate pulmonary inflammation and bleomycin-evoked fibrosis in rodent models. Eur J Pharmacol. 2013;718(1):290-298.

77. Cao M-H, Xu J, Cai H-D, et al. p38 MAPK inhibition alleviates experimental acute pancreatitis in mice. Hepatobiliary Pancreat Dis Int. 2015;14(1):101-106.

78. Stambe C, Atkins RC, Tesch GH, Masaki T, Schreiner GF, NikolicPaterson DJ. The role of p38α mitogen-activated protein kinase activation in renal fibrosis. J Am Soc Nephrol. 2004;15(2):370-379.

79. Kanno Y, Shu E, Niwa H, Kanoh H, Seishima M. Alternatively activated macrophages are associated with the α2AP production that occurs with the development of dermal fibrosis. Arthritis Res Ther. 2020;22(1):76.

80. Lavin Y, Winter D, Blecher-Gonen R, et al. Tissue-resident macrophage enhancer landscapes are shaped by the local microenvironment. Cell. 2014;159(6):1312-1326.

81. Gordon S, Taylor PR. Monocyte and macrophage heterogeneity. Nat Rev Immunol. 2005;5(12):953-964.

82. Buchacher T, Ohradanova-Repic A, Stockinger H, Fischer MB, Weber V. M2 polarization of human macrophages favors survival of the intracellular pathogen chlamydia pneumoniae. PLoS One. 2015;10 (11):e0143593.

83. Gao J, Scheenstra MR, van Dijk A, Veldhuizen EJA, Haagsman HP. A new and efficient culture method for porcine bone marrow-derived M1- and M2-polarized macrophages. Vet Immunol Immunopathol. 2018;200:7-15.

84. Zhang L, Wang Y, Wu G, Xiong W, Gu W, Wang C-Y. Macrophages: friend or foe in idiopathic pulmonary fibrosis? Respir res. 2018;19 (1):170.

85. Linnarsson S, Teichmann SA. Single-cell genomics: coming of age. Genome Biol. 2016;17(1):97.

86. Trapnell C, Cacchiarelli D, Grimsby J, et al. Pseudo-temporal ordering of individual cells reveals dynamics and regulators of cell fate decisions. Nat Biotechnol. 2014;32(4):381-386.

87. La Manno G, Soldatov R, Zeisel A, et al. RNA velocity of single cells. Nature. 2018;560(7719):494-498.

88. Bowling S, Sritharan D, Osorio FG, et al. An engineered CRISPR-Cas9 mouse line for simultaneous readout of lineage histories and gene expression profiles in single cells. Cell. 2020;181(6):1410-1422.e27.

CHAPTER 3

A NOVEL *EX VIVO* APPROACH FOR INVESTIGATING PROFIBROTIC MACROPHAGE POLARIZATION USING PRECISION-CUT LUNG SLICES

Megan Vierhout, Anmar Ayoub, Pareesa Ali, Vaishnavi Kumaran, Safaa Naiel, Takuma Issihki, Joshua F. Koenig, Martin R.J, Kolb, and Kjetil Ask

IPF is a fatal form of ILD with an uncompromising disease course and relatively short survival time. Given the limited availability of antifibrotic treatment options, there is a critical need to implement novel approaches to investigate emerging experimental treatments and disease mechanisms. Macrophages have been shown to have key implications in wound healing and fibrosis. They are remarkably interactive cells with a strong phenotypic plasticity, and swiftly adapt to their surrounding microenvironment. Thus, to maximize translation of research to lung disease, there is a need to study macrophages in multifaceted, complex systems that are representative of the lung. In this chapter, we establish a novel approach to study profibrotic macrophage polarization using PCLS. As PCLS are living tissue preparations derived from the lung that are cultured *ex vivo,* the limitations of artificially recreating the lung architecture and recapitulating the sophisticated milieu are overcome. We developed and validated a moderate-throughput, biologically-translational, viable model to study profibrotic programming of macrophages Using a polarization cocktail (PC), consisting of IL-4, IL-13, and IL-6, we show that multiple markers of macrophage profibrotic polarization, including Arginase-1, CD206, YM1, and CCL17, were induced in PCLS. Through tissue microarray-based histological assessments, we directly visualized and quantified Arginase-1 and CD206 staining in PCLS in a moderate-throughput manner. To further examine these cells and delineate phenotype of polarized macrophages, we using high-plex immunolabelling with the Iterative Bleaching Extends Multiplexity (IBEX) method, and showed that the PC effects both interstitial and alveolar macrophages. Substantiating the profibrotic properties of the system, we also showed expression of extracellular matrix components and fibrotic markers in stimulated PCLS. Finally, we demonstrated that clodronate treatment diminishes the PC effects on profibrotic macrophage readouts, supporting the specific contribution of macrophages to the profibrotic attributes observed in our PCLS. Overall, our findings support a suitable complex model for studying *ex vivo* profibrotic macrophage programming in the lung, with future capacity for investigating experimental therapeutic candidates and disease mechanisms in pulmonary fibrosis.

Author Contributions:
MV: methodology, formal analysis, investigation, writing – original draft, writing – review & editing, visualization; **AA**: methodology, investigation, writing – review & editing; **PA:** methodology, investigation, writing – review & editing; **VK:** methodology, writing – review & editing; **SN:** methodology, writing – review & editing; **TI:** methodology, writing – review & editing; **JK:** methodology, resources, writing – review & editing**; MK:** project administration, resources, supervision, writing – review & editing, funding acquisition;

KA: conceptualization, resources, supervision, writing – review & editing, project administration, funding acquisition
Submitted to *Biochemical and Biophysical Research Communications* (2024)
Uploaded as a preprint to bioRxiv (2024)

Citation: A Novel Ex Vivo Approach for Investigating Profibrotic Macrophage Polarization Using Murine Precision-Cut Lung Slices
Megan Vierhout, Anmar Ayoub, Pareesa Ali, Vaishnavi Kumaran, Safaa Naiel, Takuma Isshiki, Joshua FE Koenig, Martin RJ Kolb, Kjetil Ask
bioRxiv 2024.07.05.602278; doi: https://doi.org/10.1101/2024.07.05.602278

A Novel *Ex Vivo* Approach for Investigating Profibrotic Macrophage Polarization Using Murine Precision-Cut Lung Slices

Megan Vierhout[a,b], Anmar Ayoub[a,b], Pareesa Ali[a,b], Vaishnavi Kumaran[a,b], Safaa Naiel[a,b], Takuma Isshiki[a,b,c], Joshua F. Koenig[c,d], Martin R.J. Kolb[a,b], Kjetil Ask[a,b]

[a]Firestone Institute for Respiratory Health, Department of Medicine, McMaster University and The Research Institute of St. Joe's Hamilton, 50 Charlton Avenue East, Hamilton, Ontario, Canada L8N 4A6

[b]McMaster Immunology Research Centre, Department of Medicine, McMaster University, 1280 Main Street West, Hamilton, Ontario, Canada L8S 4L8

[c]Department of Respiratory Medicine, Toho University School of Medicine, 6-11-1 Omorinishi, Ota-ku, Tokyo, Japan 143-8540

[d]Schroeder Allergy and Immunology Research Institute, Faculty of Health Sciences, McMaster University, 1280 Main Street West, Hamilton, Ontario, Canada L8S 4L8

Corresponding Author: Dr. Kjetil Ask. Email: askkj@mcmaster.ca. Phone: +1 (905) 522-1155 ext. 33683

ABSTRACT

Idiopathic pulmonary fibrosis (IPF) is fatal interstitial lung disease characterized by excessive scarring of the lung tissue and declining respiratory function. Given its short prognosis and limited treatment options, novel strategies to investigate emerging experimental treatments are urgently needed. Macrophages, as the most abundant immune cell in the lung, have key implications in wound healing and lung fibrosis. However, they are highly plastic and adaptive to their surrounding microenvironment, and thus to maximize translation of research to lung disease, there is a need to study macrophages in multifaceted, complex systems that are representative of the lung. Precision-cut lung slices (PCLS) are living tissue preparations derived from the lung that are cultured *ex vivo,* which bypass the need for artificial recapitulation of the lung milieu and architecture. Our objective was to establish and validate a moderate-throughput, biologically-translational, viable model to study profibrotic polarization of macrophages in the lung using murine PCLS. To achieve this, we used a polarization cocktail (PC), consisting of IL-4, IL-13, and IL-6, over a 72-hour time course. We first demonstrated no adverse effects of the PC on PCLS viability and architecture. Next, we showed that multiple markers of macrophage profibrotic polarization, including Arginase-1, CD206, YM1, and CCL17 were induced in PCLS following PC treatment. Through tissue microarray-based histological assessments, we directly visualized and quantified Arginase-1 and CD206 staining in PCLS in a moderate-throughput manner. We further delineated phenotype of polarized macrophages, and using high-plex immunolabelling with the Iterative Bleaching Extends Multiplexity (IBEX) method, showed that the PC effects both interstitial and alveolar macrophages.

Substantiating the profibrotic properties of the system, we also showed expression of extracellular matrix components and fibrotic markers in stimulated PCLS. Finally, we demonstrated that clodronate treatment diminishes the PC effects on profibrotic macrophage readouts. Overall, our findings support a suitable complex model for studying ex vivo profibrotic macrophage programming in the lung, with future capacity for investigating experimental therapeutic candidates and disease mechanisms in pulmonary fibrosis.

Keywords: pulmonary fibrosis, macrophages, precision-cut lung slices, macrophage programming, profibrotic polarization, *ex vivo*

Graphical Abstract

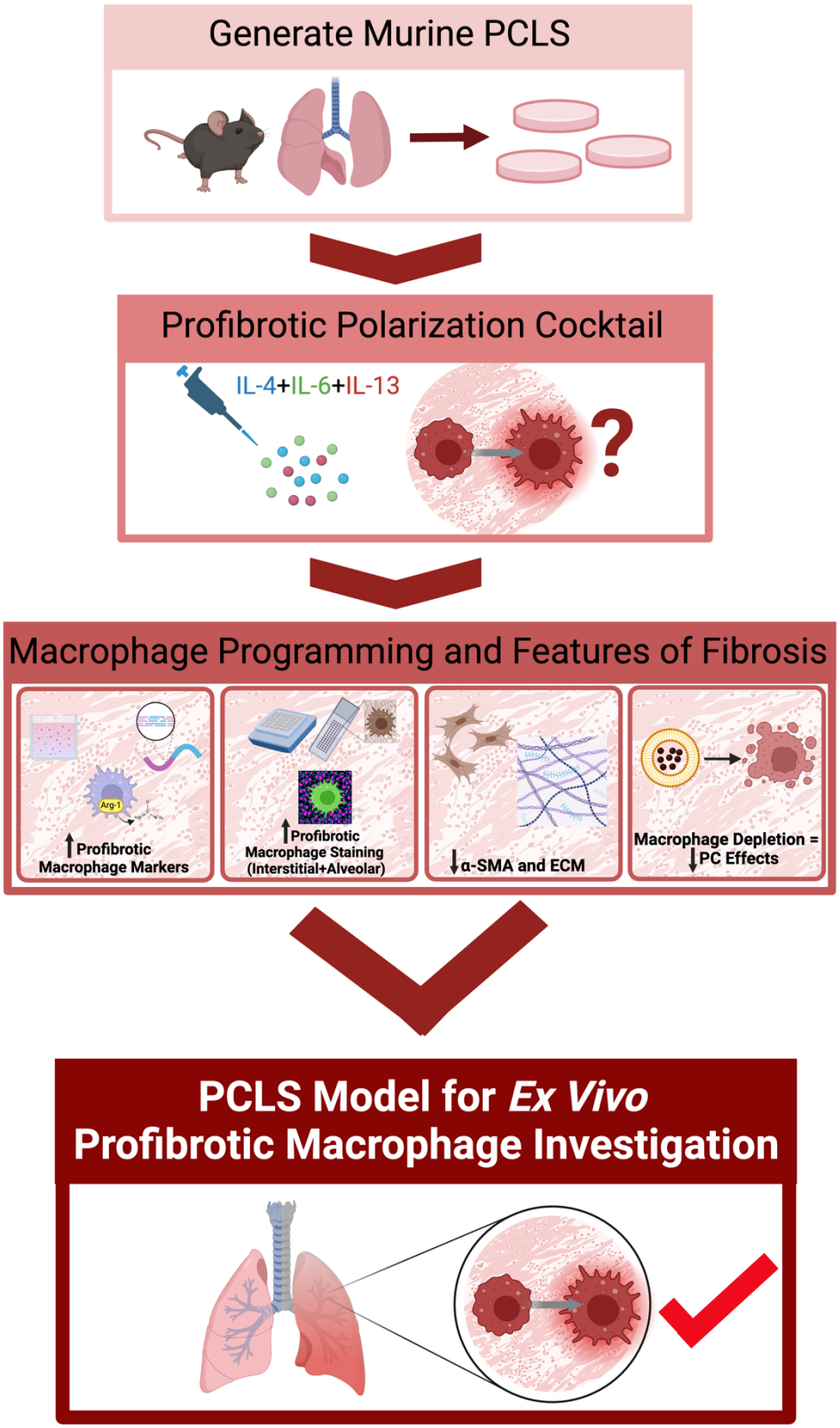

INTRODUCTION

Fibrotic interstitial lung diseases (ILD) are a group of debilitating disorders characterized by excessive scarring of the lung tissue and declining respiratory function. Idiopathic pulmonary fibrosis (IPF) is one of the most common ILD subtypes, for which the cause remains unclear and prognosis is relatively short, with patients surviving a median of 3 to 5 years after diagnosis [1]. There are only two approved antifibrotic therapies for IPF, nintedanib and pirfenidone. Despite slowing the progression of disease, neither are curative or reverse fibrosis [2,3]. Given the poor prognosis and limited treatment options for fibrotic lung disease, investigation is urgently needed to delineate pathogenesis, as well as to develop novel approaches to rapidly screen emerging experimental treatments and their respective effects on the lung microenvironment.

Macrophages, the most abundant immune cells in the lung, have vital implications in mediating the pathology of lung fibrosis [4,5]. Specifically, there is evidence supporting the contribution of profibrotic alternatively activated macrophages to aberrant wound healing [6–9], rendering these cells and their programming critical targets of interest in the context of lung fibrosis. Notably, macrophages are incredibly plastic cells with a dynamic phenotypic spectrum. They are highly interactive and swiftly adapt to their surrounding microenvironment, participating in a complex crosstalk of multifaceted signalling [9]. As such, evaluation of macrophages and their programming *in vitro*, although favoured for throughput and speed in preclinical screening studies, is limited for modelling authentic macrophage behaviour in the lung and fibrotic milieu. Therefore, to maximize translation

to disease, there is a need to study macrophages in an environment that better represents the lung.

Precision cut lung slices (PCLS) are living tissue preparations derived from the lung that are cultured *ex vivo*. Historically, PCLS were used for pulmonary airway studies, mainly focusing on smooth muscle and airway epithelial cells [10,11]. More recently, research involving PCLS has become increasingly popular for the study of numerous cellular mechanisms, fibrosis, infection, inflammation, senescence, disease-relevant stimuli, and experimental treatments [12]. A primary advantage of the PCLS system is that slices contain all resident cells of the lung and maintain intercellular interactions and cell-to-matrix relationships which are not found in traditional two-dimensional cell culture or three-dimensional organoid systems [13]. Conventional systems face limitations related to physiologically accurate lung cell and extracellular matrix (ECM) localization patterns, which are overcome in PCLS as lung structures do not need to be artificially recapitulated [14]. The nature of the PCLS model is also less time- and resource-intensive than *in vivo* disease models, and in honouring the 3 Rs of Replacement, Reduction, and Refinement, markedly decreases the number of animals needed for experiments [15]. As numerous slices can be obtained from lungs of various mammals, PCLS have been leveraged for their high-throughput potential, especially for screening compounds [16–19]. Thus, there is a need to develop readouts that are also throughput-conducive to best maximize the potential of this platform.

Recent single-cell RNA sequencing (scRNAseq) studies have demonstrated the preservation of immune cells in PCLS [20], including proliferating macrophages, alveolar

macrophages, and monocyte-derived macrophages. Despite being disconnected from the influence of the circulating immune system and thus incoming monocyte infiltration, Blomberg et al. (2023) have recently exhibited proliferative capacity of macrophages in their murine PCLS model of pre-cancer malignancy [21]. Additionally, Alsafadi et al. (2017) [22] successfully induced multiple fibrotic changes in human PCLS using a fibrotic cocktail (FC). Using this FC, Lang et al. (2023) recently showed induction of fibrosis-related marker genes in human PCLS, which were similar to a signature observed in macrophages from pulmonary fibrosis patients [23]. Overall, this evidence offers the suggestion that PCLS may constitute a suitable medium for the study of macrophage programming in the lung, and further investigation is needed to study profibrotic polarization and modes to measure this.

Our group has previously demonstrated that the addition of IL-6 to the traditional alternative programming cocktail of IL-4 and IL-13 effectuated a hyperpolarized profibrotic phenotype in murine and human macrophages *in vitro* [24]. Therefore, we postulated that the profibrotic effects of this cocktail could be applied in an appropriate *ex vivo* system, potentially contributing to the development of a novel translational model for studying pulmonary profibrotic macrophages. Here, we evaluate the potential of employing this cocktail to establish and validate a moderate-throughput, complex, viable model to study profibrotic polarization of macrophages in the lung using PCLS. We demonstrate that treatment with IL-4+IL-13+IL-6, referred to as the polarization cocktail (PC), effectively induces profibrotic programming of *ex vivo* macrophages in murine PCLS over a 72-hour time course study. We implement the use of multiple readouts, with a focus on establishing

throughput of the model, especially through quantitative histological readouts using tissue microarray-based approaches. Substantiating the profibrotic properties of the system, we also show expression of ECM and fibrotic markers in PCLS following PC treatment. Finally, we demonstrate that clodronate treatment diminishes the effects of the PC on profibrotic macrophage readouts.

METHODS

Animal Utilization

All work involving animals was approved by the McMaster University Animal Research Ethics Board (Animal Utilization Protocol #23-19) and was conducted in accordance with the Canadian Council on Animal Care guidelines. Wildtype female C57BL6/J mice (The Jackson Laboratory) aged 8–12 weeks were housed in pathogen-free conditions at the McMaster University Central Animal Facility. Mice were kept on a 12-hour light/12-hour dark cycle and provided access to water and food *ad libitum*.

PCLS Generation and Culture

Animals were anesthetized with isoflurane and exsanguinated by severing the inferior vena cava. After sacrifice, the lungs were perfused by injecting 5mL of warm PBS into the right ventricle of the heart to flush out residual blood. The trachea was cannulated and 1.3mL of 40°C 1.5% low-melting point agarose (Invitrogen) dissolved in Hanks' Balanced Salt Solution (HBSS) was slowly infiltrated into the lungs via the cannula, followed by a 0.2mL bolus of air to ensure agarose reached the lower airways. During lung inflation, mice were kept on a heating pad to maintain a warm temperature to prevent premature gelling of agarose. After inflation, mouse bodies were transferred onto ice and left to cool for 30

minutes to ensure complete gelling of agarose prior to excision of lungs. Lungs were then carefully excised, and lobes were separated. Each lobe was then affixed to a specimen holder, externally embedded in 2% agarose, and individually sliced (500µm thickness) in HBSS using a Compresstome VF-510-0Z vibrating microtome (Precisionary Instruments; speed setting: 1.5, oscillation setting: 9). PCLS cores (2mm or 4mm diameter) were obtained from full slices using a tissue puncher. **Figure 1** depicts a schematic of experimental overview for the study.

After slicing, PCLS were cultivated in DMEM culture medium supplemented with 10% fetal bovine serum, 2 mM L-Glutamine, 100 U/mL penicillin, 100 µg/mL streptomycin, and 2.5 µg/mL amphotericin B at 37°C, 5% CO_2. Medium was changed 3 times and PCLS were left in the incubator overnight to acclimate prior to treatment. At the time of treatment, PCLS were moved to 96-well plates and treated with a polarization cocktail (PC) consisting of recombinant IL-4 (40 ng/mL), IL-6 (10 ng/mL), and IL-13 (100 ng/mL; PeproTech), or a control cocktail (CC) consisting of only medium and diluent. We have previously shown that this triple cytokine combination stimulates profibrotic hyperpolarization of macrophages *in vitro* [24], however for *ex vivo* purposes we increased concentrations (while maintaining the same component ratios). Samples were harvested at 24-hour intervals over a 72-hour time course. For clodronate experiments, PCLS were subjected to a 24-hour pre-treatment period with liposomal clodronate (10-3000µM; Encapsula NanoSciences), followed by CC or PC treatment for 48 hours.

Water-Soluble Tetrazolium-1 (WST-1) Assay

PCLS (4mm diameter) were incubated (37°C, 5% CO_2) with 10µL of WST-1 reagent (Roche) in 100µL of culture media for 1 hour. After incubation, supernatant was transferred to a fresh 96-well plate and absorbance was measured at 450nm using a plate reader.

Tissue Microarray Generation and Brightfield Histology

PCLS (2mm diameter) were fixed in 10% neutral-buffered formalin for 24 hours and then transferred to 70% ethanol. Fixed tissues were embedded in paraffin. Tissue microarrays were generated from the formalin-fixed paraffin embedded (FFPE) PCLS with the TMA Master II (3D Histech Ltd), by taking 2mm punches (containing full PCLS) from the original blocks and inserting them in a host paraffin block. FFPE histology was conducted at the John Mayberry Histology Facility at the McMaster Immunology Research Centre. 5µM sections were cut using a microtome (Leica) and stained with hematoxylin and eosin (H&E) and immunohistochemical (IHC) stains for Arginase-1, CD206, and α-SMA. Antibody information can be found in **Supplementary Table 1.** IHC was completed using a Bond RX immunostainer (Leica). Full slides were digitized (20X brightfield) using an Olympus VS120 Slide Scanner (Evident Scientific) at the Firestone Molecular Imaging and Phenotyping Core Facility (MPIC). Histological quantification was performed using HALO image analysis software (version 3.5, Indica Labs). For Arginase-1, CD206, and H&E, the Multiplex IHC module was used. For α-SMA, airways and vessels were excluded and the Area Quantification module was used. To calculate Percentage of Positive Cells, total number of cells per PCLS tissue core (determined by nuclear detection with hematoxylin staining) and number of cells positive for the protein of interest in the PCLS tissue core (determined by DAB staining) were quantified. Number of stain-positive cells

was divided by number of total cells, and multiplied by 100% to obtain Percentage of Positive Cells. To calculate Percentage of Positive Area, total tissue area per PCLS tissue core (determined by optical density detection) and tissue area that was positive for the protein of interest in the PCLS tissue core (determined by DAB staining) were quantified. Positive tissue area was divided by total tissue area, and multiplied by 100% to obtain Percentage of Positive Tissue Area. To calculate H-Score, all cells in the tissue core were detected, and each cell was ranked (high, medium, low, negative) based on its average intensity of signal for protein of interest (DAB). H-Score was then quantified by accounting for the proportion and intensity of the signal ranking using the following equation: H-Score $= 100\frac{3H+2M+L}{H+M+L+N}$.

Iterative Bleaching Extends Multiplexity (IBEX) Fluorescent Histology

Multiplex staining of PCLS was achieved using IBEX, an open-source method for serial multi-marker immunolabelling [25,26]. PCLS (2mm diameter) were fixed in Cytofix/Cytoperm (BD Biosciences) diluted 1:4 in PBS, for 24 hours at 4°C. Tissue was then transferred to a 30% sucrose solution for cryoprotection for 48 hours at 4°C. Following fixation and cryoprotection, PCLS were embedded in optimal cutting temperature (OCT) compound and frozen using liquid nitrogen and isopentane. 12µM cryosections of fixed-frozen tissue were cut using a cryostat (Leica) and placed in chambered cover glasses. Tissues were incubated with the primary antibody staining solution overnight at 4°C. When needed, the secondary antibody staining solution was applied for 1 hour at 37°C. Antibody information can be found in **Supplementary Table 2.** After staining, Fluoromount-G mounting medium (Southern Biotech) was added. Multiplex imaging (20X fluorescent)

was performed using an inverted confocal microscope (Zeiss LSM 980) at the McMaster University Centre for Advanced Light Microscopy (CALM). Tile images of the entire tissue were captured using a Plan-Apochromat 20X objective (0.8 numerical aperture), with pixel dimensions of 0.124um x 0.124um and a pinhole size of 1 Airy unit. Following image acquisition, mounting medium was removed and fluorophores were bleached by applying a 1mg/mL solution of lithium borohydride (Sigma-Aldrich) for 15 minutes. Tissues were stained with the next round of antibodies and the procedure was repeated iteratively as described. For histological analysis, serial image rounds were merged in HALO image analysis software, using DAPI as the alignment fiducial channel. For α-SMA staining, airways and vessels were excluded to focus on parenchymal expression. Quantification was performed using the Highplex FL module. Total number of cells per PCLS tissue core (determined by nuclear detection with DAPI staining) and number of cells positive for the proteins of interest in the PCLS tissue core (multiple fluorophores) were quantified.

Arginase Activity Assay

PCLS (4mm diameter) were homogenized in lysis buffer (0.1% Triton-X supplemented with sodium orthovanadate, PMSF, DTT and bovine lung aprotinin) using a Bullet Blender Bead Homogenizer (Next Advance). Homogenates were then centrifuged at maximum speed to remove remaining insoluble debris, and the arginase activity assay was carried out as previously described [7]. Briefly, lysates were diluted with 25mM Tris-HCl to form a 1:1 mixture, from which 25µL was transferred to a 96-well PCR plate containing 2.5µL 10 mM manganese chloride per sample well. The plate was then incubated in a thermal cycler at 56°C for 10 minutes. 25µL of 0.5M L-arginine then added, followed by another

thermal cycler incubation at 37°C for 30 minutes. Urea standards, 200µL of sulfuric+phosphoric acid solution, and 10µL of 9% alpha-isonitrosopropiophenone were added to the plate. A final thermal cycler incubation was completed at 95°C for 30 minutes. After allowing the plate to cool for 5 minutes, 150µL from each well was transferred to a fresh 96-well flat bottom plate and absorbance was read at 550nm using a plate reader.

Enzyme Linked Immunosorbent Assay (ELISA)

YM1 and CCL17 protein levels were measured in PCLS (4mm diameter) supernatant using commercially available ELISA kits (R&D Systems), according to the manufacturer's protocol. Of note, CCL17 levels that were too low to be detected were assigned the lower limit of detection.

RNA Isolation and cDNA Synthesis

PCLS (4mm diameter) were snap frozen using liquid nitrogen and were stored at -80°C until extraction. PCLS RNA isolation protocol was adapted from previously published studies [27,28]. Six PCLS per condition were pooled and homogenized in TRIzol Reagent (Invitrogen) using a bead mill. Phase separation was completed with chloroform and gel density tubes (Qiagen). The aqueous phase was then collected and RNA was extracted using the RNeasy Fibrous Tissue Mini Kit (Qiagen). RNA was converted to cDNA via reverse transcription using qScript cDNA SuperMix (Quantabio) according to the manufacturer's instructions.

Quantitative Real-Time Polymerase Chain Reaction (PCR)

PCR was performed using the QuantStudio 3 system (Applied Biosystems), with Advanced qPCR Mastermix (Wisent) and ThermoFisher Scientific Predesigned TaqMan Gene

Expression Assay primer pairs (information found in **Supplementary Table 3**). Using *GAPDH* as the reference gene, relative expression was calculated as $2^{-\Delta CT}$.

Sircol Soluble Collagen Assay

The Sircol Soluble Collagen Assay 2.0 (Biocolor) was used to measure secreted soluble collagen in PCLS (4mm) supernatant, according to the manufacturer's instructions.

Statistical Analysis

Results were expressed as the mean ± standard error of the mean (SEM). Comparisons of two groups were performed with an unpaired two-tailed t test, while more than two groups were compared with ANOVA followed by Sidak's multiple comparisons test. Statistical analyses were performed using GraphPad Prism 10. A P value less than 0.05 was considered statistically significant.

RESULTS

Development of Optimized PCLS Experimental Workflow

In the development of our experimental workflow, our objective was to establish a robust moderate-throughput approach to lung macrophages in an *ex vivo* environment. To maximize our throughput capacity, as well as normalize the size of PCLS, we created punches (2mm or 4mm in diameter) from full-lobe slices using a handheld tissue coring tool. We found punching the cores post-slicing, as opposed to taking cores from pre-sliced lobes, allowed for better control over the uniformity of core size. **Figure 1A** contains a photographic depiction of the workflow for processing murine lungs for PCLS generation. We have also included a summary of potential technical issues faced during the slicing process and troubleshooting solutions in **Supplementary Table 4.** On average, from slicing all lobes of a murine lung we are able to obtain approximately 40 4mm PCLS or 70 2mm PCLS (500uM thickness) per mouse (taking approximately 1.5 to 2 hours from sacrifice to incubator). In developing means to increase throughput of our PCLS studies, we introduced a tissue microarray-based approach for FFPE histology (**Figure 1C**). While previous studies have performed fundamental histological assessments on PCLS, these analyses have generally been limited in throughput. Constructing tissue microarrays from PCLS allows us to achieve this and evaluate approximately 80 PCLS cores (2mm diameter) on a single slide and using a tissue thickness of 500uM maximizes the quantity of FFPE serial sections that can be used for histological staining. Additionally, extracting adequate amounts and quality of RNA from PCLS has been reported as a challenge due to limitations of small tissue mass and interference from agarose [27,29]. Using a modified protocol

derived from Stegmayr et al. (2020) [27] and Michalaki et al. (2022) [28], we isolated RNA using 6 pooled PCLS per condition (see Methods). For the purpose of gene expression readouts via PCR, we obtained adequate RNA quantity and quality, from both control and PC-treated samples (**Supplementary Figure 1**).

Murine Precision-Cut Lung Slices (PCLS) Remain Viable and Structurally Intact Throughout Culture Time course with Polarization Cocktail (PC) Treatment

First, to assess the utility and viability of our PCLS experimental system and treatment cocktail for subsequent macrophage polarization studies, we performed metabolic and histological evaluations at 24-hour intervals throughout the 72-hour culture period. Similar to previously published studies on human PCLS [22,30,31], we utilized the water-soluble tetrazolium (WST-1) assay and H&E histological staining to achieve this. Over the 72-hour time course in culture, PCLS maintained high viability and stable total cell numbers. Viability assessment of PCLS measured through mitochondrial activity using WST-1 assay (**Figure 2A**) demonstrated that CC- and PC-treated PCLS remained viable over 72 hours, and exhibited an increase in metabolic activity at the 48 and 72-hour timepoints, which may indicate tissue recovery after preparation [31]. Histological examination of H&E stained PCLS on an FFPE tissue microarray (**Figure 2B**), and quantification of cell number with HALO image analysis software (**Figure 2C**), confirmed that PCLS maintained structure and a consistent quantity of cells per total tissue area. No adverse effects from treatment with the PC were detected. Additionally, as our objective was to study and modulate macrophages in the PCLS system, we confirmed that macrophages persisted throughout the time course and were still present in the slices at the 72-hour timepoint, as also seen at

baseline (0-hour) (**Figure 2D**). Overall, this allowed us to verify the integrity and suitability of our experimental system and PC intervention for investigation of *ex vivo* macrophage polarization.

Treatment with the PC Induces Markers of Alternatively Activated Macrophages in PCLS Tissue and Supernatant

Next, we aimed to determine if the PC could polarize macrophages to an alternatively activated phenotype *ex vivo*, as we have previously shown in murine and human macrophages *in vitro* [24]. To investigate profibrotic macrophage polarization in the PCLS system, we began by measuring markers of profibrotic macrophages in the tissue (lysates) and soluble secretions (supernatant). Arginase-1, chitinase-3-like-protein-3 (YM1, gene name *Chil3*), CC chemokine ligand 17 (CC17), and cluster of differentiation 206 (CD206, gene name *MRC1*) are all established markers used to phenotype murine alternatively activated macrophages [32], which were found to be induced in PCLS with treatment of the PC (**Figure 3**). More specifically, arginase activity, determined by conversion of L-arginine to urea, was found to be increased in the lysates of PC-stimulated PCLS at all timepoints (24, 48, and 72 hours) during the time course, compared to CC-treated controls (**Figure 3A**). With regards to soluble markers, secreted YM1 and CC17 levels were increased with treatment of the PC at the 48 and 72-hour timepoints (**Figure 3B,C**), as measured by ELISA. At the gene expression level, treatment with PC led to increased gene expression of *Arg1*, *MRC1,* and *Chil3*, relative to *GAPDH*, at all timepoints throughout the time course (24, 48, and 72 hours; **Figure 3D-F**). Overall, these findings suggest the

successful polarization of profibrotic pulmonary macrophages in the *ex vivo* PCLS environment, as exhibited through various quantitative assays.

Histological Markers Characteristic of Profibrotic Macrophages are Increased Throughout Polarization Time course

Following the observations outlined in Figure 3, we proceeded to directly visualize polarized macrophages in the cocktail-treated PCLS tissue. We elevated the throughput capacity of our PCLS histological readouts through the construction of tissue microarrays containing numerous FFPE PCLS cores (see Methods), which could then be stained and analyzed on a single slide. To quantitatively assess alternatively activated macrophages throughout the time course, brightfield immunohistochemical (IHC) staining was performed on the tissue microarrays and whole-slide images were acquired. We observed that IHC staining for established alternatively activated macrophage markers, Arginase-1 and CD206, were increased with treatment of the PC (**Figure 4A,B**). Specifically, using HALO quantification we found that the percentage of positive cells, as well as staining intensity, assessed by HALO H-Score which accounts for marker staining strength and proportion, were increased at all time course intervals for both Arginase-1 (**Figure 4C**) and CD206 (**Figure 4D**). In terms of cellular localization, it was observed that Arginase-1 and CD206 positive macrophages exist in both the alveolar lumen and interstitium of PCLS **(Figure 4E).** Overall, these findings complement the results displayed in Figure 3 and visually confirm the presence of profibrotic macrophage polarization with PC treatment, as well as demonstrate the utility of a moderate-throughput histological approach for PCLS assessments.

PC Induces Polarization in Both Interstitial and Alveolar Macrophages, as Determined by Highly Multiplexed Staining (IBEX) to Assess Macrophage Phenotype

As the findings presented with traditional single-stain IHC established a foundation for characterizing the macrophages in the PC-stimulated PCLS, to better understand these cells we then sought to employ a high-content, multiplex imaging approach. Using Iterative Bleaching Extends Multiplexity (IBEX), an open-source method for serial multi-marker immunolabelling [25,26], we aimed to further investigate macrophage phenotype. Markers and antibodies used in our panel can be found in **Supplementary Table 2**. While Figure 4 conveys that Arginase-1 and CD206 IHC were increased in PCLS with treatment of the PC, and staining was present in cells that morphologically resemble macrophages, other cell types in the lung can also express these markers. To overcome the limitation of single-plex staining, we used IBEX to investigate macrophage-specific cells (defined as $CD45^{+}CD68^{+}CD11c^{+}$) in the PCLS. First, to substantiate our findings, we examined overall profibrotic polarization (characterized by Arginase-1+CD206 expression) in the macrophage population (defined as $CD45^{+}CD68^{+}CD11c^{+}Arg1^{+}CD206^{+}$ cells) (**Figure 5A**). $Arg1^{+}CD206^{+}$ macrophages were increased with PC treatment (48 hours), expressed as percentage of total cells in the PCLS (**Figure 5B**), as well as percentage of total macrophages (**Figure 5C**). Next, we aimed to evaluate if our PC could induce polarization in both interstitial (IM) and alveolar macrophages (AM), which are the two primary broad categories of macrophages found in the lung. In the context of lung fibrosis, both IM and AM are believed to play important roles in disease pathogenesis [33]. Delineating the exact contributions of IM and AM is a vital topic in the field under active investigation. Our

brightfield IHC assessments, shown in Figure 4E, portray that Arginase-1 and CD206 positive cells were present in both the interstitium and alveolar lumen in PCLS. However, it is unclear if PC treatment definitively increases quantity of macrophage-specific polarization in each of these compartments. Thus, we aimed to evaluate polarization in IM and AM using IBEX. Murine IM and AM have been historically stratified based on the presence of CD11b and SiglecF expression, respectively [34]. We therefore used these markers, in combination with the general macrophage and polarization markers used in Figure 5A-C, to examine profibrotic polarization in IM and AM (**Figure 5D,E**). We observed that PC treatment (48-hours) increased the number of $Arg1^{+}CD206^{+}$ IM, expressed as percent of total IM (**Figure 5F**), as well as $Arg1^{+}CD206^{+}$ AM, expressed as percent of total AM (**Figure 5G**). Collectively, these results support the accumulated evidence that the PC successfully induces profibrotic macrophage polarization in our PCLS system. Additionally, these profibrotic macrophages also demonstrate evidence for proliferation, as shown by Ki-67, Arginase-1, and CD206 serial section IHC (**Supplementary Figure 2**). This is aligned with the current understanding of profibrotic macrophages in the pathology of lung fibrosis, involving the processes of cellular accumulation, division, and activation [5,6].

Expression of Extracellular Matrix and Fibrotic Markers in PCLS Treated with PC

We have demonstrated the ability of the PC, consisting of IL-4, IL-13, and IL-6, to influence *ex vivo* macrophage polarization in PCLS. This is in alignment with *in vitro* studies that have shown the ability of these cytokines to hyperpolarize macrophages to the profibrotic phenotype [7,24]. Additionally, *in vivo* overexpression of IL-6 in the bleomycin

lung fibrosis model induced an exacerbation of the fibrotic response, increased frequency of lung $Arg1^{+}CD206^{+}$ macrophages, and increased gene expression of IL-4 receptor in these macrophages (thus likely rendering them more susceptible to polarization by IL-4 and IL-13), demonstrating critical interplay between these cytokines, macrophages, and fibrosis [7]. While our primary objective in this study was to establish an *ex vivo* model suitable for studying pulmonary profibrotic macrophage polarization, given the key role of macrophages in fibrogenesis we speculated that it would be logical to investigate features related to fibrosis in our system. Using IHC staining of FFPE tissue microarrays, we evaluated the expression of α-SMA in PCLS subjected to CC or PC treatment **(Figure 6A).** HALO quantification of parenchymal α-SMA staining, excluding major airways and vessels, revealed an increase in α-SMA positive area at 48 and 72 hours in the PC-stimulated PCLS (**Figure 6B**). In the culture supernatant, we observed an increase in secreted soluble collagen with PC treatment at the 72-hour timepoint, as measured with Sircol Soluble Collagen Assay (**Figure 6C**). Normalized gene expression of α-SMA (*ACTA2*), extracellular matrix (ECM) component fibronectin (*FN1*), and ECM glycoprotein tenascin-C (*TNC*) were elevated in PC-treated PCLS lysates at the 72-hour (*TNC*), or both the 48 and 72-hour (*ACTA2* and *FN1*) timepoints (**Figure 6D-F**). Of note, gene expression of these three markers (*ACTA2, FN1, TNC*) has also been shown to be increased in a published model of fibrosis in human PCLS [22]. Lastly, to better understand the phenotype $\alpha\text{-SMA}^{+}$ cells in the PCLS, we performed multiplex image analysis with IBEX. Our group has previously explored macrophage to myofibroblast transition (MMT), which is a debated scientific theory that myofibroblasts can arise from macrophage

populations. The majority of studies on MMT include evidence of cellular co-expression of both macrophage and myofibroblast markers, which we have shown in lung tissue from IPF patients [52]. Lineage-tracing studies have also demonstrated that labelled cells from the bone marrow are found as myofibroblasts in various fibrotic disorder models, including in the lung, kidney, and eye [51,56-57]. Therefore, we sought explore possible evidence for MMT in the profibrotic macrophage PCLS system. In PC-treated PCLS, the α-SMA$^+$ cell population in the parenchyma had increased co-expression of the marker profile of Arg1$^+$CD206$^+$ profibrotic macrophages (**Figure 6 G,H**). These results suggest that in addition to augmenting macrophage polarization, the PC may also have fibrosis-inducing properties in our experimental system. MMT processes may describe the increase in percentage of α-SMA$^+$ cells co-expressing markers of Arg1$^+$CD206$^+$ macrophages in our system, and serve as a potential source of α-SMA$^+$ cells.

Clodronate Treatment Diminishes Effects of PC on Profibrotic Macrophage Readouts

Finally, in order to substantiate the role of macrophages in the observed responses in the PCLS, we conducted a depletion study using liposomal clodronate. Clodronate is known for its ability to selectively deplete macrophages both *in vitro* and *in vivo* [35], and has been used in murine bleomycin studies to demonstrate that macrophages are required for lung fibrosis [36]. PCLS were pre-treated with liposomal clodronate for 24 hours, followed by 48 hours in culture with the CC or PC. Confirming clodronate-mediated depletion, macrophage quantity was decreased in PCLS, determined by counting visible alveolar macrophages in H&E stained tissue (**Figure 7A,B**). We next evaluated expression of profibrotic macrophage markers that are known to be induced by the PC. We observed that

clodronate pre-treatment diminished PC-induced arginase activity in a dose-dependent manner (**Figure 7C**). Similarly, secreted YM1 (**Figure 7D**) and CCL17 (**Figure 7E**) in PCLS supernatant exhibited a dose-dependent decrease. In IHC-stained FFPE PCLS, clodronate dose-dependent reductions in Arginase-1 (**Figure 7F,G**) and CD206 (**Figure 7H,I**) positive cells and staining intensity (H-Score) were identified. With regards to features related to fibrosis, we observed a reduction in soluble collagen with all doses of clodronate (**Figure 7J**). Additionally, there was a trend of reduction in α-SMA expression in the FFPE PCLS tissue (**Figure 7K,L**). Overall, our results suggest that macrophages have a key role in the profibrotic phenotype observed in our PCLS system.

DISCUSSION

Given the poor prognosis, debilitating symptoms, and gap in curative treatments for IPF, advancement of translational models and screening tools for preclinical therapies are especially critical. Macrophages are key regulators in tissue repair, however their plasticity and heterogeneity mean macrophage phenotypes are highly context-dependent, overall making the investigation of their precise contributions to disease challenging. In this study, we harness the potential benefits offered by the PCLS platform in establishing a novel strategy to investigate the profibrotic programming of lung macrophages, which have been demonstrated to be fundamental players in lung fibrosis [4–9]. In our model we have exhibited capacity for profibrotic macrophage programming with the treatment of a polarization cocktail, which is shown to be induced at multiple points throughout a 72-hour time course. This builds on the current literature revealing *ex vivo* immune competency in multiple PCLS disease models, including premalignancy, fibrosis, asthma, COPD, viral infection, bacterial infection, inflammation, and immunotoxicity [23,28,37–42]. Despite being disconnected from the circulating immune system, several studies have reported the presence and persistence of macrophages in PCLS. As demonstrated by Sompel et al. (2023), macrophages are the most abundant immune cell in murine PCLS [41]. Understandably, contribution to the lung macrophage population by incoming monocyte recruitment is absent in PCLS. Blomberg et al. (2023) have recently exhibited the capacity of macrophages to proliferate in a murine PCLS model of pre-cancer malignancy [21], which may contribute to the persistent presence of macrophages *ex vivo*. Additionally, scRNAseq analysis of cellular phenotype stability in PCLS demonstrated the preservation

of immune cells including proliferating macrophages, alveolar macrophages, and monocyte-derived macrophages, although alveolar macrophage quantity was reported to be decreased after 120 hours of culture [20]. In the context of fibrosis, using scRNAseq analyses on human PCLS treated with the fibrosis cocktail developed by Alsafadi et al. (2017), Lang et al. (2023) showed induction of expression of fibrosis-related marker genes shown in a population of macrophages found in pulmonary fibrosis patients [22,23]. Taken together, our findings and the published evidence support the use of PCLS as a valid platform to investigate macrophage polarization and programming in the lung.

Previous findings from our group and others have shown that *in vitro* stimulation of human and murine macrophages with a combination of IL-4, IL-13 and IL-6 resulted in enhanced profibrotic programming to a hyperpolarized phenotype [7,24,43]. In the current study, we aimed to investigate if repurposing this cytokine combination (here termed the PC) could achieve similar polarization effects in an *ex vivo* setting. Similar to the published results, we observed an increase in profibrotic macrophage markers evoked with the PC in our *ex vivo* system, including Arginase-1, CD206, YM1, CCL17, and arginase enzymatic activity [7,24,43]. To elicit profibrotic macrophage polarization, it is believed that the PC components work in synergy. IL-4 and IL-13 effectuate profibrotic macrophage polarization via IL-4 receptor alpha (IL-4Rα) signalling, and it has been shown that IL-6 upregulates IL-4Rα in macrophages *in vitro* [43,44], thus potentially increasing the propensity for polarization. It is plausible that similar processes are occurring with PC treatment *ex vivo*, however further investigations are required to delineate the molecular mechanism of action of profibrotic macrophage polarization in the PCLS.

Pulmonary macrophages are broadly categorized into IM and AM, which are both believed to participate in fibrogenic processes in lung fibrosis [9]. The delineation of their specific roles is a key topic of current investigation in the field, especially for IM which have been vastly understudied [33]. AM, residing in the lung alveoli, have been shown to alter tissue remodelling and interact with fibroblasts to enhance ECM synthesis [33,45]. IM, which are present in the lung interstitium, are less understood but are believed to be involved in initiation of fibrosis and partake in crosstalk with fibroblasts [33]. Circulating monocytes have been shown to contribute to the maintenance of both AM and IM, however both populations also demonstrate capacity for self-renewal [33]. In our PCLS model, we show the that the PC induces polarization in both IM and AM, thus demonstrating potential to be used as a tool to study these cells and their respective properties further. To target the specific role of IM in the relative absence of AM in future studies, AM could be largely washed out with repeated bronchoalveolar lavage fluid collection, prior to PCLS generation. Additionally, previous studies have shown retained functionality of these cells in PCLS, where IM were substantial antigen-uptaking cells of house dust mite extract *ex vivo* [46].

The primary objective for our study was to establish an *ex vivo* model for profibrotic macrophage programming in PCLS, using the PC. In addition to macrophage polarization, we interestingly observed other features related to fibrosis in our model, including ECM and α-SMA expression, particularly at later timepoints in the time course. The current paradigm of pathogenesis for pulmonary fibrosis is multifactorial and is believed to be initiated with insult to the lung epithelium. The resulting inflammatory response involves

recruitment of macrophages to the site of injury, which through a series of mediators eventually cascades into activation of fibroblasts and resulting ECM deposition, resulting in fibrosis [9]. One plausible explanation for the observed fibrotic characteristics in our model is that the slicing of the lungs to generate PCLS functions as an injury, which then activates an intrinsic wound healing response in the tissue. This has been suggested previously [47], and may also explain why we see increased expression of some markers in our control PCLS, including *FN1*, Arginase activity, and Arg-1 IHC, compared to baseline. Providing external cytokines through administration of the PC further exacerbates the macrophage response and involvement, thus resulting in the development of fibrosis-like features in the PCLS. Additionally, although shown to effect macrophages, the addition of the PC to PCLS culture does not solely target one cell type, and can influence a variety of cells. IL-4 and IL-13 have historically been shown to stimulate collagen synthesis in fibroblasts [48,49]. IL-4Rα signalling also plays a role in tissue remodelling, and has also been demonstrated to be essential for the development of lung fibrosis *in vivo* [50]. Thus, another potential explanation is direct modulation of fibroblasts by the PC, in addition to macrophages, cultivating fibrotic features. Furthermore, our group has previously shown that overexpression of IL-6 in a bleomycin-induced lung fibrosis model led to increased accumulation of profibrotic macrophages ($Arg1^{+}CD206^{+}$), as well as IL-4Rα expression, and worsened the fibrotic response [7]. This further supports the multifaceted interplay between the cytokines in the PC, polarized macrophages, and the fibrotic response.

Compared to traditional *in vitro* models, PCLS forgo the need for researcher-made recapitulation of the lung microenvironment, and present advantages of increased

complexity, preserved architecture, and resident cell milieu, which substantiate their translatability in the study of lung pathology [53]. The *ex vivo* system is also less demanding of resources and time relative to *in vivo* models of disease, supporting utility especially in early stages of compound testing. Our goal was to establish a translational platform to study macrophage behaviour in fibrotic systems, with moderate-throughput that could be used for a variety of readouts. We introduce an approach to expand the throughput of direct histological evaluation in organ slices by constructing tissue microarrays, which can house approximately 80 PCLS that can be stained, imaged, and analyzed on a single slide. In the era of exponentially growing interest in spatial biology, there is also reasonable potential capacity for these analyses in cultured organ slice systems, which can be performed with the use of high-content imaging pipelines such as IBEX and other established methodologies. Future assessments using comprehensive gene profiling, such as RNAseq or microarray analyses, are also achievable with the attained RNA quantity and quality from our system. Additionally, multiple PCLS studies, including in the fibrosis field, have utilized human tissue to model disease and investigate disease mechanisms. These studies are highly robust and representative of human biology, as they are derived directly from human tissue. However, working with fresh human tissue presents logistical limitations, including inconsistencies in agarose filling, variability in baseline tissue viability, amount of tissue available, and/or lack of access to human tissue altogether. Murine models are therefore convenient tools to bypass these limitations, and can be used in synergy with human models to conduct screening on preclinical mechanisms and experimental treatment candidates. Overall, given the current set-up of our system, we believe our approach has

potential for future expansion in several domains, including bleomycin pulmonary fibrosis models, PCLS generation from other species including humans, evaluation of pulmonary stretch and mechanotransduction, and testing of experimental treatments. The pipeline is scalable, and throughput could be increased further with the addition of multiple tissue slicers to simultaneously generate slices from multiple lobes, which is currently our time-limiting step.

The overarching objective for the further development of this work is maximizing the translatability of this approach for the study of disease. Several synergistic components are flow into this. Firstly, as the goal is to model human fibrotic lung disease, we aim evaluate and understand the expression of a panel of profibrotic macrophage markers found in IPF, including SPP1, MERTK, FABP4, FABP5, GPNMB, and CD63 [58,59]. As macrophages are a highly diverse and heterogenous cell type, it is important to gain a comprehensive understanding of the disease-relevant phenotypes that are being represented in models used to investigate disease processes. While we have already identified polarized alveolar and interstitial macrophage compartments in the PC-treated PCLS, further delineating macrophage subsets through the addition of a panel of disease-relevant markers would further advance the model. Adding to this repertoire, as pro-inflammatory signalling also plays a role in the pathogenesis of fibrosis, it would be advantageous to characterize the expression pattern of these mediators in our system as a stride towards the overarching goal of optimizing the disease-translational qualities of this model. Previous PCLS models of fibrosis have reported a mixed bag of induced characteristics, including profibrotic, inflammatory, and ECM-related factors, thus demonstrating the complexity of the fibrotic

milieu [22]. It would also be useful to directly compare the PC used in this study with other previously published studies that employed fibrosis-inducing cocktails. We have already drawn similarities between the PC model and established PCLS-based fibrosis models, including the published FC in human PCLS [22] and PCLS derived from bleomycin-exposed mice [55]. As also observed in the published models, the PC induced ECM (*FN1, TNC,* secreted collagen), as well as myofibroblast (*ACTA2*/α-SMA) marker expression. Interestingly, while macrophage infiltration and activation are key components of the *in vivo* bleomycin lung fibrosis model, few studies have examined the involvement of profibrotic lung-resident macrophages in *ex vivo* slices derived from these animals, warranting further investigation in this area. While this study is focused on the evaluation of macrophages, it would also be useful to assess factors related to other key fibrotic components in these models, including epithelial cell aberration, MMP expression, and inflammatory mediators. Future multi-arm studies focused on the direct cross-evaluation of the PC with established fibrotic inducers and models would allow us to fill critical knowledge gaps related to the capability of our approach and provide insight into effectively modelling the multifactorial landscape of fibrosis.

Additionally, another future directive of the model is to delineate the origin of the α-$SMA^{+}Arg1^{+}CD206^{+}$ cells in this system, understand the expression pattern of this population over time, as well as explore a hypothetical link to MMT, further investigations focusing on cellular phenotyping throughout the duration of the time course are needed. Such studies are vital for broadening comprehension of the fibrosis-related features of the model and their relationship to the surrounding cellular microenvironment. Although we

have established a foundation for these evaluations using IBEX, our study was limited to a cross-sectional snapshot at the 48-hour timepoint. Future studies are required to fully understand the timing of myofibroblast formation in this system. In relation to model optimization and comprehensive understanding, in Figure 3 it is unclear why there is an overall decrease of *MRC1* gene expression, while CD206 protein levels are sustained over time. We initially postulated that this might be partially attributed to the known decrease of alveolar macrophages in PCLS (which can express high levels of CD206) [21,54] however this has been reported to occur around 120 hours in culture, and would likely also be reflected in the protein expression. Further investigation with *in-situ* hybridization techniques to spatially examine gene expression pattern and accompanying cellular morphology would be highly useful for elucidating this.

In summary, we have established and validated a moderate-throughput, complex, viable model to study profibrotic polarization of macrophages in the lung using PCLS. Stimulation of PCLS with the PC effectively induces polarization of macrophages to a profibrotic phenotype. Our model provides means for interrogation of programming of profibrotic lung macrophages with the benefits of increased translatability, with future capacity for investigating novel therapeutic candidates and modes of action in pulmonary fibrosis.

AUTHOR CONTRIBUTIONS

MV: methodology, formal analysis, investigation, writing – original draft, writing – review & editing, visualization; **AA**: methodology, investigation, writing – review & editing; **PA:** methodology, investigation, writing – review & editing; **VK:** methodology, writing – review & editing; **SN:** methodology, writing – review & editing; **TI:** methodology, writing – review & editing; **JK:** methodology, resources, writing – review & editing**; MK:** project administration, resources, supervision, writing – review & editing, funding acquisition; **KA:** conceptualization, resources, supervision, writing – review & editing, project administration, funding acquisition

FUNDING SOURCES

This work was supported by the Canadian Institutes of Health Research (CIHR) [MV: (Doctoral Award) Grant No. 170793; SN: (Doctoral Award) Grant No. 476552, MK: Grant No. PJT-162295] and Ontario Graduate Scholarship (OGS) Program [MV].

ACKNOWLEDGEMENTS

We would like to thank Mary Jo Smith, Mary Bruni, and Xiaoxing Ma at the McMaster Immunology Research Centre John Mayberry Core Histology Facility for their technical support in FFPE immunohistochemistry. We also thank Dr. Joao Pedro Bronze de Firmino and Dr. Mouhanad Babi from the McMaster Centre for Advanced Light Microscopy (CALM) for their expertise in confocal microscopy. We thank Vitoria Murakami Olyntho for knowledgeable teaching of the IBEX method. Lastly, we express our sincere thanks to Joanna Kasinska and Fuqin Duan for their expert technical laboratory assistance.

REFERENCES

[1] R.B. Hopkins, N. Burke, C. Fell, G. Dion, M. Kolb, Epidemiology and survival of idiopathic pulmonary fibrosis from national data in Canada, Eur. Respir. J. 48 (2016) 187–195. https://doi.org/10.1183/13993003.01504-2015.

[2] R.K. Man, A. Gogikar, A. Nanda, L.S.N. Janga, H.G. Sambe, M. Yasir, S. Ramphall, A Comparison of the Effectiveness of Nintedanib and Pirfenidone in Treating Idiopathic Pulmonary Fibrosis: A Systematic Review, Cureus 16 (2024) e54268. https://doi.org/10.7759/cureus.54268.

[3] T. Yanagihara, S.G. Chong, M. Vierhout, J.A. Hirota, K. Ask, M. Kolb, Current models of pulmonary fibrosis for future drug discovery efforts, Expert Opin. Drug Discov. 15 (2020) 931–941. https://doi.org/10.1080/17460441.2020.1755252.

[4] T. Ogawa, S. Shichino, S. Ueha, K. Matsushima, Macrophages in lung fibrosis, Int. Immunol. 33 (2021) 665–671. https://doi.org/10.1093/intimm/dxab040.

[5] C.Y. Perrot, T. Karampitsakos, J.D. Herazo-Maya, Monocytes and macrophages: emerging mechanisms and novel therapeutic targets in pulmonary fibrosis, Am. J. Physiol.-Cell Physiol. 325 (2023) C1046–C1057. https://doi.org/10.1152/ajpcell.00302.2023.

[6] D.V. Pechkovsky, A. Prasse, F. Kollert, K.M.Y. Engel, J. Dentler, W. Luttmann, K. Friedrich, J. Müller-Quernheim, G. Zissel, Alternatively activated alveolar macrophages in pulmonary fibrosis-mediator production and intracellular signal transduction, Clin. Immunol. Orlando Fla 137 (2010) 89–101. https://doi.org/10.1016/j.clim.2010.06.017.

[7] E.A. Ayaub, A. Dubey, J. Imani, F. Botelho, M.R.J. Kolb, C.D. Richards, K. Ask, Overexpression of OSM and IL-6 impacts the polarization of pro-fibrotic macrophages and the development of bleomycin-induced lung fibrosis, Sci. Rep. 7 (2017) 13281. https://doi.org/10.1038/s41598-017-13511-z.

[8] Y. Yao, Y. Wang, Z. Zhang, L. He, J. Zhu, M. Zhang, X. He, Z. Cheng, Q. Ao, Y. Cao, P. Yang, Y. Su, J. Zhao, S. Zhang, Q. Yu, Q. Ning, X. Xiang, W. Xiong, C.-Y. Wang, Y. Xu, Chop Deficiency Protects Mice Against Bleomycin-induced Pulmonary Fibrosis by Attenuating M2 Macrophage Production, Mol. Ther. 24 (2016) 915–925. https://doi.org/10.1038/mt.2016.36.

[9] L. Zhang, Y. Wang, G. Wu, W. Xiong, W. Gu, C.-Y. Wang, Macrophages: friend or foe in idiopathic pulmonary fibrosis?, Respir. Res. 19 (2018) 170. https://doi.org/10.1186/s12931-018-0864-2.

[10] C. Martin, S. Uhlig, V. Ullrich, Videomicroscopy of methacholine-induced contraction of individual airways in precision-cut lung slices, Eur. Respir. J. 9 (1996) 2479–2487. https://doi.org/10.1183/09031936.96.09122479.

[11] C. Martin, S. Uhlig, V. Ullrich, Cytokine-induced bronchoconstriction in precision-cut lung slices is dependent upon cyclooxygenase-2 and thromboxane receptor activation, Am. J. Respir. Cell Mol. Biol. 24 (2001) 139–145. https://doi.org/10.1165/ajrcmb.24.2.3545.

[12] M. Lam, E. Lamanna, L. Organ, C. Donovan, J.E. Bourke, Perspectives on precision cut lung slices—powerful tools for investigation of mechanisms and therapeutic targets in lung diseases, Front. Pharmacol. 14 (2023).

https://www.frontiersin.org/articles/10.3389/fphar.2023.1162889 (accessed October 15, 2023).

[13] G. Liu, C. Betts, D.M. Cunoosamy, P.M. Åberg, J.J. Hornberg, K.B. Sivars, T.S. Cohen, Use of precision cut lung slices as a translational model for the study of lung biology, Respir. Res. 20 (2019) 162. https://doi.org/10.1186/s12931-019-1131-x.

[14] X. Wu, E.M. van Dijk, I.S.T. Bos, L.E.M. Kistemaker, R. Gosens, Mouse Lung Tissue Slice Culture, Methods Mol. Biol. Clifton NJ 1940 (2019) 297–311. https://doi.org/10.1007/978-1-4939-9086-3_21.

[15] R.C. Hubrecht, E. Carter, The 3Rs and Humane Experimental Technique: Implementing Change, Anim. Open Access J. MDPI 9 (2019) 754. https://doi.org/10.3390/ani9100754.

[16] M. Gerckens, K. Schorpp, F. Pelizza, M. Wögrath, K. Reichau, H. Ma, A.-M. Dworsky, A. Sengupta, M.G. Stoleriu, K. Heinzelmann, J. Merl-Pham, M. Irmler, H.N. Alsafadi, E. Trenkenschuh, L. Sarnova, M. Jirouskova, W. Frieß, S.M. Hauck, J. Beckers, N. Kneidinger, J. Behr, A. Hilgendorff, K. Hadian, M. Lindner, M. Königshoff, O. Eickelberg, M. Gregor, O. Plettenburg, A.Ö. Yildirim, G. Burgstaller, Phenotypic drug screening in a human fibrosis model identified a novel class of antifibrotic therapeutics, Sci. Adv. 7 (2021) eabb3673. https://doi.org/10.1126/sciadv.abb3673.

[17] C.Y. Watson, F. Damiani, S. Ram-Mohan, S. Rodrigues, P. de Moura Queiroz, T.C. Donaghey, J.H. Rosenblum Lichtenstein, J.D. Brain, R. Krishnan, R.M. Molina,

Screening for Chemical Toxicity Using Cryopreserved Precision Cut Lung Slices, Toxicol. Sci. 150 (2016) 225–233. https://doi.org/10.1093/toxsci/kfv320.

[18] F.T. Munyonho, R.D.E. Clark, D. Lin, M.S. Khatun, D. Pungan, G. Dai, J.K. Kolls, Precision-cut lung slices as an ex vivo model to study Pneumocystis murina survival and antimicrobial susceptibility, mBio 15 (2023) e01464-23. https://doi.org/10.1128/mbio.01464-23.

[19] J.Y. Lee, N.S. Reyes, S. Ravishankar, M. Zhou, M. Krasilnikov, C. Ringler, G. Pohan, C. Wilson, K.K.-H. Ang, P.J. Wolters, T. Tsukui, D. Sheppard, M.R. Arkin, T. Peng, An in vivo screening platform identifies senolytic compounds that target *p16*$^{INK4a+}$ fibroblasts in lung fibrosis, J. Clin. Invest. 134 (2024). https://doi.org/10.1172/JCI173371.

[20] N.I. Winters, C.J. Taylor, C.S. Jetter, J.E. Camarata, A.J. Gutierrez, L.T. Bui, J.J. Gokey, M. Bacchetta, N.E. Banovich, J.M.S. Sucre, J.A. Kropski, Single-cell transcriptomic assessment of cellular phenotype stability in human precision-cut lung slices, (2021) 2021.08.19.457016. https://doi.org/10.1101/2021.08.19.457016.

[21] R. Blomberg, K. Sompel, C. Hauer, A.J. Smith, B. Peña, J. Driscoll, P.S. Hume, D.T. Merrick, M.A. Tennis, C.M. Magin, Hydrogel-Embedded Precision-Cut Lung Slices Model Lung Cancer Premalignancy Ex Vivo, Adv. Healthc. Mater. 13 (2024) 2302246. https://doi.org/10.1002/adhm.202302246.

[22] H.N. Alsafadi, C.A. Staab-Weijnitz, M. Lehmann, M. Lindner, B. Peschel, M. Königshoff, D.E. Wagner, An ex vivo model to induce early fibrosis-like changes in

human precision-cut lung slices, Am. J. Physiol.-Lung Cell. Mol. Physiol. 312 (2017) L896–L902. https://doi.org/10.1152/ajplung.00084.2017.

[23] N.J. Lang, J. Gote-Schniering, D. Porras-Gonzalez, L. Yang, L.J. De Sadeleer, R.C. Jentzsch, V.A. Shitov, S. Zhou, M. Ansari, A. Agami, C.H. Mayr, B. Hooshiar Kashani, Y. Chen, L. Heumos, J.C. Pestoni, E.S. Molnar, E. Geeraerts, V. Anquetil, L. Saniere, M. Wögrath, M. Gerckens, M. Lehmann, A.Ö. Yildirim, R. Hatz, N. Kneidinger, J. Behr, W.A. Wuyts, M.-G. Stoleriu, M.D. Luecken, F.J. Theis, G. Burgstaller, H.B. Schiller, Ex vivo tissue perturbations coupled to single-cell RNA-seq reveal multilineage cell circuit dynamics in human lung fibrogenesis, Sci. Transl. Med. 15 (2023) eadh0908. https://doi.org/10.1126/scitranslmed.adh0908.

[24] E.A. Ayaub, K. Tandon, M. Padwal, J. Imani, H. Patel, A. Dubey, O. Mekhael, C. Upagupta, A. Ayoub, A. Dvorkin-Gheva, J. Murphy, P.S. Kolb, S. Lhotak, J.G. Dickhout, R.C. Austin, M.R.J. Kolb, C.D. Richards, K. Ask, IL-6 mediates ER expansion during hyperpolarization of alternatively activated macrophages, Immunol. Cell Biol. 97 (2019) 203–217. https://doi.org/10.1111/imcb.12212.

[25] A.J. Radtke, C.J. Chu, Z. Yaniv, L. Yao, J. Marr, R.T. Beuschel, H. Ichise, A. Gola, J. Kabat, B. Lowekamp, E. Speranza, J. Croteau, N. Thakur, D. Jonigk, J.L. Davis, J.M. Hernandez, R.N. Germain, IBEX: an iterative immunolabeling and chemical bleaching method for high-content imaging of diverse tissues, Nat. Protoc. 17 (2022) 378–401. https://doi.org/10.1038/s41596-021-00644-9.

[26] A.J. Radtke, E. Kandov, B. Lowekamp, E. Speranza, C.J. Chu, A. Gola, N. Thakur, R. Shih, L. Yao, Z.R. Yaniv, R.T. Beuschel, J. Kabat, J. Croteau, J. Davis, J.M.

Hernandez, R.N. Germain, IBEX: A versatile multiplex optical imaging approach for deep phenotyping and spatial analysis of cells in complex tissues, Proc. Natl. Acad. Sci. 117 (2020) 33455–33465. https://doi.org/10.1073/pnas.2018488117.

[27] J. Stegmayr, H.N. Alsafadi, W. Langwiński, A. Niroomand, S. Lindstedt, N.D. Leigh, D.E. Wagner, Isolation of high-yield and -quality RNA from human precision-cut lung slices for RNA-sequencing and computational integration with larger patient cohorts, Am. J. Physiol.-Lung Cell. Mol. Physiol. 320 (2021) L232–L240. https://doi.org/10.1152/ajplung.00401.2020.

[28] C. Michalaki, C. Dean, C. Johansson, The Use of Precision-Cut Lung Slices for Studying Innate Immunity to Viral Infections, Curr. Protoc. 2 (2022) e505. https://doi.org/10.1002/cpz1.505.

[29] M. Niehof, T. Hildebrandt, O. Danov, K. Arndt, J. Koschmann, F. Dahlmann, T. Hansen, K. Sewald, RNA isolation from precision-cut lung slices (PCLS) from different species, BMC Res. Notes 10 (2017) 121. https://doi.org/10.1186/s13104-017-2447-6.

[30] V. Neuhaus, D. Schaudien, T. Golovina, U.-A. Temann, C. Thompson, T. Lippmann, C. Bersch, O. Pfennig, D. Jonigk, P. Braubach, H.-G. Fieguth, G. Warnecke, V. Yusibov, K. Sewald, A. Braun, Assessment of long-term cultivated human precision-cut lung slices as an ex vivo system for evaluation of chronic cytotoxicity and functionality, J. Occup. Med. Toxicol. Lond. Engl. 12 (2017) 13. https://doi.org/10.1186/s12995-017-0158-5.

[31] A. Temann, T. Golovina, V. Neuhaus, C. Thompson, J.A. Chichester, A. Braun, V. Yusibov, Evaluation of inflammatory and immune responses in long-term cultured human precision-cut lung slices, Hum. Vaccines Immunother. 13 (2017) 351–358. https://doi.org/10.1080/21645515.2017.1264794.

[32] T. Rőszer, Understanding the Mysterious M2 Macrophage through Activation Markers and Effector Mechanisms, Mediators Inflamm. 2015 (2015) 816460. https://doi.org/10.1155/2015/816460.

[33] Y. Gu, T. Lawrence, R. Mohamed, Y. Liang, B.H. Yahaya, The emerging roles of interstitial macrophages in pulmonary fibrosis: A perspective from scRNA-seq analyses, Front. Immunol. 13 (2022) 923235. https://doi.org/10.3389/fimmu.2022.923235.

[34] A.V. Misharin, L. Morales-Nebreda, G.M. Mutlu, G.R.S. Budinger, H. Perlman, Flow Cytometric Analysis of Macrophages and Dendritic Cell Subsets in the Mouse Lung, Am. J. Respir. Cell Mol. Biol. 49 (2013) 503–510. https://doi.org/10.1165/rcmb.2013-0086MA.

[35] M. Naito, H. Nagai, S. Kawano, H. Umezu, H. Zhu, H. Moriyama, T. Yamamoto, H. Takatsuka, Y. Takei, Liposome-encapsulated dichloromethylene diphosphonate induces macrophage apoptosis in vivo and in vitro, J. Leukoc. Biol. 60 (1996) 337–344. https://doi.org/10.1002/jlb.60.3.337.

[36] M.A. Gibbons, A.C. MacKinnon, P. Ramachandran, K. Dhaliwal, R. Duffin, A.T. Phythian-Adams, N. van Rooijen, C. Haslett, S.E. Howie, A.J. Simpson, N. Hirani, J. Gauldie, J.P. Iredale, T. Sethi, S.J. Forbes, Ly6Chi Monocytes Direct Alternatively

Activated Profibrotic Macrophage Regulation of Lung Fibrosis, Am. J. Respir. Crit. Care Med. 184 (2011) 569–581. https://doi.org/10.1164/rccm.201010-1719OC.

[37] O. Danov, S.M. Jiménez Delgado, H. Obernolte, S. Seehase, S. Dehmel, P. Braubach, H.-G. Fieguth, G. Matschiner, M. Fitzgerald, D. Jonigk, S. Knauf, O. Pfennig, G. Warnecke, J. Wichmann, A. Braun, K. Sewald, Human lung tissue provides highly relevant data about efficacy of new anti-asthmatic drugs, PloS One 13 (2018) e0207767. https://doi.org/10.1371/journal.pone.0207767.

[38] F.E. Uhl, S. Vierkotten, D.E. Wagner, G. Burgstaller, R. Costa, I. Koch, M. Lindner, S. Meiners, O. Eickelberg, M. Königshoff, Preclinical validation and imaging of Wnt-induced repair in human 3D lung tissue cultures, Eur. Respir. J. 46 (2015) 1150–1166. https://doi.org/10.1183/09031936.00183214.

[39] L. Lauenstein, S. Switalla, F. Prenzler, S. Seehase, O. Pfennig, C. Förster, H. Fieguth, A. Braun, K. Sewald, Assessment of immunotoxicity induced by chemicals in human precision-cut lung slices (PCLS), Toxicol. In Vitro 28 (2014) 588–599. https://doi.org/10.1016/j.tiv.2013.12.016.

[40] M. Henjakovic, K. Sewald, S. Switalla, D. Kaiser, M. Müller, T.Z. Veres, C. Martin, S. Uhlig, N. Krug, A. Braun, Ex vivo testing of immune responses in precision-cut lung slices, Toxicol. Appl. Pharmacol. 231 (2008) 68–76. https://doi.org/10.1016/j.taap.2008.04.003.

[41] K. Sompel, A.J. Smith, C. Hauer, A.P. Elango, E.T. Clamby, R.L. Keith, M.A. Tennis, Precision Cut Lung Slices as a Preclinical Model for Non–Small Cell Lung Cancer

Chemoprevention, Cancer Prev. Res. (Phila. Pa.) 16 (2023) 247–258. https://doi.org/10.1158/1940-6207.CAPR-23-0004.

[42] S.K. Banerjee, S.D. Huckuntod, S.D. Mills, R.C. Kurten, R.D. Pechous, Modeling Pneumonic Plague in Human Precision-Cut Lung Slices Highlights a Role for the Plasminogen Activator Protease in Facilitating Type 3 Secretion, Infect. Immun. 87 (2019) e00175-19. https://doi.org/10.1128/IAI.00175-19.

[43] M.R. Fernando, J.L. Reyes, J. Iannuzzi, G. Leung, D.M. McKay, The Pro-Inflammatory Cytokine, Interleukin-6, Enhances the Polarization of Alternatively Activated Macrophages, PLOS ONE 9 (2014) e94188. https://doi.org/10.1371/journal.pone.0094188.

[44] J. Mauer, B. Chaurasia, J. Goldau, M.C. Vogt, J. Ruud, K.D. Nguyen, S. Theurich, A.C. Hausen, J. Schmitz, H.S. Brönneke, E. Estevez, T.L. Allen, A. Mesaros, L. Partridge, M.A. Febbraio, A. Chawla, F.T. Wunderlich, J.C. Brüning, Interleukin-6 signaling promotes alternative macrophage activation to limit obesity-associated insulin resistance and endotoxemia, Nat. Immunol. 15 (2014) 423–430. https://doi.org/10.1038/ni.2865.

[45]T. Shi, L. Denney, H. An, L.-P. Ho, Y. Zheng, Alveolar and lung interstitial macrophages: Definitions, functions, and roles in lung fibrosis, J. Leukoc. Biol. 110 (2021) 107–114. https://doi.org/10.1002/JLB.3RU0720-418R.

[46] F.M. Hoffmann, J.L. Berger, I. Lingel, Y. Laumonnier, I.P. Lewkowich, I. Schmudde, P. König, Distribution and Interaction of Murine Pulmonary Phagocytes in the Naive

and Allergic Lung, Front. Immunol. 9 (2018) 1046. https://doi.org/10.3389/fimmu.2018.01046.

[47] K.S.S. Putri, A. Adhyatmika, C.E. Boorsma, H. Habibie, M.J.R. Ruigrok, P. Heukels, W. Timens, M.H. de Jager, W.L.J. Hinrichs, P. Olinga, B.N. Melgert, Osteoprotegerin is an Early Marker of the Fibrotic Process and of Antifibrotic Treatment Responses in Ex Vivo Lung Fibrosis, Lung 202 (2024) 331–342. https://doi.org/10.1007/s00408-024-00691-5.

[48] C. Fertin, J.F. Nicolas, P. Gillery, B. Kalis, J. Banchereau, F.X. Maquart, Interleukin-4 stimulates collagen synthesis by normal and scleroderma fibroblasts in dermal equivalents, Cell. Mol. Biol. 37 (1991) 823–829.

[49] M. Jinnin, H. Ihn, K. Yamane, K. Tamaki, Interleukin-13 Stimulates the Transcription of the Human α2(I) Collagen Gene in Human Dermal Fibroblasts *, J. Biol. Chem. 279 (2004) 41783–41791. https://doi.org/10.1074/jbc.M406951200.

[50]B. Singh, R.K. Kasam, V. Sontake, T.A. Wynn, S.K. Madala, Repetitive intradermal bleomycin injections evoke T-helper cell 2 cytokine-driven pulmonary fibrosis, Am. J. Physiol.-Lung Cell. Mol. Physiol. 313 (2017) L796–L806. https://doi.org/10.1152/ajplung.00184.2017.

[51] M.-P.D. Campli, A. Azouz, A. Assabban, J. Scaillet, M. Splittgerber, A.V. Keymeulen, F. Libert, M. Remmelink, A.L. Moine, P. Lemaitre, S. Goriely, The mononuclear phagocyte system contributes to fibrosis in post-transplant obliterans bronchiolitis, Eur. Respir. J. 57 (2021). https://doi.org/10.1183/13993003.00344-2020.

[52] M. Vierhout, A. Ayoub, S. Naiel, P. Yazdanshenas, S.D. Revill, A. Reihani, A. Dvorkin-Gheva, W. Shi, K. Ask, Monocyte and macrophage derived myofibroblasts: Is it fate? A review of the current evidence, Wound Repair Regen. 29 (2021) 548–562. https://doi.org/10.1111/wrr.12946.

[53] G. Liu, L. Särén, H. Douglasson, X.-H. Zhou, P.M. Åberg, A. Ollerstam, C.J. Betts, K. Balogh Sivars, Precision cut lung slices: an ex vivo model for assessing the impact of immunomodulatory therapeutics on lung immune responses, Arch. Toxicol. 95 (2021) 2871–2877. https://doi.org/10.1007/s00204-021-03096-y.

[54] E. Mitsi, R. Kamng'ona, J. Rylance, C. Solórzano, J. Jesus Reiné, H.C. Mwandumba, D.M. Ferreira, K.C. Jambo, Human alveolar macrophages predominately express combined classical M1 and M2 surface markers in steady state, Respir Res 19 (2018) 66. https://doi.org/10.1186/s12931-018-0777-0.

[55] M. Cedilak, M. Banjanac, D. Belamarić, A. Paravić Radičević, I. Faraho, K. Ilić, S. Čužić, I. Glojnarić, V. Eraković Haber, M. Bosnar, Precision-cut lung slices from bleomycin treated animals as a model for testing potential therapies for idiopathic pulmonary fibrosis, Pulm Pharmacol Ther 55 (2019) 75–83. https://doi.org/10.1016/j.pupt.2019.02.005.

[56] X.-M. Meng, S. Wang, X.-R. Huang, C. Yang, J. Xiao, Y. Zhang, K.-F. To, D.J. Nikolic-Paterson, H.-Y. Lan, Inflammatory macrophages can transdifferentiate into myofibroblasts during renal fibrosis, Cell Death Dis 7 (2016) e2495. https://doi.org/10.1038/cddis.2016.402.

[57] A.M. Abu El-Asrar, G. De Hertogh, E. Allegaert, M.I. Nawaz, S. Abouelasrar Salama, P.W. Gikandi, G. Opdenakker, S. Struyf, Macrophage-Myofibroblast Transition Contributes to Myofibroblast Formation in Proliferative Vitreoretinal Disorders, Int J Mol Sci 24 (2023) 13510. https://doi.org/10.3390/ijms241713510.

[58] C. Morse, T. Tabib, J. Sembrat, K.L. Buschur, H.T. Bittar, E. Valenzi, Y. Jiang, D.J. Kass, K. Gibson, W. Chen, A. Mora, P.V. Benos, M. Rojas, R. Lafyatis, Proliferating SPP1/MERTK-expressing macrophages in idiopathic pulmonary fibrosis, Eur Respir J 54 (2019) 1802441. https://doi.org/10.1183/13993003.02441-2018.

[59]T. Fabre, A.M.S. Barron, S.M. Christensen, S. Asano, K. Bound, M.P. Lech, M.H. Wadsworth, X. Chen, C. Wang, J. Wang, J. McMahon, F. Schlerman, A. White, K.M. Kravarik, A.J. Fisher, L.A. Borthwick, K.M. Hart, N.C. Henderson, T.A. Wynn, K. Dower, Identification of a broadly fibrogenic macrophage subset induced by type 3 inflammation, Sci Immunol 8 (2023) eadd8945. https://doi.org/10.1126/sciimmunol.add8945.

Figure 1

A


i.
ii.
iii.
iv.
v.
2mm
4mm

B

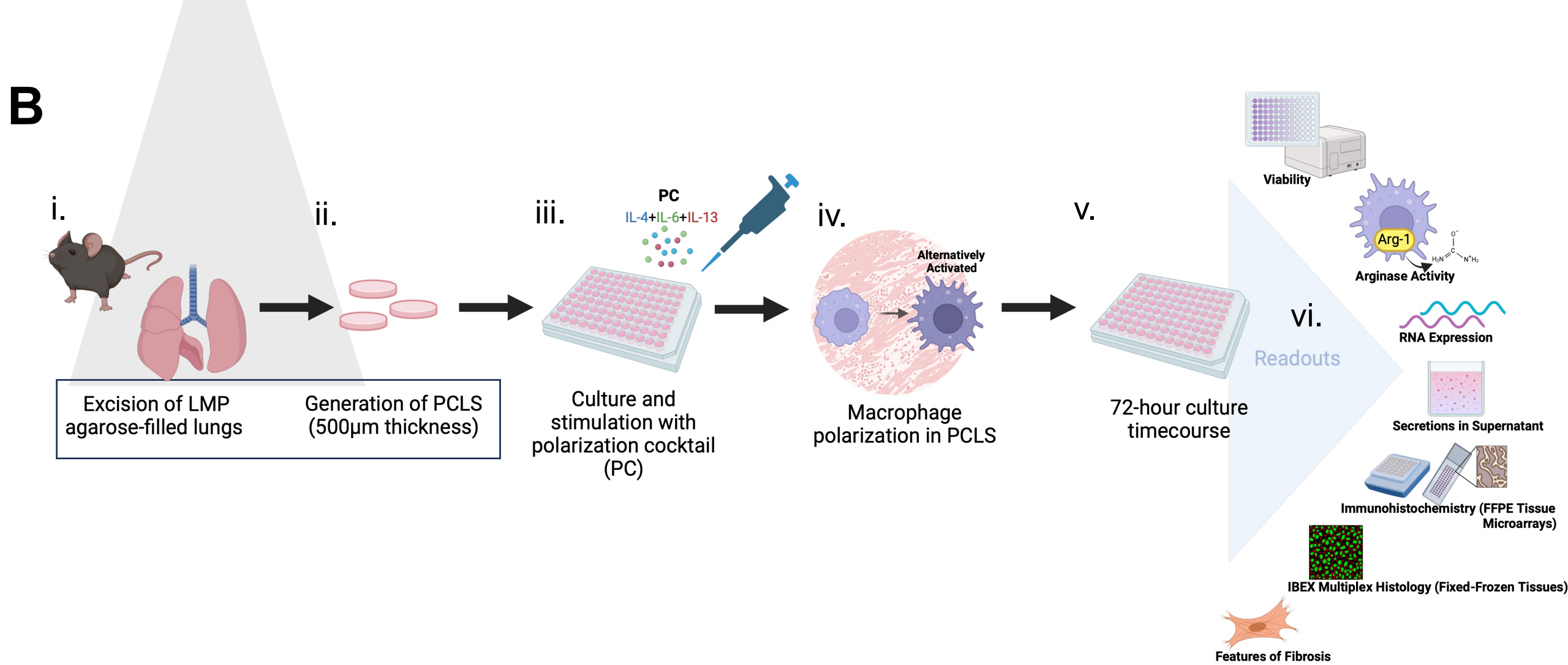
i.
ii.
iii.
PC
IL-4+IL-6+IL-13
iv.
Alternatively Activated
v.
Excision of LMP agarose-filled lungs
Generation of PCLS (500µm thickness)
Culture and stimulation with polarization cocktail (PC)
Macrophage polarization in PCLS
72-hour culture timecourse
vi.
Readouts
Viability
Arg-1
Arginase Activity
RNA Expression
Secretions in Supernatant
Immunohistochemistry (FFPE Tissue Microarrays)
IBEX Multiplex Histology (Fixed-Frozen Tissues)
Features of Fibrosis

C

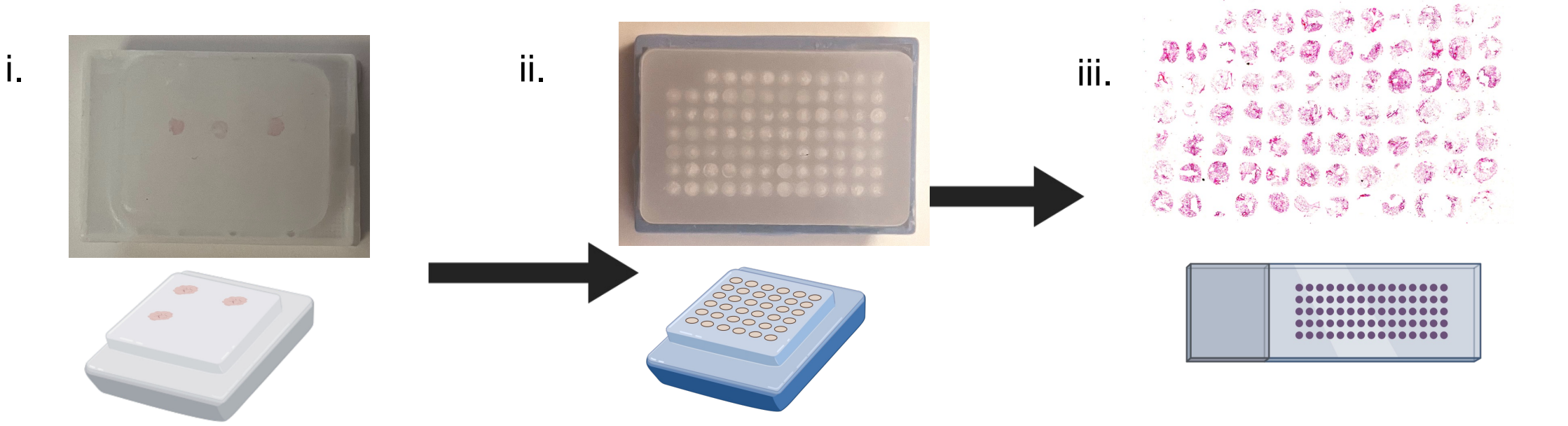
i.
ii.
iii.
PCLS FFPE block
Punches inserted in host tissue microarray (TMA) block
TMA sections stained for histological evaluation and quantitative assessment

Figure 1. Schematic of overall experimental workflow. (**A)** Processing of murine lung for generation of PCLS. i. After sacrifice, lungs are infiltrated via the trachea with 1.5% low-melting point (LMP) agarose. Tissue is left to cool on ice in order for agarose to completely solidify prior to excision of lungs. ii. Filled lungs are excised from the body. iii. Lobes are separated to be sliced one at a time. iv. PCLS (500μm thickness) are generated from slicing each lobe using a Compresstome vibrating microtome. v. PCLS cores (2mm or 4mm in diameter) are punched from full lobe slices. **(B)** Experimental pipeline and readouts. i.,ii. Lungs are removed, sliced, and cored to create PCLS. After slicing, PCLS are placed in culture medium and left in incubator overnight to acclimate prior to treatment. iii. PCLS are moved to 96-well plates and treated with polarization cocktail (PC; IL-4+IL-6+IL-13). Baseline samples can also be harvested at this time (Day 0). iv.,v. Macrophage polarization occurs over 72-hour time course. Samples are harvested at 24-hour intervals throughout the time course. vi. Various readouts can be conducted on the polarized and control PCLS, including viability assays (WST-1), arginase activity assay, RNA expression, measurement of secreted components in supernatant, traditional brightfield immunohistochemistry (on FFPE PCLS, in tissue microarrays), multiplex immunostaining with Iterative Bleaching Extends Multiplexity method (IBEX; on fixed-frozen PCLS), and evaluation of fibrotic features (determined via histology, RNA expression, and secretions in supernatant). **(C)** Tissue microarray (TMA) generation from FFPE PCLS for histological evaluations. i. Original FFPE blocks containing PCLS. ii. 2mm punches are taken and inserted in parent TMA blocks. iii. Sections are taken from TMA and stained for histological evaluations, including quantitative assessment with HALO Image Analysis

Software. Note: After fixation and prior to embedding, a small amount of eosin can be added to the ethanol storage solution to lightly colour the tissue, increasing ease of visibility during the embedding process. Figure created using BioRender.com.

Figure 2

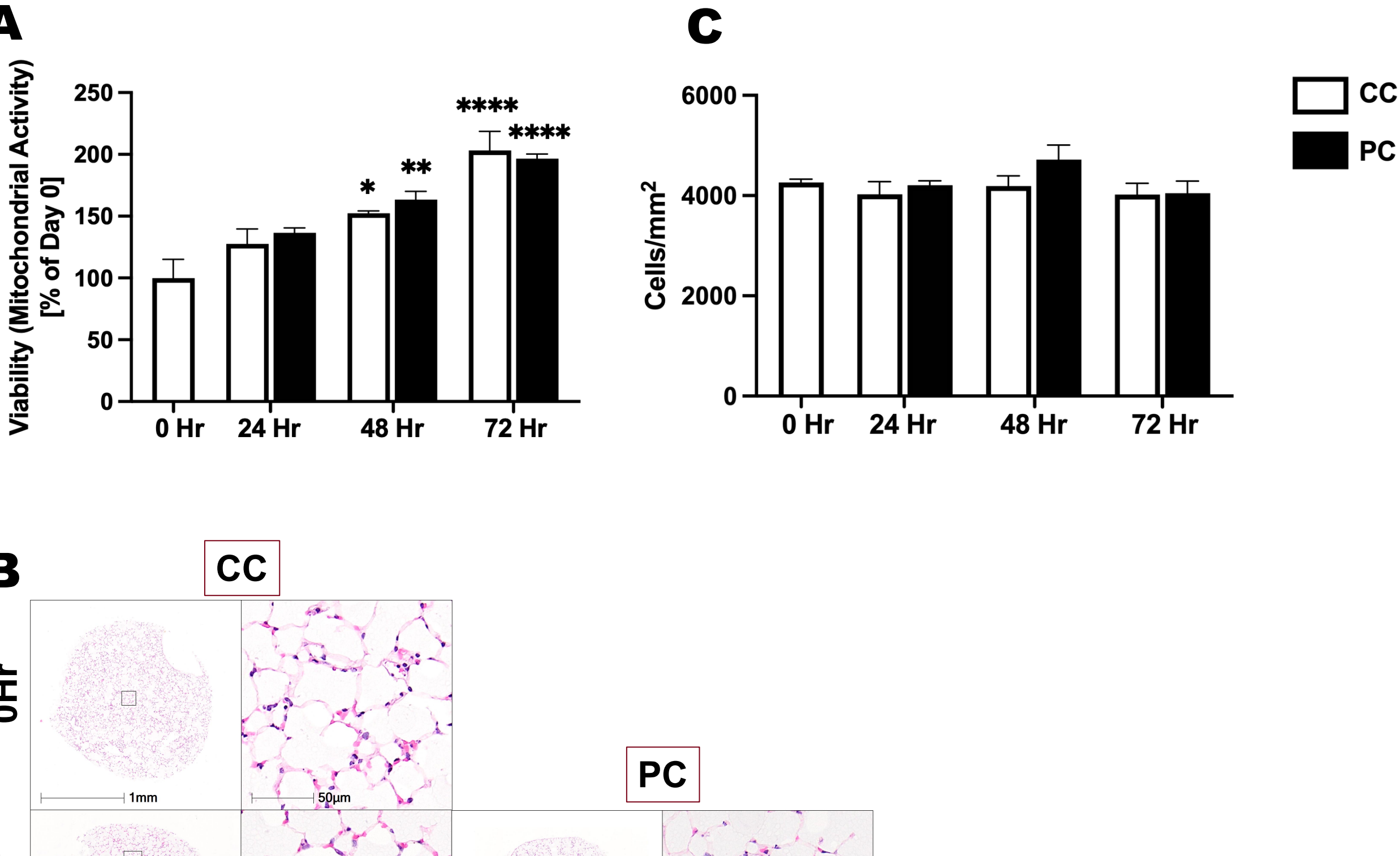
A
Viability (Mitochondrial Activity) [% of Day 0]
250
200
150
100
50
0
*
**
****
****
0 Hr
24 Hr
48 Hr
72 Hr
C
Cells/mm2
6000
4000
2000
0
0 Hr
24 Hr
48 Hr
72 Hr
CC
PC
B
CC
PC
0Hr
24Hr
48Hr
72Hr
1mm
50µm
D
0Hr
0Hr
72Hr - CC
72Hr- PC
50µm

Figure 2. Murine Precision-Cut Lung Slices Maintain Viability and Structural Integrity in Culture Throughout Polarization Cocktail Treatment Time course. (A) Viability of precision-cut lung slices (PCLS) cultured with control cocktail (CC) or polarization cocktail (PC), assessed via water-soluble tetrazolium-1 (WST-1) assay. Absorbance values are expressed as percent of signal measured at Day 0. (n=3 mice, 5 slices per condition). **(B)** Hematoxylin and eosin (H&E) staining of PCLS (formalin-fixed, paraffin-embedded) throughout 72-hour time course. **(C)** Cell count per mm^2 of tissue, quantified from whole slide images of H&E stained tissue microarrays using HALO image analysis platform (n=3 mice, 3-4 slices per condition). **(D)** Presence of macrophages in PCLS at baseline and 72-hour timepoint shown in H&E stained tissues. Arrows point to macrophages in alveolar spaces. * indicates $P<0.05$, ** indicates $P<0.01$, *** indicates $P<0.001$, and **** indicates $P<0.0001$, where * represents a significant difference compared to baseline (Day 0). Data are displayed as mean ± S.E.M.

Figure 3

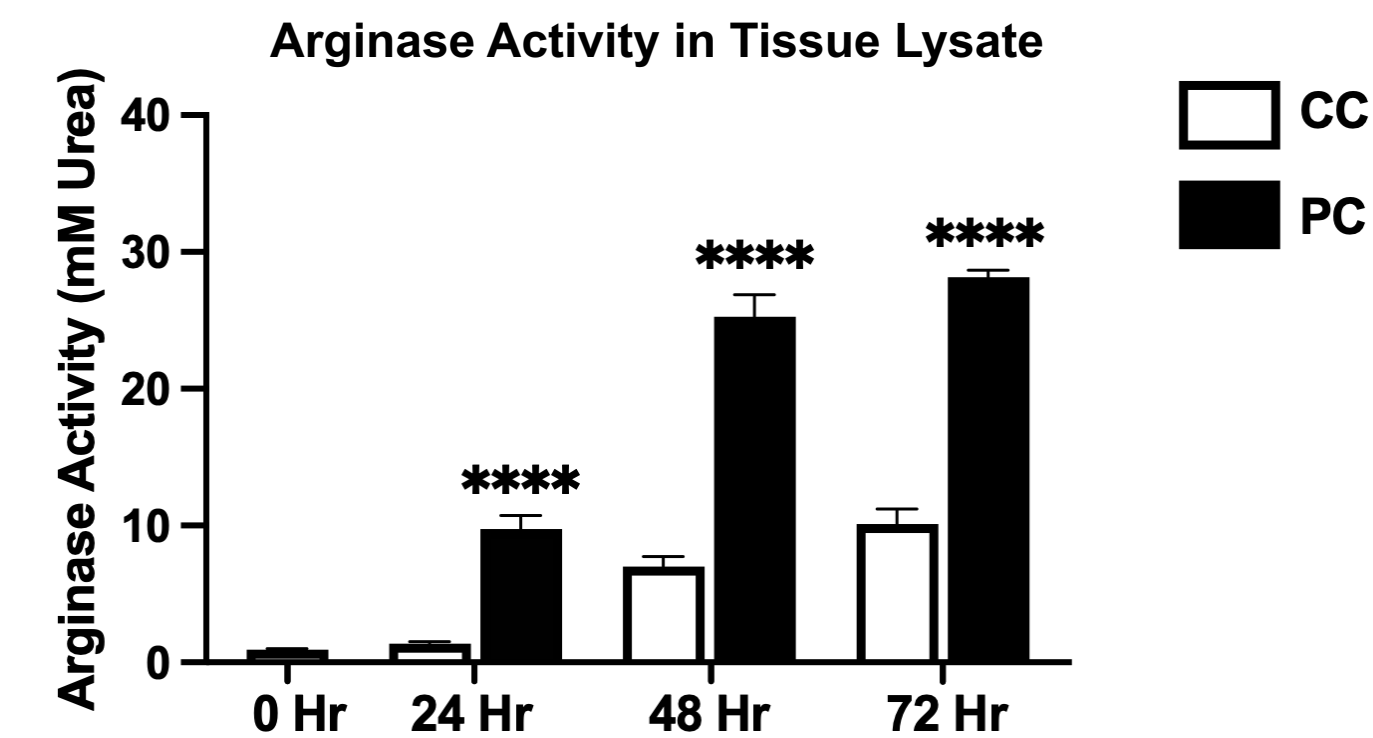
A
Arginase Activity in Tissue Lysate
Arginase Activity (mM Urea)
40
30
20
10
0
****
****
****
0 Hr
24 Hr
48 Hr
72 Hr
CC
PC

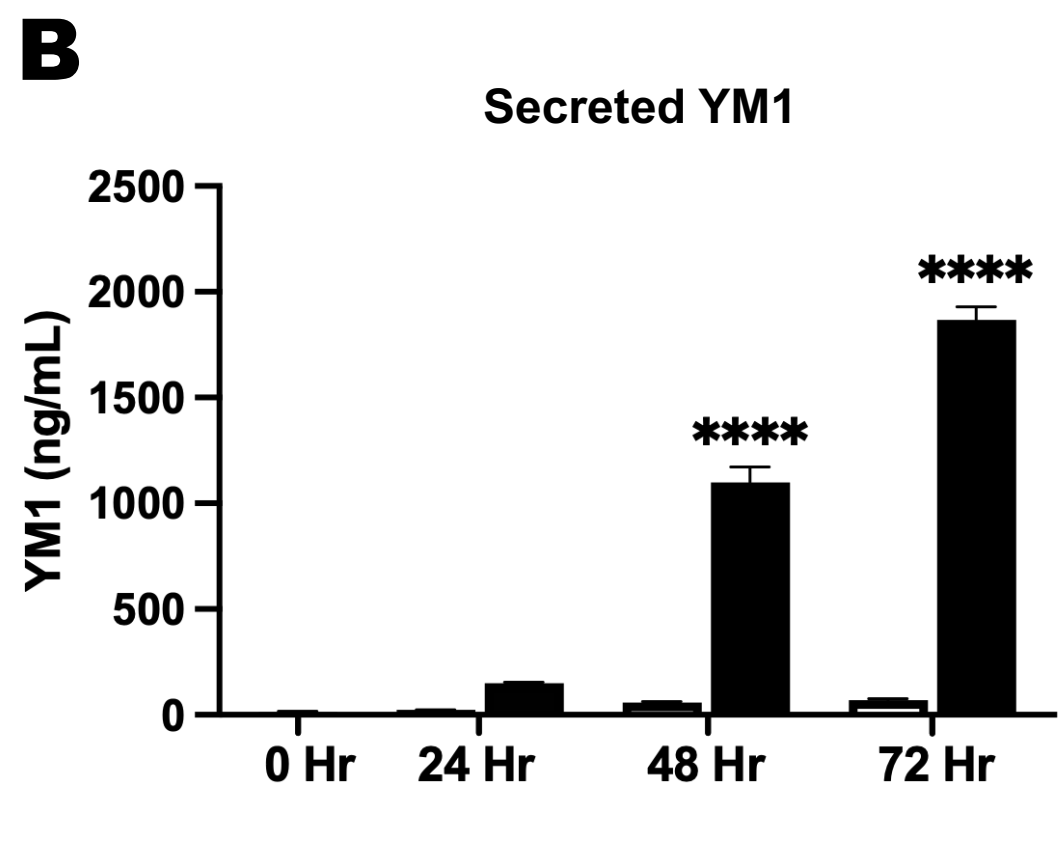
B
Secreted YM1
YM1 (ng/mL)
2500
2000
1500
1000
500
0
****
****
0 Hr
24 Hr
48 Hr
72 Hr

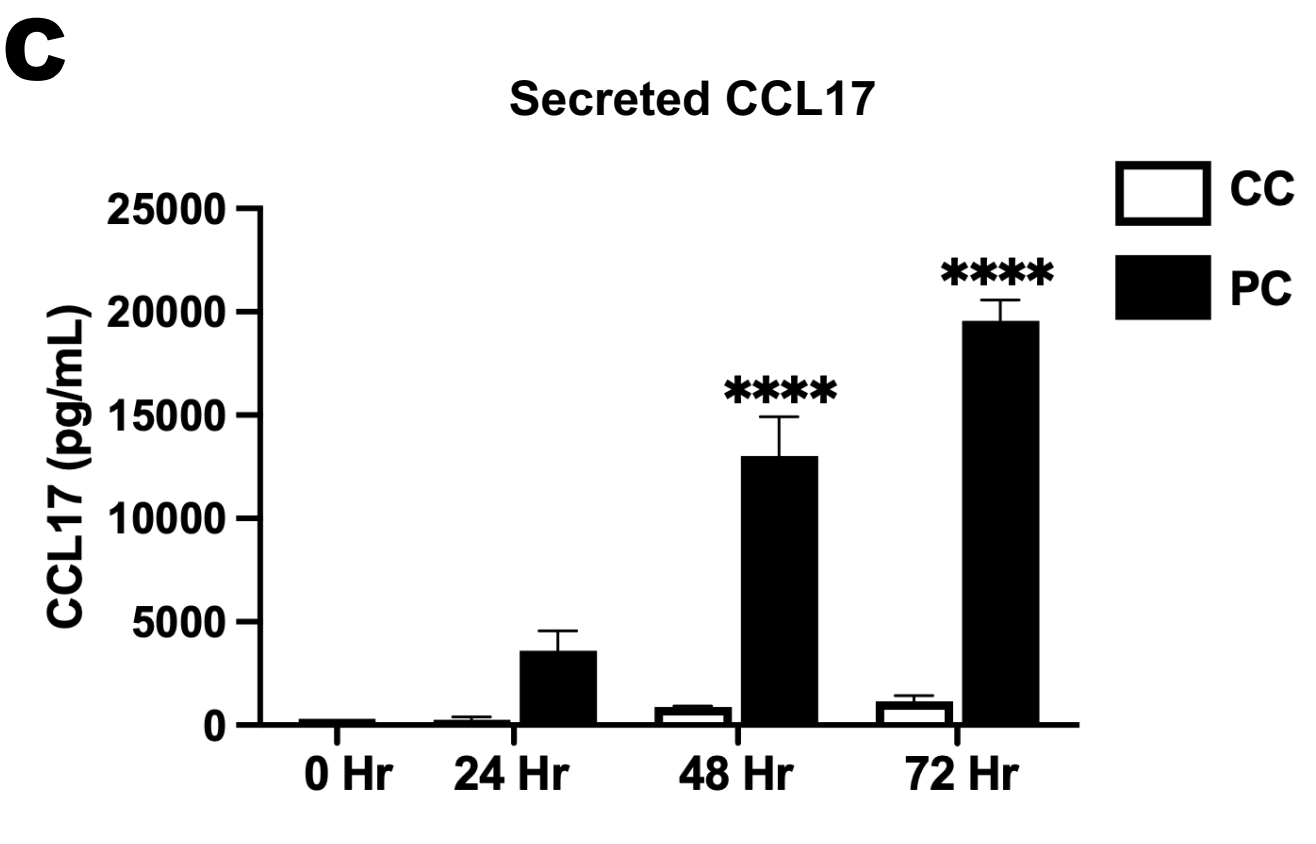
C
Secreted CCL17
CCL17 (pg/mL)
25000
20000
15000
10000
5000
0
****
****
0 Hr
24 Hr
48 Hr
72 Hr
CC
PC

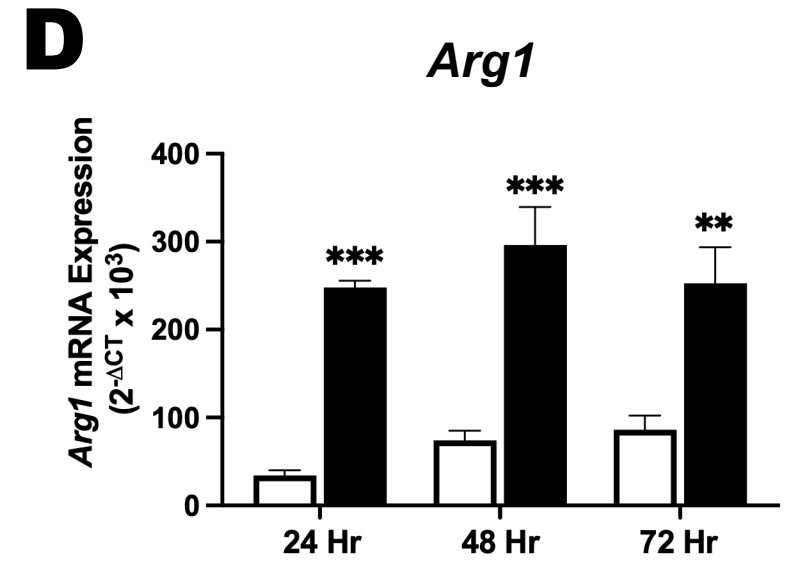
D
Arg1
Arg1 mRNA Expression
(2-ΔCT x 10³)
400
300
200
100
0
***
***
**
24 Hr
48 Hr
72 Hr

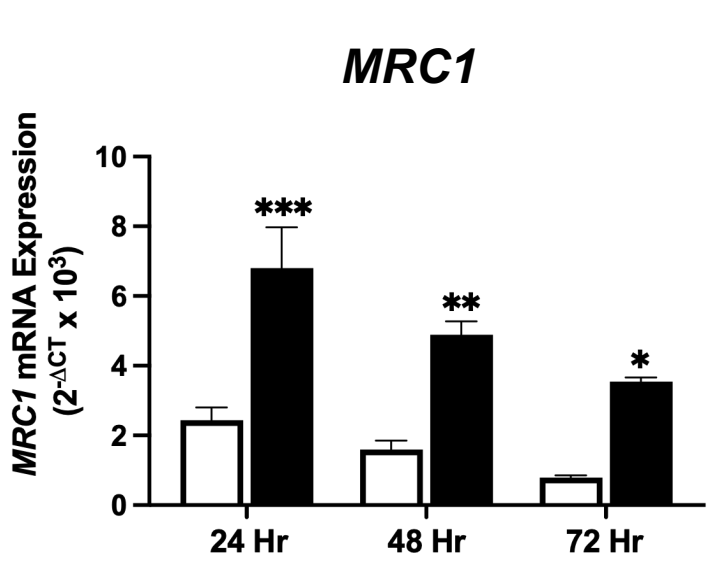
E
MRC1
MRC1 mRNA Expression
(2-ΔCT x 10³)
10
8
6
4
2
0
***
**
*
24 Hr
48 Hr
72 Hr

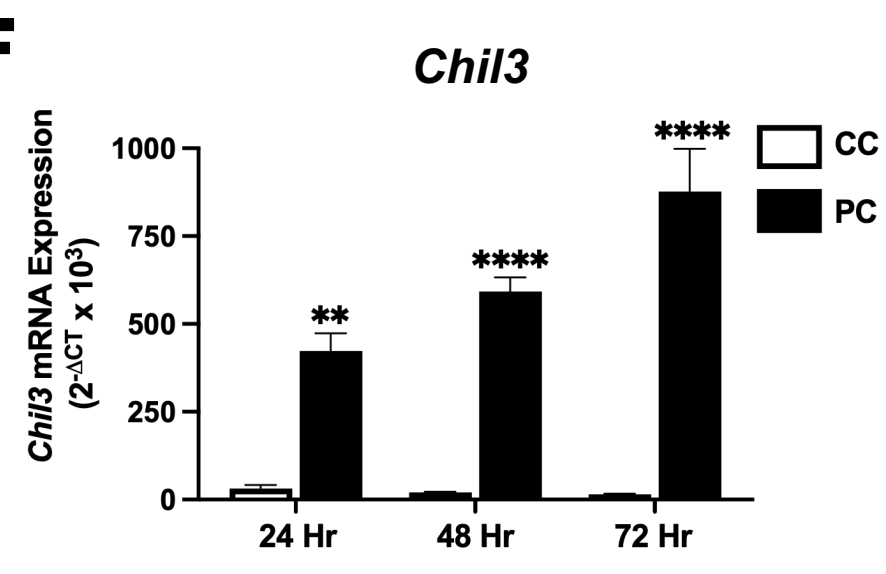
F
Chil3
Chil3 mRNA Expression
(2-ΔCT x 10³)
1000
750
500
250
0
**
****
****
24 Hr
48 Hr
72 Hr
CC
PC

Figure 3. Treatment with the Polarization Cocktail Induces Markers of Alternatively Activated Macrophages in Precision-Cut Lung Slice Tissue and Supernatant. (A) Arginase activity measured as mM Urea in PCLS tissue homogenates (n=3 mice, 3-4 slices per condition). **(B,C)** Secreted Chitinase-3-like protein 3 (YM1) and CC chemokine ligand 17 (CCL17) protein levels in PCLS supernatant measured via ELISA (n=3 mice). **(D,E,F)** Normalized gene expression of Arginase 1 (*Arg1*), CD206 (*MRC1*) and YM1 (*Chil3*) in PCLS tissue, relative to *GAPDH* (n=3 mice, 6 slices pooled per condition). * indicates $P<0.05$; ** indicates $P<0.01$; *** indicates $P<0.001$; and **** indicates $P<0.0001$; where * represents a significant difference between the two treatment groups at the respective timepoint. Data are displayed as mean ± S.E.M.

Figure 4

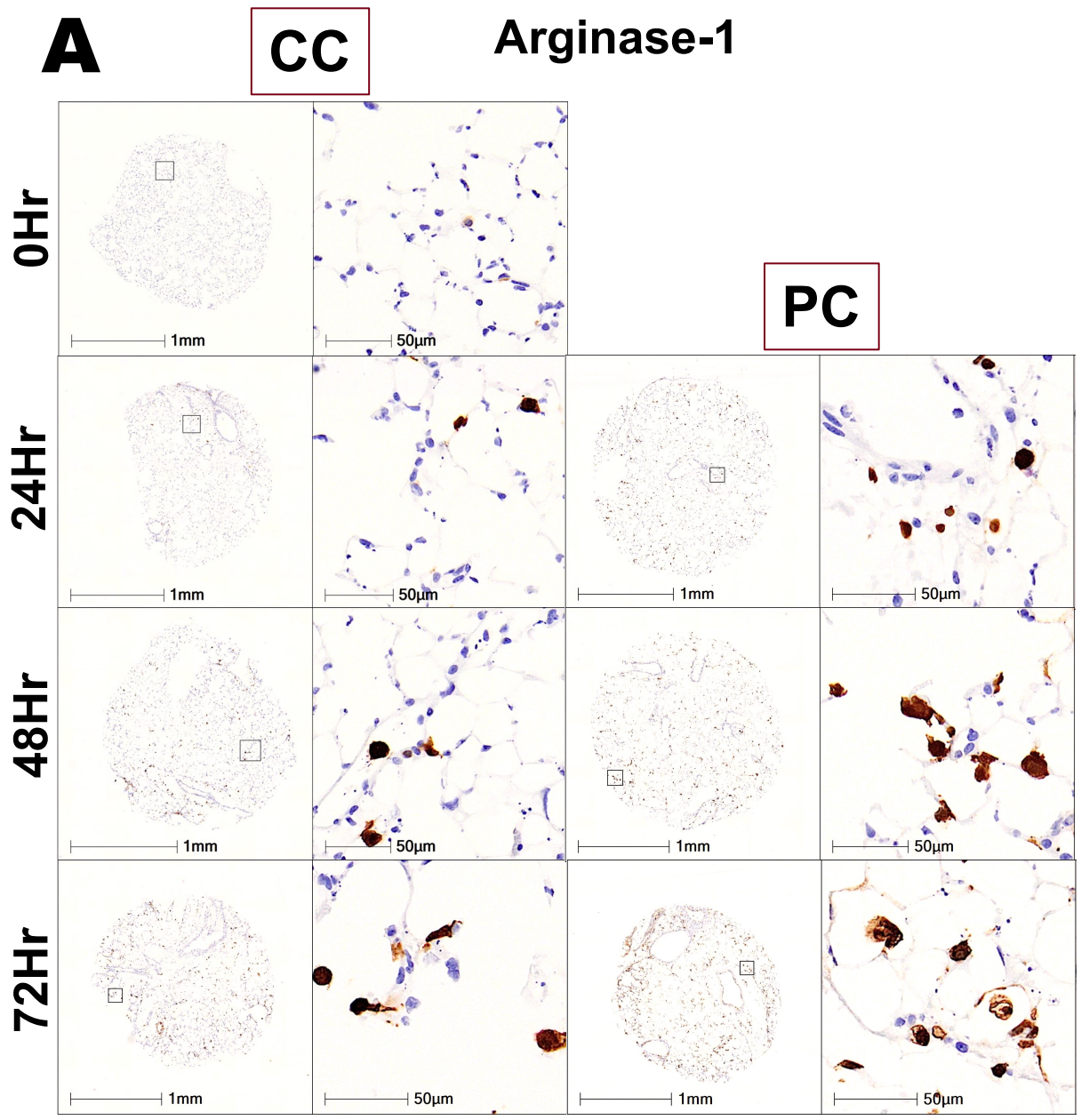
A
CC
Arginase-1
PC
0Hr
24Hr
48Hr
72Hr
1mm
50µm

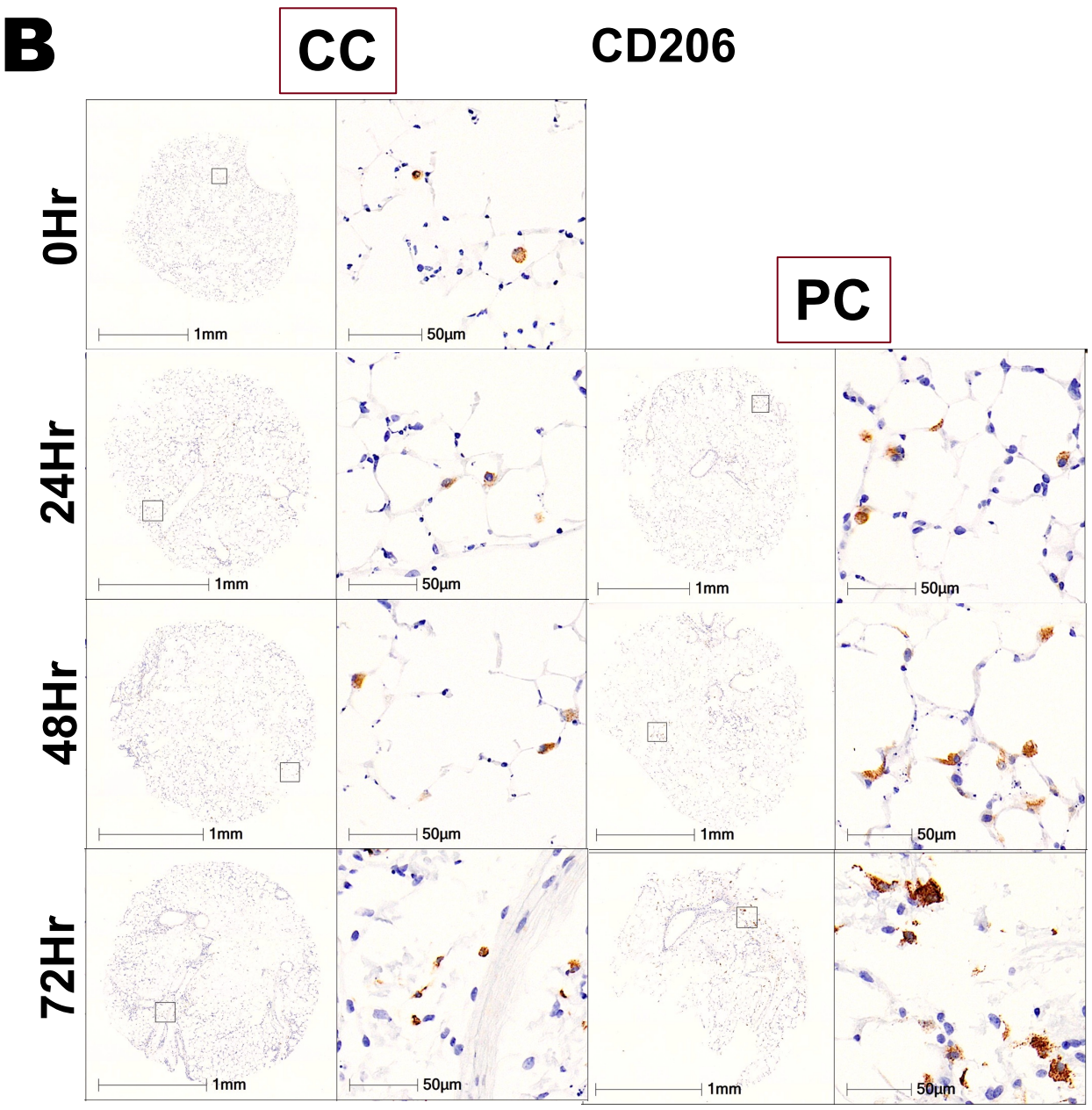
B
CC
CD206
PC
0Hr
24Hr
48Hr
72Hr
1mm
50µm

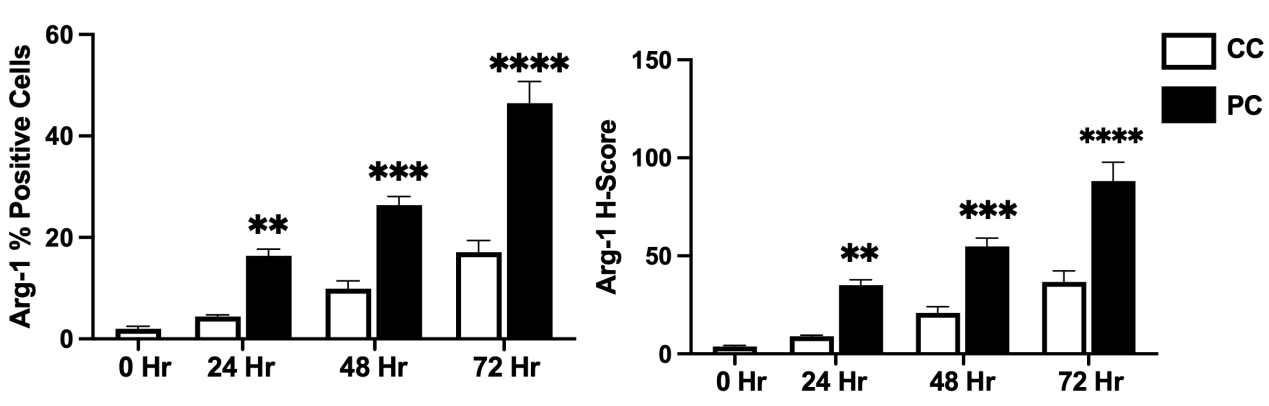
C
Arg-1 Cell Positivity
Arg-1 % Positive Cells
0 Hr
24 Hr
48 Hr
72 Hr
**
***
****

Arg-1 Staining Intensity
Arg-1 H-Score
CC
PC
**
***
****

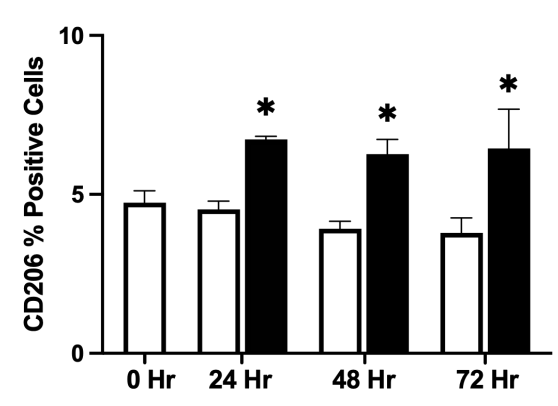
D
CD206 Cell Positivity
CD206 % Positive Cells
*

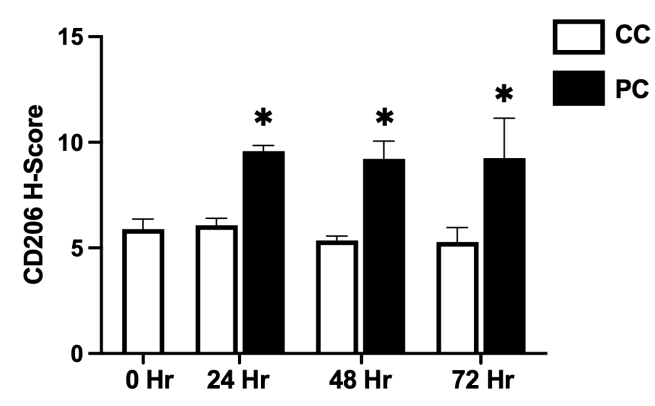
CD206 Staining Intensity
CD206 H-Score
CC
PC
*

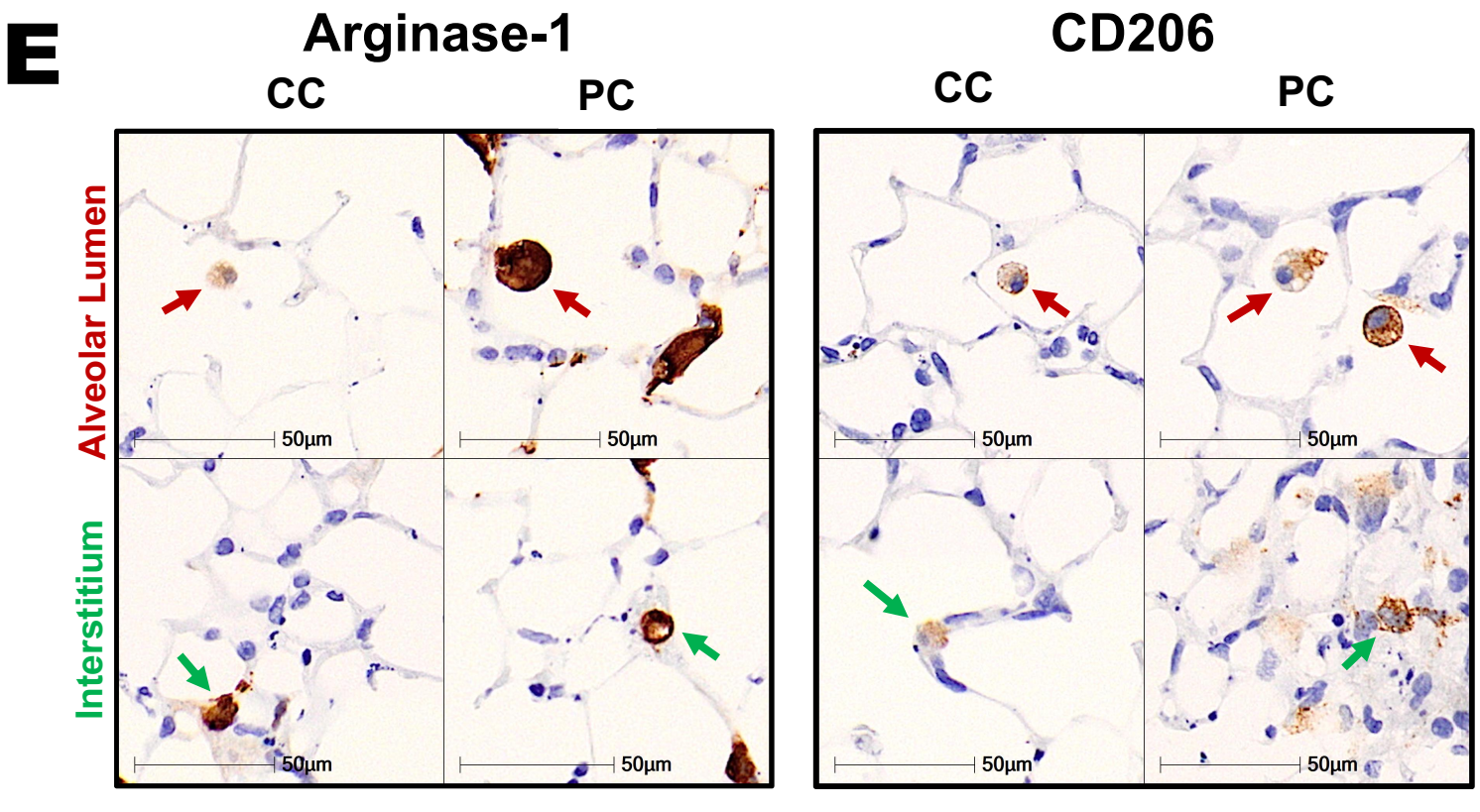
E
Arginase-1
CD206
CC
PC
Alveolar Lumen
Interstitium
50µm

Figure 4. Histological Markers Characteristic of Profibrotic Macrophages are Increased Throughout Polarization Time course. (A) Representative images of Arginase-1 immunohistochemical (IHC) staining in CC- and PC-treated PCLS throughout time course. **(B)** Representative images of CD206 IHC staining in CC- and PC-treated PCLS throughout time course. **(C)** HALO quantification of Arginase-1 cell positivity and staining intensity (H-Score). **(D)** HALO quantification of CD206 cell positivity and staining intensity (H-Score). **(E)** Arginase-1 and CD206 expression in macrophages located in both the alveolar lumen and interstitium, indicated by red and green arrows, respectively (72-hour timepoint). (n=3 mice, 3-4 slices per condition). * indicates $P<0.05$; *** indicates $P<0.001$; and **** indicates $P<0.001$; where * represents a significant difference between the two treatment groups at the respective timepoint. Data are displayed as mean ± S.E.M.

Figure 5

A Arg1⁺CD206⁺ Macrophages

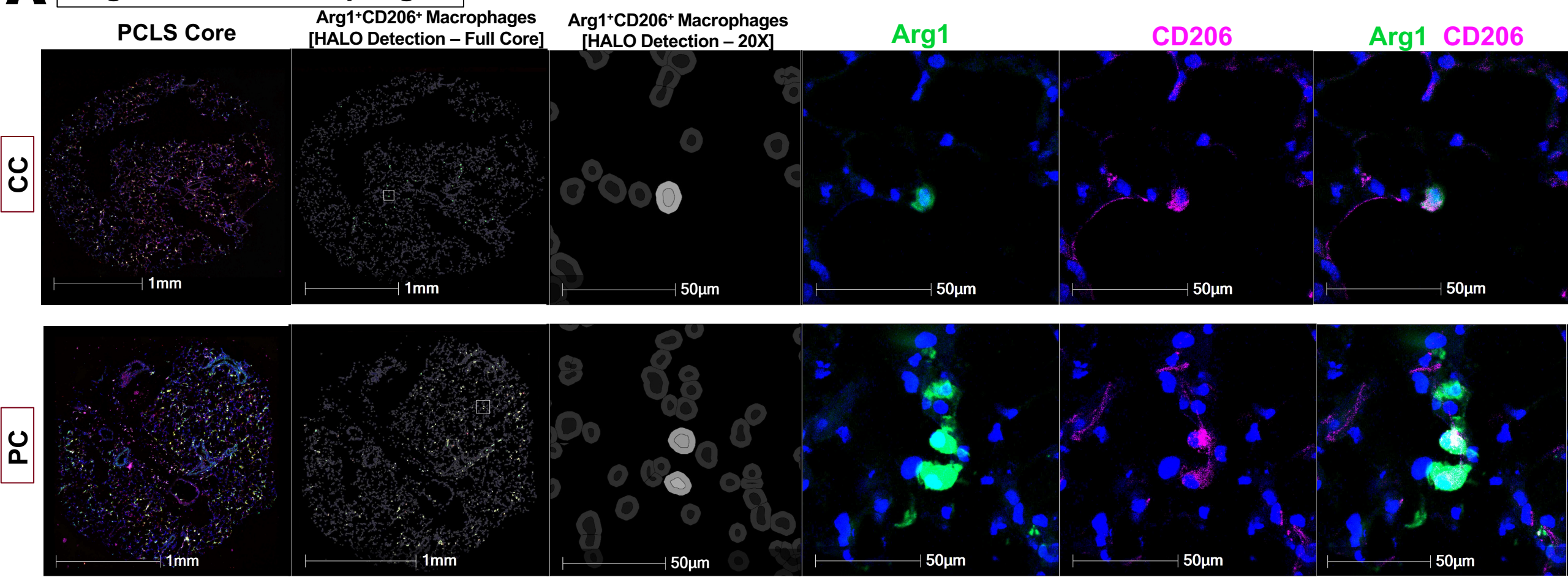

Arg1⁺CD206⁺ Macrophages=
CD45⁺CD68⁺CD11c⁺Arg1⁺CD206⁺

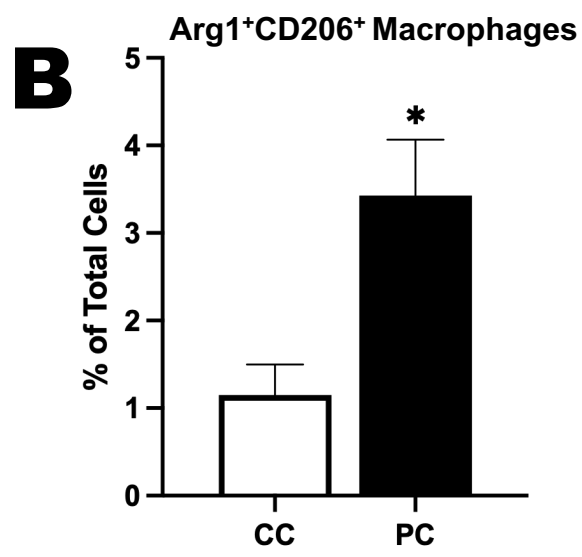

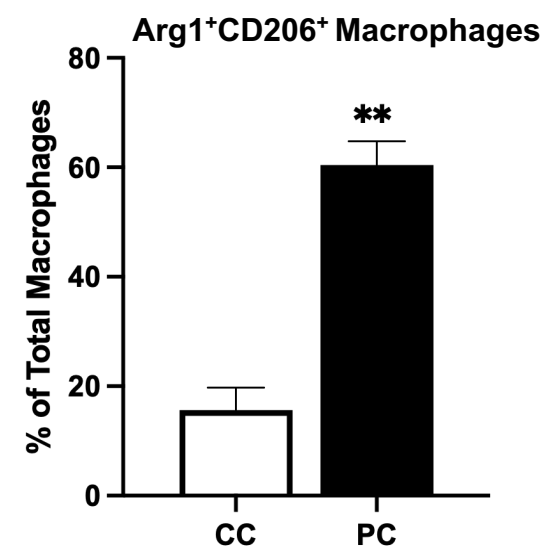

D Arg1⁺CD206⁺ Interstitial Macrophages

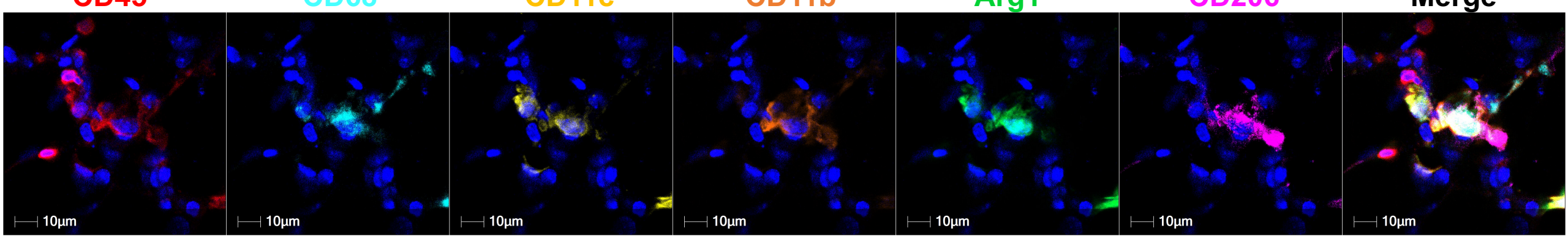

E Arg1⁺CD206⁺ Alveolar Macrophages

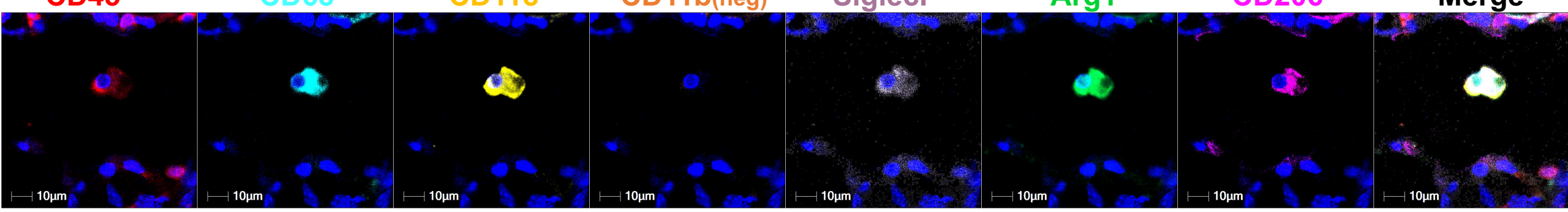

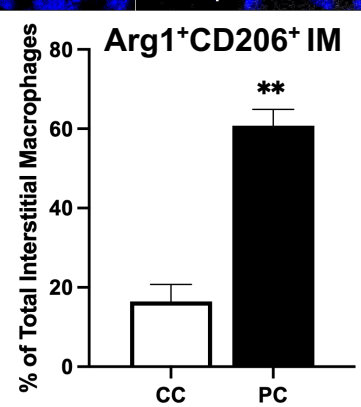

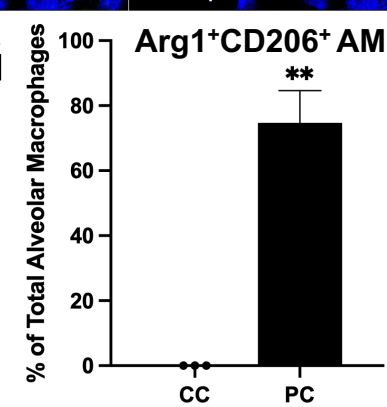

Figure 5. PC Induces Polarization in Both Interstitial and Alveolar Macrophages, as Determined by Highly Multiplexed Staining (IBEX) to Assess Macrophage Phenotype in PCLS. (A) Confocal fluorescent images of fixed-frozen multiplex stained (IBEX) PCLS treated with the CC and PC (48-hour timepoint). Markup for HALO detection of $Arg1^{+}CD206^{+}$ profibrotic macrophages (defined as $CD45^{+}CD68^{+}CD11c^{+}Arg1^{+}CD206^{+}$ cells) , as well as 20X representative images of Arginase-1 (green) and CD206 (magenta) staining in these cells, are shown. Cell nuclei are stained with DAPI (blue). **(B,C)** HALO quantification of $Arg1^{+}CD206^{+}$ profibrotic macrophages in CC- and PC-treated PCLS, expressed as percent of total cells and percent of total macrophages (n=3 mice). (**D,E)** Representative images of staining panels for $Arg1^{+}CD206^{+}$ interstitial macrophages (IM) (defined as $CD45^{+}CD68^{+}CD11c^{+}CD11b^{+}Arg1^{+}CD206^{+}$ cells) and $Arg1^{+}CD206^{+}$ alveolar macrophages (AM) (defined as $CD45^{+}CD68^{+}CD11c^{+}CD11b^{-}SiglecF^{+}Arg1^{+}CD206^{+}$ cells) in PCLS. Cell nuclei are stained with DAPI (blue). **(F)** HALO quantification $Arg1^{+}CD206^{+}$ IM, expressed as percent of total IM. **(G)** HALO quantification $Arg1^{+}CD206^{+}$ AM, expressed as percent of total AM. (n=3 mice). * indicates $P<0.05$; and ** indicates $P<0.01$; where * represents a significant difference between the two treatment groups. Data are displayed as mean ± S.E.M.

Figure 6

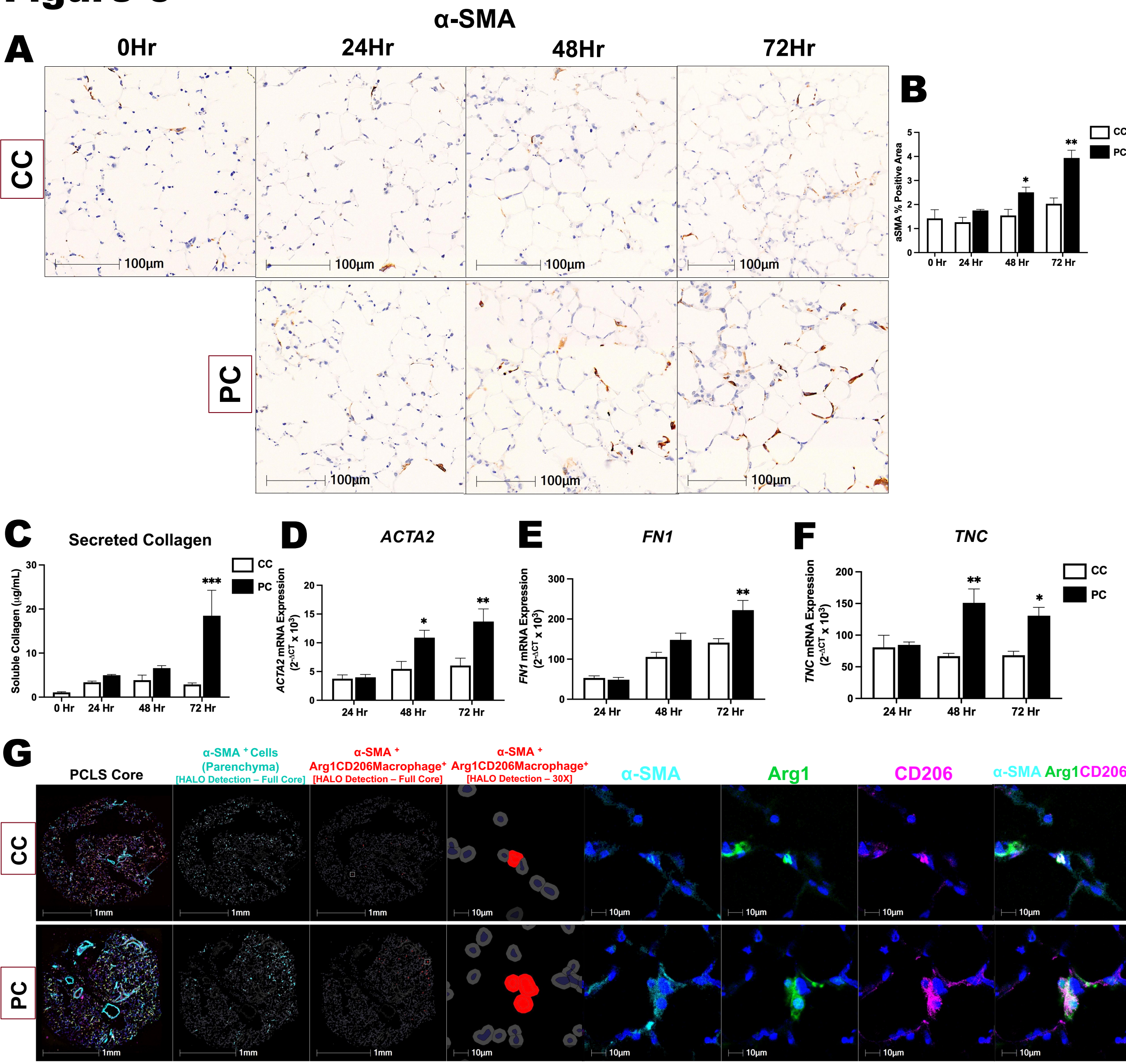
A
α-SMA
0Hr
24Hr
48Hr
72Hr
CC
PC
100µm
B
aSMA % Positive Area
CC
PC
0 Hr
24 Hr
48 Hr
72 Hr
C
Secreted Collagen
Soluble Collagen (µg/mL)
D
ACTA2
ACTA2 mRNA Expression
E
FN1
FN1 mRNA Expression
F
TNC
TNC mRNA Expression
G
PCLS Core
α-SMA + Cells (Parenchyma)
[HALO Detection – Full Core]
α-SMA + Arg1CD206Macrophage+
[HALO Detection – Full Core]
α-SMA + Arg1CD206Macrophage+
[HALO Detection – 30X]
α-SMA
Arg1
CD206
α-SMA Arg1CD206
1mm
10µm
H
α-SMA +Arg1+CD206+ Cells
% of aSMA+ Cells

Figure 6. Expression of Extracellular Matrix and Fibrotic Markers in PCLS Treated with PC. (A) α-SMA IHC staining in CC- and PC-treated PCLS throughout time course. **(B)** HALO quantification of α-SMA positive parenchymal area (n=3 mice, 3-4 slices per condition). **(C)** Secreted soluble collagen in PCLS supernatant measured with Sircol Soluble Collagen Assay (n=3 mice). **(D,E,F)** Normalized gene expression of α-SMA (*ACTA2*), Fibronectin (*FN1*) and Tenascin-C (*TNC*) in PCLS tissue, relative to *GAPDH* (n=3 mice, 6 slices pooled per condition). **(G)** Confocal fluorescent images of multiplex stained (IBEX) PCLS treated with the CC and PC (48-hour timepoint). Markup for HALO detection of α-SMA+ cells (parenchyma), and cells that co-express α-SMA and markers for $Arg1^{+}CD206^{+}$ macrophages, is shown. 30X magnification images (CC- and PC-treated PCLS) of α-SMA (turquoise), Arg1 (green) staining, and CD206 (magenta) staining are also shown. Cell nuclei are stained with DAPI (blue). **(H)** HALO quantification of α-SMA and $Arg1^{+}CD206^{+}$ profibrotic macrophage marker co-expression in CC- and PC-treated PCLS, expressed as percent of $\alpha\text{-SMA}^{+}$ cells in the parenchyma (n=3 mice). * indicates $P<0.05$; ** indicates $P<0.01$; and *** indicates $P<0.001$; where * represents a significant difference between the two treatment groups at the respective timepoint. Data are displayed as mean ± S.E.M.

Figure 7

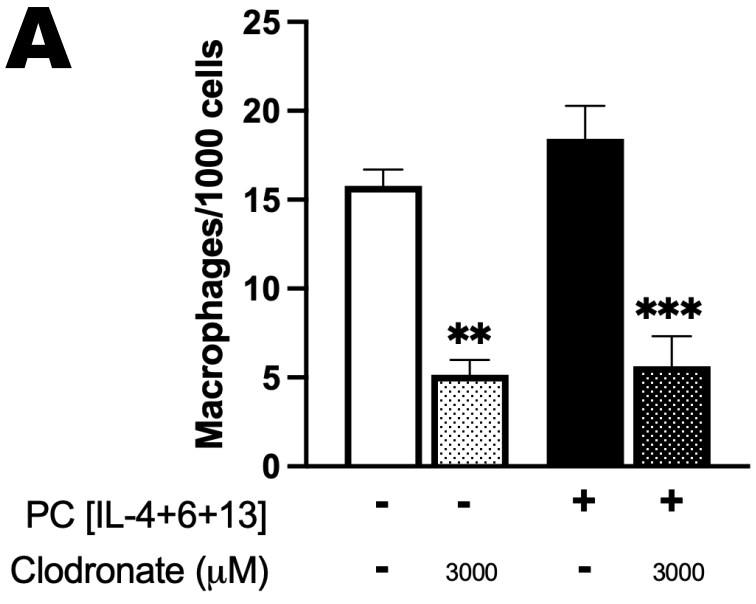
A
Macrophages/1000 cells
25
20
15
10
5
0
**
***
PC [IL-4+6+13]
Clodronate (μM)
- - + +
- 3000 - 3000

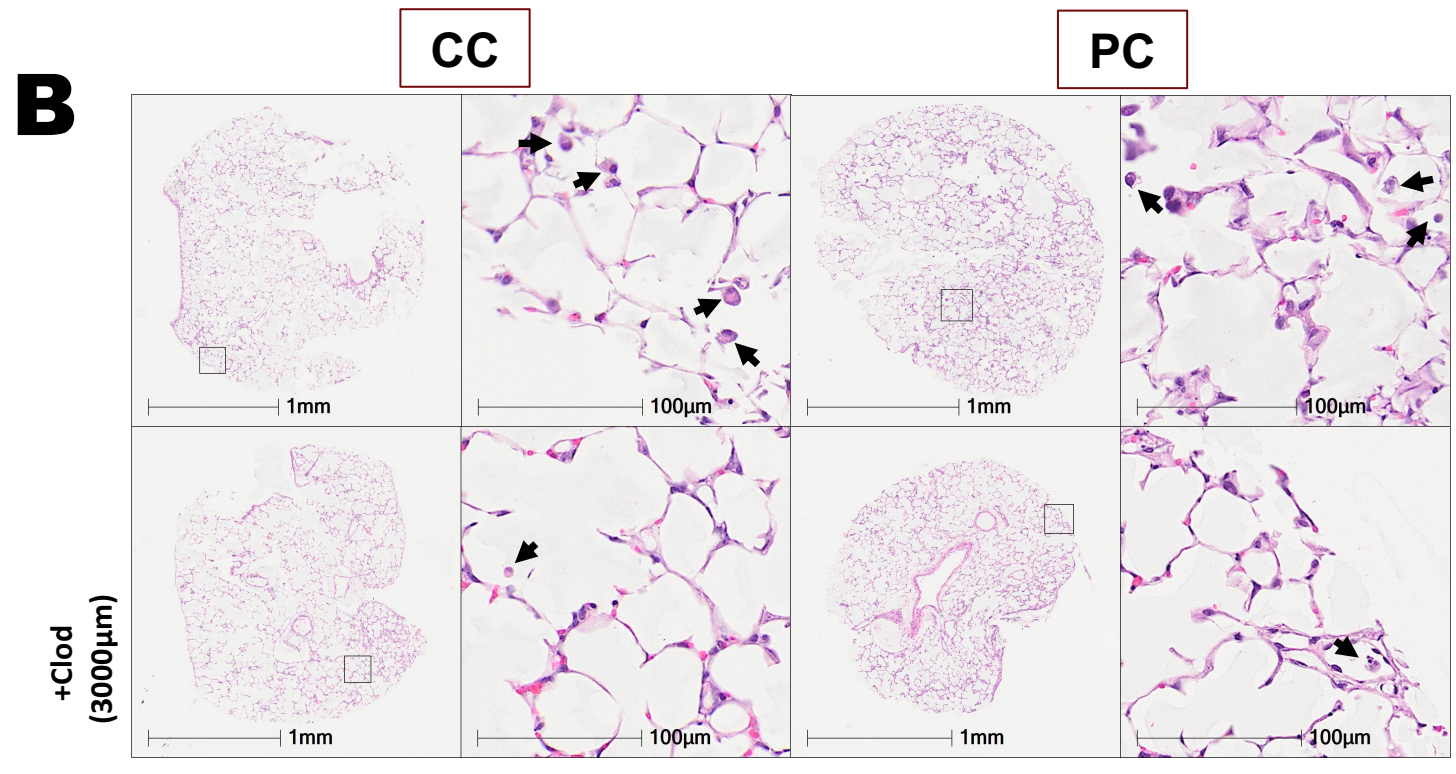
B
CC
PC
+Clod (3000μm)
1mm
100μm

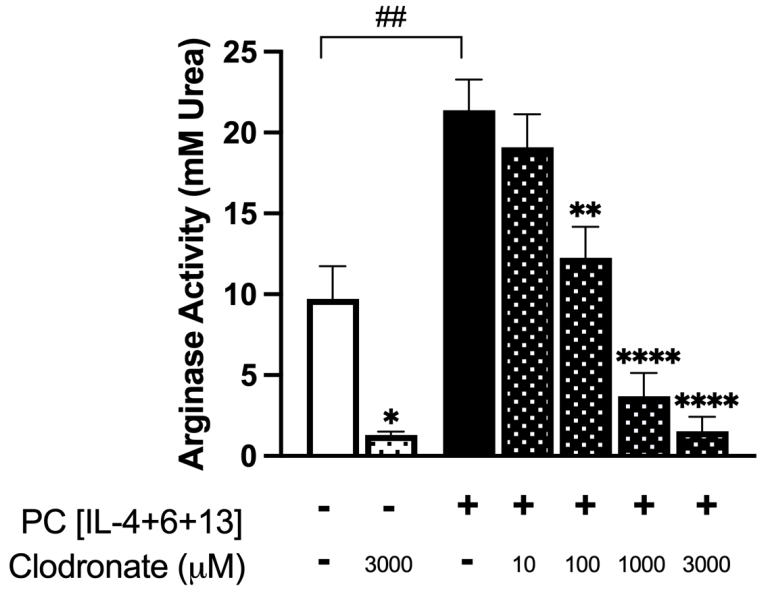
C
Arginase Activity
Arginase Activity (mM Urea)
##
*
**
****
PC [IL-4+6+13]
Clodronate (μM)
- - + + + + +
- 3000 - 10 100 1000 3000

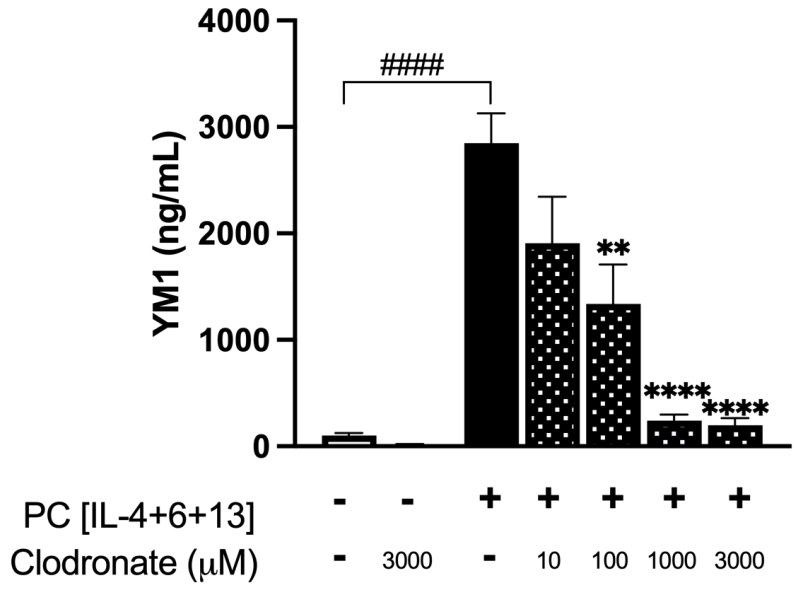
D
Secreted YM1
YM1 (ng/mL)
4000
3000
2000
1000
0
####
**
****
PC [IL-4+6+13]
Clodronate (μM)
- - + + + + +
- 3000 - 10 100 1000 3000

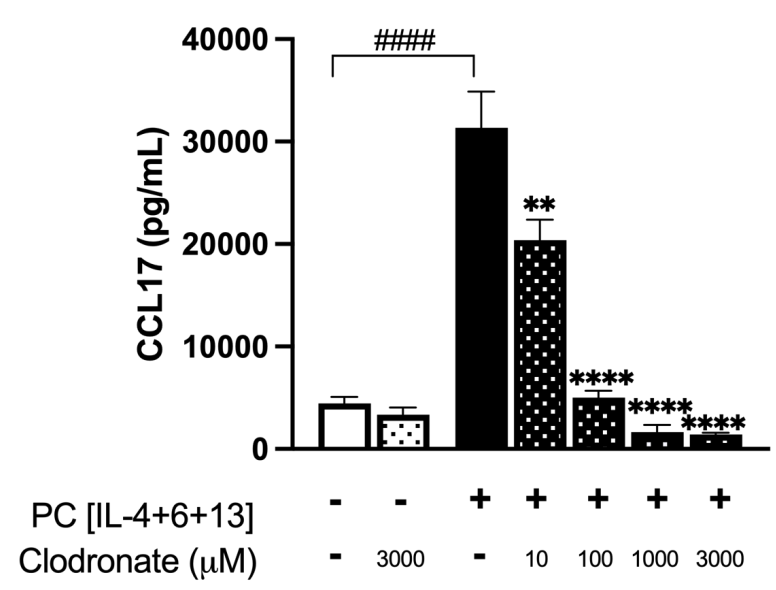
E
Secreted CCL17
CCL17 (pg/mL)
40000
30000
20000
10000
0
####
**
****
PC [IL-4+6+13]
Clodronate (μM)
- - + + + + +
- 3000 - 10 100 1000 3000

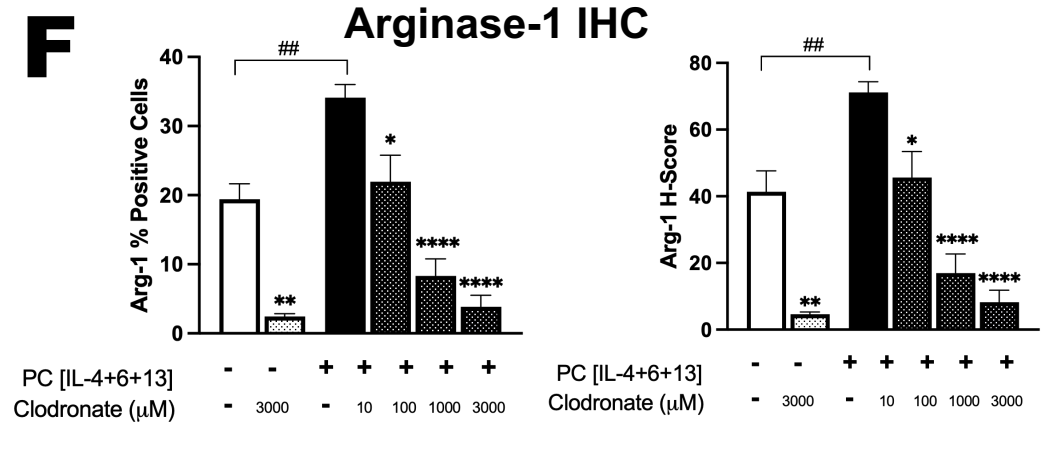
F
Arginase-1 IHC
Arg-1 % Positive Cells
Arg-1 H-Score
##
*
**
****
PC [IL-4+6+13]
Clodronate (μM)
- - + + + + +
- 3000 - 10 100 1000 3000

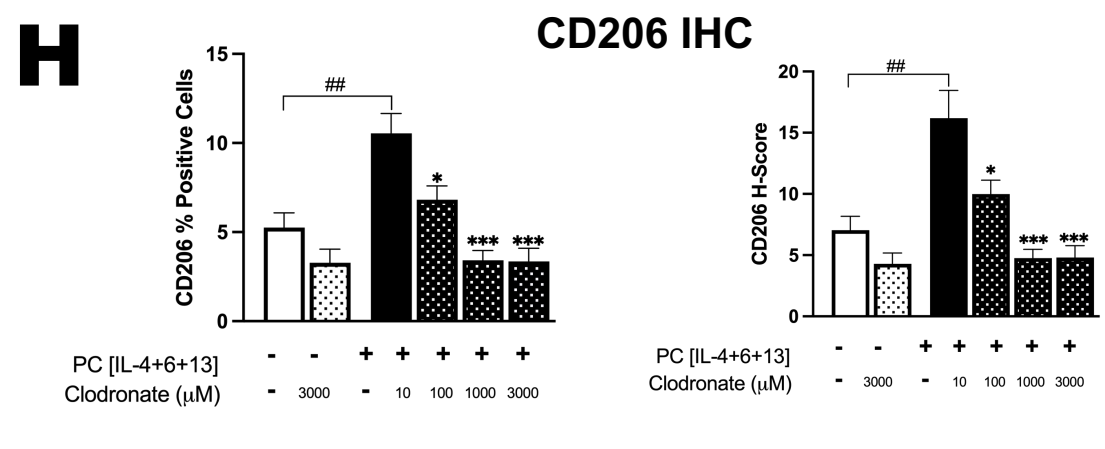
H
CD206 IHC
CD206 % Positive Cells
CD206 H-Score
##
*
***
PC [IL-4+6+13]
Clodronate (μM)
- - + + + + +
- 3000 - 10 100 1000 3000

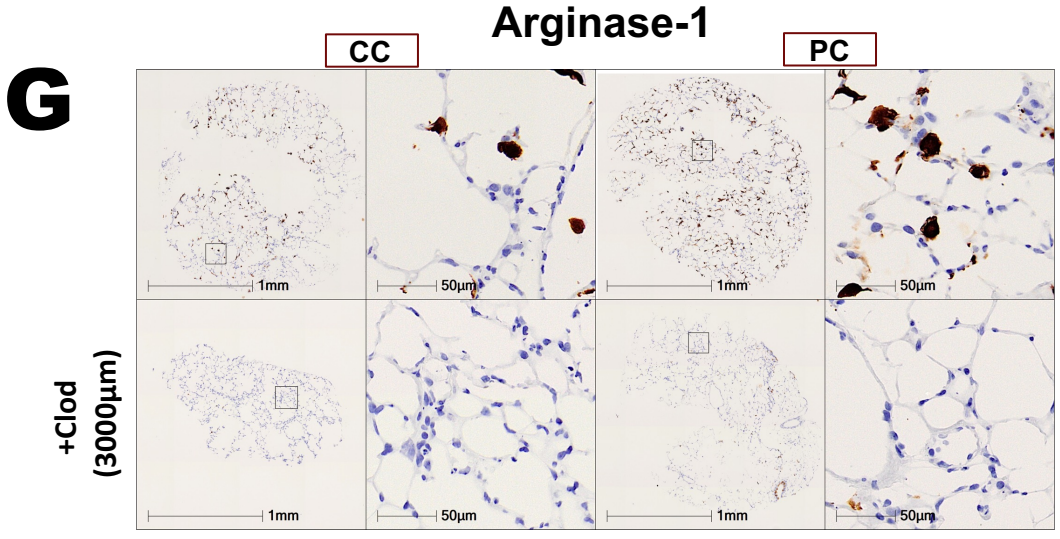
G
Arginase-1
CC
PC
+Clod (3000μm)
1mm
50μm

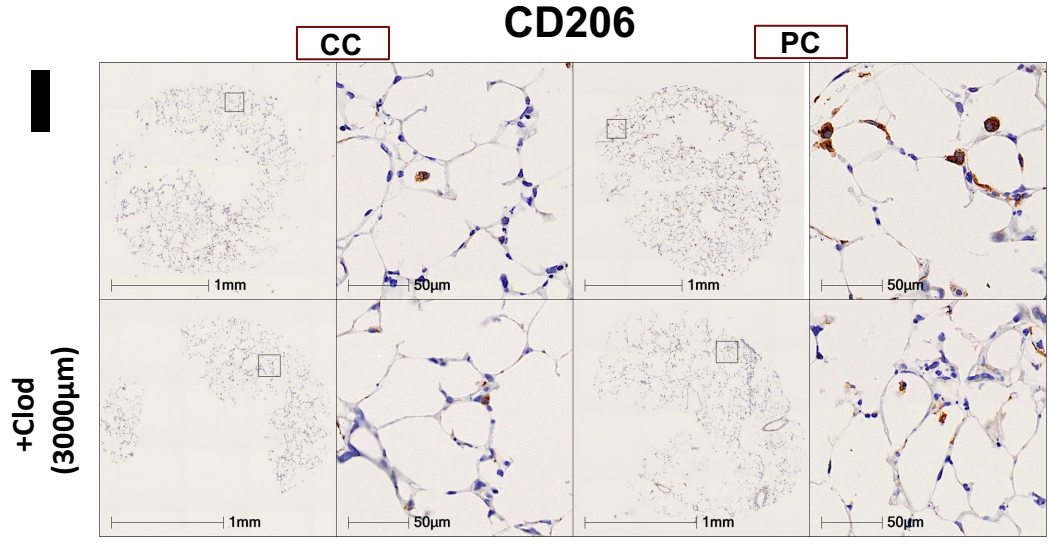
I
CD206
CC
PC
+Clod (3000μm)
1mm
50μm

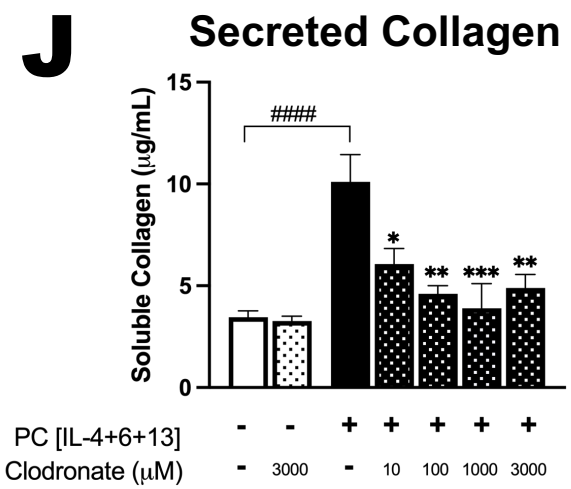
J
Secreted Collagen
Soluble Collagen (μg/mL)
####
*
**
***
PC [IL-4+6+13]
Clodronate (μM)
- - + + + + +
- 3000 - 10 100 1000 3000

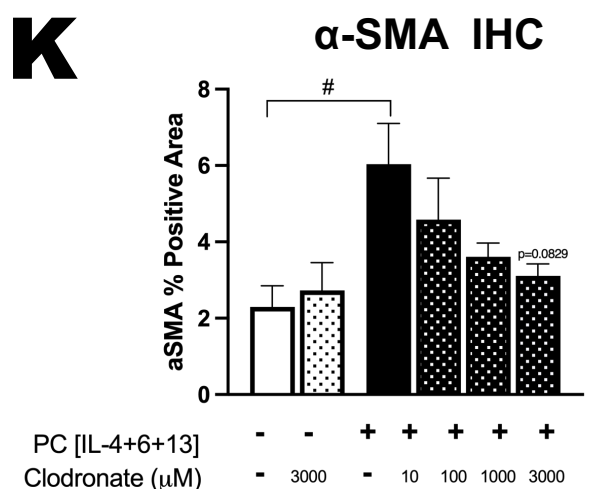
K
α-SMA IHC
aSMA % Positive Area
#
p=0.0829
PC [IL-4+6+13]
Clodronate (μM)
- - + + + + +
- 3000 - 10 100 1000 3000

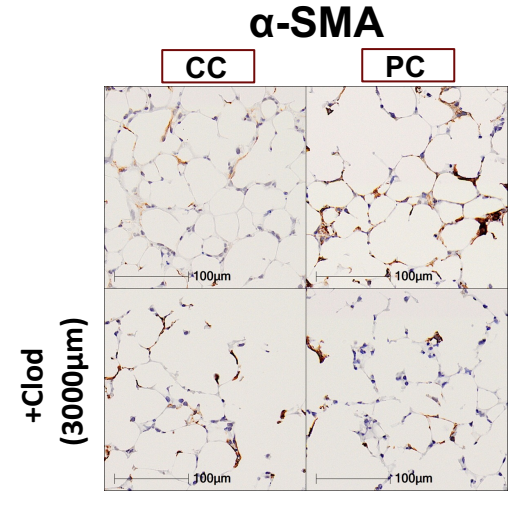
L
α-SMA
CC
PC
+Clod (3000μm)
100μm

Figure 7. Clodronate Treatment Diminishes Effects of PC on Profibrotic Macrophage Readouts. PCLS were pre-treated with liposomal clodronate for 24 hours, followed by 48 hours in culture +/- PC. **(A)** Macrophage quantity per 1000 cells in PCLS, determined by counting visible alveolar macrophages in H&E stained tissue (n=3). **(B)** H&E images of CC- and PC-treated PCLS, +/- clodronate pre-treatment. Black arrows point to alveolar macrophages. **(C)** Arginase activity in PCLS homogenates treated with CC or PC, +/- clodronate pre-treatment (n=3 mice, 3 slices per condition). **(D,E)** Secreted YM1 and CCL17 protein levels in PCLS supernatant measured via ELISA (n=3 mice). **(F)** HALO quantification of Arginase-1 IHC cell positivity and staining intensity (H-Score). **(G)** Representative images of Arginase-1 IHC staining in CC- and PC-treated PCLS, +/- clodronate pre-treatment. **(H)** HALO quantification of CD206 IHC cell positivity and staining intensity (H-Score). **(I)** Representative images of CD206 IHC staining in CC- and PC-treated PCLS, +/- clodronate pre-treatment. (n=3 mice, 3-4 slices per condition). **(J)** Secreted soluble collagen in PCLS supernatant measured with Sircol Soluble Collagen Assay (n=3 mice). **(K)** HALO quantification of α-SMA positive parenchymal area (n=3 mice, 3-4 slices per condition). **(L)** Representative images of α-SMA IHC staining in CC- and PC-treated PCLS, +/- clodronate pre-treatment. *,# indicates $P<0.05$; **,## indicates $P<0.01$; *** indicates $P<0.001$; and ****,#### indicates $P<0.0001$; where * represents a significant difference between the clodronate pre-treated groups (patterned bars) and their respective CC or PC control group (solid-colored bars), and # represents a significant difference between the CC and PC groups (solid-colored bars). Data are displayed as mean ± S.E.M.

SUPPLEMENTARY MATERIAL

Supplementary Table 1: Antibody Information for FFPE IHC

Target Name	Clone	Host Species	Supplier	Catalog Number
α-SMA	1A4	Mouse	Agilent Dako	M0851
Arginase-1	D4E3M	Rabbit	Cell Signaling Technology	Cs93668
CD206	-	Rabbit	Abcam	ab64693

Supplementary Table 2: Antibody Information for IBEX

Target Name	Clone	Host Species	Supplier	Catalog Number	Fluorophore
α-SMA	1A4	Mouse	Invitrogen	M0851	eFluor660
Arginase-1	D4E3M	Rabbit	Cell Signaling Technology	Cs93668	-
CD11b	M1/70	Rat	BD Biosciences	557397	PE
CD11c	N418	Hamster	Invitrogen	MCD11C20	AF488
CD206	C068C2	Rat	BioLegend	141709	AF488
CD45	30-F11	Rat	BioLegend	103144	AF594
CD68	FA-11	Rat	BioLegend	137004	AF647
Siglec F	E50-2440	Rat	BD Biosciences	552126	PE
Anti-Rabbit	-	Goat	Invitrogen	A11008	AF488

Supplementary Table 3: Taqman PCR Primer Information

Gene	Catalog # (ThermoFisher Scientific)
ACTA2	Mm01546133_m1
Arg1	Mm00475988_m1
Chil3	Mm00657889_mH
FN1	Mm01256744_m1
GAPDH	Mm99999915_g1
MRC1	Mm00485148_m1
Tnc	Mm00495662_m1

Supplementary Table 4: Troubleshooting Issues in Generation of Murine PCLS

Issue	Potential Reasons	Solutions
Uneven filling of lung lobes	• Premature gelling of agarose in proximal airways	• Ensure LMP agarose is at a temperature of 40°C (no less than 37°C) directly prior to infiltration[1] • Utilize heating pad and/or heat lamp to keep mouse body warm[1] • Pour warm (37°C) HBSS on lungs directly prior to infiltration[1] • Inject bolus of air (~0.2mL) into lungs to push agarose into distal airways[1]
Lungs are not fully inflated after agarose infiltration	• Premature gelling of agarose in proximal airways	• See above[1]
	• Too small of volume of agarose used for infiltration	• Inject volume equivalent to total lung capacity of mouse (~1mL-1.3mL, depending on size of animal)[2]
Agarose leakage while filling lung	• Premature gelling of agarose in proximal airways, leading to blockage and subsequent rupture/damage	• See above[1]
	• Infiltration volume exceeded total lung capacity	• See above[2]
Agarose leakage after filling lung	• Canula and/or syringe removed before agarose fully solidified	• Leave canula and syringe in place while mouse body is on ice and agarose fully solidifies (30 minutes)
	• Canula loose and/or ligature not secured tightly enough	• Ensure depth of canula insertion in the trachea is not too shallow. Secure tightly with double-knotted ligature
Tissue is not being sliced by vibratome	• Inadequate infiltration of lungs with agarose	• See above[1,2]
	• Tissue is not properly secured to vibratome specimen holder	• Ensure bottom side of tissue is completely glued to specimen holder. Do not allow glue to touch anywhere else on tissue
Tissue tearing while slicing	• Lung tissue is overfilled with agarose	• See above[2]
	• Inappropriate vibratome speed and/or oscillation	• Lower vibratome speed and/or raise oscillation

Supplementary Figure 1: RNA Extraction Quantity and Quality Measures from Murine PCLS

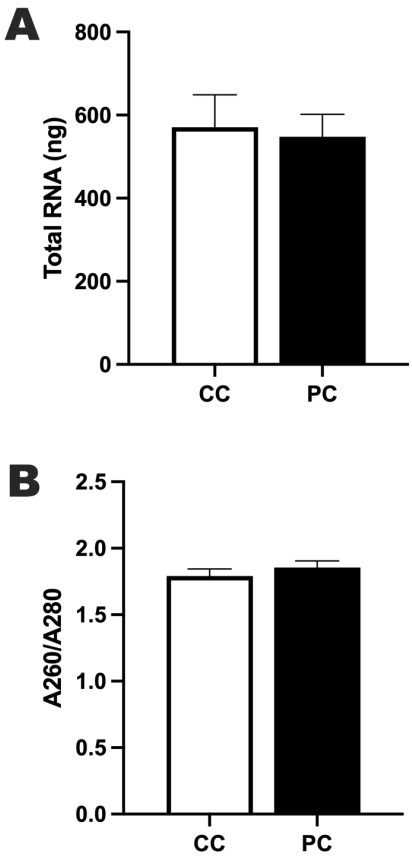

Figure S1. RNA Extraction Quantity and Quality Measures from Murine PCLS. Six PCLS (4mm diameter) were pooled for each sample. **(A)** Total RNA extracted from each sample. **(B)** A260/A260 ratio. n=18 PCLS from 3 mice. Results represent mean ± S.E.M. with samples taken from all timepoints.

Supplementary Figure 2: Ki-67 Immunohistochemical Staining Throughout Polarization Time Course

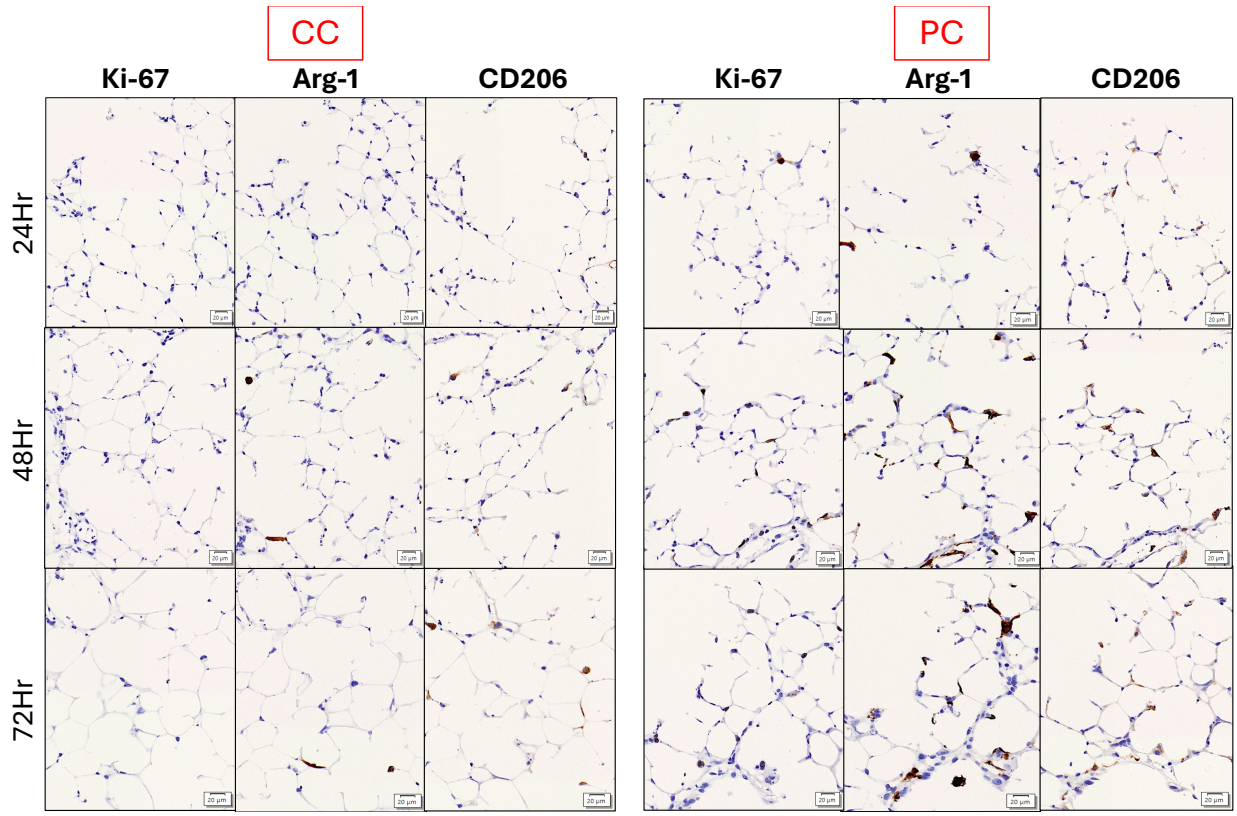

Figure S2. Immunohistochemical staining on serial slide sections throughout polarization time course. Representative images of serial sections of CC- and PC-treated PCLS stained with Ki-67, Arginase-1 and CD206.

CHAPTER 4

Highly Multiplexed Imaging for Cellular Phenotyping in Murine Precision-Cut Lung Slices Using Iterative Bleaching Extends Multiplexity (IBEX)

Megan Vierhout, Mouhanad Babi, Joao Bronze de Firmino, Andrea Radtke, Ziv Yaniv, Martin R.J. Kolb, Joshua F. Koenig*, Kjetil Ask*

This chapter contains an invited submission on our developed protocol for cellular phenotyping in precision-cut lung slices using highly multiplexed imaging (IBEX). This complements the work presented in chapter 3, and delves deeper into the specifics of the protocol. Although IBEX has been shown to work on a multitude of organs, tissues, and species, to our knowledge it has not previously been reported in cultured *ex vivo* organ slices, which adds to the novelty of the paper. Although cellular phenotyping in PCLS and other *ex vivo* organ slice models is critical for understanding the disease-like features of these systems, this has been traditionally challenging due to the interference of agarose and relatively small tissue mass. This hinders the overall ability to comprehensively assess effects of stimulated responses and treatments. Here, we present a protocol for immunophenotyping in PCLS using IBEX, demonstrating its utility and application through our work on assessing profibrotic pulmonary macrophage phenotype. This platform has high potential for versatility and can be applied to *ex vivo* cultured slices from other organ systems.

Author Contributions:
MV: conceptualization, methodology, formal analysis, investigation, writing – original draft, writing – review & editing; **MB**: methodology, software, writing – original draft; **JBdF**: methodology; **AR**: methodology, resources; **ZY:** methodology, resources; **MK:** supervision, funding acquisition, resources; **JFK**: supervision, resources, methodology; **KA:** conceptualization, supervision, project administration, funding acquisition, resources.

To be submitted to STAR (invited)

Highly Multiplexed Imaging for Cellular Phenotyping in Murine Precision-Cut Lung Slices Using Iterative Bleaching Extends Multiplexity (IBEX)

Megan Vierhout[1,2,8]*, Mouhanad Babi[3], Vitoria M. Olyntho[2,4], Andrea J. Radtke[5], Ziv Yaniv[6], Martin R.J. Kolb[1,2], Kjetil Ask[1,2,7]**, Joshua F.E. Koenig[2,4,7,9]***

Affiliations:

[1]Firestone Institute for Respiratory Health, The Research Institute of St. Joe's Hamilton, Department of Medicine, McMaster University, Hamilton, ON, Canada

[2]McMaster Immunology Research Centre, Department of Medicine, McMaster University, Hamilton, ON, Canada

[3]McMaster Centre for Advanced Light Microscopy, McMaster University, Hamilton, ON, Canada

[4]Schroeder Allergy and Immunology Research Institute, Faculty of Health Sciences, McMaster University, Hamilton, ON, Canada

[5]Center for Advanced Tissue Imaging, Laboratory of Immune System Biology, National Institute of Allergy and Infectious Diseases, National Institutes of Health, Bethesda, MD, USA

[6]Bioinformatics and Computational Bioscience Branch, National Institute of Allergy and Infectious Diseases, National Institutes of Health, Bethesda, MD, USA

[7]These authors contributed equally and share senior authorship

[8]Technical contact

[9]Lead contact

*Correspondence: vierhom@mcmaster.ca

**Correspondence: askkj@mcmaster.ca

***Correspondence: koenigjf@mcmaster.ca

HIGHLIGHTS

- Pipeline for detailed cellular immunophenotyping in *ex vivo* cultured precision-cut lung slices (PCLS)
- Fixation, preservation, staining, and imaging of cultured PCLS for high-quality quantitative multiplex microscopy
- Application of iterative staining and bleaching with IBEX to maximize marker quantity
- Techniques to increase throughput and conserve time
- Tunable to various cell types and treatment conditions. Expandable to *ex vivo* slices from other organs

SUMMARY

Ex vivo precision-cut lung slices (PCLS) serve as a translational model for investigating mechanisms related to lung disease, however capacity for comprehensive cellular phenotyping is limited. Here, we present a protocol for immunophenotyping in PCLS using Iterative Bleaching Extends Multiplexity (IBEX). We specifically assess pulmonary macrophage phenotype in murine PCLS following culture with a cytokine cocktail to induce profibrotic programming. We include details for the complete pipeline for fixed-frozen sample preparation, cryosectioning, blocking, staining, microscopy, bleaching, and image quantification.

For complete details on the use, execution, and application of this protocol, please refer to Vierhout et al. (2024).[1]

GRAPHICAL ABSTRACT

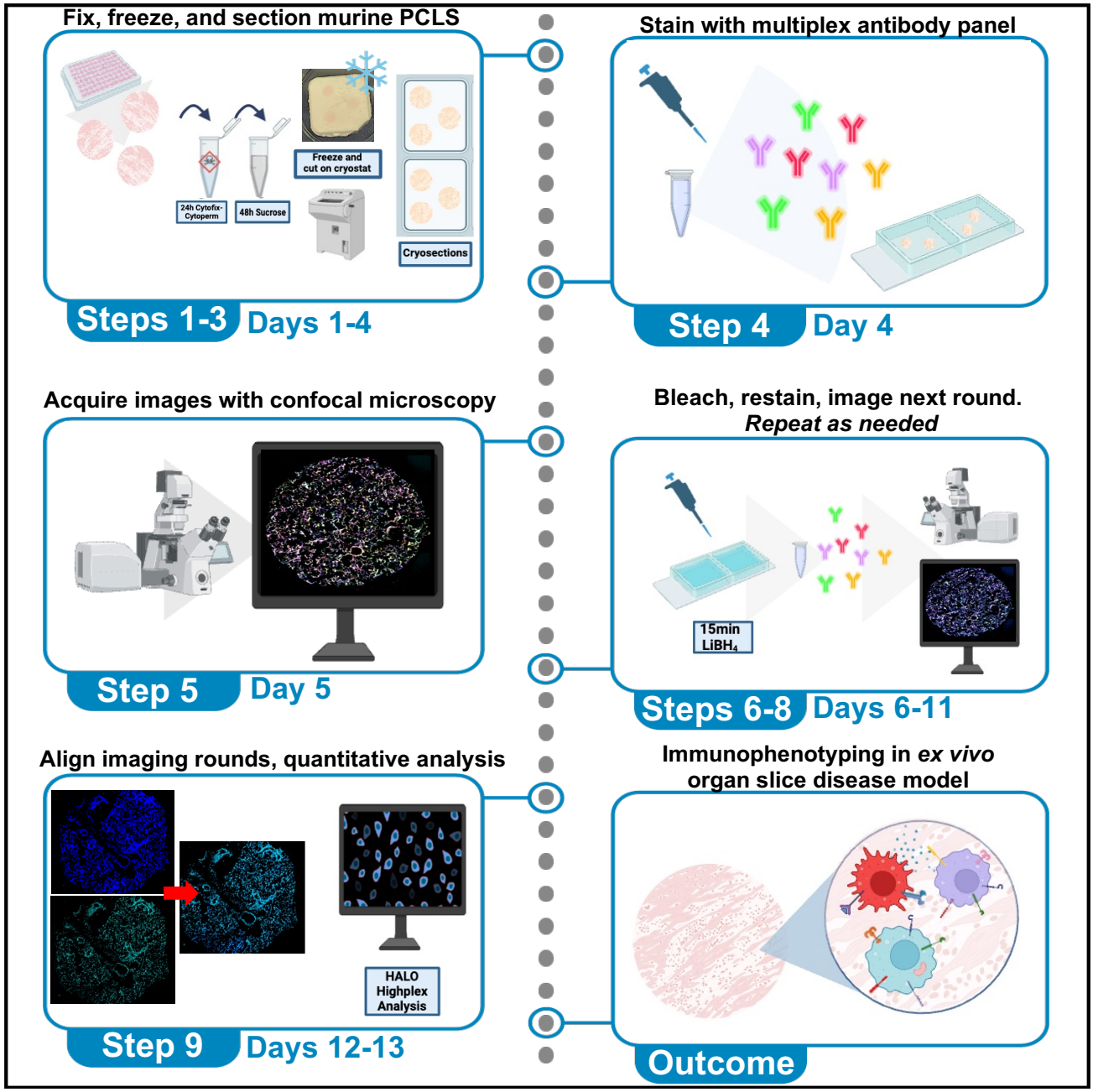

BEFORE YOU BEGIN

We present a protocol for immunophenotyping in PCLS using IBEX – an open-source method for high-content immunostaining and imaging.[2,3] We present a protocol for using IBEX on PCLS generated from C57Bl/6 mice (500μM thickness, 2mm diameter) to evaluate macrophage phenotype following *ex vivo* culture with a profibrotic polarization cocktail, as previously described.[1] PCLS contain all pulmonary cell types and avoid the need for scientist-made artificial recapitulation of the lung, as they maintain the lung's natural cellular interactions, microenvironment, and architecture.[4] The utilization of such biologically-translational models is highly useful to study plastic, phenotypically-diverse cells like macrophages, which are believed to be key players in multiple respiratory diseases including fibrosis.[5,6] Macrophages are highly interactive and dynamically respond to their microenvironment, and so their activation states are limitedly reproduced in monoculture systems grown on plastic.[7–9] An *ex vivo* approach allows for the flexibility to induce disease-like states with endless options for stimuli, and so a comprehensive understanding of the induced cellular phenotype is required to establish robust systems. However, the small tissue mass of PCLS and requirement to fill the lung tissue with agarose prior to slicing pose challenges for various downstream applications including RNA isolation and flow cytometry.[10] This limits the capacity for cellular phenotyping in PCLS, and thus hinders the overall ability to comprehensively assess effects of stimulated responses and treatments, for which understanding is critical in in disease-model systems. In order to overcome this challenge, as well as confirm that the profibrotic macrophage markers we observed through supernatant, lysate, and traditional brightfield

immunohistochemistry assays[1] were indeed being induced in macrophage-specific cells in the lung, we performed cellular phenotyping with a panel of commercially-available antibodies using IBEX. Using HALO image analysis platform, we performed a quantitative evaluation to compare control and profibrotic cocktail-treated PCLS. Additionally, as alveolar and interstitial macrophages are both thought to play important roles in lung fibrosis, we dove deeper into phenotyping and examined these subpopulations using the markers in our panel. IBEX has proven useful for multiplex immunostaining of multiple organs, tissue types and species,[2,3] however, to our knowledge its application has not been previously reported in *ex vivo* cultured organ slices. This platform is highly tunable to various antibody marker panels and treatment conditions, and can be applied to *ex vivo* cultured slices from other organ systems and species. A repository of IBEX-validated antibodies can be found in the public IBEX Knowledge Base.[11]

Institutional permissions

All procedures involving animals were approved by the McMaster Animal Research Ethics Board (AUP# 23-19), and were performed in accordance with the guidelines of the Canadian Council on Animal Care (CCAC). Ensure required ethics approvals from relevant institutions are obtained prior to beginning the work.

PCLS preparation

Timing: 1 day, 1.5 to 2 hours per mouse to slice all 5 lung lobes

1. Generate PCLS using fresh murine lung tissue, according to previous protocol.[1]
    a. Sacrifice mice, cannulate trachea, and inflate lung with agarose.

b. Slice lung tissue using Compresstome vibrating microtome, or available precision tissue slicing apparatus (500µM thickness).

c. Using manual coring tool, punch 2mm cores from full lobe slices.

2. Once slicing and coring is complete, leave PCLS to normalize overnight in culture medium in incubator (37°C, 5% CO_2), prior to beginning any treatment/stimulation.

Note: Detailed methods and troubleshooting guide on PCLS generation can be found in Vierhout et al.[1]

Culture and stimulation of PCLS

Timing: 24 to 72 hours

3. Culture PCLS with polarization cocktail to stimulate profibrotic programming of macrophages, according to previous protocol.[1]

a. Treat PCLS with polarization cocktail (IL-4+IL-6+IL-13) in culture medium. Culture 1 PCLS per well in a 96-well plate.

Note: We have previously tested macrophage polarization readouts at various time points (24, 48, and 72 hours). For this experiment, PCLS were cultured for 48 hours. Select culture time based on desired outcomes.

Preparation of buffers for fixation and cryoprotection

Timing: 10 minutes

4. Prepare fixation/permeabilization solution.

Critical: Cytofix/Cytoperm™ contains formaldehyde and is toxic. Wear gloves, lab coat, and appropriate personal protective equipment (PPE). Avoid direct contact. Only handle open containers in a fume hood.

a. Dilute Cytofix/Cytoperm™ 1:4 in 1X phosphate-buffered saline (PBS) in a 50mL conical tube.

b. Wrap outside of tube with aluminum foil to protect solution from light.

c. Store at 4°C.

5. Prepare cryoprotection solution.

a. Add sucrose (30% w/v) to 1X PBS in autoclaved 100mL glass bottle.

Note: Sucrose is slow to dissolve. Lightly swirl the capped bottle periodically until dissolved.

b. Store at 4°C.

Preparation of staining buffer

Timing: 10 minutes

6. Prepare Triton-BSA buffer, to be used for blocking and as an antibody diluent during staining.

a. Add bovine serum albumin (BSA) to 1X PBS (1% w/v) in autoclaved 100mL glass bottle.

b. Add Triton X-100 (0.3% v/v) to BSA-PBS mixture.

Note: Triton X-100 is viscous and can be difficult to transfer by pipette. Use small syringe instead of pipette.

c. Lightly swirl capped bottle until BSA and Triton are dissolved.

d. Store at 4°C.

KEY RESOURCES TABLE

REAGENT or RESOURCE	SOURCE	IDENTIFIER
Antibodies		
Mouse aSMA eFluor660 (1:200 dilution)	Invitrogen	Cat#50-9760-82; RRID AB_2574362
Rabbit Arginase-1 (1:50 dilution)	Cell Signaling Technology	Cat#Cs93668; RRID AB_2800207
Rat CD11b PE (1:100 dilution)	BD Biosciences	Cat#557397; RRID AB_396680
Hamster CD11c AF488 (1:200 dilution)	Invitrogen	Cat#MCD11C20; RRID AB_10373244
Rat CD206 AF488 (1:100 dilution)	BioLegend	Cat#141709; RRID AB_10933252
Rat CD45 AF594 (1:20 dilution)	BioLegend	Cat#103144; RRID AB_2563458
Rat CD68 AF647 (1:100 dilution)	BioLegend	Cat#137004; RRID AB_2044002
Rat Siglec F PE (1:50 dilution)	BD Biosciences	Cat#552126; RRID AB_394341
Goat Anti-Rabbit AF488 (1:50 dilution)	Invitrogen	Cat#A-11008; RRID AB_143165
Fc Block (1:100 dilution)	BD Biosciences	Cat#553141; RRID AB_394656
Chemicals, peptides, and recombinant proteins		
Recombinant murine Interleukin 4	Peprotech	Cat#214-14
Recombinant murine Interleukin 6	Peprotech	Cat#216-16
Recombinant murine Interleukin 13	Peprotech	Cat#210-13
Cytofix/Cytoperm™	BD Biosciences	Cat#554722; RRID AB_2869010
Sucrose	Sigma-Aldrich	Cat#S0389
Triton X-100	Sigma-Aldrich	Cat#93443
DAPI (1:1000 dilution)	Invitrogen	Cat#D1306
Chrome-Alum Gelatin	Newcomer Supply	Cat#1033A
Fluoromount-G mounting medium	Southern Biotech	Cat#0100-01
Lithium Borohydride (LiBH4)	Sigma-Aldrich	Cat#222356
Optimal Cutting Temperature (OCT) Compound	Sakura	Cat#4583
Isopentane	Sigma-Aldrich	Cat#A1933

Bovine serum albumin	Sigma-Aldrich	Cat#A9418
Sulfuric acid	Sigma-Aldrich	Cat#258105
Liquid nitrogen	N/A	N/A
Software and algorithms		
HALO image analysis software	Indica Labs	Highplex FL module; RRID SCR_018350
Other		
Mouse: C57Bl/6	The Jackson Laboratory	Cat#000664; RRID MGI:2159769
Compresstome vibrating microtome	Precisionary Instruments	VF-510-0Z
Incubator	N/A	N/A
Small paintbrush (to handle PCLS)	N/A	N/A
Cryomold (Intermediate)	Tissue-Tek	Cat#62534-15
Chambered coverglasses	Lab-Tek	Cat#155380
Cryostat	Leica	CM3050 S; RRID SCR_016844
Humidity chamber for slide staining	N/A	N/A
Vacuum aspirator	N/A	N/A
Warm room or oven (37°C)	N/A	N/A
Confocal microscope	Zeiss	LSM 980; RRID SCR_025048

MATERIALS AND EQUIPMENT

Fixation/permeabilization solution

Reagent	Final concentration	Amount
Cytofix/Cytoperm™	25% (v/v)	4 mL
1X PBS	N/A	6 mL
Total Volume		**10 mL**

Fixation/permeabilization solution can be stored at +4°C for up to 2 weeks (keep solution protected from light by wrapping outside of tube with aluminum foil).

Critical: Cytofix/Cytoperm™ contains formaldehyde and is toxic. Wear gloves, lab coat, and appropriate PPE. Avoid direct contact. Only handle open containers in a fume hood.

Cryoprotection solution

Reagent	Final concentration	Amount
Sucrose	30% (w/v)	33 g
1X PBS	N/A	100 mL
Total Volume		**100 mL**

Cryoprotection solution can be stored at +4°C for up to 3 months.

Staining buffer

Reagent	Final concentration	Amount
BSA	1% (w/v)	1 g
Triton X-100	0.3% (v/v)	0.3 mL
1X PBS	N/A	100 mL
Total Volume		**100 mL**

Staining buffer can be stored at +4°C for up to 1 week.

STEP-BY-STEP METHOD DETAILS

Note: Tissue processing and staining protocols are adapted from IBEX protocols by Radtke et al. (2020 and 2022).[2,3]

Harvesting cultured PCLS for fixation/permeabilization

Timing: 20 minutes and 1 day

This step outlines the harvesting of PCLS from culture plates after incubation, and proper sample handling for fixation and permeabilization of the tissue.

Note: Perform this step in a biological safety cabinet (BSC).

1. Prepare pre-labelled 1.5 mL Eppendorf tubes and pipette 500uL of fixation/permeabilization solution into each tube.
2. Remove PCLS culture plate from incubator and place in BSC.

3. Harvest PCLS from culture plate and put in Eppendorf tubes containing fixation/permeabilization solution (1 PCLS per tube).
4. Close lids and transfer tubes to 4°C.
5. Leave PCLS to fix/permeabilize for 24 hours (4°C).

Cryoprotection

Timing: 30 minutes and 2 days

This step explains the transfer of fixed/permeabilized PCLS tissue to sucrose solution for cryoprotection, in preparation for the subsequent freezing step.

Note: Perform this step in a BSC.

6. Prepare pre-labelled 1.5 mL Eppendorf tubes and pipette 1mL of 30% sucrose into each tube.
7. For each sample, also prepare a second 1.5 mL Eppendorf tubes and pipette 1mL of cold 1X PBS into each tube.
8. Remove PCLS from Cytofix/Cytoperm™ and place in PBS tube for 5 minutes to rinse off fixative.
9. Transfer PCLS to 30% sucrose tubes (1 PCLS per tube).
10. Leave PCLS to cryoprotect for 48 hours (4°C).

Note: At end of 48-hour cryoprotection period, PCLS should be sunken to bottom of Eppendorf tube.

OCT Embedding and Freezing

Timing: 1 hour

This step describes the embedding of fixed/permeabilized/cryoprotected PCLS in optimal cutting temperature (OCT) compound. The freezing protocol uses isopentane to achieve gradual freezing to avoid compromising the tissue with freezing artifacts.

11. Fill cryomolds with OCT.

Note: Take care to avoid creating large bubbles. If bubbles are present, attempt to pop them with a pipette tip. Carefully move remaining bubbles to the edges of the mold, away from where the tissue will be embedded.

12. Carefully remove PCLS from sucrose and place in OCT-filled cryomolds.

Note: 3 PCLS (same treatment condition, biological/technical replicates) can be placed in each cryomold.

Critical: If using biological replicates, take note of the placement of PCLS from each mouse in the cryomold (as seen in **Figure 1A**).

13. Put liquid nitrogen in foam cryo-dewar and place dewar in fume hood.

Critical: Wear appropriate PPE and eye protection while handling liquid nitrogen.

14. Pour approximately 250mL of isopentane in clean 500mL glass beaker.

15. Carefully place beaker in liquid nitrogen cryo-dewar.

Critical: Right before freezing, push all PCLS down to bottom of cryomold to ensure all are frozen in same plane (as seen in **Figure 1B**). Keep cryomold level when handling to prevent movement and slanting of tissue.

16. Using large forceps, submerge bottom surface of cryomold in isopentane to gradually freeze PCLS in OCT (**Figure 1C**).

Critical: Only submerge the bottom surface (not the entire cryomold) in isopentane. Full submersion may lead to irregular freezing and formation of freezing artifacts.

Critical: Perform freezing in fume hood. Take care to avoid direct contact with liquid nitrogen and wear appropriate PPE and eye protection.

17. Remove frozen blocks from cryomolds.

Note: If freezing multiple samples, temporarily place each frozen filled cryomold at -20°C or -80°C to prevent thawing while processing rest of samples.

18. Using a scalpel, carefully cut off a small piece from the bottom right corner of the block to serve as a reference landmark for the placement of the frozen tissues in the same block (**Figure 1D**).

19. Store blocks at -80°C until cryosectioning.

Note: We have found that labelled 12-well plates work well for block storage, but any suitable preferred container can be used.

Pause point: Fixed-frozen PCLS in OCT blocks can be stored long-term at -80°C. We have tested up to 6 months with no observed compromise of the PCLS, and the original IBEX protocol states that tissues can be left frozen for several years[2].

Cryosectioning

Timing: 3 hours

This step outlines cutting the OCT-embedded PCLS with a cryostat. Cryosections are adhered to chambered coverglasses for subsequent staining, imaging, and bleaching.

20. Coat chambered coverglasses (**Figure 2A**) with an even layer of chrome-alum gelatin adhesive using a cotton swab dipped in the solution.
21. Leave chambers to dry at 37°C for 1 hour.

Optional: Coverglasses can also be coated the day before cryosectioning and left to dry at room temperature overnight.

22. Take OCT blocks out of -80°C freezer and store at -20°C for one hour prior to cryosectioning.

Critical: Wear cut-resistant gloves while operating cryostat and take precaution while handling sharp objects.

23. Using cryostat, cut fixed-frozen PCLS (three per OCT block) at thickness of 12um. Carefully place cryosections in chambered coverglasses and allow tissue to adhere completely flat (**Figure 2B**).

Critical: Pre-cool coverglasses by keeping them in the cryostat chamber. A cold surface prevents automatic sticking of the freshly cut section, and allows for gentle maneuvering while it is being placed in the coverglass. Once the cryosection is in the correct position, warm the bottom surface of the coverglass with thumb to cause cryosection to adhere.

Critical: Ensure that OCT does not curl under tissue and impede full contact of tissue with coverglass surface.

24. Label lid and side of each coverglass with sample IDs.
25. Leave coverglasses with adhered cryosections to dry for 1 hour at 37°C, or overnight at room temperature.

Pause point: Dried PCLS cryosections can be left at room temperature for up to 3 days before staining.

Blocking and Staining

Timing: 1.5 hours and overnight

This step describes the Fc-blocking and staining of PCLS cryosections with panel of primary antibodies for downstream multiplex microscopy.

26. Prepare blocking buffer by diluting Fc block 1:100 in staining buffer (Triton-BSA).
27. Rehydrate tissue by adding 1mL of 1X PBS to each chamber and incubating for 5 minutes.
28. Aspirate 1X PBS with vacuum aspiration system, taking care not to damage or scratch tissue.
29. Add 250uL of blocking buffer to each chamber and incubate for 1 hour at room temperature.
30. While samples are blocking, make antibody staining mixtures in staining buffer. With our current set up, 4 antibody-fluorophore conjugates (AF488, PE, AF594, AF647) plus DAPI can be imaged in one panel round.

Note: Antibody dilutions used are indicated in key resource table. Add Fc block at 1:100 to antibody staining panel.

Critical: Briefly centrifuge antibodies before pipetting to reduce non-specific signal from unbound fluorophore.

31. Set up staining humidity chamber by filling with tap water.

32. After blocking is complete, aspirate blocking solution and add 250uL of antibody staining solution to each chamber.
33. Incubate in humidity chamber (covered to protect samples from light) overnight at 4°C

Washing, secondary antibody staining (optional), and mounting

Timing: 20 minutes (no secondary antibody staining) or 1.5hrs (secondary antibody staining)

This step explains washing to clear unbound primary antibody, secondary antibody staining (if needed), and addition of mounting media to chambered coverglasses prior to imaging.

34. Carefully remove humidity chamber from 4°C fridge.
35. Aspirate antibody staining mixture.

Critical: If using multiple staining mixtures, take caution not to use same aspirator tip between staining mixtures.

36. Add 2mL 1X PBS per chamber, leave to soak for 2 minutes, and aspirate.
37. Repeat step 36 twice more for a total of 3 washes.

Optional: If adding secondary antibody, prepare in staining buffer with Fc block and incubate in humidity chamber for 1 hour at 37°C. Repeat triple PBS wash as described in steps 36 and 37.

38. After washing, add 1mL of Fluoromount G mounting medium to each chamber, taking care to not create bubbles.
39. Protect chambers from light and store at 4°C until imaging

Pause point: Samples can be stored for two to three days before imaging, however best image quality is obtained when performed on same day of staining.

Imaging PCLS with confocal microscopy

Timing: 1 day, 20 minutes set up and 20 to 30 minutes image acquisition per full PCLS

This step describes set-up of the confocal microscope for efficient multiplex imaging of the full PCLS tissues through acquisition of a tiled image.

Note: This protocol has been written with specific detail to the Zeiss LSM 980 microscope, however a similar workflow can be adapted to any commercial line-scanning confocal.

40. Start computer and microscope.
    a. Turn on computer connected to microscope.
    b. Switch on Zeiss LSM 980 confocal microscope.
    c. Open Zeiss ZEN Blue software.

    Note: Ideally, the system is turned on at least an hour prior to the experiment to allow for warm-up.
41. Wipe bottom of chamberglass with Kimwipe and lens cleaning solution to clean away fingerprints and debris, then load it on microscope stage.

Note: Ideally, start with the brightest sample when optimizing the acquisition settings for the experiment.

42. If available, use the AI sample finder feature in the Acquisition tab of ZEN Blue to capture an overview image of the slide.

43. While in the Locate tab, use the 10× objective and the eyepiece (in widefield epifluorescence mode) to focus on the sample using the DAPI channel or another bright channel. Switch to the 20× (NA 0.8) objective and refocus the sample.
44. In the Acquisition tab, configure confocal acquisition tracks in Imaging Setup (**Figure 3A-C**).
    a. Select all fluorophores ("Dyes") to detect based on staining panel.
    b. Combine some of the spectrally-distinct channels into single confocal tracks (e.g., Track 1: DAPI and AF594, Track 2: AF488 and AF647) to increase speed of acquisition while imaging full PCLS with multiple fluorophores. For 5 colours (DAPI, AF488, PE, AF594, AF647), 3 confocal tracks are sufficient.
    c. Adjust detection range for each channel to minimize spectral overlap between fluorophores and select the appropriate excitation lasers.

    Note: Use Thermofisher Spectraviewer as a guide to visualize excitation and emission spectra of each fluorophore in panel, as well as overlap. (https://www.thermofisher.com/order/fluorescence-spectraviewer)

    d. Select "Frame" track switching to minimize spectral overlap and accommodate different dichroic mirrors.
45. In the Acquisition Mode window, maximize resolution by adjusting pixel size to Nyquist (click on the Confocal button beside Sampling).

46. To maximize speed, set the scan zoom to 0.6× – 1.0×, increase scan speed to the maximum (unless the image noise becomes significantly high) and enable bidirectional scanning.
47. Finetune laser settings for optimal imaging of each marker (**Figure 3D**).

Critical: Do not look directly at laser with eyes at any point during experiment.

a. For each confocal track, go "Live" to preview each fluorophore.
b. Set pinhole size to 1 Airy unit (AU).
c. Adjust laser powers and detector gains to best detect each fluorophore without saturating pixels.
    i. Use Range Indicator feature to ensure that pixels are not saturated.
d. Adjust the histogram maximum display range accordingly to easily view image (or click on Best Fit).

Critical: If comparing intensities across multiple tissues/samples stained for the same markers, all samples must be imaged with identical settings.

Note: To ensure that settings are kept consistent, open a previous image and click on Reuse button to load previous settings.

48. Set up tile scan to image full PCLS tissue.

a. Enable the tile function. In the Tile Viewer, draw a polygon contour around the tissue border using the overview image generated by the AI Sample Finder.

Note: If this feature is not available, acquire a preview tile scan using a low-magnification lens (e.g., 5×) with a low-resolution acquisition setting. Drag and drop the overview tile into the Navigation window and draw the tissue contour.

b. Draw tile regions around all tissues on the slide (**Figure 3E**). This will allow the microscope to automatically image all three tissues in a row, minimizing needed hands-on time.

c. Under the Focus Surface and Support Points section of the Tiles tab, add support points across tissue tile regions (also seen in **Figure 3E**). Ensure that the Focus Strategy is set to use the Z Values defined in Tiled Setup.

   i. For full 2 mm diameter PCLS, place at least 10 support points.

   ii. Verify support points by enabling live view in the DAPI channel and ensure that the sample is in focus across all support points.

49. Click on Start Experiment to begin image acquisition. In our experience, this takes approximately 20-30 mins per full PCLS tissue.

Fluorophore bleaching and restaining

Timing: 45 minutes and overnight

This step explains inactivation of fluorophores (bleaching) in the stained sample with reducing agent lithium borohydride ($LiBH_4$), and subsequent restaining of the tissue with a new round of antibodies.

50. After image acquisition is complete, carefully remove all mounting medium out of chamber with pipette.

51. Wash by adding 2mL 1X PBS to each chamber. Leave to soak for 2 minutes and aspirate with vacuum aspirator.
52. Repeat step 51 twice more for a total of 3 washes.
53. Prepare bleaching solution.

Critical: $LiBH_4$ is highly flammable! Perform all $LiBH_4$ handling and bleaching steps in fume hood.

   a. Weigh $LiBH_4$ in a small glass beaker using a microbalance.
   b. Add distilled water to dissolve $LiBH_4$ to a final concentration of 1mg/mL.

54. Add 1mL of bleaching solution to each chamber and leave to incubate for 15 minutes.

Note: Small bubbles will form around tissue. If bubbling is not observed, this may indicate $LiBH_4$ reagent has oxidized and is no longer effective, and needs to be replaced.

55. After incubation, carefully remove bleaching solution with pipette and place in waste beaker.
   a. Neutralize $LiBH_4$ waste by carefully adding sulfuric acid in a drop-wise manner, until solution no longer bubbles. Dispose by pouring on absorbent pad.
56. Wash sample by adding 2mL 1X PBS to each chamber. Leave to soak for 2 minutes and aspirate.

Note: Tissue may become more prone to lifting and/or slipping after bleaching. Take caution to keep direct suction from the vacuum away from the tissue.

57. Repeat step 56 twice more for a total of 3 washes.

58. Perform next round of antibody staining, as previously described in steps 30-39.

***Note**:* Blocking step is not required before restaining.

***Note**:* DAPI and AF594 do not bleach and should not be included in restaining rounds.

Imaging of subsequent staining rounds

Timing: 1 day, 20 minutes set up and 20 to 30 minutes image acquisition per full PCLS

This step outlines the imaging of subsequent staining rounds, and the critical need to ensure that the same Z plane in the tissue is being imaged across rounds to allow for successful image fusion of multiple rounds.

59. Set up microscope and imaging parameters as described above in steps 40 to 49.
    a. If using same panel of fluorophores, laser track settings can be re-used.
    b. Adjust gain and laser power for each marker, keeping settings consistent across samples.
60. When setting up tile scans, focus each support point using DAPI and match with DAPI image in the same area from previous round to ensure the same Z plane is being imaged (**Figure 3F**).

Note: Bleaching, restaining, and imaging of subsequent rounds can be repeated as desired for experimental purposes. However, we have noticed an increase in autofluorescence with each round of bleaching and thus suggest placing markers with lower expression in earlier staining rounds.

Image fusing and quantitative analysis

Timing: 2 days

This final step outlines the use of HALO image analysis software to fuse multiple rounds into a single image for each PCLS tissue, as well as quantitative analysis of markers and cellular phenotypes.

61. Import all images into HALO image analysis software.

Optional: For ease of image management, rename all channels from fluorophore names (e.g. AF488) to marker names (e.g. CD206).

62. Register serial imaging rounds on same tissue with image registration tool, selecting the setting for serial stain registration.

63. Fuse images using fuse serial stain tool.

    a. Select middle staining round (ie. round two out of three) as registration target.

    b. Select DAPI as fusing reference channel.

    c. Verify alignment of fusion by simultaneously turning on DAPI channels from all rounds. **Figure 4A** displays an example of successful alignment of DAPI channels from sequential rounds in a fused image.

        i. If rounds are not properly aligned, adjust the image fusion by manually adding reference points with the landmark tool.

64. In fused images, assign distinct pseudocolour to each channel for ease of visualization.

65. Adjust histogram settings to have optimal visualization for each channel, keeping settings consistent across all images.
66. To now analyze fused multiplex images (examples seen in **Figure 4B**), launch Highplex FL analysis module to develop algorithm for detection of markers.
    a. Select dyes to quantify. If want to use all, select "autofill".
    b. Set phenotypes for cell types to quantify, based on marker criteria. In this paper, we quantify general macrophages (**Figure 4C i.** "Phenotype 1", defined as $CD45^+CD68^+CD11c^+$ cells) and profibrotic macrophages (**Figure 4C ii.** "Phenotype 2", defined as $CD45^+CD68^+CD11c^+Arg1^+CD206^+$ cells), as we were interested in evaluating if our IL-4+IL-6+IL-13 polarization cocktail could induce this phenotype in PCLS.
    c. Use "real-time tuning" window to set parameters for nuclear detection on DAPI channel.
    d. Use "real-time tuning" window to set parameters for detection of each marker.
    e. Name and save analysis algorithm to study folder.
67. Run analysis with developed Highplex algorithm on all tissues.
    a. Resulting analysis will yield detection of all nuclei (DAPI, as seen in **Figure 4D i**.), cellular positivity for each individual stain (example for CD45 shown in **Figure 4D ii.**), and multiplex analysis for each defined phenotype (example for $Arg1^+CD206^+$ Macrophages seen in **Figure 4D iii.**).

EXPECTED OUTCOMES

PCLS are 1iving tissue preparations that contain all pulmonary cell types, and preserve the cellular interactions, architecture, and microenvironment of the lung, thus ultimately serving as a powerful biologically-translational model for respiratory research[4]. This is especially critical when studying plastic, phenotypically-diverse cells like macrophages that are highly responsive to cues in their microenvironment and limitedly recapitulated in traditional two-dimensional *in vitro* cell culture systems[7]. The *ex vivo* nature of the system provides versatility, as an endless range of mediators and compounds can be applied to stimulate disease-like states and experimental treatment angles. In these experimental systems, it is essential to have a comprehensive understanding of induced cellular phenotype. However, due to the requirement of agarose instillation to generate slices, as well as the relatively small mass of tissue, downstream applications such as RNA assessment and flow cytometry have proved challenging[10], thus creating barriers for cellular phenotyping in PCLS. While immunostaining on PCLS has been performed previously, this has initially been done on full fixed slices rather than cryosections, thus increasing the susceptibility to autofluorescence by the large amount of agarose gel content. Hoffman et al. (2018) have demonstrated robust multiplex staining in PCLS, but acknowledge the limitation of content throughput with immunostaining due to constraint of available fluorophores that can be used at once[12], which our work aims to overcome with iterative rounds of staining. This protocol provides a detailed, multi-step breakdown of a pipeline for processing, sectioning, iterative rounds of staining+imaging+bleaching (using IBEX), and quantitative analysis of highly multiplexed immunolabelling for the

determination of macrophage phenotype in PCLS. Using a customizable panel of commercially-available antibodies conjugated to different fluorophores across the spectrum (see **Key Resources Table**), we specifically visualized and detected macrophages ($CD45^+CD68^+CD11c^+$ cells) in the control and polarization cocktail-treated (IL-4+IL-6+IL-13) PCLS (**Figure 5A**). Using established profibrotic macrophage markers Arginase-1 and CD206, we were also able to specifically detect macrophages that had a profibrotic phenotype ($CD45^+CD68^+CD11c^+Arg1^+CD206^+$ cells). Using HALO image analysis platform, we were able to specifically quantify profibrotic macrophages in full-tissue images, based on cellular marker co-positivity (using the inputted custom phenotype criteria). Using the pipeline described in this protocol, we demonstrated visually and quantitatively that PCLS treated with our polarization cocktail had a significant increase in profibrotic ($Arg1^+CD206^+$) macrophages, expressed as percentage of total cells and percentage of macrophages (**Figure 5B,C,** as seen in Vierhout et al. 2024[1]). Delving deeper into the phenotype of these macrophages, we also used additional markers to define alveolar and interstitial macrophages, which are broadly the two main macrophage populations in the lung, and are both believed to play critical roles in lung fibrosis[13]. We observed that our polarization cocktail was able to program both alveolar and interstitial macrophages to a profibrotic phenotype (**Figure 6,** as seen in Vierhout et al. 2024[1]). Overall, this protocol is suitable and feasible for visual and quantitative macrophage phenotyping in murine PCLS. It has potential for customizability to other panels and *ex vivo* tissue slice systems, especially due to the versatile and open-source nature of IBEX.

LIMITATIONS

The major limiting timestep in this protocol is time spent imaging. Microscope set up requires approximately 20 minutes per tissue, and image acquisition then takes approximately 20-30 minutes for a full PCLS (2mm diameter) using 5 colours. We have introduced modifications to minimize time, such as including three PCLS per chamberglass, placing two channels on a laser track, and setting up acquisition for three tiled images at once so they are automatically sequentially imaged by the microscope. However, if testing multiple treatment conditions with multiple biological/technical replicates, timing presents a limitation for throughput of the readout. We suggest using high-content quantitative imaging in synergy with other readouts suitable for higher throughput, such as brightfield immunohistochemistry and protein assessments. Examples of this in the context of our research question can be found in our full study[1].

TROUBLESHOOTING

Problem 1: Difficulty sectioning tissue using cryostat (related to Step 23).

Potential solution:

- Make sure tissue OCT blocks are left to warm up at -20°C (either in cryostat chamber or -20°C freezer) for 1 hour before sectioning. Blocks that are too cold will not cut well.
- If tissue seems teared/fragmented, freezing artifacts may be present. Ensure that cryoprotection step, as well as gradual freezing of OCT block using isopentane (and

only submerging the bottom surface, not the whole cryomold), are properly followed.

- As PCLS tissues are limited in size/thickness and can be easily depleted, it is best to use a few extra "practice" samples to test cryostat set up prior to cutting precious samples.

Problem 2: Non-specific signal/background in microscopy images (related to Steps 47-49).

Potential solution:

- Check IBEX reagent resource repository on public IBEX Knowledge-Base[11] to check if antibody of concern has been used before and the accompanying conditions.
- Include unstained tissue, which is subjected to all parts of the protocol but is incubated in staining buffer without antibodies/DAPI, to determine if background may be caused by any component of the tissue processing/staining protocol, or imaging settings.
- Perform antibody optimization:
    - Optimize antibody concentrations with single-stained tissues prior to full experiment. We typically use a range of test concentrations, including 1:20, 1:50, 1:100, and 1:200.

- If using secondary antibodies, run a secondary-only control to determine if background is caused by non-specific binding of secondary antibody (**Figure 7**).

Problem 3: High autofluorescence in microscopy images (related to Step 47-49).

Potential solution:

- Ensure tissue does not dry out at any point during the protocol.
- If increased autofluorescence is seen in subsequent staining/imaging rounds after bleaching, ensure that $LiBH_4$ is kept on tissue for no longer than 15 minutes. Reducing bleaching time to 10 minutes may also be useful.
- Put markers with weaker signal in earlier staining rounds.

Problem 4: Tissue loss after washing/bleaching (related to Step 56, and all wash/aspiration steps).

Potential solution:

- Ensure slides are always freshly coated with chrome-alum gelatin adhesive (same day of cryosectioning or day before).
- When cryosectioning, ensure that no OCT curls underneath tissue, which would interfere with adherence to coverglass.
- When aspirating liquids from chambers, take care to not scrape or aspirate tissue.

Problem 5: Difficulty with image fusion – serial images are not properly aligned (related to Step 63).

Potential solution:

- In our experience, HALO works well to fuse and align the images easily approximately 90% of the time. For the other 10% of the time, further adjustment is needed by manually adding reference points with the landmark tool to correct the alignment.
- During image acquisition, it is important to ensure that the same Z plane is being imaged in the tissue across all rounds. If the same cells are not imaged, fusion/alignment and accurate multiplex detection will not work.
- If tissue loss/movement occurs with bleaching, washing, and aspiration across rounds, this will also affect image fusion (See Problem 4 above for potential solution).

RESOURCE AVAILABILITY

Lead contact

Further information and requests for resources and reagents should be directed to and will be fulfilled by the lead contact, Joshua F.E. Koenig (koenigjf@mcmaster.ca).

Technical contact

Questions about the technical specifics of performing the protocol should be directed to the technical contact, Megan Vierhout (vierhom@mcmaster.ca).

Materials availability

This study did not generate new unique reagents.

Data and code availability

This study did not generate new datasets or code; originally published data can be found in our original manuscript.[1] Any additional information required to reanalyze the data reported in this paper is available from the lead contact or technical contact upon request.

ACKNOWLEDGEMENTS

This work was supported by funding from the Canadian Institutes of Health Research (CIHR) [MV: (Doctoral Award) Grant No. 170793, MK: Grant No. PJT-162295] and the Ontario Graduate Scholarship (OGS) Program [MV].

We sincerely thank Dr. Joao Pedro Bronze de Firmino at the McMaster Centre for Advanced Light Microscopy (CALM) for expert assistance with confocal microscopy. We also genuinely thank Joanna Kasinska and Fuqin Duan for their technical assistance.

The graphical abstract was created using BioRender.com.

AUTHOR CONTRIBUTIONS

MV: conceptualization, methodology, formal analysis, investigation, writing – original draft, writing – review & editing; **MB**: methodology, software, writing – original draft, writing – review & editing; **VMO:** methodology; **AJR**: methodology, resources; **ZY:** methodology, resources; **MRJK:** supervision, funding acquisition, resources; **KA:** conceptualization, supervision, project administration, funding acquisition, resources;

JFEK: conceptualization, supervision, funding acquisition, resources, methodology, writing – original draft, writing – review & editing.

DECLARATION OF INTERESTS

The authors declare no competing interests.

REFERENCES

1. Vierhout, M., Ayoub, A., Ali, P., Kumaran, V., Naiel, S., Isshiki, T., Koenig, J.F., Kolb, M.R., and Ask, K. (2024). A Novel Ex Vivo Approach for Investigating Profibrotic Macrophage Polarization Using Murine Precision-Cut Lung Slices. bioRxiv, 2024.07.05.602278. https://doi.org/10.1101/2024.07.05.602278.
2. Radtke, A.J., Chu, C.J., Yaniv, Z., Yao, L., Marr, J., Beuschel, R.T., Ichise, H., Gola, A., Kabat, J., Lowekamp, B., et al. (2022). IBEX: an iterative immunolabeling and chemical bleaching method for high-content imaging of diverse tissues. Nat Protoc *17*, 378–401. https://doi.org/10.1038/s41596-021-00644-9.
3. Radtke, A.J., Kandov, E., Lowekamp, B., Speranza, E., Chu, C.J., Gola, A., Thakur, N., Shih, R., Yao, L., Yaniv, Z.R., et al. (2020). IBEX: A versatile multiplex optical imaging approach for deep phenotyping and spatial analysis of cells in complex tissues. Proceedings of the National Academy of Sciences *117*, 33455–33465. https://doi.org/10.1073/pnas.2018488117.
4. Lam, M., Lamanna, E., Organ, L., Donovan, C., and Bourke, J.E. (2023). Perspectives on precision cut lung slices—powerful tools for investigation of mechanisms and therapeutic targets in lung diseases. Front Pharmacol *14*, 1162889. https://doi.org/10.3389/fphar.2023.1162889.
5. Zhang, L., Wang, Y., Wu, G., Xiong, W., Gu, W., and Wang, C.-Y. (2018). Macrophages: friend or foe in idiopathic pulmonary fibrosis? Respiratory Research *19*, 170. https://doi.org/10.1186/s12931-018-0864-2.

6. Aegerter, H., Lambrecht, B.N., and Jakubzick, C.V. (2022). Biology of lung macrophages in health and disease. Immunity *55*, 1564–1580. https://doi.org/10.1016/j.immuni.2022.08.010.

7. Wei, Y., Wang, M., Ma, Y., Que, Z., and Yao, D. (2021). Classical Dichotomy of Macrophages and Alternative Activation Models Proposed with Technological Progress. Biomed Res Int *2021*, 9910596. https://doi.org/10.1155/2021/9910596.

8. Bain, C.C., and MacDonald, A.S. (2022). The impact of the lung environment on macrophage development, activation and function: diversity in the face of adversity. Mucosal Immunol *15*, 223–234. https://doi.org/10.1038/s41385-021-00480-w.

9. Morales-Nebreda, L., Misharin, A.V., Perlman, H., and Budinger, G.R.S. (2015). The heterogeneity of lung macrophages in the susceptibility to disease. European Respiratory Review *24*, 505–509. https://doi.org/10.1183/16000617.0031-2015.

10. Neuhaus, V., Schaudien, D., Golovina, T., Temann, U.-A., Thompson, C., Lippmann, T., Bersch, C., Pfennig, O., Jonigk, D., Braubach, P., et al. (2017). Assessment of long-term cultivated human precision-cut lung slices as an ex vivo system for evaluation of chronic cytotoxicity and functionality. J Occup Med Toxicol *12*, 13. https://doi.org/10.1186/s12995-017-0158-5.

11. Yaniv, Z., Anidi, I., Arakkal, L., Arroyo-Mejias, A., Beuschel, R.T., Börner, K., Chu, C.J., Clatworthy, M., Colautti, J., Croteau, J., et al. (2024). Iterative Bleaching Extends Multiplexity (IBEX) Knowledge-Base. Version v0.2.0 (Zenodo). https://doi.org/10.5281/zenodo.13122300 https://doi.org/10.5281/zenodo.13122300.

12. Hoffmann, F.M., Berger, J.L., Lingel, I., Laumonnier, Y., Lewkowich, I.P., Schmudde, I., and König, P. (2018). Distribution and Interaction of Murine Pulmonary Phagocytes in the Naive and Allergic Lung. Front Immunol *9*, 1046. https://doi.org/10.3389/fimmu.2018.01046.

13. Gu, Y., Lawrence, T., Mohamed, R., Liang, Y., and Yahaya, B.H. (2022). The emerging roles of interstitial macrophages in pulmonary fibrosis: A perspective from scRNA-seq analyses. Front Immunol *13*, 923235. https://doi.org/10.3389/fimmu.2022.923235.

Figure 1

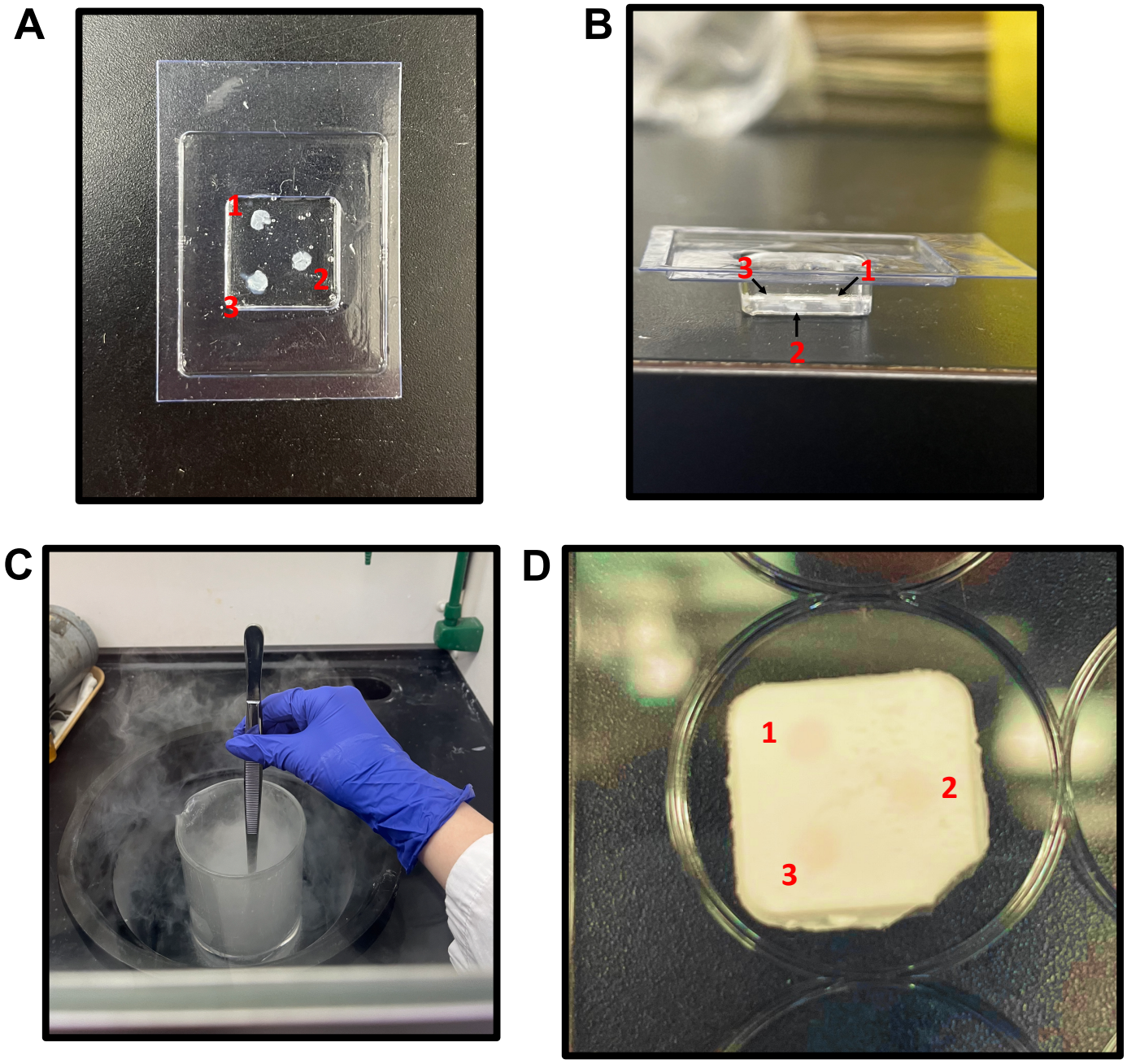

Figure 1: Embedding and freezing fixed PCLS in OCT
A: 3 PCLS in liquid OCT in cryomold; overhead perspective.
B: 3 PCLS in liquid OCT in cryomold; lateral perspective.
C: Freezing PCLS+OCT in beaker of isopentane placed in liquid nitrogen.
D: Frozen PCLS embedded in OCT. Bottom right corner of OCT is cut to indicate orientation of samples.

Figure 2

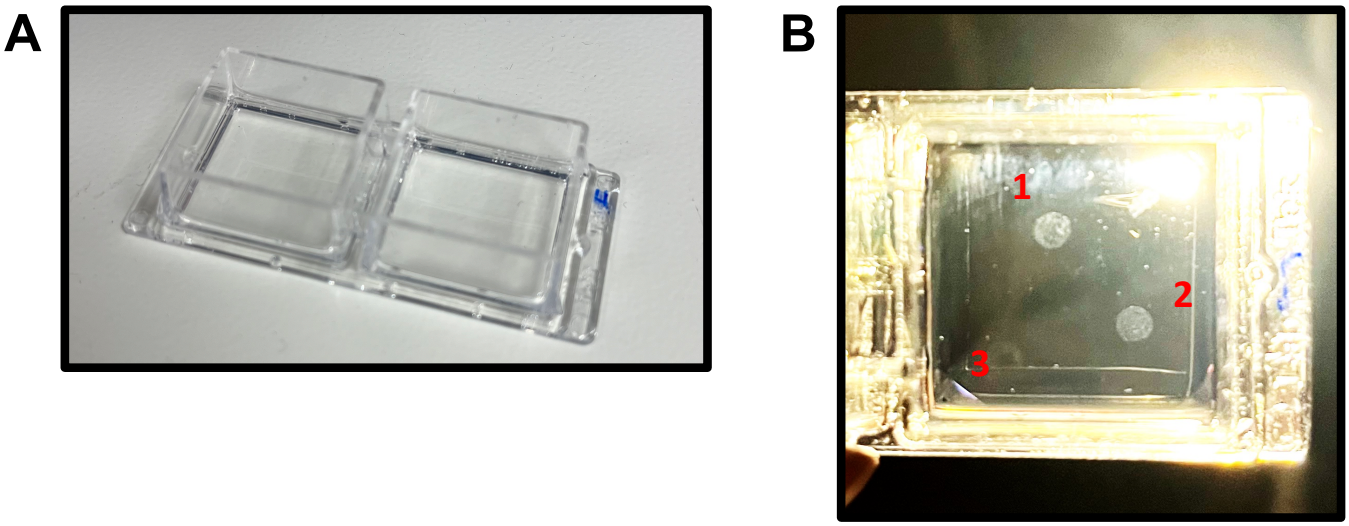

Figure 2: Chambered coverglass for PCLS staining
A: Chambered coverglass used for IBEX staining.
B: PCLS cryosections (3) cut on chambered coverglass.

Figure 3

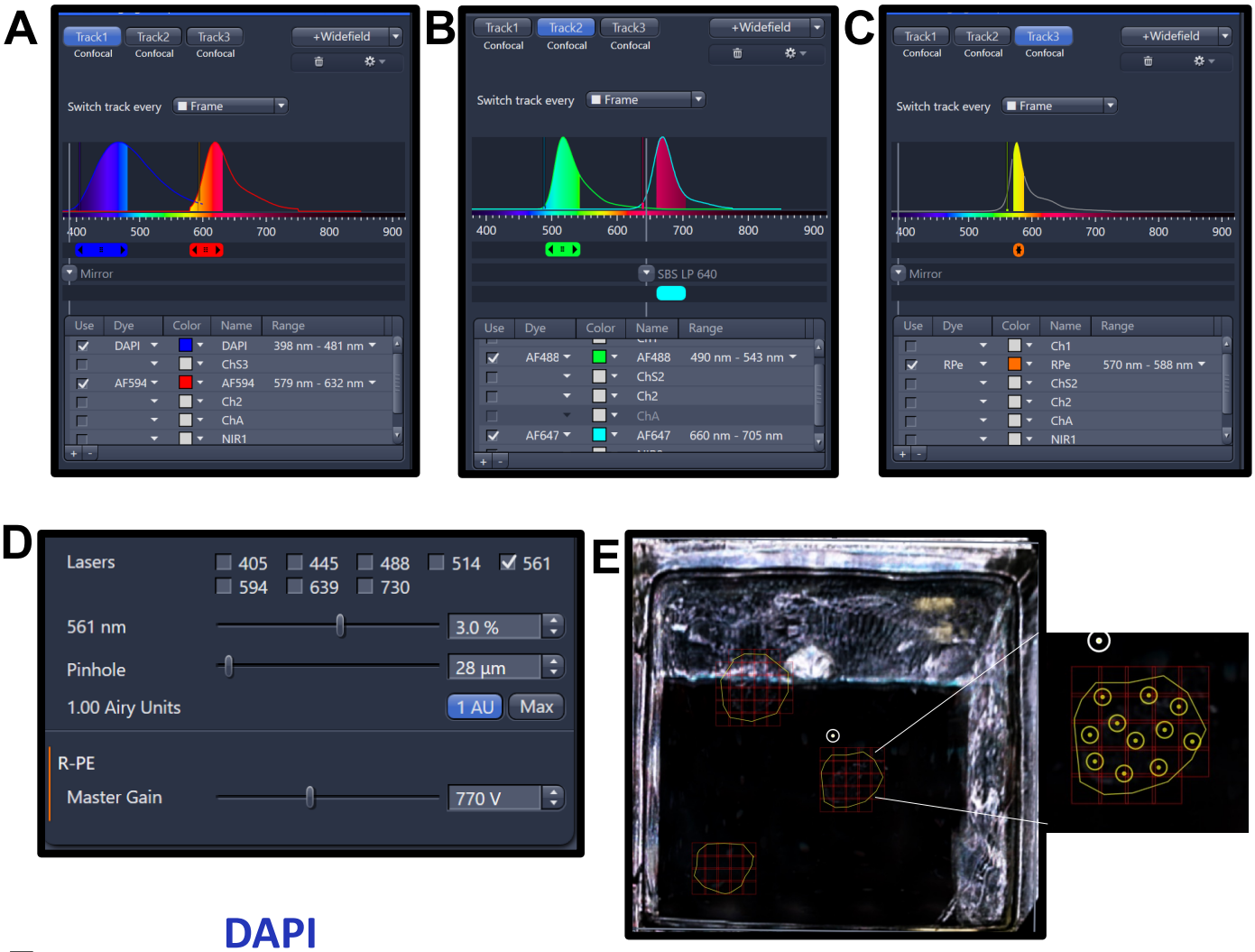

Figure 3: Settings for image acquisition on confocal microscope (Zeiss LSM 980)
A,B,C: Optimized track and channel setup, with fluorescence detection ranges adjusted to minimize spectral overlap between dyes.
D: Example of laser power and gain settings for channel.
E: Tile regions drawn on sample finder overview to capture the full tissue, with focus support points (yellow) distributed across the field.
F: Alignment of Z-plane across multiple rounds of imaging, based on DAPI channel.

Figure 4

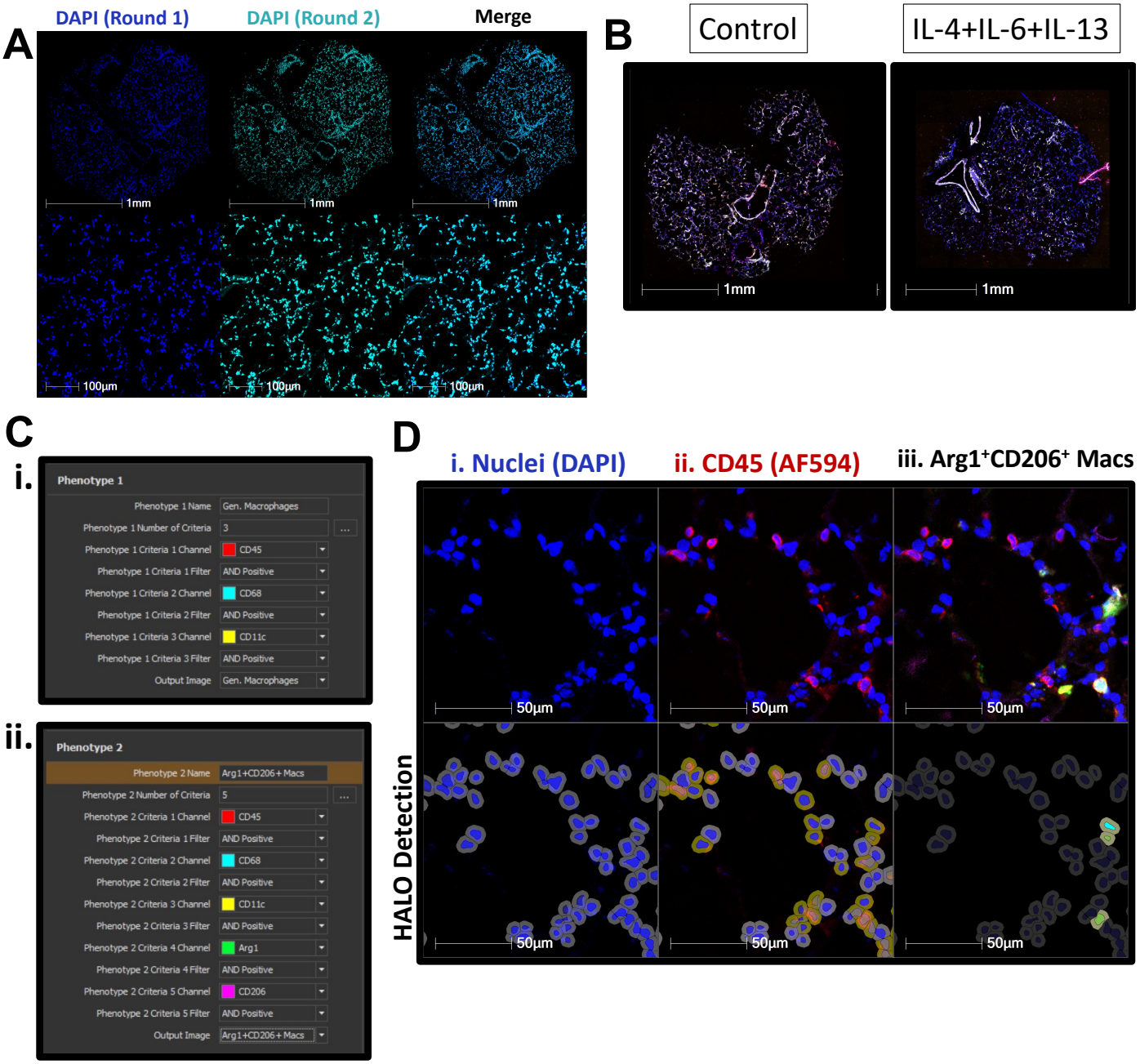

Figure 4: Image analysis using HALO Highplex FL Module

A: Alignment of DAPI channels from sequential staining rounds on PCLS (used as a reference channel during image fusion).

B: Examples of fused multiplex PCLS images from multiple staining rounds.

C: Set phenotypes for i. General Macrophages and ii. Profibrotic ($Arg1^{+}CD206^{+}$) Macrophages, defined by positivity of markers.

D: Example of markup of HALO analysis, showing i. DAPI (nuclear), ii. CD45 (single stain), and iii. profibrotic macrophage (multiplex) detection.

Figure 5 Macrophages (CD45⁺CD68⁺CD11c⁺ cells) with profibrotic (Arg1⁺CD206⁺) phenotype

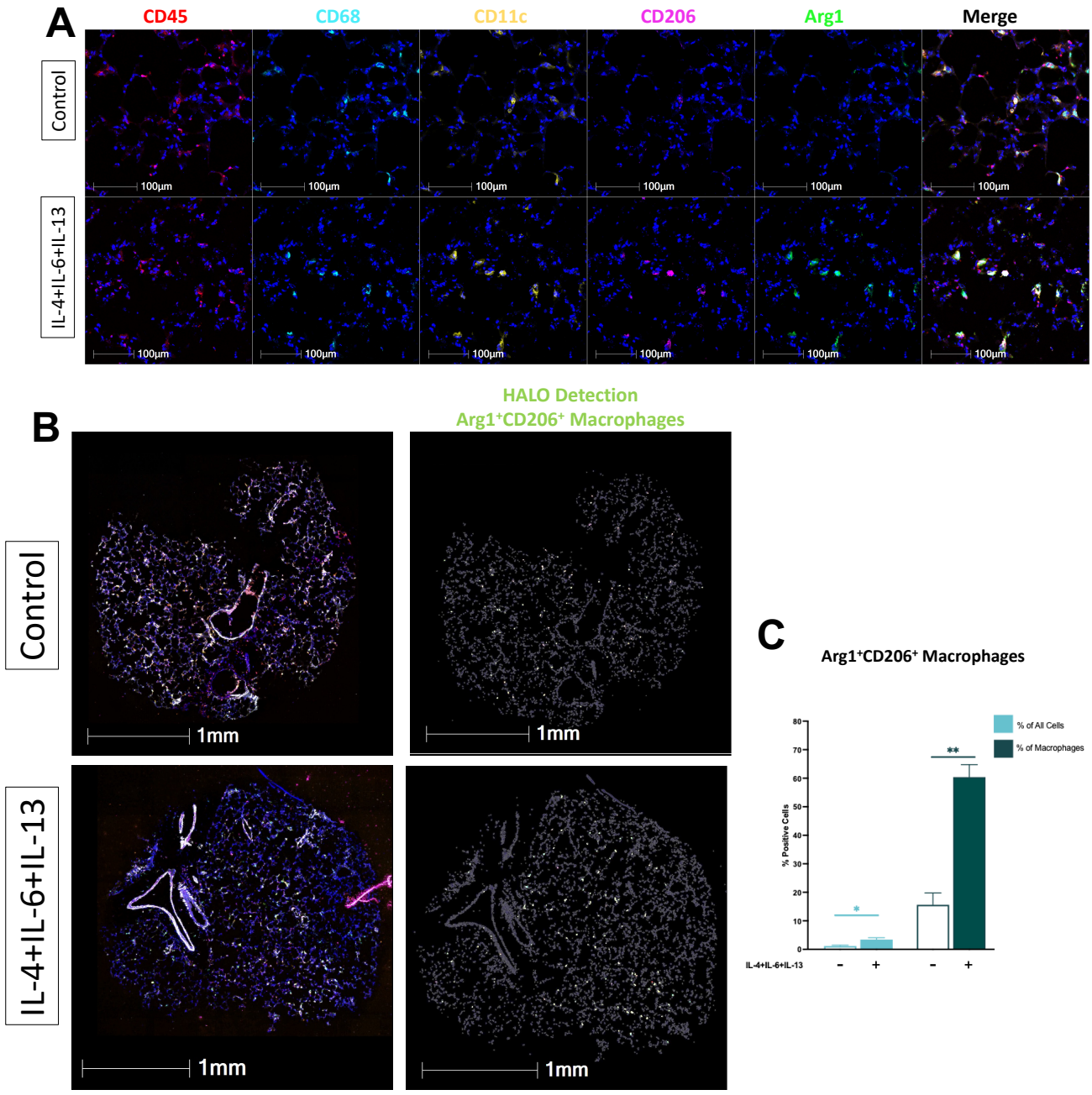

Figure 5: Quantifying profibrotic macrophage phenotype in PCLS
A: Markers defining profibrotic macrophage phenotype.
B: HALO detection of profibrotic macrophages in full PCLS.
C: Quantification of profibrotic macrophages in control and treated PCLS, expressed as % total cells and % total macrophages (graph adapted from Vierhout et al. 2024[1]).

Figure 6

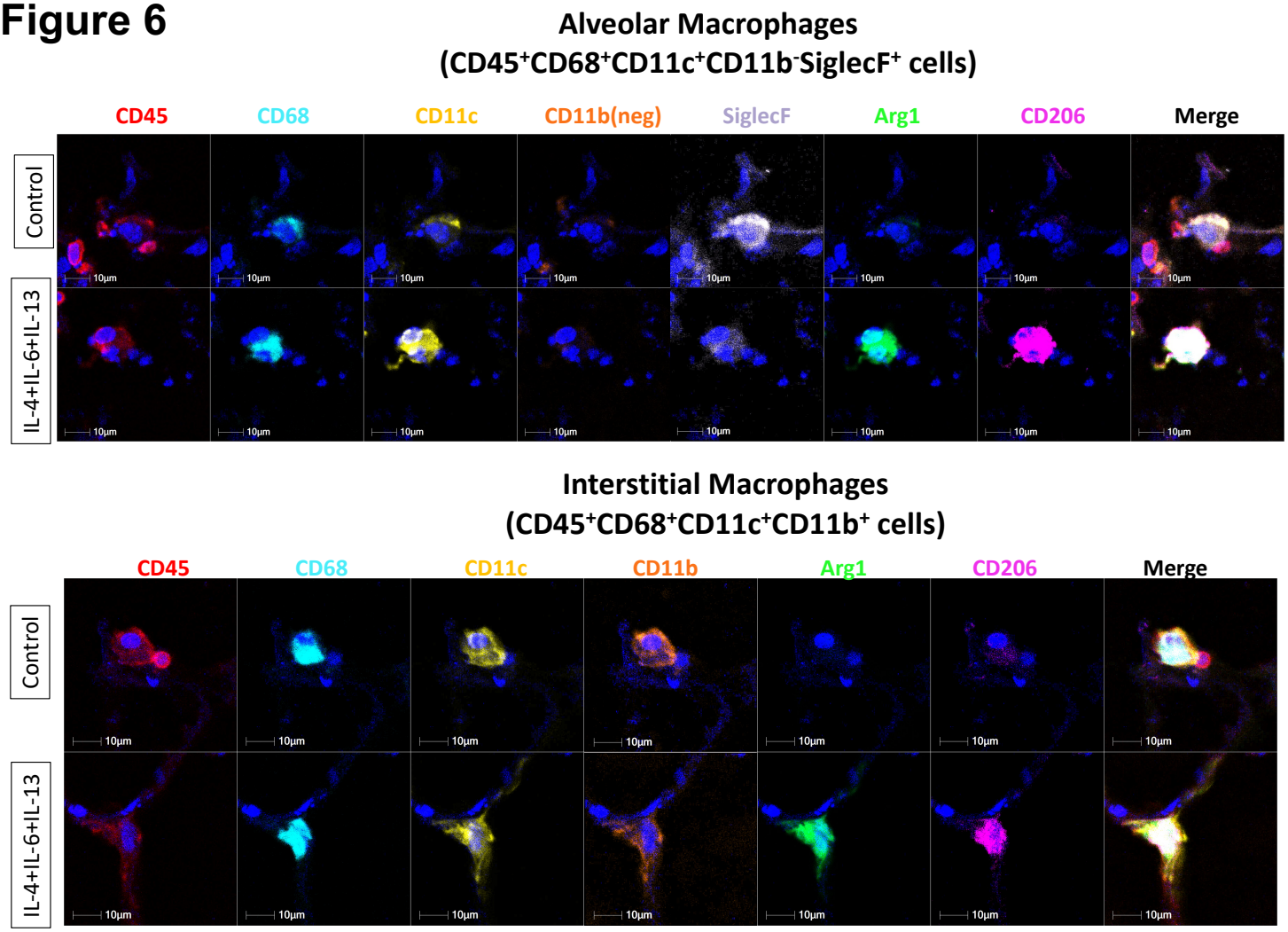

Figure 6: Marker panels defining alveolar and interstitial macrophage populations
A: Alveolar macrophages in control and treated PCLS.
B: Interstitial macrophages in control and treated PCLS.

Figure 7

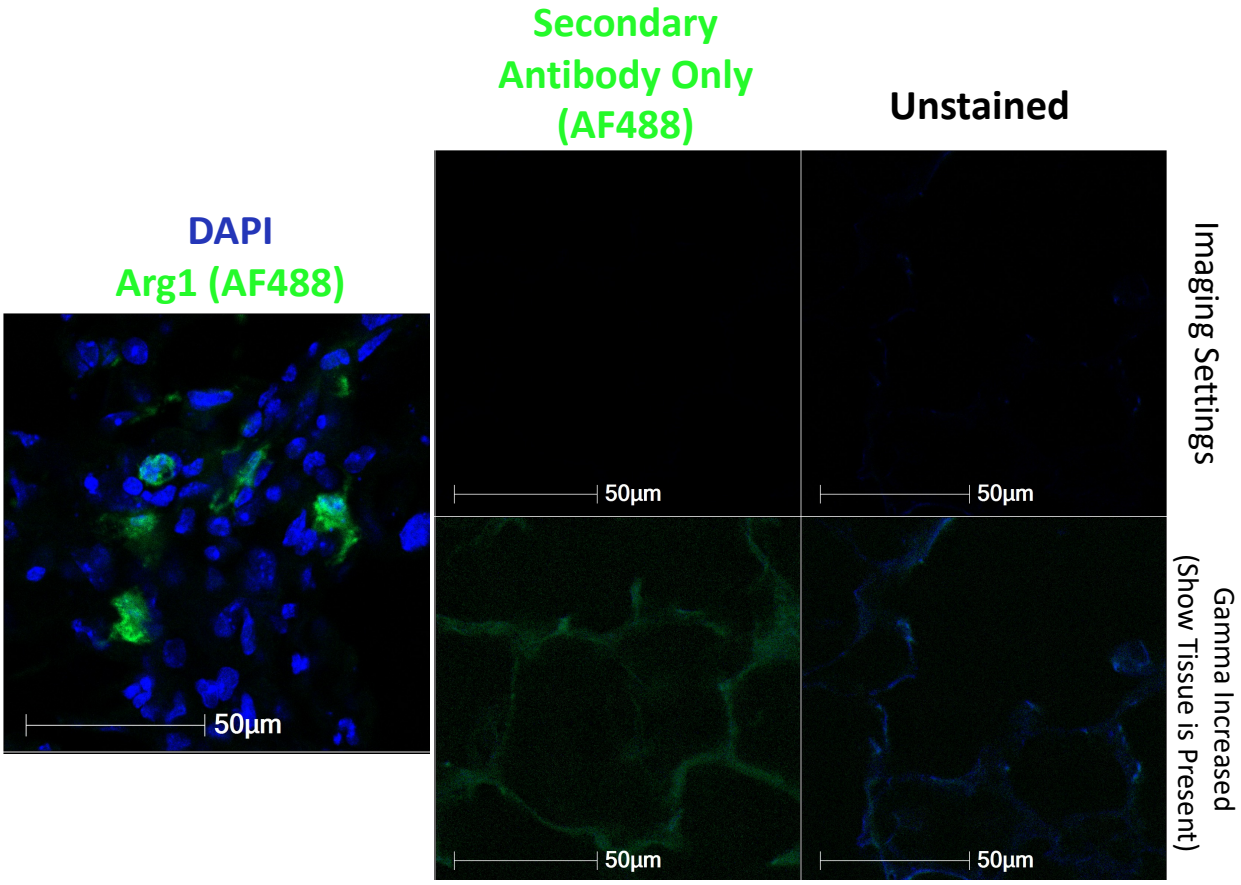

Figure 7: Determination of non-specific signal and/or autofluorescence using only secondary antibody and unstained tissue. The top row shows the same settings used to acquire the stained sample image on the left, while the bottom row is the same image with gamma settings increased to show presence of tissue.

CHAPTER 5

IDENTIFICATION OF ABERRANT METABOLIC PHENOTYPE IN CIRCULATING MONOCYTES IN IDIOPATHIC PULMONARY FIBROSIS THROUGH TRANSCRIPTOMIC PROFILING AND IMPLICATIONS ON PROFIBROTIC MACROPHAGE POLARIZATION

Megan Vierhout, Anna Dvorkin-Gheva, Anmar Ayoub, Safaa Naiel, Quan Zhou, Alexander Noble, Albina Tyker, Pareesa Ali, J.C. Cutz, Asghar Naqvi, Martin R.J. Kolb, Kjetil Ask*, Nathan Hambly*

Elevated blood monocyte count has been reported in IPF patients and shown to be linked to poor disease outcomes. These monocytes are believed to migrate into the lung and differentiate into profibrotic macrophages which contribute to fibrogenesis. However, little is known about their properties in IPF. In this chapter, we investigated these macrophage precursor cells in IPF through exploring the transcriptomic attributes of monocytes isolated from the blood of IPF patients and controls using RNA sequencing. We found that both monocytes in the blood, and profibrotic macrophages in the lung, were increased in IPF patients. Our transcriptomic findings identified an aberrant metabolic profile in IPF, as well as potential association of monocytic attributes with features related to disease severity. We then applied this information to delve into mechanistic studies on the contribution of the identified aberrant features to profibrotic macrophage polarization, using macrophage and precision-cut lung slice polarization systems. Overall, this chapter outlines a translational study, using patient-derived signatures and identification of targets of interest to modulate profibrotic cell behaviour, offering insight into the activation status of these cells in IPF.

AUTHOR CONTRIBUTIONS

MV: methodology, formal analysis, investigation, writing – original draft, writing – review & editing, visualization; **ADG**: formal analysis, investigation, visualization, data curation; **AA:** methodology, investigation; **SN:** methodology; **QZ:** methodology; **AT:** methodology, resources; **PA:** methodology**; JCC:** formal analysis, resources; **AN:** formal analysis, resources; **MK:** project administration, resources, supervision, funding acquisition; **KA:** conceptualization, resources, supervision, writing – review & editing, project administration, funding acquisition; **NH:** conceptualization, resources, supervision, project administration, funding acquisition.

To be submitted

Identification of Aberrant Metabolic Phenotype in Circulating Monocytes in Idiopathic Pulmonary Fibrosis Through Transcriptomic Profiling and Implications on Profibrotic Macrophage Polarization

Megan Vierhout[1,2], Anna Dvorkin-Gheva[1], Anmar Ayoub[1,2], Safaa Naiel[1,2], Quan Zhou[1,2], Alexander Noble[1,2], Albina Tyker[1], Pareesa Ali[1,2], J.C. Cutz[3], Asghar Naqvi[3], Martin R.J. Kolb[1,2], Kjetil Ask[1,2]*, Nathan Hambly[2]*

Affiliations:

[1]Firestone Institute for Respiratory Health, Department of Medicine, McMaster University and The Research Institute of St. Joe's Hamilton, Hamilton, Ontario, Canada

[2]McMaster Immunology Research Centre, Department of Medicine, McMaster University, Hamilton, Ontario, Canada

[3]Division of Anatomical Pathology, Department of Pathology and Molecular Medicine, McMaster University, Hamilton, Ontario, Canada

***Corresponding Authors**: Dr. Nathan Hambly and Dr. Kjetil Ask.

Contact Email: hamblyn@mcmaster.ca; askkj@mcmaster.ca

Key words: monocyte, macrophage, transcriptomics, macrophage polarization, cellular metabolism, idiopathic pulmonary fibrosis

ABSTRACT

Patients with idiopathic pulmonary fibrosis (IPF) have shown elevated circulating monocyte counts linked to poor outcomes. These monocytes are believed to migrate into the lung and differentiate into profibrotic macrophages, however little is known about their properties. Here, we investigated the transcriptomic attributes of monocytes from IPF patients and identified an aberrant metabolic profile. We then mechanistically assessed this in profibrotic macrophages.

RNA sequencing was performed on CD14+ blood monocytes from IPF patients and controls. Monocyte-derived profibrotic macrophages were histologically assessed in IPF surgical lung biopsies. Mechanistic *in-vitro* (THP-1 and RAW264.7) and *ex-vivo* [murine precision-cut lung slices (PCLS)] studies employed a profibrotic macrophage hyperpolarization cocktail (IL-4+IL-6+IL-13) +/- dichloroacetate (PDK inhibitor). Profibrotic macrophage activation was evaluated via protein expression of CCL18, IL-10, Arginase-1, CD206, and YM1.

Both monocytes (blood) and profibrotic macrophages (lung) were increased in IPF patients. Transcriptomic analyses revealed downregulation of oxidative phosphorylation (OXPHOS) in IPF monocytes, aligning with the finding that PDK4, a gatekeeper kinase between glycolysis and OXPHOS, was drastically upregulated. Inhibition of PDK (and thus promotion of OXPHOS) using dichloroacetate *in-vitro* decreased CCL18, Arginase-1, and IL-10, supporting that downregulated OXPHOS is associated with a profibrotic macrophage phenotype. This was confirmed in PCLS studies, where inhibiting PDK reduced profibrotic macrophage markers Arginase-1, CD206, and YM1.

Our results highlight a novel metabolic target in monocytes and macrophages in pulmonary fibrosis. Mechanistic studies reveal that this altered metabolic state influences profibrotic macrophage polarization, offering insight into alternative activation states of these cells in IPF.

INTRODUCTION

Idiopathic pulmonary fibrosis (IPF) is a fatal, progressive disease involving excessive scarring of the lung tissue. IPF is associated with early mortality, with a median survival of just 3 to 5 years after diagnosis [1]. Currently, there are no curative pharmacologic therapies for IPF. Lung transplant is a beneficial option for IPF patients, however eligibility is generally restricted to a relatively short time frame. Additionally, many IPF patients die while awaiting lung transplant, suggesting that transplant referral is often initiated too late in the disease course [2]. The disease trajectory of IPF is often unpredictable, and periods of rapid patient decline or acute symptom worsening, also termed acute exacerbations, can be deadly [3]. Overall, methods for prognostication and prediction of acute exacerbations in IPF are urgently needed to optimize transplant referral and optimize patient-centred treatment strategies.

Elevated circulating monocyte count has been reported in multiple cohorts of IPF patients [4–7]. Additionally, monocyte levels have been shown to be associated with poor disease outcomes, and even potentially predictive of acute exacerbations [6]. A 52-gene risk profile for mortality in IPF patients using peripheral blood mononuclear cells not only showcased the possibility of disease outcome prediction in circulating cells, but demonstrated that monocytes were the main cellular source of the features related to high risk [8]. This suggests that monocyte characteristics may be related to profibrotic processes in IPF. Furthermore, as precursor cells for macrophages, it has been demonstrated that circulating monocytes contribute to profibrotic macrophage populations in the fibrotic lung [9]. Thus, the phenotype of monocytes needs to be further elucidated to understand their potential

relationship to pulmonary profibrotic macrophage programming and progression in the landscape of IPF.

Here, we perform transcriptomic profiling on $CD14^{+}CD16^{-}$ blood monocytes, as the most common monocyte subset, isolated from IPF patients. We demonstrate their increased quantity in IPF, as well as association with disease features such as lung function decline. We also uncover an aberrant metabolic phenotype classified by decreased oxidative phosphorylation (OXPHOS) and increased OXHPOS gatekeeper enzyme PDK4, which we mechanistically explore further through macrophage polarization studies.

METHODS

Research Ethics

Collection and utilization of human lung tissues and blood was approved by the Hamilton Integrated Research Ethics Board (HiREB# 11-3559 and 13-523-C; and HiREB# 2017). Work involving animals was approved by the McMaster Animal Research Ethics Board (AUP# 23-19).

Tissue Microarray Creation

Human lung tissue microarrays were constructed from formalin-fixed paraffin-embedded (FFPE) surgical lung biopsies from IPF patients and non-fibrotic controls, with the guidance of molecular pathologists (AN and JCC). Regions of interest were selected from hematoxylin and eosin (H&E) stained slides of the parent surgical lung biopsy blocks. Using a TMA Master II (3D Histech Ltd), cores from parent blocks were punched and inserted into host paraffin blocks. Two tissue microarrays were used in this study: tissue microarray 1 containing 0.6mm cores from IPF patients (cores taken from both fibrotic and non-fibrotic regions) (n=24) and controls (non-involved areas of lung cancer resections) (n=17); and tissue microarray 2 containing 2mm cores from IPF patients (fibrotic areas) (n=55). Demographic information is included in Supplementary Table 1.

For tissue microarrays containing murine precision-cut lung slices (PCLS), full tissues were inserted in host blocks using 2mm cores.

In-situ Hybridization (RNAscope®)

RNAscope® (ACD Bio) fluorescent in-situ hybridization for *CCL18, CD68, MAFB, CD163,* and *MRC1* was performed using commercially available assays. Staining was

completed at the John Mayberry Core Histology Facility at the McMaster Immunology Research Centre, using the Leica Bond RX immunostainer.

Immunohistochemistry

Immunohistochemical (IHC) staining was performed at the John Mayberry Core Histology Facility at the McMaster Immunology Research Centre. Staining of CD206 (Abcam ab64693) and CD163 (Abcam ab182422) on human lung tissue microarrays was performed using the Leica Bond RX. For murine PCLS, tissues were fixed in 10% formalin for 24 hours and then transferred to 70% ethanol. Fixed tissues were subsequently embedded in paraffin. IHC staining on PCLS tissue microarrays was completed for Arginase-1 (Cell Signalling Cs93668) and CD206 (Abcam ab64693) on the Leica Bond RX.

Slide Imaging and Histological Quantification

Slides were imaged using the Olympus VS120 Slide Scanner (20x brightfield, 40x fluorescent). Full slide images of tissue microarrays were quantitatively analyzed using the Area Quantification module in HALO Image Analysis Software (Indica Labs).

$CD14^+$ Monocyte Isolation

Peripheral blood was obtained from IPF patients and control subjects at the Firestone Institute for Respiratory Health. $CD14^+CD16^-$ monocytes were directly isolated from whole blood collected in K_2EDTA tubes (BD) using immunomagnetic negative selection (STEMCELL Technologies). Cells were then counted, pelleted and lysed with RNA lysis buffer. Lysates were stored at -80°C until RNA extraction. For this study, monocytes were obtained from 49 IPF patients and 12 control subjects. Demographic information is included in Supplementary Table 2 and Supplementary Table 3.

RNA Isolation

RNA was isolated from monocyte lysates using a spin column extraction kit, following the manufacturer's instructions (Macherey-Nagel). Prior to sequencing, RNA quality was measured using a High Sensitivity RNA ScreenTape® Device at the McMaster Farncombe Metagenomics Facility to confirm an RNA Integrity Number (RIN) of 7 or higher (average RIN>9).

For FFPE lung tissue cores, RNA was isolated using an FFPE-specific spin column extraction kit, following the manufacturer's instructions (Macherey-Nagel).

NanoString Gene Expression

NanoString gene expression was conducted using RNA isolated from FFPE lung samples. RNA was assessed using the nCounter Analysis System at the McMaster Farncombe Metagenomics Facility. Gene expression was normalized using the total counts normalization method, and was processed and analyzed using nSolver and R. *ACTB, B2M, PGK1, POLR2A, PPBI, RPLP2,* and *UBC* were used as housekeeping genes.

Bulk RNA Sequencing

RNA sequencing on monocyte samples was conducted at the McMaster Farncombe Metagenomics Facility. Directional library preparation was performed using poly-A mRNA enrichment (New England Biolabs). Bulk RNA sequencing was completed using the Illumina HiSeq 1500, with single end reads of 75 base pairs and an average sequencing depth of 9.1 million clusters.

Reads were mapped using HISAT2 [10] with hg38 (UCSC) reference genome and counted using HTSeq [11]. Genes with low expression across samples were removed, and *TMM*

normalization [12] and *voom* transformation [13] were performed in R. *Limma* package was used for differential expression (DE) analysis [14]. BH correction for multiple testing was used to correct p values [15], with $p < 0.05$ denoting statistical significance. Volcano plots were created with *EnhancedVolcano* package in R. For enrichment analysis using published datasets, gene set enrichment analysis (GSEA) was used. MATLAB Clustergram function and *gplots* package in R were used to generate the heatmap with hierarchical clustering. For visualization of clusters, *rgl* package in R was used for principal component analysis and plots. STRING was used for enrichment of Gene Ontology (GO) processes and pathways (querying STRING clusters, Reactome, KEGG, and Wikipathways databases). GSEA of differentially expressed genes between IPF and control and between the clusters was determined using HALLMARK, C2cp, and C5 gene set databases.

Analysis of Public IPF Single Cell RNA Sequencing Datasets

Human IPF single cell RNA sequencing data was obtained from published publicly available datasets. Data were either visualized using R or the IPF Cell Atlas (GSE135893[16], GSE136831 [17]; https://www.ipfcellatlas.com)

Cell Culture

RAW 264.7 macrophages were cultivated in DMEM supplemented with 10% FBS, 2 mM L-Glutamine, 100 U/mL penicillin, 100 µg/mL streptomycin, and 2.5 µg/mL amphotericin B. For polarization assays, cells were treated with recombinant IL-4 (20 ng/mL), IL-6 (5 ng/mL), and IL-13 (50 ng/mL) (Peprotech) with or without dichloroacetate (DCA; Sigma-Aldrich) at a range of concentrations (10-25mM) for 24 hours.

THP-1 monocytes were cultivated in RPMI supplemented with 10% FBS, 100 U/mL penicillin, and 100 µg/mL streptomycin. THP-1 were differentiated into adherent macrophages with treatment of 10ng/mL phorbol 12-myristate 13-acetate (PMA) for 72 hours. For polarization assays, cells were treated with recombinant IL-4 (20 ng/mL), IL-6 (20 ng/mL), and IL-13 (20 ng/mL) (Peprotech) for 72 hours, followed by treatment with DCA (10mM or 20mM; Sigma-Aldrich) for an additional 72 hours.

Generation and Culture of PCLS

Murine PCLS were generated from 8–12-week female C57Bl/6 mice (The Jackson Laboratory), as previously described (Vierhout et al. 2024, [18]). Briefly, PCLS were cut using a Compresstome (Precisionary) at 500µM thickness and punched at 2mm or 4mm diameter, and were cultivated in DMEM culture medium supplemented with 10% fetal bovine serum, 2 mM L-Glutamine, 100 U/mL penicillin, 100 µg/mL streptomycin, and 2.5 µg/mL amphotericin B (37°C, 5% CO2). For polarization assays, PCLS were treated recombinant IL-4 (40 ng/mL), IL-6 (10 ng/mL), and IL-13 (100 ng/mL) (Peprotech) with or without DCA at a range of concentrations (10-25mM) for 48 hours.

Water Soluble Tetrazolium 1 (WST-1) Assay

10µL of WST-1 reagent (Roche) per well was added to 100µL of culture medium with cells or PCLS. The plate was incubated for 1 hour at 37°C, prior to reading absorbance of supernatant at a wavelength of 450 nm.

Arginase Activity Assay

Arginase activity was determined as previously described [19]. Briefly, cells were either directly lysed in the culture plate, or PCLS were homogenized using a Bullet Bead

Homogenizer (Next Advance) in lysis buffer (0.1% Triton-X supplemented with protease inhibitors). Cell or tissue lysates were then diluted with 25mM Tris-HCl and 10 mM manganese chloride was added, followed by a heated incubation at 56°C for 10 minutes. This was followed by addition of 0.5 M L-arginine and a subsequent heated incubation at 37°C for 30 minutes. Urea standards, sulphuric+phosphoric acid solution, and 9% α-ISPF were added to the plate, followed by a final incubation at 95°C for 30 minutes. Absorbance was then read at a wavelength of 550 nm.

Enzyme Linked Immunosorbent Assay (ELISA)

IL-10, CCL18, and YM1 ELISAs were performed according to the manufacturer's instructions (R&D Systems).

Western Blotting

Western blotting was performed as previously described [20]. Briefly, total protein from cell lysates was separated based on molecular weight on SDS polyacrylamide electrophoresis gels. Proteins were then transferred to a PVDF membrane using wet transfer. After transfer, membranes were blocked at room temperature for one hour in 5% BSA. Proteins were detected with ECL substrate and membranes were imaged using a ChemiDoc XRS Imaging System (Bio-Rad). Signal was quantified using ImageJ software. Primary antibodies used for western blotting were Arginase-1 (BD, 610708), IL-10 (Abcam, ab133575), CCL18 (Abcam, ab300057), α-tubulin (Cell Signalling Technology, 2144S), and β-Actin (Sigma-Aldrich, A5316), and secondary antibodies were Anti-rabbit (Cell Signalling Technology, 7074S) and Anti-mouse (Cell Signalling Technology, 7076S).

Statistical Analysis

Statistical analysis of data was performed using GraphPad Prism (Version 10). For comparisons between two groups, significance was determined using an unpaired two-tailed t-test or Mann-Whitney test, based on normality. For more than three-groups, one-way ANOVA with Tukey's or Kruskal-Wallis post hoc testing was used, based on normality. Normality of the data was determined with a Shapiro-Wilk test. A p value of less than 0.05 was considered statistically significant.

RESULTS

Circulating Monocytes and Monocyte-Derived Macrophages in IPF Patient Blood and Lung Samples.

To begin, we first substantiated the finding of increased monocyte count in IPF in our cohort. CD14+ monocytes were isolated from the blood of IPF patients and control subjects and cell count was obtained directly after. We found that monocyte quantity was increased in IPF patients compared to control subjects (**Figure 1A**). We also observed a negative correlation between monocyte count and forced vital capacity (FVC) in IPF patients (**Figure 1B**), which is accordance with the finding that monocyte count is linked to poor outcomes in IPF. Next, in order to verify the presence of monocyte-derived macrophages in the lung, we examined CD14 gene expression in various lung cell populations using a published scRNAseq dataset on lung explant tissue removed at the time of surgery from IPF and non-fibrotic controls (IPF Cell Atlas, GSE135893[16]). CD14 expression was found to be highest in monocytes, macrophages, and proliferating macrophages (**Figure 1C**), supporting that these cell populations in the lung are derived from CD14 circulating

cells. Further supporting the presence of monocyte-derived macrophages in the IPF lung, we performed dual RNAscope in-situ hybridization to show colocalization of MAFB (monocytic transcription factor) and CD68 (macrophage marker) (**Figure 1D**) in the i. airway and ii. interstitium of IPF FFPE lung tissue. Additionally, supporting profibrotic programming of $MAFB^{+}$ cells, triplex in-situ hybridization showed colocalization of MAFB (monocytic transcription factor), CD163 (alternatively activated macrophage marker) and MRC1 (gene name for CD206, alternatively activated macrophage marker) in IPF lung tissue (Figure 1E). Overall, these results demonstrate increase of CD14 monocytes in IPF in our cohort, and support the presence of monocyte-derived profibrotic macrophages in the lung.

Macrophages Expressing Markers of Profibrotic Alternative Activation are Increased in IPF Lung Tissue.

Next, we performed a quantitative assessment of profibrotic macrophages in IPF lung. Using a tissue microarray containing surgical lung biopsy tissue from IPF patients (n=24) and controls (n=17) (tissue microarray 1), we performed immunohistochemical staining for established profibrotic macrophage markers CD206 and CD163. After quantifying full slide images with HALO image analysis software, we found that both CD206 (**Figure 2A,B**) and CD163 (**Figure 2C,D**) staining was increased IPF lung tissue (in both fibrotic and non-fibrotic areas) compared to control tissue. A second tissue microarray was constructed using FFPE lung biopsies from multiple IPF patients to be used for analyses with clinical parameters (n=55) (tissue microarray 2). Using this TMA, we performed correlational analyses of FVC with macrophage immunohistochemistry, and found that

FVC is negatively correlated with both CD206 (**Figure 2E**) and CD163 (**Figure 2F**). Notably, no active smokers were included in correlational analyses as smoking has been shown to markedly elevate pulmonary macrophage number [21], thus acting as a confounding variable. Additionally, using in-situ hybridization, colocalization of CCL18 and CD68 mRNA transcripts were observed in IPF lung, supporting that macrophages have an alternatively activated phenotype in IPF (**Figure 2G**). Adding to this, CCL18 gene expression was shown to be elevated in RNA isolated from FFPE tissue punches taken from IPF lung (**Figure 2H**), compared to control.

Transcriptomic Analysis Reveals Differentially Expressed Genes in IPF Monocytes Which Show General Similarities to Features of Macrophage Activation and Fibrosis. To elucidate the widely unknown characteristics of monocytes in IPF, we performed bulk RNA sequencing on RNA isolated from IPF and control monocytes. Differential expression analysis yielded 474 significantly differentially expressed (DE) genes (**Figure 3A)**. Recently, Wang et al. published a comprehensive list of "Known Pulmonary Fibrosis Genes" that includes human genes associated with lung fibrosis from multiple published datasets [22]. To first obtain an overall understanding potential fibrosis-related properties of the monocytes, we compared the 474 DE genes in our dataset to the published list and found an overlap of 104 genes (**Figure 3B)**. Shared genes (from upregulated genes in our dataset) are listed. Gene names that are bolded have been reported to be associated with macrophage polarization, while those highlighted in blue have been reported to be involved in monocyte recruitment and monocyte-to-macrophage differentiation. Additionally, highly DE genes in our dataset that overlap with this list are marked on the volcano plot in

Figure 3A. Overall, this suggests that the transcriptomic characteristics of monocytes in IPF are related to known fibrotic processes. Subsequently, to further and more precisely investigate the potential similarities of our dataset to known IPF-related features, we performed gene set enrichment analysis (GSEA) to compare our dataset to published IPF datasets. To examine the similarities of our data with known properties of circulating cells in IPF, and to gauge if monocytes may have biomarker potential in IPF, we used a published 52-gene signature in peripheral blood mononuclear cells (PBMC) for outcome prediction in IPF (GSE28042 [8]). GSEA revealed significant enrichment; specifically, genes from the published PBMC dataset related to longer transplant-free survival were enriched in donors in our dataset (and thus downregulated in IPF), which supports similarities between the two datasets (**Figure 3C**). As it is believed that monocytes contribute to cell populations in the lung in IPF, we next aimed to evaluate potential similarities with IPF lung tissue. Using two published datasets on gene expression signatures in lung tissue from IPF patients (GSE53845 and GSE92592 [23,24]), we found that genes upregulated in our donors (and thus downregulated in IPF samples) were found to be enriched in the controls of the published studies (**Figure 3D**). This further substantiates the potential fibrosis-related transcriptomic features of monocytes in IPF.

Patient Clusters in Our Dataset Show Association with Features Related to Disease Severity, Including Lung Function and Transplant-Free Survival.

To further visualize our data, we created a heatmap of DE genes (fold change ≥ 1.5), which displayed three clusters, as determined by hierarchical clustering (**Figure 4A**). Principal component analysis showed separation of these clusters, primarily along the PC1 axis

(**Figure 4B**). To assess associations between the transcriptomic characteristics of monocytes and disease severity, we then classified the patients in our dataset into categories of lung function severity based on FVC and DLCO, according to the literature [25,26]. We examined the stratification of these severity categories across the three clusters and found that composition of each cluster seemed to gradually increase in overall lung function severity (from 1 to 3, with 3 having the highest percentage of severe) (**Figure 4C**). We also found a gradual increase in the percentage death or transplant (assessed in three-year period following study visit) across the clusters. The Fisher Exact test was used to demonstrate significant differences in the composition of the clusters (**Figure 4D**). Overall, this demonstrates the potential relevance of monocyte profile and phenotype to disease outcomes in IPF.

Gene Ontology Enrichment, Pathway, and Gene Set Enrichment Analysis Reveal Downregulation in Metabolism and Mitochondrial Function in IPF Monocytes.

Building on the findings of association to features of fibrosis and clinical measures, we then aimed to further investigate the specific dysregulated processes and pathways that define monocyte profile in IPF. Comparing IPF to control subjects, we first performed Gene Ontology (GO) analysis. This yielded the discovery of multiple enriched processes, with the highest amount relating to *Metabolic, biosynthetic, and catabolic processes* (**Figure 5A**). When examining the top 15 enriched GO processes, we also observed that all except one process were downregulated, and a large proportion of processes were related to metabolism (yellow) and some to cellular translation (green) (**Figure 5B**). Similarly, pathway analysis revealed downregulation of processes related to metabolism and

translation, as well as upregulation of immune activation (red) (**Figure 5C**). As these findings were indicative of metabolic dysregulation, to further explore perturbed processes related to metabolism in the data, we performed a gene set enrichment analysis. This revealed downregulation of multiple processes related to mitochondrial oxidative phosphorylation (OXPHOS) in monocytes in IPF (**Figure 5D**). Interestingly, this aligns with the finding that pyruvate dehydrogenase kinase 4 (PDK4), a gatekeeper kinase that inhibits OXPHOS, is the most highly upregulated protein-coding DE gene in our dataset (**Figure 5E**). To further assess the potential suitability of PDK4 as a target in IPF monocytes, we examined its overall expression in lung cell populations using the IPF Cell Atlas (GSE136831 [17]). This confirmed PDK4 expression in macrophage and alveolar macrophage cell populations in the lung (**Figure 5F)**, as well as increased expression in IPF versus control (**Figure 5G**). In summary, this suggests aberrant mitochondrial function and metabolism as a possible phenotypic feature of monocytes in IPF.

Cluster Comparison with GSEA Reveals Multiple Differentially Regulated Processes in Most Severe Cluster, Including Downregulated Mitochondrial Function and Upregulated Fibrosis-Related Processes.

After investigating the differential characteristics between IPF and control in Figure 5, we then proceeded to analyze the differences between the IPF patients in each cluster in our dataset. Using GSEA on the DE genes between each cluster comparison, we found numerous differentially regulated processes between clusters (**Figure 6A**). Information for networking modules and corresponding node numbers are included in **Supplementary Spreadsheet 1**. Comparisons with cluster 3, as the “most severe cluster” based on Figure

4, had the highest amount of regulated processes, including multiple upregulated processes related to fibrosis, such as wound healing, cell adhesion and ECM, and EMT (**Figure 6B**). Processes related to monocyte recruitment and activation, including monocyte infiltration and differentiation, and immune response, were also found to be upregulated. Lastly, and notably relating to the aberrant mitochondrial findings reported in Figure 5, processes related to mitochondrial function were downregulated. Adding to our previous results, we examined the expression of PDK4 across clusters, and observed that expression gradually increases from cluster 1 to 3 (**Figure 6C**). Taken together, these results further substantiate aberrant mitochondrial/metabolic function in IPF monocytes.

Effect of PDK Inhibition with DCA on Macrophage Polarization in Monocytic Macrophage Cell Lines.

Given our findings thus far supporting evidence for monocyte-derived profibrotic macrophages in IPF lung, aberrant metabolism and decreased OXPHOS, and the link of PDK4 as a highly upregulated gene in the IPF monocytes that is a master OXPHOS regulator, we aimed to conduct mechanistic studies targeting this access to investigate the potential effects on profibrotic macrophage polarization. PDK4 is one of four isoforms of pyruvate dehydrogenase kinase, which has been reported to have the highest kinase activity [27], however all isoforms inhibit OXPHOS. We employed the use of dicholoroacetate (DCA) a well-established pan-PDK inhibitor and orphan drug that has passed human toxicity trials [28], to study this axis. Using our polarization cocktail (PC) consisting of IL-4, IL-13 and IL-6, which we have shown induces hyperpolarization of macrophages to a profibrotic phenotype [19], we investigated the effects of DCA treatment, and thus

OXPHOS induction, on macrophage polarization in RAW 264.7 (murine) and THP-1 (human) cells. We first tested a range of DCA concentrations for effects on viability and determined that concentrations of up to 25mM are suitable for intervention (**Figure 7A**), which is in-line with previous studies [29,30]. DCA treatment was shown to decrease Arginase activity (**Figure 7B)**, as well as IL-10 secretion (**Figure 7C**), in a dose-dependent manner. These findings were corroborated with Arginase-1 and IL-10 protein assessment via western blotting (**Figure 7 D-F)**. In THP-1-derived macrophages, treatment with DCA resulted in decreased CCL18, which is a known human profibrotic macrophage marker in IPF [31], in both the supernatant and cell lysates (**Figure 7 G,H)**. Overall, these results support that intervention of the PDK axis interferes with PC-mediated profibrotic macrophage programming *in vitro,* and thus the overall involvement of metabolically dysfunctional monocytes and macrophages in fibrosis-related processes.

Effect of PDK Inhibition with DCA on Macrophage Polarization in Precision-Cut Lung Slices.

Lastly, to conduct mechanistic studies using a system that is translational to lung biology, we employed our *ex vivo* precision-cut lung slice (PCLS) system for studying pulmonary macrophage polarization (Vierhout et al., [18]). It is well-known that macrophages are incredibly plastic cells with an extensive phenotypic range that cannot be adequately captured in traditional two-dimensional *in vitro* culture. Thus, we extended our mechanistic studies to PCLS to gain insight on the effects of PDK inhibition on profibrotic macrophage polarization the lung. We generated PCLS from murine lungs and treated them with the PC (IL-4, IL-13 and IL-6) to induce profibrotic macrophage polarization. After testing effects

on viability up to a DCA concentration of 25mM (**Figure 8A**), we found a dose-dependent decrease of Arginase activity with DCA treatment in activity in polarized PCLS (**Figure 8B**). In the supernatant, it was observed that YM1 secretion was decreased with all concentrations of DCA treatment (**Figure 8C**). Using quantitative histological assessments on tissue microarrays containing FFPE PCLS, it was observed that DCA treatment decreased Arginase-1 IHC in a dose-dependent manner (**Figure 8D,E**). Additionally, CD206 IHC was decreased with 25mM DCA (**Figure 8F,G**). Overall, these results support the mechanistic involvement of the PDK axis, and thus metabolic processes, in PC-mediated polarization, as well as the contribution of this mechanism to profibrotic macrophage polarization in the lung overall.

DISCUSSION

In this study we conduct transcriptomic profiling to unveil the characteristics of circulating monocytes in IPF, which were previously largely understudied. Consistent with the published literature, we show a significant increase in the quantity of monocytes in IPF [4–7], as well as a negative correlation with forced vital capacity. We demonstrate that the discovered differentially expressed gene signature in IPF monocytes draws parallels with known pulmonary fibrosis genes, monocyte recruitment, monocyte to macrophage differentiation, and macrophage polarization. Through GSEA, we also show similarities between our monocyte dataset and published IPF datasets from both PBMC and lung tissue [8,23,24]. Cluster analysis of the data separated the study subjects into three clusters, which were seemingly associated with lung function severity. Cluster 3 had the highest percent composition of severe disease (based on FVC, DLCO, and death/transplant), followed by Cluster 2, and then Cluster 1. Overall, this suggests that at the transcriptomic level, IPF monocytes carry known characteristics of disease, which may also be of clinical relevance. This provides supportive evidence for the proposed biomarker potential of monocytes in IPF. It also suggests that monocytes are involved in underlying processes driving disease in IPF, which could potentially constitute novel interventional avenues.

Through analyses of differential pathways and processes in the IPF vs. control monocytes, as well comparison of the IPF monocytes across clusters, we uncovered evidence for metabolic and mitochondrial dysregulation. Interestingly, there is growing interest in mitochondrial dysfunction in IPF, which is suggested to be a driving factor of disease [32,33]. Recently, it was shown that mitochondrial transfer is an effective treatment for

pulmonary fibrosis, as this led to decreased fibrosis in the murine bleomycin model as well as a humanized spheroid model [34]. Furthermore, and relevant to our study, it has been found that dysmorphic mitochondria accumulate in alveolar macrophages in IPF patients [35]. These macrophages also displayed decreased capacity for OXPHOS, similar to what we observed in our monocytes. Adding to this further, metabolic investigation of profibrotic alveolar macrophages in murine pulmonary fibrosis models showed increased glycolytic programming, but no dependence on OXPHOS [36]. It has also been previously reported that recruited alveolar macrophages, which are derived from circulating monocytes, have an increased glycolytic capacity, which is in contrast to resident alveolar macrophages which rely on TCA cycle/OXPHOS [37]. Taken together, this evidence supports that monocyte-derived macrophages in the lung have a similar metabolic phenotype to what was found in our circulating monocytes. This suggests that monocytes retain these aberrant features after transitioning into macrophages in the lung, plausibly contributing to processes that drive disease. Previous studies have also shown that CD64 is upregulated in monocytes in IPF and correlated with extent of fibrosis, and we also see significant upregulation of this marker in our cohort [88]. Further substantiating the recruitment of monocytes in IPF, CCR2, which is a receptor that is critical for monocyte trafficking, is among the top 15 differentially expressed genes in IPF in our dataset. It is well-established that macrophages undergo metabolic reprogramming to adapt their internal machinery to achieve different activation and polarization states [38,39]. Given the potential evidence for retention of monocytic aberrant features from the circulation to the lung, it is plausible to postulate that these cells are primed for profibrotic behaviour prior

to entering the lung tissue. Further studies employing lineage tracing strategies will need to be done to validate such behaviour in monocyte-derived alveolar macrophages in fibrosis, as well as elucidate contribution of aberrant monocytes to interstitial macrophage populations in the lung, which are generally much less studied than the alveolar compartment [40].

PDK4 has previously been reported as a "targetable kinase" in IPF, with PDK4 IHC-stained positive alveolar macrophages reported in the IPF lung [41]. This is consistent with the results we found for PDK4 expression using the IPF Cell Atlas, as well as our monocyte data. In monocytes specifically, increased PDK4 expression has been reported in multiple cancers, as well as ARDS and coronary artery disease, and is linked to poor outcomes [42–46]. Many cancer cells exhibit a phenomenon termed the Warburg effect, which is a shift from OXPHOS to glycolysis even in the presence of oxygen [47]. This is associated with PDK, as the master gatekeeper between OXPHOS and glycolysis [47]. This altered metabolism contributes to cellular strategies to adapt and evade apoptosis. Therefore, resistance to apoptosis as a result of altered metabolic programming may also be a contributing factor for the increased monocyte counts observed in IPF.

In our study, we targeted the PDK axis with DCA, which is a well-established pan-PDK inhibitor and an orphan drug that has passed human toxicity trials [28]. There are four isoforms of PDK, with PDK4 reported to have the highest kinase activity, however all isoforms are known to inhibit OXPHOS [27]. Therefore, we decided to target the PDK axis as a whole to investigate the potential mechanistic effects on profibrotic macrophage polarization. With DCA treatment, we observed decreases in various profibrotic

macrophage markers *in vitro*, including Arginase-1, IL-10, and CCL18. Interestingly, this is in contrast with the published literature that has historically reported increased OXPHOS in "M2" macrophages [48]. However, these studies primarily use IL-4 and IL-13 stimulation, while our polarization cocktail also introduced IL-6 to this combination. IL-6 is a pleiotropic cytokine with both pro-inflammatory and pro-fibrotic capacities, which our group has also shown to not only hyperpolarize macrophages *in vitro*, but bolster profibrotic effects *in vivo* as well [19,49]. This is in accordance with findings in IPF that have shown accompaniment of IL-4 and IL-13 with inflammatory cytokines [50,51], supporting that addition of a proinflammatory component to our polarization cocktail would effectuate a phenotype that is more representative of IPF. Similar to the diverse and transient nature of immune activation of macrophages in IPF, which have been shown to have a mix of anti- and proinflammatory markers, it is likely that metabolic programming exists on a spectrum as well in profibrotic macrophages, giving them remarkable plasticity and adaptability.

Intriguingly, DCA has been previously investigated for the treatment of pulmonary fibrosis in a murine bleomycin model [52]. When administered through drinking water, DCA, and thus promotion of OXPHOS, led to a decrease in fibrosis, myofibroblast activation, and ECM deposition in the lung [52]. Study assessments were primarily focused on fibroblasts, and thus, further investigations on the macrophage-specific effects of DCA in *in vivo* pulmonary fibrosis models are required. In our *ex vivo* mechanistic evaluations, we observed decreased markers of profibrotic macrophage polarization with DCA treatment in our PCLS model for macrophage programming. While PCLS are disconnected from the

influence of the circulating immune system, monocytes can still enter the lung and give rise to alveolar macrophage populations at normal physiological state [53], and so it is plausible that some of the alveolar macrophages in the PCLS have monocytic origins. We have previously reported the capability of our PCLS system to induce profibrotic polarization in both alveolar and interstitial macrophages [18]. To better understand the interplay between metabolic and immune activation in *ex vivo* lung macrophages, further phenotypic analysis of macrophages following by DCA treatment, such as through high-content imaging using IBEX [18,54,55], would be useful to conduct in future studies. Additionally, both THP-1 and RAW 264.7 cell lines are leukemic cell lines, and so would naturally display a different metabolic profile than primary macrophages. Thus, such intervention studies should also be performed in primary cells.

Lastly, the transcriptomic observations in this work have set the stage for a follow-up study to conduct functional assessments of the aberrant metabolic phenotype we observed. This can be achieved using extracellular flux analysis, such as with an Agilent Seahorse XF Analyzer, to directly measure mitochondrial respiration and glycolysis using freshly-isolated live cells. While our transcriptomic profile did show downregulation of gene expression associated with OXPHOS and mitochondrial function, we cannot definitively conclude that glycolytic programming was enhanced in the IPF monocytes to compensate for this shift. Therefore, metabolic functional assessments would be useful for providing functional metabolic insight through measuring glycolysis, as well as mitochondrial respiration. Functional assessments on DCA-treated cells would also be critical for demonstrating that PDK-inhibition by this drug is driving the phenotypic change we see,

which we cannot currently definitively claim is not, at least in part, also due to off-target effects. These studies should be conducted in an external cohort of IPF patients, and be compared to monocytes from age-matched controls, for which availability was limited in our study. The older age of the IPF compared to the control subjects is a limitation of our study, and may be implicated in some of the transcriptional factors we observe. Further studies on larger, age-matched populations are required.

In summary, our results highlight district characteristics in monocytes in IPF, which may be related to underlying disease-driving process in IPF. This work unveils novel metabolic target in monocytes in IPF, which may contribute to macrophage profibrotic activity in the lung. Mechanistic studies reveal that altering metabolic state influences profibrotic macrophage polarization *ex vivo* and *in vitro*, overall offering insight into alternative activation states of these cells in IPF.

Figure 1

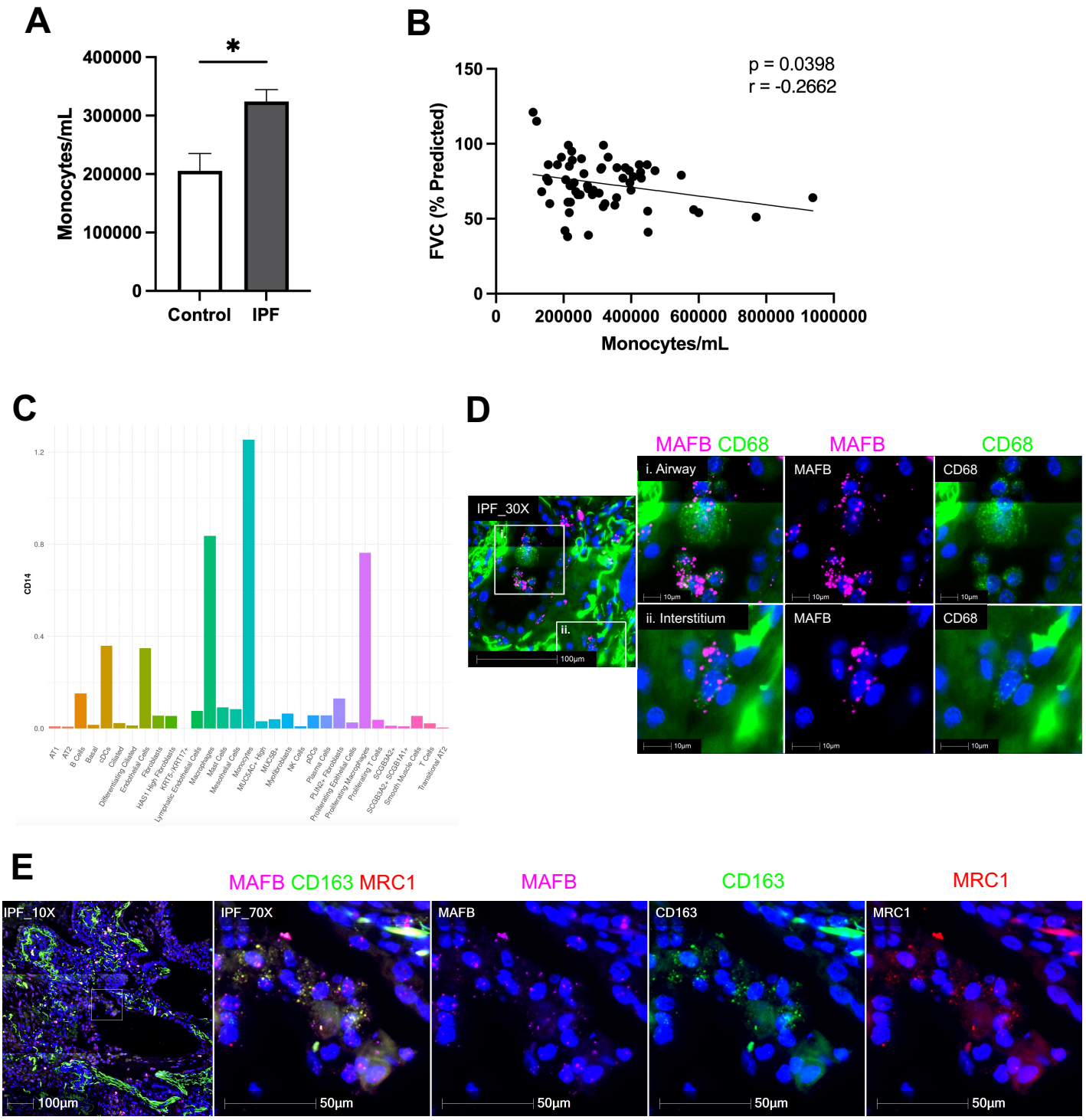
A
*
400000
300000
200000
100000
0
Monocytes/mL
Control
IPF
B
p = 0.0398
r = -0.2662
150
100
50
0
FVC (% Predicted)
0
200000
400000
600000
800000
1000000
Monocytes/mL
C
CD14
1.2
0.8
0.4
0.0
AT1
AT2
B Cells
Basal
cDCs
Ciliated
Differentiating Ciliated
Endothelial Cells
Fibroblasts
HAS1 High Fibroblasts
KRT5-/KRT17+
Lymphatic Endothelial Cells
Macrophages
Mast Cells
Mesothelial Cells
Monocytes
MUC5AC+ High
MUC5B+
Myofibroblasts
NK Cells
pDCs
Plasma Cells
PLIN2+ Fibroblasts
Proliferating Epithelial Cells
Proliferating Macrophages
Proliferating T Cells
SCGB3A2+ SCGB1A1+
Smooth Muscle Cells
T Cells
Transitional AT2
D
MAFB CD68
MAFB
CD68
IPF_30X
i.
ii.
100µm
i. Airway
ii. Interstitium
MAFB
CD68
10µm
E
MAFB CD163 MRC1
MAFB
CD163
MRC1
IPF_10X
IPF_70X
MAFB
CD163
MRC1
100µm
50µm

Figure 1: Circulating Monocytes and Monocyte-Derived Macrophages in IPF Patient Blood and Lung Samples.

A: CD14+ monocyte quantity in blood isolated from IPF and control patients, expressed as monocytes per mL blood. * indicates $P < 0.05$, data are displayed as mean ± S.E.M. **B:** Correlation of FVC (% predicted) with monocyte count in IPF patient samples (Pearson's correlation). **C:** CD14 expression in lung cell populations, determined from scRNAseq analysis on lung explant tissue removed at the time of surgery from IPF (n=12) and non-fibrotic controls (n=10) using the IPF Cell Atlas (GSE135893 [16]). **D:** Dual RNAscope in-situ hybridization showing colocalization of MAFB (monocytic transcription factor) and CD68 (macrophage marker) in the i. airway and ii. interstitium of IPF lung tissue. **E:** Triple RNAscope in-situ hybridization showing colocalization of MAFB (monocytic transcription factor), CD163 (alternatively activated macrophage marker), and MRC1 (gene name for CD206, alternatively activated macrophage marker) in IPF lung tissue.

Figure 2

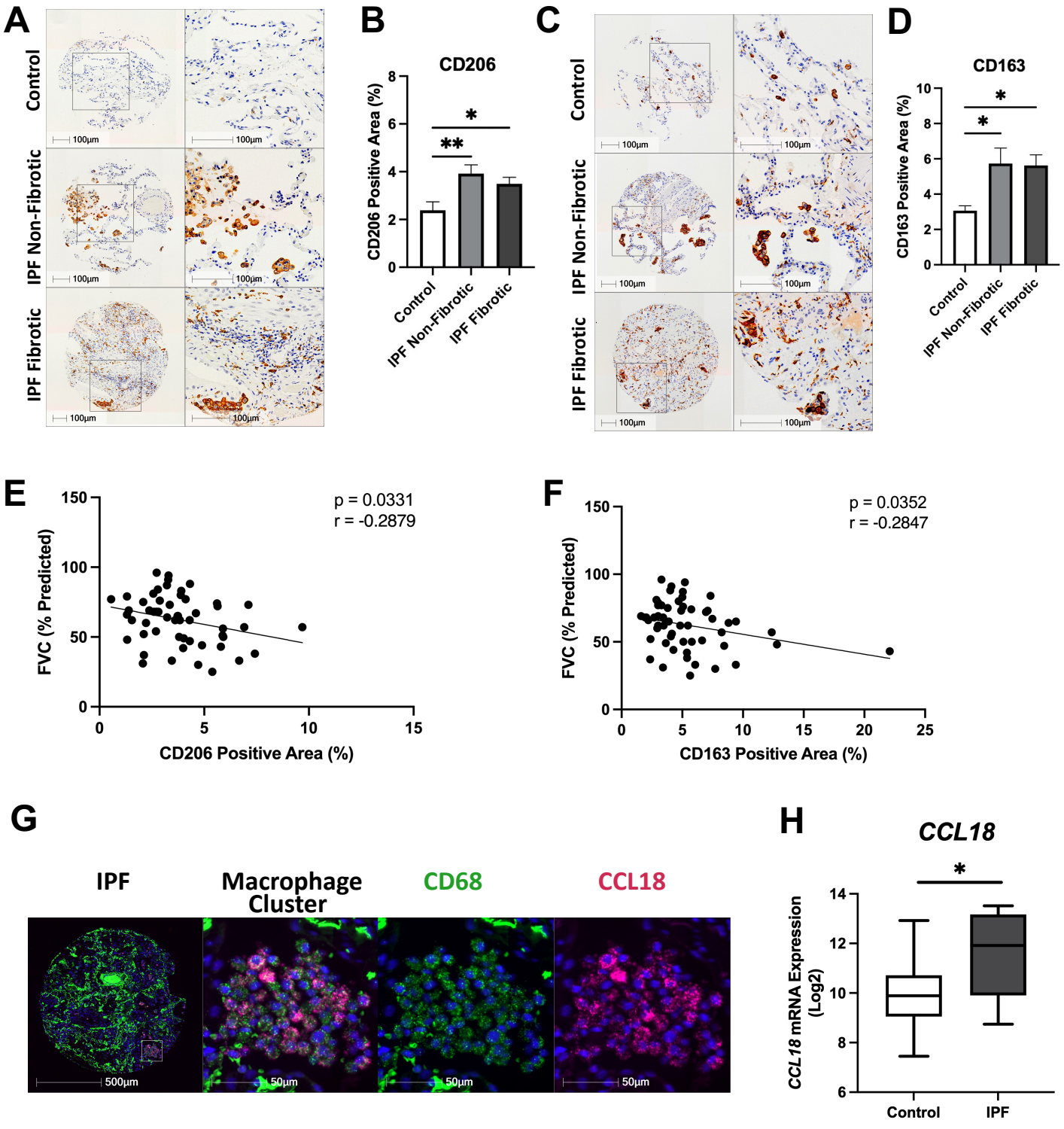
A
Control
IPF Non-Fibrotic
IPF Fibrotic
100µm
B
CD206
CD206 Positive Area (%)
Control
IPF Non-Fibrotic
IPF Fibrotic
C
D
CD163
CD163 Positive Area (%)
E
p = 0.0331
r = -0.2879
FVC (% Predicted)
CD206 Positive Area (%)
F
p = 0.0352
r = -0.2847
CD163 Positive Area (%)
G
IPF
Macrophage Cluster
CD68
CCL18
500µm
50µm
H
CCL18
CCL18 mRNA Expression (Log2)

Figure 2: Macrophages Expressing Markers of Profibrotic Alternative Activation are Increased in IPF Lung Tissue.

A, B: CD206 and **C,D:** CD163 immunohistochemical staining in FFPE surgical lung biopsies from IPF patients (n=24) and non-fibrotic control subjects (n=17) (tissue microarray 1), quantified with HALO image analysis platform. Data are displayed as mean ± S.E.M. **E, F:** Correlation of FVC (% predicted) with CD206 and CD163 immunohistochemical staining in IPF patients (n=55; tissue microarray 2; Pearson's correlation). **G:** Dual RNAscope in-situ hybridization exhibiting colocalization of CD68 and CCL18 mRNA transcripts in IPF lung. **H:** CCL18 mRNA expression from FFPE tissue cores taken from in IPF (n=11) and control (n=11) surgical lung biopsies, displayed as box and whisker plot. * indicates $P < 0.05$; ** indicates $P < 0.01$.

Figure 3

A

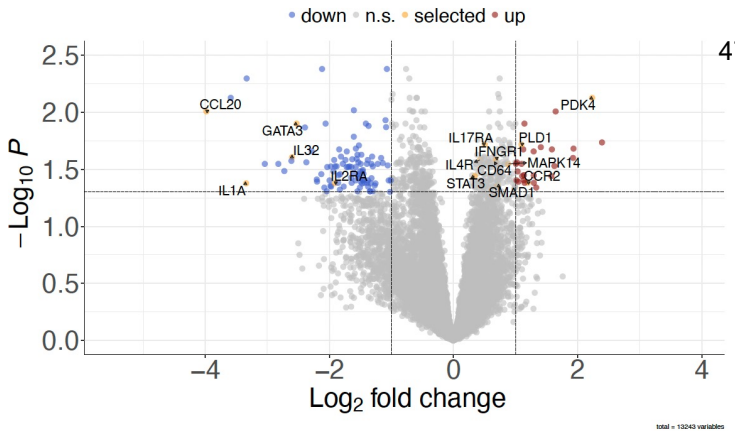

B

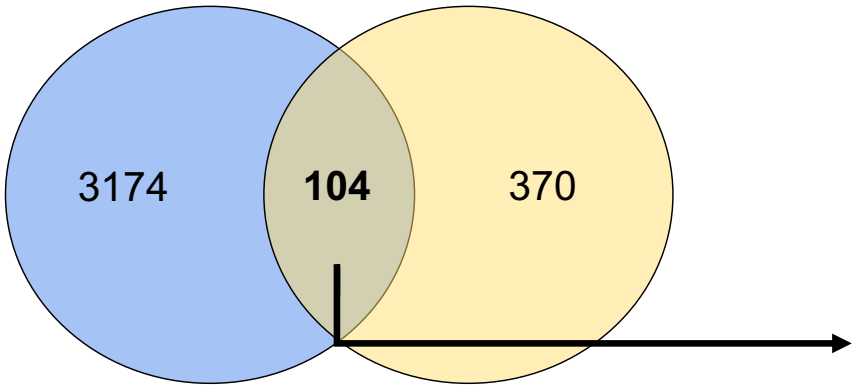

Overlapping Upregulated Genes:

1. PDK4	**20. SOAT1**
2. CCR2	**21. FZD1**
3. PLD1	**22. MLKL**
4. FOS	**23. TNFRSF1A**
5. NLRC4	24. MTHFR
6. KREMEN1	25. TANK
7. ERLIN1	26. ARHGAP26
8. IRAK3	**27. IL17RA**
9. MAPK14	**28. MAP3K7**
10. CR1	**29. PPARD**
11. HHEX	**30. MCU**
12. CLEC4D	**31. NUMB**
13. CHUK	**32. IL4R**
14. TBK1	**33. PTPN6**
15. SMAD1	**34. DNAJC5**
16. HPS6	**35. STAT3**
17. DGAT2	**36. FYN**
18. CD64	**37. IRAK4**
19. IFNGR1	

Bold: Associated with macrophage polarization
Blue: Monocyte recruitment and mono-to-mac differentiation

C **GSEA: IPF Blood Dataset (PBMC)**

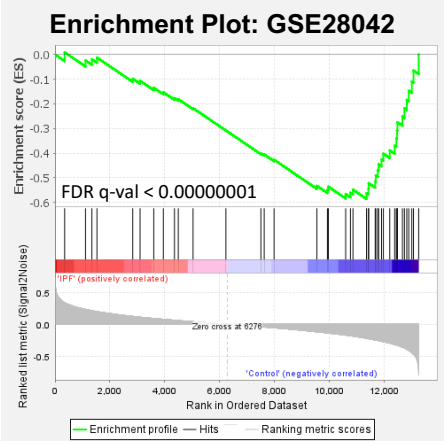

D **GSEA: IPF Lung Datasets (Biopsies/Explants)**

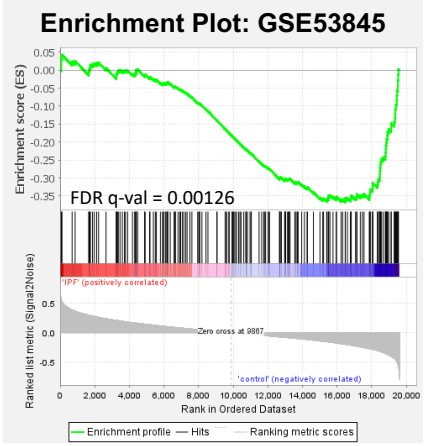

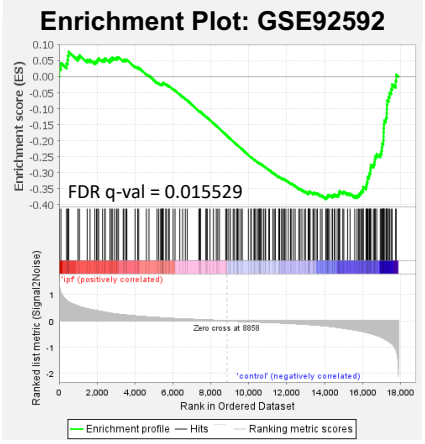

Figure 3: Transcriptomic Analysis Reveals Differentially Expressed Genes in IPF Monocytes Which Show General Similarities to Features of Macrophage Activation and Fibrosis.

A: Volcano plot displaying differentially expressed (DE) genes in monocytes from IPF versus control subjects. 474 genes were found to be significantly differentially expressed. Marked genes in plot overlap with known list of pulmonary fibrosis genes published by Wang et al. (2020) [22]. **B:** Venn diagram comparing DE genes in our dataset (474) to a published list of known pulmonary fibrosis genes (3278) [22]. Shared genes (from upregulated genes in our dataset) are listed. Gene names that are bolded have been reported to be associated with macrophage polarization, while those highlighted in blue have been reported to be involved in monocyte recruitment and monocyte-to-macrophage differentiation. **C:** Gene set enrichment analysis (GSEA) of our dataset and a published 52-gene signature in peripheral blood mononuclear cells (PBMC) for outcome prediction in IPF [8]. Specifically, genes from the published dataset related to longer transplant-free survival were enriched in donors in our dataset (and thus downregulated in IPF). **D:** GSEA of our dataset and two published datasets on gene expression signatures in lung tissue from IPF patients [23,24]. Specifically, genes upregulated in our donors (and thus downregulated in IPF samples) were found to be enriched in the controls of the published IPF lung datasets.

Figure 4

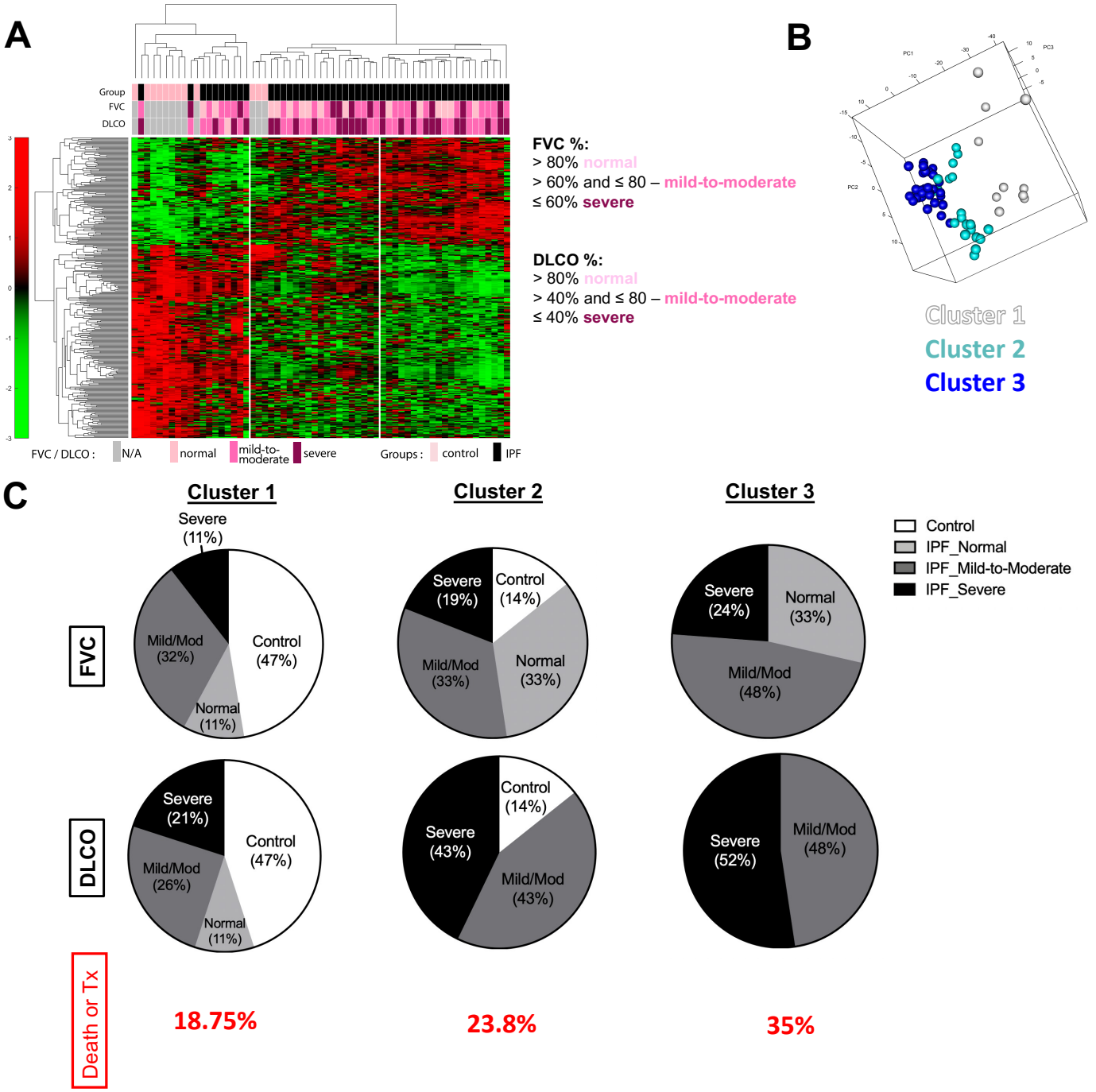

D

Disease	Cluster 1		Cluster 2		Cluster 3	
	FVC	DLCO	FVC	DLCO	FVC	DLCO
Control	9 (47%)	9 (47%)	3 (14%)	3 (14%)	0	0
IPF						
Normal	2 (11%)	2 (11%)	7 (33%)	0	6 (29%)	0
Mild/Mod	6 (32%)	5 (26%)	7 (33%)	9 (43%)	10 (48%)	10 (48%)
Severe	2 (11%)	4 (21%)	4 (19%)	9 (43%)	5 (24%)	11 (52%)
Total	**19**		**21**		**21**	

FVC: Fisher Exact test p-value = 0.01317
DLCO: Fisher Exact test p-value = 0.001998

Figure 4: Patient Clusters in Our Dataset Show Association with Features Related to Disease Severity, Including Lung Function and Transplant-Free Survival.

A: Heatmap of differentially expressed genes (FC ≥ 1.5) arranged by patient clusters (Cluster 1- left, Cluster 2- middle, Cluster 3- right). Group (IPF or control) and FVC and DLCO categories are marked above the plot, with lung function ranges defining each category of severity for FVC and DLCO denoted to the right of the heatmap. **B:** Principal component analysis plot displaying separation of clusters. **C:** Pie charts depicting composition of each cluster based on categories of FVC and DLCO. Percentage of death or transplant (Tx) in the three-year period following study sample collection for each cluster is included in red. **D:** Table displaying stratification of subjects in each cluster based on lung function category. The Fisher Exact test was used to demonstrate significant differences in the composition of the clusters.

Figure 5

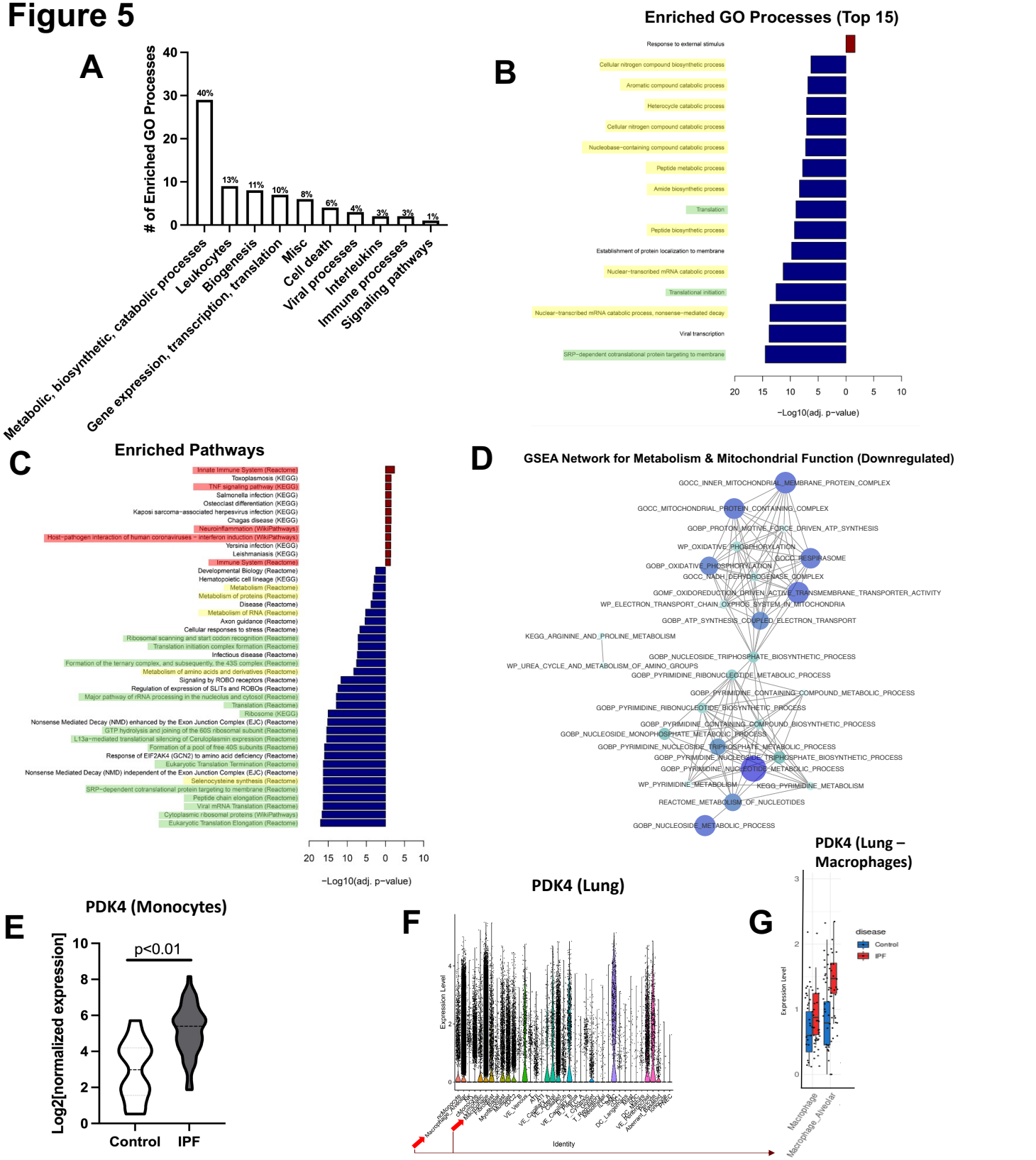
A
# of Enriched GO Processes
40%
13%
11%
10%
8%
6%
4%
3%
3%
1%
Metabolic, biosynthetic, catabolic processes
Leukocytes
Biogenesis
Gene expression, transcription, translation
Misc
Cell death
Viral processes
Interleukins
Immune processes
Signaling pathways
B
Enriched GO Processes (Top 15)
Response to external stimulus
Cellular nitrogen compound biosynthetic process
Aromatic compound catabolic process
Heterocycle catabolic process
Cellular nitrogen compound catabolic process
Nucleobase−containing compound catabolic process
Peptide metabolic process
Amide biosynthetic process
Translation
Peptide biosynthetic process
Establishment of protein localization to membrane
Nuclear−transcribed mRNA catabolic process
Translational initiation
Nuclear−transcribed mRNA catabolic process, nonsense−mediated decay
Viral transcription
SRP−dependent cotranslational protein targeting to membrane
−Log10(adj. p−value)
C
Enriched Pathways
Innate Immune System (Reactome)
Toxoplasmosis (KEGG)
TNF signaling pathway (KEGG)
Salmonella infection (KEGG)
Osteoclast differentiation (KEGG)
Kaposi sarcoma−associated herpesvirus infection (KEGG)
Chagas disease (KEGG)
Neuroinflammation (WikiPathways)
Host−pathogen interaction of human coronaviruses − interferon induction (WikiPathways)
Yersinia infection (KEGG)
Leishmaniasis (KEGG)
Immune System (Reactome)
Developmental Biology (Reactome)
Hematopoietic cell lineage (KEGG)
Metabolism (Reactome)
Metabolism of proteins (Reactome)
Disease (Reactome)
Metabolism of RNA (Reactome)
Axon guidance (Reactome)
Cellular responses to stress (Reactome)
Ribosomal scanning and start codon recognition (Reactome)
Translation initiation complex formation (Reactome)
Infectious disease (Reactome)
Formation of the ternary complex, and subsequently, the 43S complex (Reactome)
Metabolism of amino acids and derivatives (Reactome)
Signaling by ROBO receptors (Reactome)
Regulation of expression of SLITs and ROBOs (Reactome)
Major pathway of rRNA processing in the nucleolus and cytosol (Reactome)
Translation (Reactome)
Ribosome (KEGG)
Nonsense Mediated Decay (NMD) enhanced by the Exon Junction Complex (EJC) (Reactome)
GTP hydrolysis and joining of the 60S ribosomal subunit (Reactome)
L13a−mediated translational silencing of Ceruloplasmin expression (Reactome)
Formation of a pool of free 40S subunits (Reactome)
Response of EIF2AK4 (GCN2) to amino acid deficiency (Reactome)
Eukaryotic Translation Termination (Reactome)
Nonsense Mediated Decay (NMD) independent of the Exon Junction Complex (EJC) (Reactome)
Selenocysteine synthesis (Reactome)
SRP−dependent cotranslational protein targeting to membrane (Reactome)
Peptide chain elongation (Reactome)
Viral mRNA Translation (Reactome)
Cytoplasmic ribosomal proteins (WikiPathways)
Eukaryotic Translation Elongation (Reactome)
−Log10(adj. p−value)
D
GSEA Network for Metabolism & Mitochondrial Function (Downregulated)
GOCC_INNER_MITOCHONDRIAL_MEMBRANE_PROTEIN_COMPLEX
GOCC_MITOCHONDRIAL_PROTEIN_CONTAINING_COMPLEX
GOBP_PROTON_MOTIVE_FORCE_DRIVEN_ATP_SYNTHESIS
WP_OXIDATIVE_PHOSPHORYLATION
GOCC_RESPIRASOME
GOBP_OXIDATIVE_PHOSPHORYLATION
GOCC_NADH_DEHYDROGENASE_COMPLEX
GOMF_OXIDOREDUCTION_DRIVEN_ACTIVE_TRANSMEMBRANE_TRANSPORTER_ACTIVITY
WP_ELECTRON_TRANSPORT_CHAIN_OXPHOS_SYSTEM_IN_MITOCHONDRIA
GOBP_ATP_SYNTHESIS_COUPLED_ELECTRON_TRANSPORT
KEGG_ARGININE_AND_PROLINE_METABOLISM
GOBP_NUCLEOSIDE_TRIPHOSPHATE_BIOSYNTHETIC_PROCESS
WP_UREA_CYCLE_AND_METABOLISM_OF_AMINO_GROUPS
GOBP_PYRIMIDINE_RIBONUCLEOTIDE_METABOLIC_PROCESS
GOBP_PYRIMIDINE_CONTAINING_COMPOUND_METABOLIC_PROCESS
GOBP_PYRIMIDINE_RIBONUCLEOTIDE_BIOSYNTHETIC_PROCESS
GOBP_PYRIMIDINE_CONTAINING_COMPOUND_BIOSYNTHETIC_PROCESS
GOBP_NUCLEOSIDE_MONOPHOSPHATE_METABOLIC_PROCESS
GOBP_PYRIMIDINE_NUCLEOSIDE_TRIPHOSPHATE_METABOLIC_PROCESS
GOBP_PYRIMIDINE_NUCLEOSIDE_TRIPHOSPHATE_BIOSYNTHETIC_PROCESS
GOBP_PYRIMIDINE_NUCLEOTIDE_METABOLIC_PROCESS
WP_PYRIMIDINE_METABOLISM
KEGG_PYRIMIDINE_METABOLISM
REACTOME_METABOLISM_OF_NUCLEOTIDES
GOBP_NUCLEOSIDE_METABOLIC_PROCESS
E
PDK4 (Monocytes)
p<0.01
Log2[normalized expression]
Control
IPF
F
PDK4 (Lung)
Expression Level
Identity
G
PDK4 (Lung – Macrophages)
disease
Control
IPF
Expression Level
Macrophage
Macrophage_Alveolar

Figure 5: Gene Ontology Enrichment, Pathway, and Gene Set Enrichment Analysis Reveal Downregulation in Metabolism and Mitochondrial Function in IPF Monocytes.

A: Category breakdown of all Gene Ontology Processes that were found to be enriched in our dataset (IPF vs. control). Percentage composition of the total number of enriched processes is denoted above each bar. **B**: Top 15 Gene Ontology (GO) Biological Processes that were enriched in IPF versus control monocytes. Red bars represent upregulated processes, while blue bars represent downregulated processes. Processes related to metabolism are marked in yellow; processes related to cellular translation mechanisms are marked in green. **C:** All pathways that were found to be enriched in our dataset. Red bars represent upregulated pathways, while blue bars represent downregulated pathways. Processes related to immune system activation are marked in red; processes related to metabolism are marked in yellow; processes related to cellular translation mechanisms are marked in green. **D:** Network of Gene Set Enrichment Analysis (GSEA) for metabolism and mitochondria modules (found to be downregulated in IPF). Node size represents normalized enrichment score, while node colour intensity represents adjusted p-value. **E:** Violin plot of expression of PDK4 in our monocyte dataset (most highly upregulated protein-coding DE gene in our dataset). **F:** Violin plot of overall expression of PDK4 in cell populations in lung tissue from IPF patients (n=32) and non-fibrotic controls (n=28) determined by scRNAseq (IPF Cell Atlas, GSE136831 [17]). Red arrows point to macrophage and alveolar macrophage populations. **G:** PDK4 macrophage and alveolar

macrophage expression in IPF and control subjects (Cell Atlas, subset of plot for GSE136831 [17]).

Figure 6

A

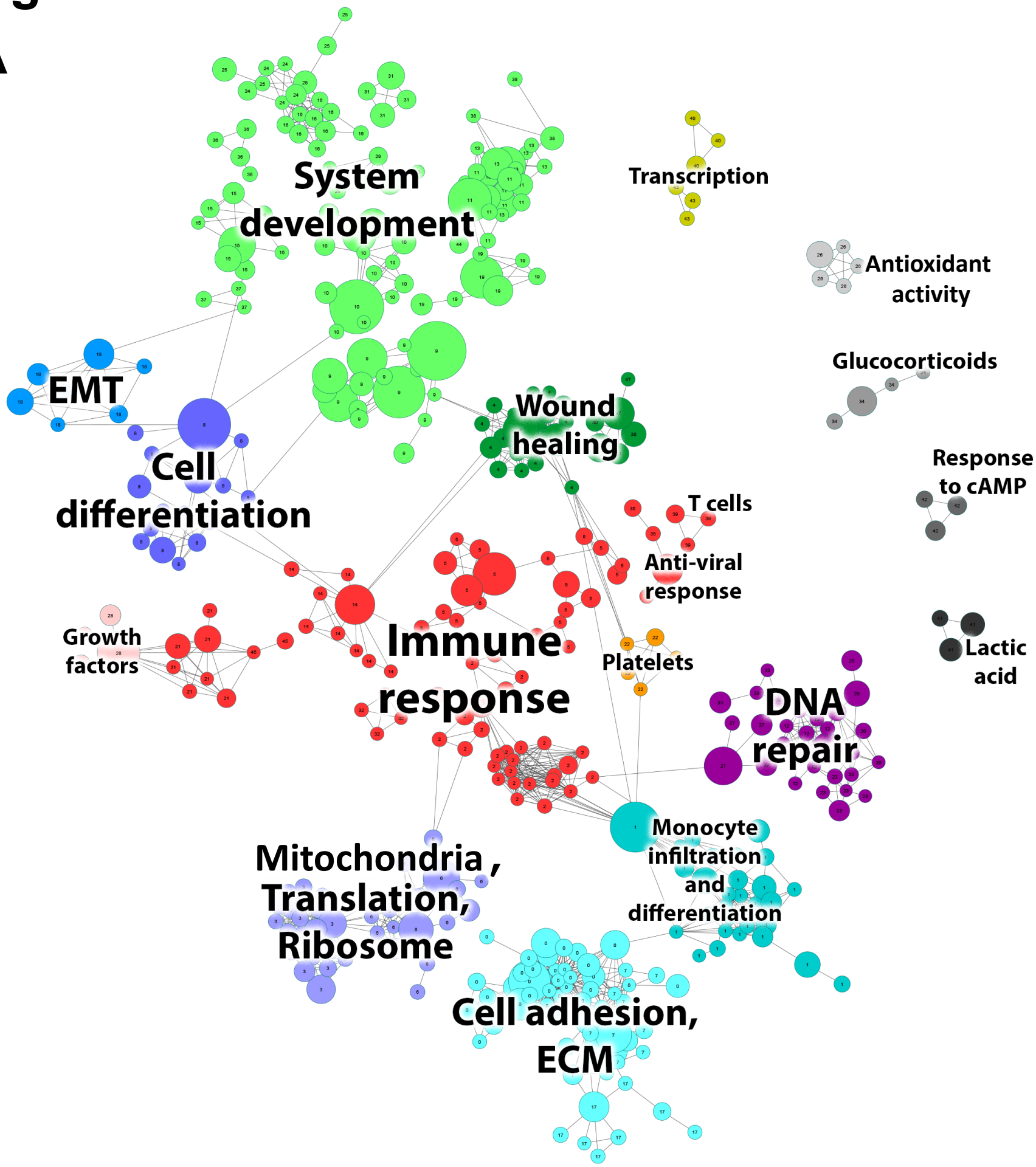
System development
Transcription
Antioxidant activity
Glucocorticoids
Response to cAMP
Lactic acid
EMT
Cell differentiation
Wound healing
T cells
Anti-viral response
Growth factors
Immune response
Platelets
DNA repair
Monocyte infiltration and differentiation
Mitochondria , Translation, Ribosome
Cell adhesion, ECM

C

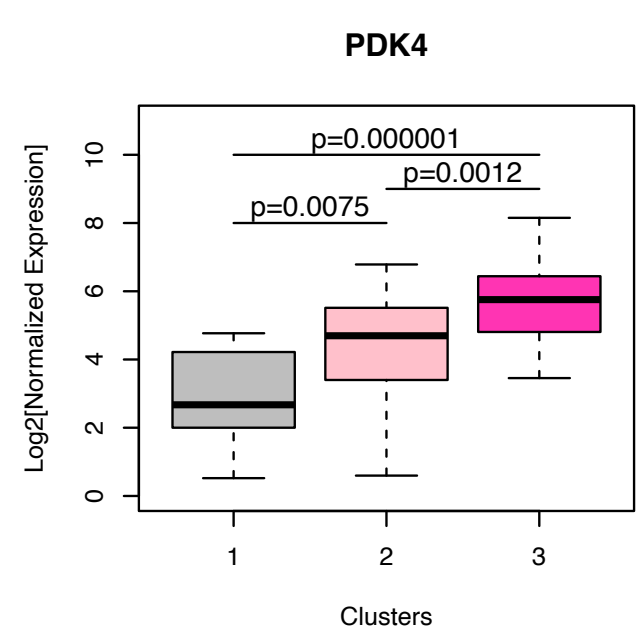
PDK4
Log2[Normalized Expression]
p=0.000001
p=0.0012
p=0.0075
0
2
4
6
8
10
1
2
3
Clusters

B

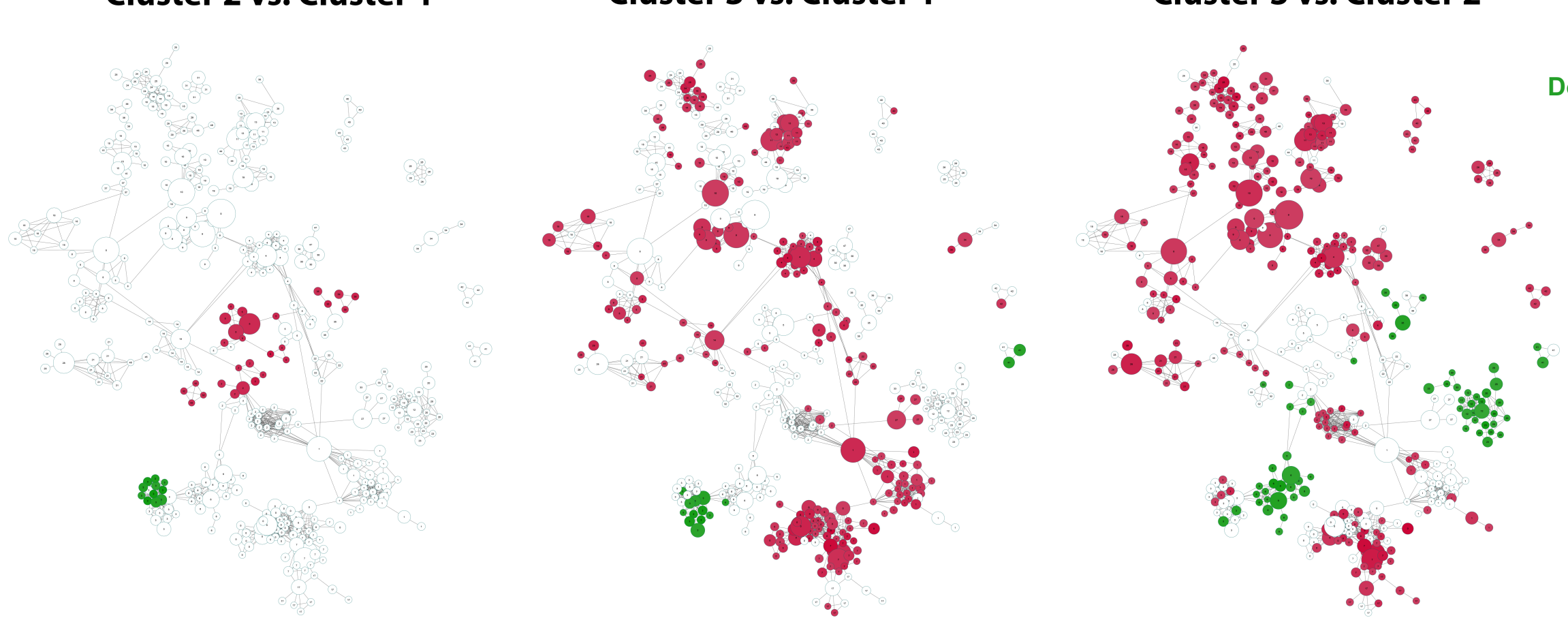
Cluster 2 vs. Cluster 1
Cluster 3 vs. Cluster 1
Cluster 3 vs. Cluster 2
Upregulated
Downregulated

Figure 6: Cluster Comparison with GSEA Reveals Multiple Differentially Regulated Processes in Most Severe Cluster, Including Downregulated Mitochondrial Function and Upregulated Fibrosis-Related Processes.

A: GSEA network displaying all differentially regulated processes found through comparison of cluster transcriptomic profiles. Each node is marked with a number corresponding to the module it belongs to. Subnetworks of modules are labelled and colour-coded. Information for modules and corresponding node numbers are included in Supplementary Spreadsheet 1. **B:** Regulation (upregulation-red, downregulation-green) of network processes for each cluster pair comparison. **C:** PDK4 expression stratified by cluster.

Figure 7

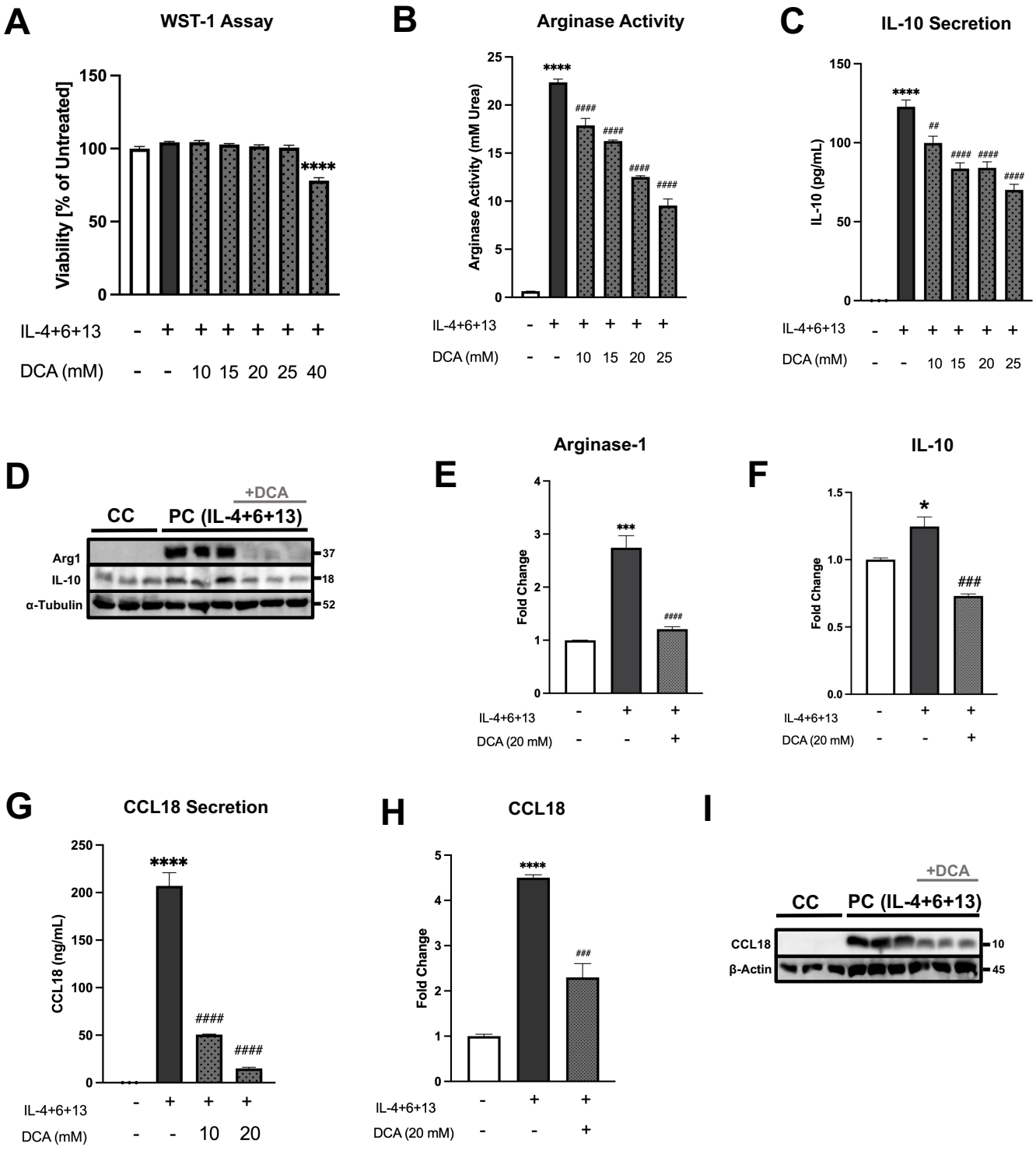
A
WST-1 Assay
Viability [% of Untreated]
150
100
50
0
****
IL-4+6+13 - + + + + + +
DCA (mM) - - 10 15 20 25 40
B
Arginase Activity
Arginase Activity (mM Urea)
25
20
15
10
5
0
****
####
IL-4+6+13 - + + + + +
DCA (mM) - - 10 15 20 25
C
IL-10 Secretion
IL-10 (pg/mL)
150
100
50
0
****
##
####
IL-4+6+13 - + + + + +
DCA (mM) - - 10 15 20 25
D
+DCA
CC
PC (IL-4+6+13)
Arg1
IL-10
α-Tubulin
37
18
52
E
Arginase-1
Fold Change
4
3
2
1
0
***
####
IL-4+6+13 - + +
DCA (20 mM) - - +
F
IL-10
Fold Change
1.5
1.0
0.5
0.0
*
###
IL-4+6+13 - + +
DCA (20 mM) - - +
G
CCL18 Secretion
CCL18 (ng/mL)
250
200
150
100
50
0
****
####
####
IL-4+6+13 - + + +
DCA (mM) - - 10 20
H
CCL18
Fold Change
5
4
3
2
1
0
****
###
IL-4+6+13 - + +
DCA (20 mM) - - +
I
+DCA
CC
PC (IL-4+6+13)
CCL18
β-Actin
10
45

Figure 7: Effect of PDK Inhibition with DCA on Macrophage Polarization in Monocytic Macrophage Cell Lines. RAW 264.7 macrophages were polarized with IL-4, IL-6, and IL-13, and treated with DCA for 24 hours. **A:** Viability was measured in RAW 264.7 cells with WST-1 assay, displayed as percentage of signal in untreated condition. **B:** Arginase activity expressed as mM Urea in cell lysates. **C:** Secreted IL-10 protein levels in RAW 264.7 supernatant measured via ELISA. **D:** Western blot images and subsequent quantification of **E:** Arginase-1 and **F:** IL-10 protein expression levels.

THP-1 cells were differentiated into macrophages using PMA, and then treated with a polarization cocktail (PC; IL-4, IL-6, and IL-13) for 72 hours. Cells were then treated with DCA for 72 hours. **G:** Secreted CCL-18 protein levels in THP-1 supernatant measured via ELISA. **H:** CCL18 protein expression levels measured with Western Blot. *,$^{\#}$ indicates $P < 0.05$; **,$^{\#\#}$ indicates $P < 0.01$; ***,$^{\#\#\#}$ indicates $P < 0.001$; and ****,$^{\#\#\#\#}$ indicates $P < 0.001$; where * represents a difference between the CC and PC control samples, and $^{\#}$ represents a difference between the treatment group and the PC stimulated control. N=2-3 technical replicates per condition. Data are displayed as mean ± S.E.M.

Figure 8

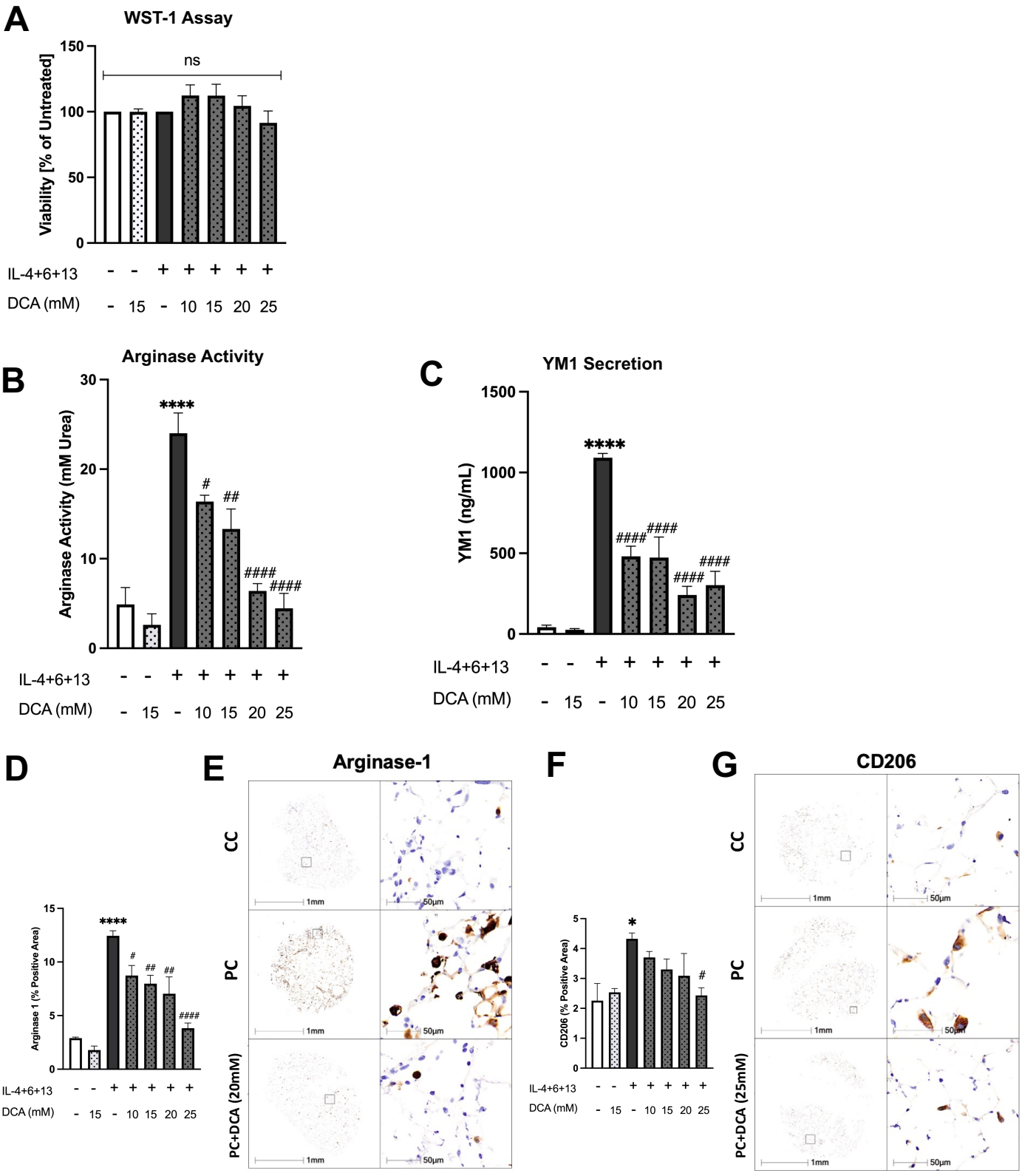
A
WST-1 Assay
Viability [% of Untreated]
ns
IL-4+6+13
DCA (mM)
B
Arginase Activity
Arginase Activity (mM Urea)
C
YM1 Secretion
YM1 (ng/mL)
D
Arginase 1 (% Positive Area)
E
Arginase-1
CC
PC
PC+DCA (20mM)
F
CD206 (% Positive Area)
G
CD206
PC+DCA (25mM)
1mm
50µm

Figure 8: Effect of PDK Inhibition with DCA on Macrophage Polarization in Precision-Cut Lung Slices (PCLS).

A: Tissue viability measured in PCLS with WST-1 assay, expressed as percentage of signal in untreated control. **B:** Arginase activity measured as mM Urea in tissue homogenates. **C:** Secreted YM1 protein levels in PCLS supernatant measured via ELISA. **D,E:** Quantification of Arginase-1 immunohistochemical staining in PCLS (expressed as % positive area), performed with HALO image analysis software. **F,G:** Quantification of CD206 immunohistochemical staining in PCLS (expressed as % positive area), performed with HALO image analysis software.. *,# indicates $P < 0.05$; **,## indicates $P < 0.01$; ***,### indicates $P < 0.001$; and ****,#### indicates $P < 0.001$; where * represents a difference between the unstimulated and stimulated controls, and # represents a difference between the treatment group and the stimulated control. N=3 mice, 3-4 slices per condition. Data are displayed as mean ± S.E.M.

AUTHOR CONTRIBUTIONS

MV: methodology, formal analysis, investigation, writing – original draft, writing – review & editing, visualization; **ADG**: formal analysis, investigation, visualization, data curation; **AA:** methodology, investigation; **SN:** methodology; **QZ:** methodology; **AT:** methodology, resources; **PA:** methodology**; JCC:** formal analysis, resources; **AN:** formal analysis, resources; **MK:** project administration, resources, supervision, funding acquisition; **KA:** conceptualization, resources, supervision, writing – review & editing, project administration, funding acquisition; **NH:** conceptualization, resources, supervision, project administration, funding acquisition.

ACKNOWLEDGEMENTS

We extend our gratitude to the McMaster John Mayberry Core Histology Facility (Mary Jo Smith and Mary Bruni) for their assistance with histological staining. We also thank the McMaster Farncombe Metagenomics Facility (Christine King, Liliana De Sousa, and Leanne Blanchard) for their assistance with NanoString and RNA sequencing experiments. We deeply thank Joanna Kasinska and Fuqin Duan for their knowledgeable laboratory technical expertise.

REFERENCES

[1] V. Cottin, A. Schmidt, L. Catella, F. Porte, C. Fernandez-Montoya, K. Le Lay, S. Bénard, Burden of Idiopathic Pulmonary Fibrosis Progression: A 5-Year Longitudinal Follow-Up Study, PLoS One 12 (2017) e0166462. https://doi.org/10.1371/journal.pone.0166462.

[2] N. Mogulkoc, M.H. Brutsche, P.W. Bishop, S.M. Greaves, A.W. Horrocks, J.J. Egan, Pulmonary Function in Idiopathic Pulmonary Fibrosis and Referral for Lung Transplantation, Am J Respir Crit Care Med 164 (2001) 103–108. https://doi.org/10.1164/ajrccm.164.1.2007077.

[3] M.M. Juarez, A.L. Chan, A.G. Norris, B.M. Morrissey, T.E. Albertson, Acute exacerbation of idiopathic pulmonary fibrosis—a review of current and novel pharmacotherapies, J Thorac Dis 7 (2015) 499–519. https://doi.org/10.3978/j.issn.2072-1439.2015.01.17.

[4] A.K.Y. Teoh, H.E. Jo, D.C. Chambers, K. Symons, E.H. Walters, N.S. Goh, I. Glaspole, W. Cooper, P. Reynolds, Y. Moodley, T.J. Corte, Blood monocyte counts as a potential prognostic marker for idiopathic pulmonary fibrosis: analysis from the Australian IPF registry, Eur Respir J 55 (2020) 1901855. https://doi.org/10.1183/13993003.01855-2019.

[5] M.K.D. Scott, K. Quinn, Q. Li, R. Carroll, H. Warsinske, F. Vallania, S. Chen, M.A. Carns, K. Aren, J. Sun, K. Koloms, J. Lee, J. Baral, J. Kropski, H. Zhao, E. Herzog, F.J. Martinez, B.B. Moore, M. Hinchcliff, J. Denny, N. Kaminski, J.D. Herazo-Maya, N.H. Shah, P. Khatri, Increased monocyte count as a cellular biomarker for poor

outcomes in fibrotic diseases: a retrospective, multicentre cohort study, Lancet Respir Med 7 (2019) 497–508. https://doi.org/10.1016/S2213-2600(18)30508-3.

[6] K. Kawamura, K. Ichikado, K. Anan, Y. Yasuda, Y. Sekido, M. Suga, H. Ichiyasu, T. Sakagami, Monocyte count and the risk for acute exacerbation of fibrosing interstitial lung disease: A retrospective cohort study, Chron Respir Dis 17 (2020) 1479973120909840. https://doi.org/10.1177/1479973120909840.

[7] M. Kreuter, J.S. Lee, A. Tzouvelekis, J.M. Oldham, P.L. Molyneaux, D. Weycker, M. Atwood, K.-U. Kirchgaessler, T.M. Maher, Monocyte Count as a Prognostic Biomarker in Patients with Idiopathic Pulmonary Fibrosis, Am J Respir Crit Care Med 204 (2021) 74–81. https://doi.org/10.1164/rccm.202003-0669OC.

[8] J.D. Herazo-Maya, J. Sun, P.L. Molyneaux, Q. Li, J.A. Villalba, A. Tzouvelekis, H. Lynn, B.M. Juan-Guardela, C. Risquez, J.C. Osorio, X. Yan, G. Michel, N. Aurelien, K.O. Lindell, M.J. Klesen, M.F. Moffatt, W.O. Cookson, Y. Zhang, J.G. Garcia, I. Noth, A. Prasse, Z. Bar-Joseph, K.F. Gibson, H. Zhao, E.L. Herzog, I.O. Rosas, T.M. Maher, N. Kaminski, Validating a 52-gene risk profile for outcome prediction in Idiopathic Pulmonary Fibrosis: an international multicentre cohort study, Lancet Respir Med 5 (2017) 857–868. https://doi.org/10.1016/S2213-2600(17)30349-1.

[9] L. Zhang, Y. Wang, G. Wu, W. Xiong, W. Gu, C.-Y. Wang, Macrophages: friend or foe in idiopathic pulmonary fibrosis?, Respiratory Research 19 (2018) 170. https://doi.org/10.1186/s12931-018-0864-2.

[10] D. Kim, B. Langmead, S.L. Salzberg, HISAT: a fast spliced aligner with low memory requirements, Nat Methods 12 (2015) 357–360. https://doi.org/10.1038/nmeth.3317.

[11] S. Anders, P.T. Pyl, W. Huber, HTSeq—a Python framework to work with high-throughput sequencing data, Bioinformatics 31 (2015) 166–169. https://doi.org/10.1093/bioinformatics/btu638.

[12] M.D. Robinson, A. Oshlack, A scaling normalization method for differential expression analysis of RNA-seq data, Genome Biology 11 (2010) R25. https://doi.org/10.1186/gb-2010-11-3-r25.

[13] C.W. Law, Y. Chen, W. Shi, G.K. Smyth, voom: precision weights unlock linear model analysis tools for RNA-seq read counts, Genome Biol 15 (2014) R29. https://doi.org/10.1186/gb-2014-15-2-r29.

[14] M.E. Ritchie, B. Phipson, D. Wu, Y. Hu, C.W. Law, W. Shi, G.K. Smyth, limma powers differential expression analyses for RNA-sequencing and microarray studies, Nucleic Acids Res 43 (2015) e47. https://doi.org/10.1093/nar/gkv007.

[15] Y. Benjamini, Y. Hochberg, Controlling the False Discovery Rate: A Practical and Powerful Approach to Multiple Testing, Journal of the Royal Statistical Society: Series B (Methodological) 57 (1995) 289–300. https://doi.org/10.1111/j.2517-6161.1995.tb02031.x.

[16] A.C. Habermann, A.J. Gutierrez, L.T. Bui, S.L. Yahn, N.I. Winters, C.L. Calvi, L. Peter, M.-I. Chung, C.J. Taylor, C. Jetter, L. Raju, J. Roberson, G. Ding, L. Wood, J.M.S. Sucre, B.W. Richmond, A.P. Serezani, W.J. McDonnell, S.B. Mallal, M.J. Bacchetta, J.E. Loyd, C.M. Shaver, L.B. Ware, R. Bremner, R. Walia, T.S. Blackwell, N.E. Banovich, J.A. Kropski, Single-cell RNA sequencing reveals profibrotic roles of

distinct epithelial and mesenchymal lineages in pulmonary fibrosis, Sci Adv 6 (2020) eaba1972. https://doi.org/10.1126/sciadv.aba1972.

[17] T.S. Adams, J.C. Schupp, S. Poli, E.A. Ayaub, N. Neumark, F. Ahangari, S.G. Chu, B.A. Raby, G. DeIuliis, M. Januszyk, Q. Duan, H.A. Arnett, A. Siddiqui, G.R. Washko, R. Homer, X. Yan, I.O. Rosas, N. Kaminski, Single-cell RNA-seq reveals ectopic and aberrant lung-resident cell populations in idiopathic pulmonary fibrosis, Sci Adv 6 (2020) eaba1983. https://doi.org/10.1126/sciadv.aba1983.

[18] M. Vierhout, A. Ayoub, P. Ali, V. Kumaran, S. Naiel, T. Isshiki, J.F. Koenig, M.R. Kolb, K. Ask, A Novel Ex Vivo Approach for Investigating Profibrotic Macrophage Polarization Using Murine Precision-Cut Lung Slices, bioRxiv (2024) 2024.07.05.602278. https://doi.org/10.1101/2024.07.05.602278.

[19] E.A. Ayaub, K. Tandon, M. Padwal, J. Imani, H. Patel, A. Dubey, O. Mekhael, C. Upagupta, A. Ayoub, A. Dvorkin-Gheva, J. Murphy, P.S. Kolb, S. Lhotak, J.G. Dickhout, R.C. Austin, M.R.J. Kolb, C.D. Richards, K. Ask, IL-6 mediates ER expansion during hyperpolarization of alternatively activated macrophages, Immunol Cell Biol 97 (2019) 203–217. https://doi.org/10.1111/imcb.12212.

[20] T. Yanagihara, Q. Zhou, K. Tsubouchi, S. Revill, A. Ayoub, M. Gholiof, S.G. Chong, A. Dvorkin-Gheva, K. Ask, W. Shi, M.RJ. Kolb, Intrinsic BMP inhibitor Gremlin regulates alveolar epithelial type II cell proliferation and differentiation, Biochemical and Biophysical Research Communications 656 (2023) 53–62. https://doi.org/10.1016/j.bbrc.2023.03.020.

[21] A. Strzelak, A. Ratajczak, A. Adamiec, W. Feleszko, Tobacco Smoke Induces and Alters Immune Responses in the Lung Triggering Inflammation, Allergy, Asthma and Other Lung Diseases: A Mechanistic Review, International Journal of Environmental Research and Public Health 15 (2018) 1033. https://doi.org/10.3390/ijerph15051033.

[22] Y. Wang, J.K. Yella, S. Ghandikota, T.C. Cherukuri, H.H. Ediga, S.K. Madala, A.G. Jegga, Pan-transcriptome-based candidate therapeutic discovery for idiopathic pulmonary fibrosis, Ther Adv Respir Dis 14 (2020) 1753466620971143. https://doi.org/10.1177/1753466620971143.

[23] D.J. DePianto, S. Chandriani, A.R. Abbas, G. Jia, E.N. N'Diaye, P. Caplazi, S.E. Kauder, S. Biswas, S.K. Karnik, C. Ha, Z. Modrusan, M.A. Matthay, J. Kukreja, H.R. Collard, J.G. Egen, P.J. Wolters, J.R. Arron, Heterogeneous gene expression signatures correspond to distinct lung pathologies and biomarkers of disease severity in idiopathic pulmonary fibrosis, Thorax 70 (2015) 48–56. https://doi.org/10.1136/thoraxjnl-2013-204596.

[24] M.J. Schafer, T.A. White, K. Iijima, A.J. Haak, G. Ligresti, E.J. Atkinson, A.L. Oberg, J. Birch, H. Salmonowicz, Y. Zhu, D.L. Mazula, R.W. Brooks, H. Fuhrmann-Stroissnigg, T. Pirtskhalava, Y.S. Prakash, T. Tchkonia, P.D. Robbins, M.C. Aubry, J.F. Passos, J.L. Kirkland, D.J. Tschumperlin, H. Kita, N.K. LeBrasseur, Cellular senescence mediates fibrotic pulmonary disease, Nat Commun 8 (2017) 14532. https://doi.org/10.1038/ncomms14532.

[25] P.-S. Bellaye, C. Shimbori, T. Yanagihara, D.A. Carlson, P. Hughes, C. Upagupta, S. Sato, N. Wheildon, T. Haystead, K. Ask, M. Kolb, Synergistic role of HSP90α and

HSP90β to promote myofibroblast persistence in lung fibrosis, European Respiratory Journal 51 (2018). https://doi.org/10.1183/13993003.00386-2017.

[26] M. Kolb, H.R. Collard, Staging of idiopathic pulmonary fibrosis: past, present and future, European Respiratory Review 23 (2014) 220–224. https://doi.org/10.1183/09059180.00002114.

[27] M.K. Jha, S. Jeon, K. Suk, Pyruvate Dehydrogenase Kinases in the Nervous System: Their Principal Functions in Neuronal-glial Metabolic Interaction and Neuro-metabolic Disorders, Curr Neuropharmacol 10 (2012) 393–403. https://doi.org/10.2174/157015912804143586.

[28] C.L.R. van Doorn, G.K. Schouten, S. van Veen, K.V. Walburg, J.J. Esselink, M.T. Heemskerk, F. Vrieling, T.H.M. Ottenhoff, Pyruvate Dehydrogenase Kinase Inhibitor Dichloroacetate Improves Host Control of Salmonella enterica Serovar Typhimurium Infection in Human Macrophages, Front Immunol 12 (2021) 739938. https://doi.org/10.3389/fimmu.2021.739938.

[29] A. Al-Azawi, S. Sulaiman, K. Arafat, J. Yasin, A. Nemmar, S. Attoub, Impact of Sodium Dichloroacetate Alone and in Combination Therapies on Lung Tumor Growth and Metastasis, Int J Mol Sci 22 (2021) 12553. https://doi.org/10.3390/ijms222212553.

[30] L.H. Stockwin, S.X. Yu, S. Borgel, C. Hancock, T.L. Wolfe, L.R. Phillips, M.G. Hollingshead, D.L. Newton, Sodium dichloroacetate selectively targets cells with defects in the mitochondrial ETC, International Journal of Cancer 127 (2010) 2510–2519. https://doi.org/10.1002/ijc.25499.

[31] A. Prasse, D.V. Pechkovsky, G.B. Toews, W. Jungraithmayr, F. Kollert, T. Goldmann, E. Vollmer, J. Müller-Quernheim, G. Zissel, A Vicious Circle of Alveolar Macrophages and Fibroblasts Perpetuates Pulmonary Fibrosis via CCL18, American Journal of Respiratory and Critical Care Medicine (2012). https://doi.org/10.1164/rccm.200509-1518OC.

[32] J.D. Cala-Garcia, G.J. Medina-Rincon, P.A. Sierra-Salas, J. Rojano, F. Romero, The Role of Mitochondrial Dysfunction in Idiopathic Pulmonary Fibrosis: New Perspectives for a Challenging Disease, Biology (Basel) 12 (2023) 1237. https://doi.org/10.3390/biology12091237.

[33] M. Bueno, J. Calyeca, M. Rojas, A.L. Mora, Mitochondria dysfunction and metabolic reprogramming as drivers of idiopathic pulmonary fibrosis, Redox Biology 33 (2020) 101509. https://doi.org/10.1016/j.redox.2020.101509.

[34] T. Huang, R. Lin, Y. Su, H. Sun, X. Zheng, J. Zhang, X. Lu, B. Zhao, X. Jiang, L. Huang, N. Li, J. Shi, X. Fan, D. Xu, T. Zhang, J. Gao, Efficient intervention for pulmonary fibrosis via mitochondrial transfer promoted by mitochondrial biogenesis, Nat Commun 14 (2023) 5781. https://doi.org/10.1038/s41467-023-41529-7.

[35] E. Tsitoura, E. Vasarmidi, E. Bibaki, A. Trachalaki, C. Koutoulaki, G. Papastratigakis, S. Papadogiorgaki, G. Chalepakis, N. Tzanakis, K.M. Antoniou, Accumulation of damaged mitochondria in alveolar macrophages with reduced OXPHOS related gene expression in IPF, Respiratory Research 20 (2019) 264. https://doi.org/10.1186/s12931-019-1196-6.

[36] N. Xie, H. Cui, J. Ge, S. Banerjee, S. Guo, S. Dubey, E. Abraham, R.-M. Liu, G. Liu, Metabolic characterization and RNA profiling reveal glycolytic dependence of profibrotic phenotype of alveolar macrophages in lung fibrosis, American Journal of Physiology-Lung Cellular and Molecular Physiology 313 (2017) L834–L844. https://doi.org/10.1152/ajplung.00235.2017.

[37] K.J. Mould, L. Barthel, M.P. Mohning, S.M. Thomas, A.L. McCubbrey, T. Danhorn, S.M. Leach, T.E. Fingerlin, B.P. O'Connor, J.A. Reisz, A. D'Alessandro, D.L. Bratton, C.V. Jakubzick, W.J. Janssen, Cell Origin Dictates Programming of Resident versus Recruited Macrophages during Acute Lung Injury, Am J Respir Cell Mol Biol 57 (2017) 294–306. https://doi.org/10.1165/rcmb.2017-0061OC.

[38] B.-K. Min, S. Park, H.-J. Kang, D.W. Kim, H.J. Ham, C.-M. Ha, B.-J. Choi, J.Y. Lee, C.J. Oh, E.K. Yoo, H.E. Kim, B.-G. Kim, J.-H. Jeon, D.Y. Hyeon, D. Hwang, Y.-H. Kim, C.-H. Lee, T. Lee, J. Kim, Y.-K. Choi, K.-G. Park, A. Chawla, J. Lee, R.A. Harris, I.-K. Lee, Pyruvate Dehydrogenase Kinase Is a Metabolic Checkpoint for Polarization of Macrophages to the M1 Phenotype, Front. Immunol. 10 (2019). https://doi.org/10.3389/fimmu.2019.00944.

[39] J.V. den Bossche, L.A. O'Neill, D. Menon, Macrophage Immunometabolism: Where Are We (Going)?, Trends in Immunology 38 (2017) 395–406. https://doi.org/10.1016/j.it.2017.03.001.

[40] Y. Gu, T. Lawrence, R. Mohamed, Y. Liang, B.H. Yahaya, The emerging roles of interstitial macrophages in pulmonary fibrosis: A perspective from scRNA-seq

analyses, Front Immunol 13 (2022) 923235. https://doi.org/10.3389/fimmu.2022.923235.

[41] H. Higo, K. Ohashi, S. Tomida, S. Okawa, H. Yamamoto, S. Sugimoto, S. Senoo, G. Makimoto, K. Ninomiya, T. Nakasuka, K. Nishii, A. Taniguchi, T. Kubo, E. Ichihara, K. Hotta, N. Miyahara, Y. Maeda, S. Toyooka, K. Kiura, Identification of targetable kinases in idiopathic pulmonary fibrosis, Respir Res 23 (2022) 20. https://doi.org/10.1186/s12931-022-01940-y.

[42] T. Chen, L. Ye, J. Zhu, B. Tan, Q. Yi, Y. Sun, Q. Xie, H. Xiang, R. Wang, J. Tian, H. Xu, Inhibition of Pyruvate Dehydrogenase Kinase 4 Attenuates Myocardial and Mitochondrial Injury in Sepsis-Induced Cardiomyopathy, The Journal of Infectious Diseases (2023) jiad365. https://doi.org/10.1093/infdis/jiad365.

[43] K. Yuan, N.-Y. Shao, J.K. Hennigs, M. Discipulo, M.E. Orcholski, E. Shamskhou, A. Richter, X. Hu, J.C. Wu, V.A. de Jesus Perez, Increased Pyruvate Dehydrogenase Kinase 4 Expression in Lung Pericytes Is Associated with Reduced Endothelial-Pericyte Interactions and Small Vessel Loss in Pulmonary Arterial Hypertension, Am J Pathol 186 (2016) 2500–2514. https://doi.org/10.1016/j.ajpath.2016.05.016.

[44] Z. Zhang, S. Han, S. Ouyang, Z. Zeng, Z. Liu, J. Sun, W. Kang, PDK4 Constitutes a Novel Prognostic Biomarker and Therapeutic Target in Gastric Cancer, Diagnostics (Basel) 12 (2022) 1101. https://doi.org/10.3390/diagnostics12051101.

[45] P. Du, R. Guo, K. Gao, S. Yang, B. Yao, H. Cui, M. Zhao, S. Jia, Identification of differentially expressed genes and the role of PDK4 in CD14+ monocytes of coronary

artery disease, Biosci Rep 41 (2021) BSR20204124. https://doi.org/10.1042/BSR20204124.

[46] Y. Jiang, B.R. Rosborough, J. Chen, S. Das, G.D. Kitsios, B.J. McVerry, R.K. Mallampalli, J.S. Lee, A. Ray, W. Chen, P. Ray, Single cell RNA sequencing identifies an early monocyte gene signature in acute respiratory distress syndrome, JCI Insight 5 (2020). https://doi.org/10.1172/jci.insight.135678.

[47] E. Atas, M. Oberhuber, L. Kenner, The Implications of PDK1–4 on Tumor Energy Metabolism, Aggressiveness and Therapy Resistance, Front Oncol 10 (2020) 583217. https://doi.org/10.3389/fonc.2020.583217.

[48] A. Viola, F. Munari, R. Sánchez-Rodríguez, T. Scolaro, A. Castegna, The Metabolic Signature of Macrophage Responses, Front. Immunol. 10 (2019). https://doi.org/10.3389/fimmu.2019.01462.

[49] E.A. Ayaub, A. Dubey, J. Imani, F. Botelho, M.R.J. Kolb, C.D. Richards, K. Ask, Overexpression of OSM and IL-6 impacts the polarization of pro-fibrotic macrophages and the development of bleomycin-induced lung fibrosis, Sci Rep 7 (2017) 13281. https://doi.org/10.1038/s41598-017-13511-z.

[50] C.K. Watson, D. Schloesser, K. Fundel-Clemens, C. Lerner, S. Gabler, P. Baskaran, C.T. Wohnhaas, S. Dichtl, H.J. Huber, K. Ask, F. Gantner, C. Viollet, M.J. Thomas, F. Ramirez, P.J. Murray, K.C. El Kasmi, Antifibrotic Drug Nintedanib Inhibits CSF1R to Promote IL-4–associated Tissue Repair Macrophages, Am J Respir Cell Mol Biol 68 (2023) 366–380. https://doi.org/10.1165/rcmb.2022-0021OC.

[51] J.M. Parker, I.N. Glaspole, L.H. Lancaster, T.J. Haddad, D. She, S.L. Roseti, J.P. Fiening, E.P. Grant, C.M. Kell, K.R. Flaherty, A Phase 2 Randomized Controlled Study of Tralokinumab in Subjects with Idiopathic Pulmonary Fibrosis, Am J Respir Crit Care Med 197 (2018) 94–103. https://doi.org/10.1164/rccm.201704-0784OC.

[52] J. Goodwin, H. Choi, M. Hsieh, M.L. Neugent, J.-M. Ahn, H.N. Hayenga, P.K. Singh, D.B. Shackelford, I.-K. Lee, V. Shulaev, S. Dhar, N. Takeda, J. Kim, Targeting Hypoxia-Inducible Factor-1α/Pyruvate Dehydrogenase Kinase 1 Axis by Dichloroacetate Suppresses Bleomycin-induced Pulmonary Fibrosis, Am J Respir Cell Mol Biol 58 (2018) 216–231. https://doi.org/10.1165/rcmb.2016-0186OC.

[53] W. T'Jonck, C.C. Bain, The role of monocyte-derived macrophages in the lung: It's all about context, The International Journal of Biochemistry & Cell Biology 159 (2023) 106421. https://doi.org/10.1016/j.biocel.2023.106421.

[54] A.J. Radtke, C.J. Chu, Z. Yaniv, L. Yao, J. Marr, R.T. Beuschel, H. Ichise, A. Gola, J. Kabat, B. Lowekamp, E. Speranza, J. Croteau, N. Thakur, D. Jonigk, J.L. Davis, J.M. Hernandez, R.N. Germain, IBEX: an iterative immunolabeling and chemical bleaching method for high-content imaging of diverse tissues, Nat Protoc 17 (2022) 378–401. https://doi.org/10.1038/s41596-021-00644-9.

[55] A.J. Radtke, E. Kandov, B. Lowekamp, E. Speranza, C.J. Chu, A. Gola, N. Thakur, R. Shih, L. Yao, Z.R. Yaniv, R.T. Beuschel, J. Kabat, J. Croteau, J. Davis, J.M. Hernandez, R.N. Germain, IBEX: A versatile multiplex optical imaging approach for deep phenotyping and spatial analysis of cells in complex tissues, Proceedings of the

National Academy of Sciences 117 (2020) 33455–33465. https://doi.org/10.1073/pnas.2018488117.

SUPPLEMENTAL INFORMATION

Supplementary Figure 1: Arginase-1 Full Length Blot for Figure 7D-E

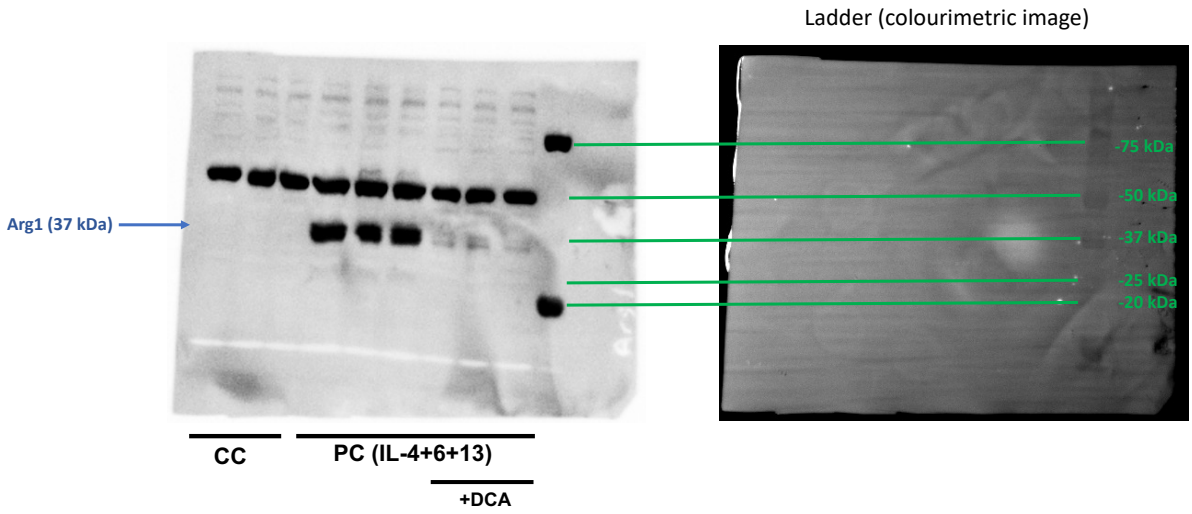

Supplementary Figure 2: IL-10 Full Length Blot for Figure 7D,F

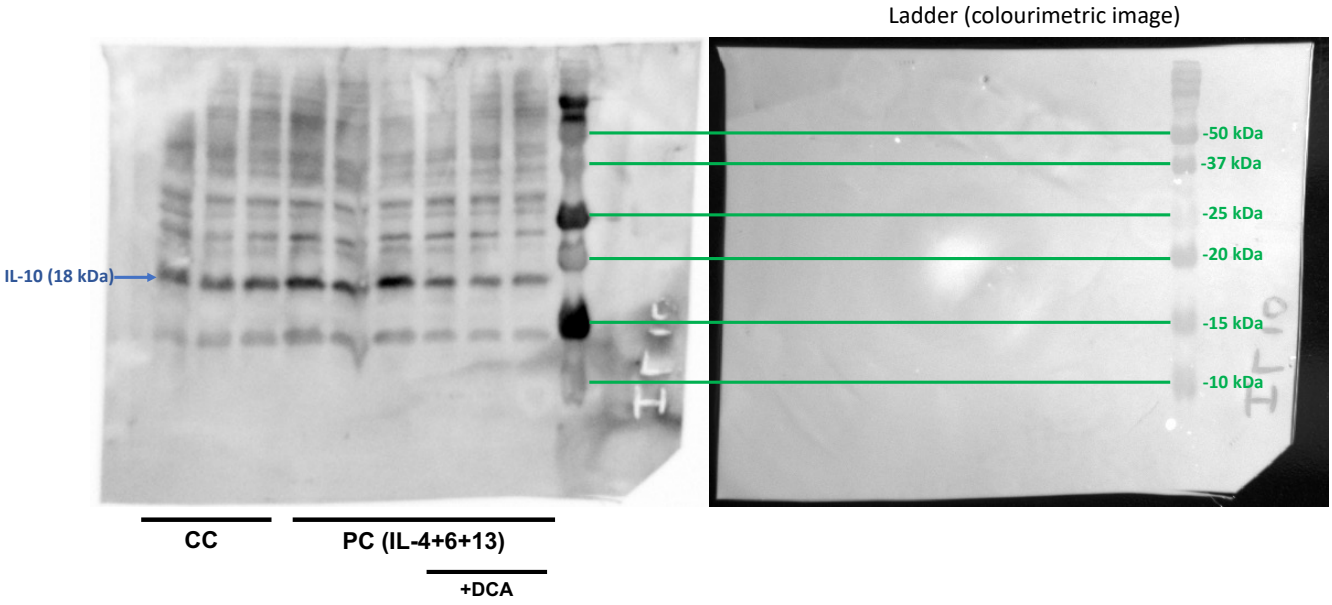

Supplementary Figure 3: α-Tubulin Full Length Blot for Figure 7D-F

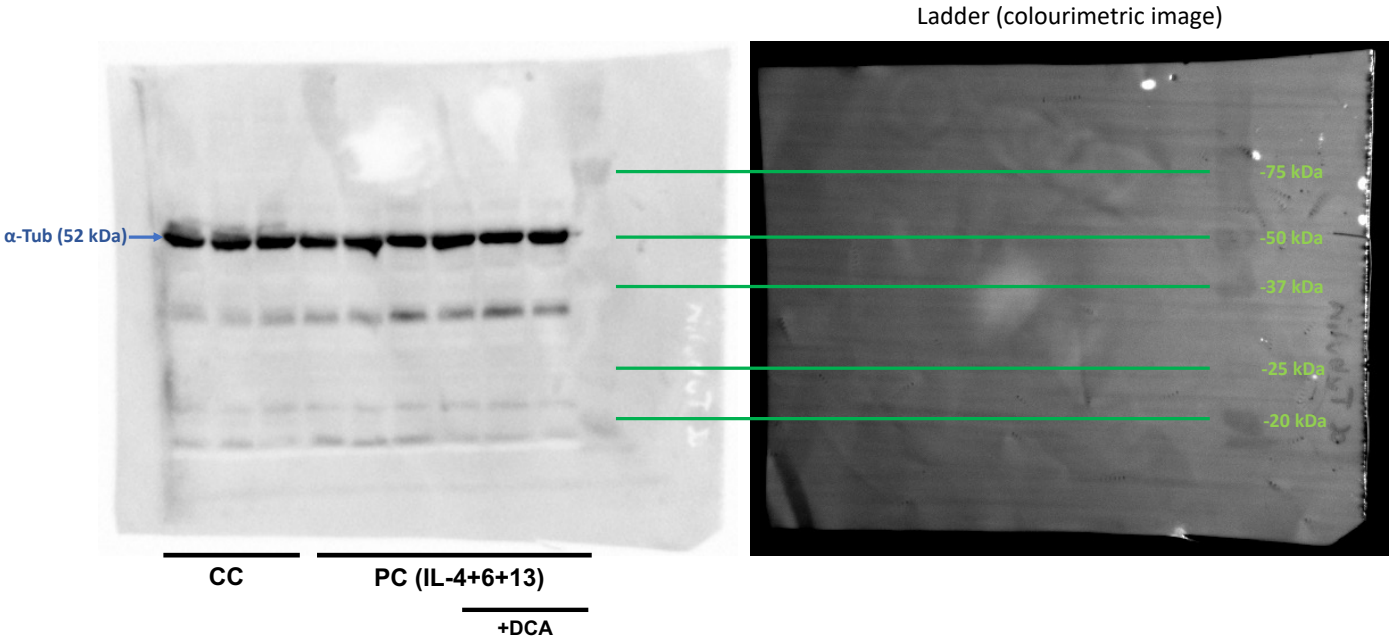

Supplementary Figure 4: CCL18 Full Length Blot for Figure 7H-I

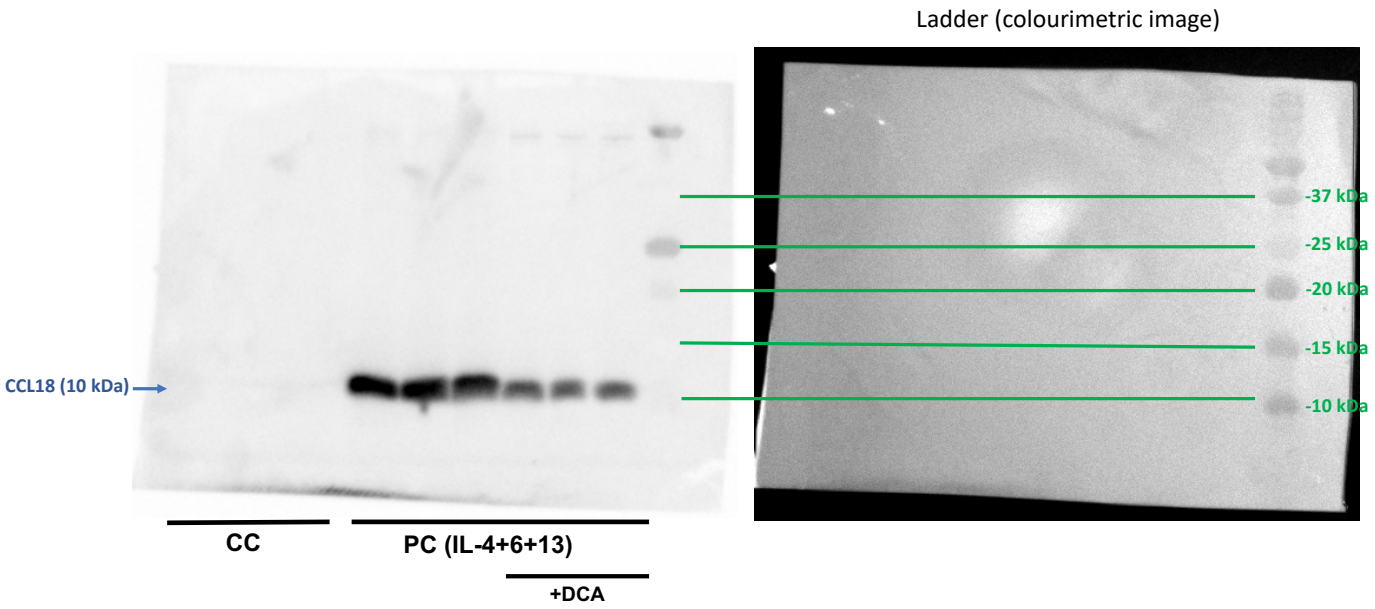

Supplementary Figure 5: β-Actin Full Length Blot for Figure 7H-I

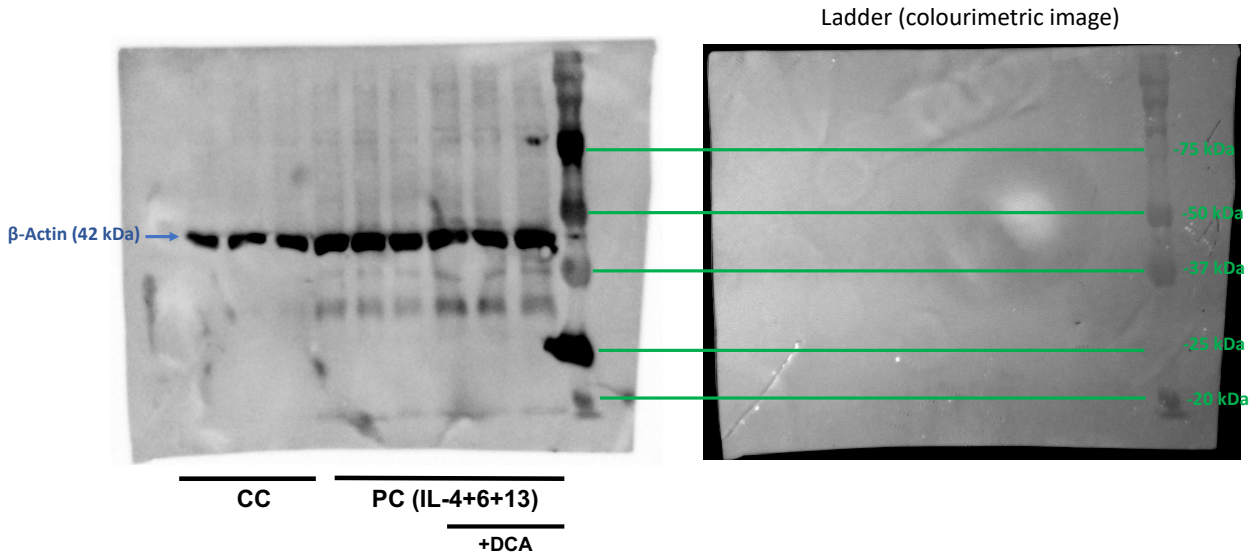

Supplementary Table 1: Demographic Characteristics for Tissue Microarrays

Characteristic	IPF (TMA 1)	IPF (TMA 2)
Sex - Male (%)	70.8	66.7
Age (years)	59.0 ± 10.1	63.1 ± 10.3
FVC (% predicted)	62.9 ± 23.2	62.7 ± 17.5
FEV1 (% predicted)	68.1 ± 16.5	67 ± 18.6
DLCO (% predicted)	42.8 ± 10.9	45.6 ± 16

Demographic information for the control group subjects was not available.

Supplementary Table 2: Demographic Characteristics for IPF Monocyte Subjects

Characteristic	IPF
Sex - Male (%)	89.8
Age (years)	74.2 ± 1.0
FVC (% predicted)	72.0 ± 2.5
FEV1 (% predicted)	80.7 ± 2.6
DLCO (% predicted)	45.7 ± 2.6

Supplementary Table 3: Demographic Characteristics for Donor Monocyte Subjects

Characteristic	Donor
Sex - Male (%)	80
Age (years)	44.8 ± 4.5
FVC (% predicted)	106.0 ± 5.0
FEV1 (% predicted)	106.2 ± 6.0

Supplementary Spreadsheet 1: Information for Processes in GSEA Network in Figure 5

Cell adhesion, ECM
0
GOBP_CELL_ADHESION_MEDIATED_BY_INTEGRIN
GOBP_CELL_MATRIX_ADHESION
GOBP_CELL_SUBSTRATE_ADHESION
GOBP_CELL_SUBSTRATE_JUNCTION_ORGANIZATION
GOBP_FOCAL_ADHESION_ASSEMBLY
GOBP_INTEGRIN_MEDIATED_SIGNALING_PATHWAY
GOBP_POSITIVE_REGULATION_OF_CELL_SUBSTRATE_ADHESION
GOBP_POSITIVE_REGULATION_OF_SUBSTRATE_ADHESION_DEPENDENT_CELL_SPREADING
GOBP_REGULATION_OF_CELL_ADHESION_MEDIATED_BY_INTEGRIN
GOBP_REGULATION_OF_CELL_MATRIX_ADHESION
GOBP_REGULATION_OF_CELL_SUBSTRATE_ADHESION
GOCC_INTEGRIN_COMPLEX
GOCC_PLASMA_MEMBRANE_SIGNALING_RECEPTOR_COMPLEX
GOCC_PROTEIN_COMPLEX_INVOLVED_IN_CELL_ADHESION
GOCC_RECEPTOR_COMPLEX
GOMF_INTEGRIN_BINDING
HALLMARK_EPITHELIAL_MESENCHYMAL_TRANSITION
KEGG_ARRHYTHMOGENIC_RIGHT_VENTRICULAR_CARDIOMYOPATHY_ARVC
KEGG_DILATED_CARDIOMYOPATHY
KEGG_ECM_RECEPTOR_INTERACTION
KEGG_FOCAL_ADHESION
KEGG_HYPERTROPHIC_CARDIOMYOPATHY_HCM
KEGG_MEDICUS_REFERENCE_ITGA_B_FAK_CDC42_SIGNALING_PATHWAY
KEGG_MEDICUS_REFERENCE_ITGA_B_FAK_RAC_SIGNALING_PATHWAY
KEGG_MEDICUS_REFERENCE_ITGA_B_RHOGAP_RHOA_SIGNALING_PATHWAY
KEGG_MEDICUS_REFERENCE_ITGA_B_RHOGEF_RHOA_SIGNALING_PATHWAY
KEGG_MEDICUS_REFERENCE_ITGA_B_RHOG_RAC_SIGNALING_PATHWAY
KEGG_MEDICUS_REFERENCE_ITGA_B_TALIN_VINCULIN_SIGNALING_PATHWAY
PID_INTEGRIN_CS_PATHWAY
REACTOME_INTEGRIN_CELL_SURFACE_INTERACTIONS
REACTOME_SYNDECAN_INTERACTIONS
WP_ARRHYTHMOGENIC_RIGHT_VENTRICULAR_CARDIOMYOPATHY
WP_FOCAL_ADHESION
WP_FOCAL_ADHESION_PI3K_AKT_MTOR_SIGNALING_PATHWAY
WP_HIPPO_MERLIN_SIGNALING_DYSREGULATION
WP_INTEGRIN_MEDIATED_CELL_ADHESION

7
GOCC_BASEMENT_MEMBRANE
GOCC_COLLAGEN_CONTAINING_EXTRACELLULAR_MATRIX
GOCC_EXTERNAL_ENCAPSULATING_STRUCTURE
GOMF_EXTRACELLULAR_MATRIX_STRUCTURAL_CONSTITUENT
PID_INTEGRIN1_PATHWAY
PID_INTEGRIN3_PATHWAY
PID_SYNDECAN_1_PATHWAY
REACTOME_ASSEMBLY_OF_COLLAGEN_FIBRILS_AND_OTHER_MULTIMERIC_STRUCTURES
REACTOME_DEGRADATION_OF_THE_EXTRACELLULAR_MATRIX
REACTOME_ECM_PROTEOGLYCANS
REACTOME_ELASTIC_FIBRE_FORMATION
REACTOME_EXTRACELLULAR_MATRIX_ORGANIZATION
REACTOME_LAMININ_INTERACTIONS
REACTOME_MET_ACTIVATES_PTK2_SIGNALING
REACTOME_MET_PROMOTES_CELL_MOTILITY
REACTOME_MOLECULES_ASSOCIATED_WITH_ELASTIC_FIBRES
REACTOME_NON_INTEGRIN_MEMBRANE_ECM_INTERACTIONS
REACTOME_SIGNALING_BY_MET
WP_SMALL_CELL_LUNG_CANCER

17
GOBP_COLLAGEN_CATABOLIC_PROCESS
GOBP_COLLAGEN_METABOLIC_PROCESS
GOBP_EXTERNAL_ENCAPSULATING_STRUCTURE_ORGANIZATION
GOBP_EXTRACELLULAR_MATRIX_ASSEMBLY
GOBP_EXTRACELLULAR_MATRIX_DISASSEMBLY
GOBP_POSITIVE_REGULATION_OF_EXTRACELLULAR_MATRIX_ORGANIZATION
GOBP_REGULATION_OF_COLLAGEN_METABOLIC_PROCESS
GOBP_REGULATION_OF_EXTRACELLULAR_MATRIX_ORGANIZATION

Monocyte infiltration and differentiation
1
GOBP_ADENYLATE_CYCLASE_INHIBITING_G_PROTEIN_COUPLED_RECEPTOR_SIGNALING_PATHWAY
GOBP_ADENYLATE_CYCLASE_MODULATING_G_PROTEIN_COUPLED_RECEPTOR_SIGNALING_PATHWAY
GOCC_PLATELET_ALPHA_GRANULE
GOCC_PLATELET_ALPHA_GRANULE_LUMEN
GOCC_PLATELET_ALPHA_GRANULE_MEMBRANE
KEGG_MEDICUS_PATHOGEN_KSHV_VGPCR_TO_GNB_G_ERK_SIGNALING_PATHWAY
REACTOME_ADORA2B_MEDIATED_ANTI_INFLAMMATORY_CYTOKINES_PRODUCTION
REACTOME_ADRENALINE_NORADRENALINE_INHIBITS_INSULIN_SECRETION
REACTOME_ANTI_INFLAMMATORY_RESPONSE_FAVOURING_LEISHMANIA_PARASITE_INFECTION
REACTOME_AQUAPORIN_MEDIATED_TRANSPORT
REACTOME_CELL_SURFACE_INTERACTIONS_AT_THE_VASCULAR_WALL
REACTOME_DAG_AND_IP3_SIGNALING
REACTOME_ESTROGEN_DEPENDENT_NUCLEAR_EVENTS_DOWNSTREAM_OF_ESR_MEMBRANE_SIGNALING
REACTOME_EXTRA_NUCLEAR_ESTROGEN_SIGNALING
REACTOME_FCGR3A_MEDIATED_IL10_SYNTHESIS
REACTOME_GABA_B_RECEPTOR_ACTIVATION
REACTOME_GABA_RECEPTOR_ACTIVATION
REACTOME_GLUCAGON_LIKE_PEPTIDE_1_GLP1_REGULATES_INSULIN_SECRETION
REACTOME_GLUCAGON_SIGNALING_IN_METABOLIC_REGULATION
REACTOME_GPER1_SIGNALING
REACTOME_G_ALPHA_S_SIGNALLING_EVENTS
REACTOME_G_ALPHA_Z_SIGNALLING_EVENTS
REACTOME_HEMOSTASIS
REACTOME_LEISHMANIA_INFECTION
REACTOME_PLATELET_ACTIVATION_SIGNALING_AND_AGGREGATION
REACTOME_PLATELET_AGGREGATION_PLUG_FORMATION
REACTOME_REGULATION_OF_INSULIN_SECRETION
REACTOME_RESPONSE_TO_ELEVATED_PLATELET_CYTOSOLIC_CA2
REACTOME_VASOPRESSIN_REGULATES_RENAL_WATER_HOMEOSTASIS_VIA_AQUAPORINS
WP_CALCIUM_REGULATION_IN_CARDIAC_CELLS
WP_MYOMETRIAL_RELAXATION_AND_CONTRACTION_PATHWAYS

Immune response
2

GOCC_LUMENAL_SIDE_OF_ENDOPLASMIC_RETICULUM_MEMBRANE
GOCC_MHC_PROTEIN_COMPLEX
KEGG_ANTIGEN_PROCESSING_AND_PRESENTATION
KEGG_MEDICUS_REFERENCE_EGF_EGFR_ACTIN_SIGNALING_PATHWAY
KEGG_MEDICUS_REFERENCE_MICROTUBULE_DEPOLYMERIZATION
KEGG_MEDICUS_REFERENCE_MICROTUBULE_DEPOLYMERIZATION_AT_THE_MINUS_ENDS
KEGG_MEDICUS_REFERENCE_MICROTUBULE_RHOA_SIGNALING_PATHWAY
KEGG_MEDICUS_REFERENCE_PROMOTION_OF_MICROTUBULE_GROWTH
KEGG_MEDICUS_REFERENCE_RETROGRADE_AXONAL_TRANSPORT
KEGG_MEDICUS_VARIANT_MUTATION_CAUSED_ABERRANT_ABETA_TO_ANTEROGRADE_AXONAL_TRANSPORT
KEGG_MEDICUS_VARIANT_MUTATION_CAUSED_ABERRANT_HTT_TO_ANTEROGRADE_AXONAL_TRANSPORT
KEGG_MEDICUS_VARIANT_MUTATION_CAUSED_ABERRANT_HTT_TO_RETROGRADE_AXONAL_TRANSPORT
KEGG_MEDICUS_VARIANT_MUTATION_CAUSED_ABERRANT_SNCA_TO_ANTEROGRADE_AXONAL_TRANSPORT
KEGG_PATHOGENIC_ESCHERICHIA_COLI_INFECTION
REACTOME_ACTIVATION_OF_AMPK_DOWNSTREAM_OF_NMDARS
REACTOME_FORMATION_OF_TUBULIN_FOLDING_INTERMEDIATES_BY_CCT_TRIC
REACTOME_GAP_JUNCTION_ASSEMBLY
REACTOME_GAP_JUNCTION_TRAFFICKING_AND_REGULATION
REACTOME_INTERFERON_ALPHA_BETA_SIGNALING
REACTOME_INTERFERON_GAMMA_SIGNALING
REACTOME_INTERFERON_SIGNALING
REACTOME_ISG15_ANTIVIRAL_MECHANISM
REACTOME_L1CAM_INTERACTIONS
REACTOME_RHO_GTPASES_ACTIVATE_IQGAPS
REACTOME_SARS_COV_2_ACTIVATES_MODULATES_INNATE_AND_ADAPTIVE_IMMUNE_RESPONSES
REACTOME_SNRNP_ASSEMBLY
REACTOME_TRNA_PROCESSING_IN_THE_NUCLEUS
WP_PATHOGENIC_ESCHERICHIA_COLI_INFECTION

5

BIOCARTA_CSK_PATHWAY
GOBP_ACTIVATION_OF_IMMUNE_RESPONSE
GOBP_ANTIBACTERIAL_HUMORAL_RESPONSE
GOBP_ANTIGEN_RECEPTOR_MEDIATED_SIGNALING_PATHWAY
GOBP_ANTIMICROBIAL_HUMORAL_RESPONSE
GOBP_COMPLEMENT_ACTIVATION_CLASSICAL_PATHWAY
GOBP_HUMORAL_IMMUNE_RESPONSE
GOBP_IMMUNE_RESPONSE_REGULATING_CELL_SURFACE_RECEPTOR_SIGNALING_PATHWAY
GOBP_NEGATIVE_REGULATION_OF_T_CELL_RECEPTOR_SIGNALING_PATHWAY
GOBP_T_CELL_RECEPTOR_SIGNALING_PATHWAY
HALLMARK_COAGULATION
KEGG_COMPLEMENT_AND_COAGULATION_CASCADES
KEGG_MEDICUS_REFERENCE_TCR_PLCG_ITPR_SIGNALING_PATHWAY
PID_CD8_TCR_PATHWAY
REACTOME_GENERATION_OF_SECOND_MESSENGER_MOLECULES
REACTOME_PD_1_SIGNALING
WP_COMPLEMENT_AND_COAGULATION_CASCADES
WP_COMPLEMENT_SYSTEM
WP_MODULATORS_OF_TCR_SIGNALING_AND_T_CELL_ACTIVATION
WP_T_CELL_RECEPTOR_SIGNALING_PATHWAY

14

GOBP_HETEROTYPIC_CELL_CELL_ADHESION
GOBP_INTERLEUKIN_4_PRODUCTION
GOBP_POSITIVE_REGULATION_OF_CD4_POSITIVE_ALPHA_BETA_T_CELL_DIFFERENTIATION
GOBP_POSITIVE_REGULATION_OF_INTERLEUKIN_4_PRODUCTION
GOBP_POSITIVE_REGULATION_OF_T_HELPER_CELL_DIFFERENTIATION
GOBP_REGULATION_OF_CD4_POSITIVE_ALPHA_BETA_T_CELL_DIFFERENTIATION
GOBP_REGULATION_OF_CELL_CELL_ADHESION
GOBP_REGULATION_OF_HETEROTYPIC_CELL_CELL_ADHESION
GOBP_REGULATION_OF_T_HELPER_CELL_DIFFERENTIATION

21

GOMF_CHEMOKINE_ACTIVITY
GOMF_CYTOKINE_ACTIVITY
KEGG_CYTOKINE_CYTOKINE_RECEPTOR_INTERACTION
REACTOME_INTERLEUKIN_10_SIGNALING
WP_CYTOKINES_AND_INFLAMMATORY_RESPONSE
WP_IMMUNE_INFILTRATION_IN_PANCREATIC_CANCER
WP_OVERVIEW_OF_PROINFLAMMATORY_AND_PROFIBROTIC_MEDIATORS

32

HP_ABNORMALITY_OF_SERUM_CYTOKINE_LEVEL
HP_ABNORMAL_CIRCULATING_INTERFERON_CONCENTRATION
HP_ABNORMAL_CIRCULATING_INTERLEUKIN_CONCENTRATION
HP_INCREASED_CIRCULATING_INTERFERON_GAMMA_CONCENTRATION

45

BIOCARTA_INFLAM_PATHWAY
KEGG_HEMATOPOIETIC_CELL_LINEAGE

Mitochondria,Translation, Ribosome

3

GOBP_MITOCHONDRIAL_GENE_EXPRESSION
GOBP_MITOCHONDRIAL_TRANSLATION
GOCC_CYTOSOLIC_LARGE_RIBOSOMAL_SUBUNIT
GOCC_MITOCHONDRIAL_LARGE_RIBOSOMAL_SUBUNIT
GOCC_MITOCHONDRIAL_PROTEIN_CONTAINING_COMPLEX
GOCC_MITOCHONDRIAL_SMALL_RIBOSOMAL_SUBUNIT
GOCC_ORGANELLAR_RIBOSOME
GOCC_RIBOSOMAL_SUBUNIT
GOCC_SMALL_RIBOSOMAL_SUBUNIT
GOMF_STRUCTURAL_CONSTITUENT_OF_RIBOSOME
KEGG_MEDICUS_REFERENCE_TRANSLATION_INITIATION
KEGG_RIBOSOME
REACTOME_EUKARYOTIC_TRANSLATION_ELONGATION
REACTOME_EUKARYOTIC_TRANSLATION_INITIATION
REACTOME_MITOCHONDRIAL_TRANSLATION
REACTOME_RESPONSE_OF_EIF2AK4_GCN2_TO_AMINO_ACID_DEFICIENCY
REACTOME_SARS_COV_1_MODULATES_HOST_TRANSLATION_MACHINERY
REACTOME_SRP_DEPENDENT_COTRANSLATIONAL_PROTEIN_TARGETING_TO_MEMBRANE
REACTOME_TRANSLATION
WP_CYTOPLASMIC_RIBOSOMAL_PROTEINS

6

GOBP_AMINO_ACID_ACTIVATION
GOBP_NCRNA_PROCESSING
GOBP_RNA_MODIFICATION
GOBP_TRNA_METABOLIC_PROCESS
GOBP_TRNA_MODIFICATION
GOBP_TRNA_PROCESSING
GOCC_90S_PRERIBOSOME
GOMF_3_5_EXONUCLEASE_ACTIVITY
GOMF_CATALYTIC_ACTIVITY_ACTING_ON_A_TRNA
GOMF_CATALYTIC_ACTIVITY_ACTING_ON_RNA
GOMF_EXONUCLEASE_ACTIVITY_ACTIVE_WITH_EITHER_RIBO_OR_DEOXYRIBONUCLEIC_ACIDS_AND_PRODUCING_5_PHOSPHOMONOESTERS
GOMF_LIGASE_ACTIVITY
GOMF_LIGASE_ACTIVITY_FORMING_CARBON_OXYGEN_BONDS
GOMF_RNA_METHYLTRANSFERASE_ACTIVITY
GOMF_TRNA_BINDING
KEGG_AMINOACYL_TRNA_BIOSYNTHESIS
REACTOME_MITOCHONDRIAL_TRNA_AMINOACYLATION
REACTOME_TRNA_AMINOACYLATION
REACTOME_TRNA_PROCESSING

Wound healing

4

GOBP_HEMOSTASIS
GOBP_HOMOTYPIC_CELL_CELL_ADHESION
GOBP_NEGATIVE_REGULATION_OF_COAGULATION
GOBP_NEGATIVE_REGULATION_OF_RESPONSE_TO_WOUNDING
GOBP_NEGATIVE_REGULATION_OF_WOUND_HEALING
GOBP_PLATELET_ACTIVATION
GOBP_PLATELET_AGGREGATION
GOBP_POSITIVE_REGULATION_OF_COAGULATION
GOBP_POSITIVE_REGULATION_OF_RESPONSE_TO_WOUNDING
GOBP_POSITIVE_REGULATION_OF_WOUND_HEALING
GOBP_REGULATION_OF_BODY_FLUID_LEVELS
GOBP_REGULATION_OF_COAGULATION
GOBP_REGULATION_OF_HOMOTYPIC_CELL_CELL_ADHESION
GOBP_REGULATION_OF_PLATELET_ACTIVATION
GOBP_REGULATION_OF_PLATELET_AGGREGATION
GOBP_REGULATION_OF_RESPONSE_TO_WOUNDING
GOBP_REGULATION_OF_WOUND_HEALING
GOBP_RESPONSE_TO_WOUNDING
GOBP_WOUND_HEALING
REACTOME_FORMATION_OF_FIBRIN_CLOT_CLOTTING_CASCADE

30

GOBP_NEGATIVE_REGULATION_OF_TRANSFORMING_GROWTH_FACTOR_BETA_RECEPTOR_SIGNALING_PATHWAY
GOBP_REGULATION_OF_CELLULAR_RESPONSE_TO_TRANSFORMING_GROWTH_FACTOR_BETA_STIMULUS
GOBP_RESPONSE_TO_TRANSFORMING_GROWTH_FACTOR_BETA
GOBP_TRANSFORMING_GROWTH_FACTOR_BETA_RECEPTOR_SIGNALING_PATHWAY

47

GOBP_REGULATION_OF_CELLULAR_RESPONSE_TO_GROWTH_FACTOR_STIMULUS
GOBP_REGULATION_OF_FIBROBLAST_GROWTH_FACTOR_RECEPTOR_SIGNALING_PATHWAY

Cell differentiation
8
GOBP_ASTROCYTE_DIFFERENTIATION
GOBP_GLIAL_CELL_DIFFERENTIATION
GOBP_NEGATIVE_REGULATION_OF_AXONOGENESIS
GOBP_NEGATIVE_REGULATION_OF_AXON_EXTENSION
GOBP_NEGATIVE_REGULATION_OF_CELL_CELL_ADHESION
GOBP_NEGATIVE_REGULATION_OF_CELL_DEVELOPMENT
GOBP_NEGATIVE_REGULATION_OF_CELL_DIFFERENTIATION
GOBP_NEGATIVE_REGULATION_OF_LYMPHOCYTE_DIFFERENTIATION
GOBP_NEGATIVE_REGULATION_OF_NEURON_DIFFERENTIATION
GOBP_POSITIVE_REGULATION_OF_GLIAL_CELL_DIFFERENTIATION
GOBP_POSITIVE_REGULATION_OF_GLIOGENESIS
GOBP_REGULATION_OF_ASTROCYTE_DIFFERENTIATION
GOBP_REGULATION_OF_GLIAL_CELL_DIFFERENTIATION
GOBP_REGULATION_OF_GLIOGENESIS
GOBP_REGULATION_OF_OLIGODENDROCYTE_DIFFERENTIATION
GOBP_SEMAPHORIN_PLEXIN_SIGNALING_PATHWAY

System development

9

GOBP_AMEBOIDAL_TYPE_CELL_MIGRATION
GOBP_ANGIOGENESIS_INVOLVED_IN_WOUND_HEALING
GOBP_ARTERY_DEVELOPMENT
GOBP_ARTERY_MORPHOGENESIS
GOBP_BLOOD_VESSEL_MORPHOGENESIS
GOBP_CELLULAR_RESPONSE_TO_VASCULAR_ENDOTHELIAL_GROWTH_FACTOR_STIMULUS
GOBP_ENDOTHELIAL_CELL_CHEMOTAXIS
GOBP_ENDOTHELIAL_CELL_PROLIFERATION
GOBP_EPITHELIAL_CELL_PROLIFERATION
GOBP_PLACENTA_BLOOD_VESSEL_DEVELOPMENT
GOBP_PLACENTA_DEVELOPMENT
GOBP_POSITIVE_REGULATION_OF_ENDOTHELIAL_CELL_PROLIFERATION
GOBP_POSITIVE_REGULATION_OF_EPITHELIAL_CELL_PROLIFERATION
GOBP_REGULATION_OF_EPITHELIAL_CELL_PROLIFERATION
GOBP_VASCULATURE_DEVELOPMENT

10

GOBP_COLUMNAR_CUBOIDAL_EPITHELIAL_CELL_DEVELOPMENT
GOBP_COLUMNAR_CUBOIDAL_EPITHELIAL_CELL_DIFFERENTIATION
GOBP_DIGESTIVE_SYSTEM_DEVELOPMENT
GOBP_EPIDERMIS_DEVELOPMENT
GOBP_EPITHELIAL_CELL_DEVELOPMENT
GOBP_EPITHELIAL_CELL_DIFFERENTIATION
GOBP_GLANDULAR_EPITHELIAL_CELL_DIFFERENTIATION
GOBP_INTESTINAL_EPITHELIAL_CELL_DIFFERENTIATION
GOBP_NEGATIVE_REGULATION_OF_EPITHELIAL_CELL_DIFFERENTIATION
GOBP_NEUROEPITHELIAL_CELL_DIFFERENTIATION
GOBP_POLARIZED_EPITHELIAL_CELL_DIFFERENTIATION
GOBP_REGULATION_OF_EPITHELIAL_CELL_DIFFERENTIATION
GOBP_SKIN_DEVELOPMENT
GOBP_SKIN_EPIDERMIS_DEVELOPMENT

11

GOBP_ACTIN_MEDIATED_CELL_CONTRACTION
GOBP_CARDIAC_MUSCLE_CONTRACTION
GOBP_CELL_COMMUNICATION_BY_ELECTRICAL_COUPLING
GOBP_HEART_PROCESS
GOBP_REGULATION_OF_BLOOD_CIRCULATION
GOBP_REGULATION_OF_CARDIAC_MUSCLE_CONTRACTION
GOBP_REGULATION_OF_HEART_CONTRACTION
GOBP_REGULATION_OF_STRIATED_MUSCLE_CONTRACTION
GOBP_REGULATION_OF_SYSTEM_PROCESS
GOBP_REGULATION_OF_VASOCONSTRICTION
GOBP_STRIATED_MUSCLE_CONTRACTION

13

GOBP_MULTICELLULAR_ORGANISMAL_MOVEMENT
GOBP_MUSCLE_CONTRACTION
GOBP_MUSCLE_SYSTEM_PROCESS
GOBP_NEGATIVE_REGULATION_OF_MUSCLE_CONTRACTION
GOBP_POSITIVE_REGULATION_OF_SMOOTH_MUSCLE_CONTRACTION
GOBP_REGULATION_OF_MUSCLE_CONTRACTION
GOBP_REGULATION_OF_MUSCLE_SYSTEM_PROCESS
GOBP_REGULATION_OF_SMOOTH_MUSCLE_CONTRACTION
GOBP_RELAXATION_OF_MUSCLE
GOBP_SKELETAL_MUSCLE_CONTRACTION

15

GOBP_BIOMINERAL_TISSUE_DEVELOPMENT
GOBP_BONE_MINERALIZATION
GOBP_NEGATIVE_REGULATION_OF_BIOMINERAL_TISSUE_DEVELOPMENT
GOBP_OSSIFICATION
GOBP_OSTEOBLAST_DIFFERENTIATION
GOBP_OSTEOBLAST_PROLIFERATION
GOBP_REGULATION_OF_OSSIFICATION
GOBP_REGULATION_OF_OSTEOBLAST_DIFFERENTIATION
GOBP_REGULATION_OF_OSTEOBLAST_PROLIFERATION

16

GOBP_KIDNEY_EPITHELIUM_DEVELOPMENT
GOBP_KIDNEY_MORPHOGENESIS
GOBP_MESONEPHRIC_TUBULE_MORPHOGENESIS
GOBP_MESONEPHROS_DEVELOPMENT
GOBP_METANEPHROS_DEVELOPMENT
GOBP_NEPHRON_EPITHELIUM_DEVELOPMENT
GOBP_NEPHRON_MORPHOGENESIS
GOBP_RENAL_TUBULE_DEVELOPMENT
WP_DEVELOPMENT_OF_URETERIC_COLLECTION_SYSTEM

19

GOBP_ENDOCRINE_HORMONE_SECRETION
GOBP_ENDOCRINE_PROCESS
GOBP_HORMONE_TRANSPORT
GOBP_LIPID_EXPORT_FROM_CELL
GOBP_NEGATIVE_REGULATION_OF_HORMONE_SECRETION
GOBP_NEGATIVE_REGULATION_OF_SECRETION
GOBP_REGULATION_OF_HORMONE_LEVELS
GOBP_REGULATION_OF_MORPHOGENESIS_OF_AN_EPITHELIUM
GOBP_REGULATION_OF_MORPHOGENESIS_OF_A_BRANCHING_STRUCTURE

25

GOBP_GLAND_MORPHOGENESIS
GOBP_LUNG_MORPHOGENESIS
GOBP_MORPHOGENESIS_OF_A_BRANCHING_STRUCTURE
GOBP_RESPIRATORY_SYSTEM_DEVELOPMENT
GOBP_SALIVARY_GLAND_DEVELOPMENT

29

GOBP_CHONDROCYTE_DIFFERENTIATION
GOBP_POSITIVE_REGULATION_OF_CARTILAGE_DEVELOPMENT
GOBP_REGULATION_OF_CARTILAGE_DEVELOPMENT
GOBP_REGULATION_OF_CHONDROCYTE_DIFFERENTIATION

31

GOBP_EAR_DEVELOPMENT
GOBP_EAR_MORPHOGENESIS
GOBP_INNER_EAR_MORPHOGENESIS
GOBP_SENSORY_ORGAN_MORPHOGENESIS

36

GOBP_ENDODERM_FORMATION
GOBP_FORMATION_OF_PRIMARY_GERM_LAYER
GOBP_MESODERM_DEVELOPMENT
GOBP_MESODERM_MORPHOGENESIS

37

GOBP_AORTIC_VALVE_MORPHOGENESIS
GOBP_HEART_VALVE_DEVELOPMENT
GOBP_SEMI_LUNAR_VALVE_DEVELOPMENT

38

REACTOME_ION_HOMEOSTASIS
REACTOME_MUSCLE_CONTRACTION
WP_STRIATED_MUSCLE_CONTRACTION_PATHWAY

44

GOBP_POSITIVE_REGULATION_OF_NERVOUS_SYSTEM_PROCESS
GOBP_REGULATION_OF_NERVOUS_SYSTEM_PROCESS

46

GOBP_BONE_GROWTH
GOBP_CARTILAGE_DEVELOPMENT

DNA Repair

12

KEGG_HOMOLOGOUS_RECOMBINATION
PID_ATM_PATHWAY
PID_FANCONI_PATHWAY
REACTOME_DISEASES_OF_DNA_REPAIR
REACTOME_DNA_DOUBLE_STRAND_BREAK_REPAIR
REACTOME_DNA_REPAIR
REACTOME_HDR_THROUGH_HOMOLOGOUS_RECOMBINATION_HRR
REACTOME_HDR_THROUGH_SINGLE_STRAND_ANNEALING_SSA
REACTOME_HOMOLOGOUS_DNA_PAIRING_AND_STRAND_EXCHANGE
REACTOME_RESOLUTION_OF_D_LOOP_STRUCTURES
REACTOME_RESOLUTION_OF_D_LOOP_STRUCTURES_THROUGH_SYNTHESIS_DEPENDENT_STRAND_ANNEALING_SDSA

23

GOBP_DNA_TEMPLATED_DNA_REPLICATION
GOCC_NUCLEAR_REPLICATION_FORK
GOCC_REPLICATION_FORK
GOCC_REPLISOME
REACTOME_POLYMERASE_SWITCHING_ON_THE_C_STRAND_OF_THE_TELOMERE

27

GOBP_ACTIN_FILAMENT_BUNDLE_ORGANIZATION
GOBP_ACTIN_FILAMENT_ORGANIZATION
GOBP_ACTIN_NUCLEATION
GOBP_NEGATIVE_REGULATION_OF_SUPRAMOLECULAR_FIBER_ORGANIZATION

33

GOBP_NEGATIVE_REGULATION_OF_TELOMERE_MAINTENANCE
GOBP_NEGATIVE_REGULATION_OF_TELOMERE_MAINTENANCE_VIA_TELOMERE_LENGTHENING
GOBP_REGULATION_OF_TELOMERE_MAINTENANCE_VIA_TELOMERE_LENGTHENING
GOCC_CHROMOSOME_TELOMERIC_REGION

20

GOMF_CATALYTIC_ACTIVITY_ACTING_ON_DNA
GOMF_HELICASE_ACTIVITY
KEGG_MEDICUS_REFERENCE_CORE_NER_REACTION
KEGG_MEDICUS_REFERENCE_HOMOLOGOUS_RECOMBINATION
KEGG_NUCLEOTIDE_EXCISION_REPAIR
WP_DNA_REPAIR_PATHWAYS_FULL_NETWORK
WP_NUCLEOTIDE_EXCISION_REPAIR_IN_XERODERMA_PIGMENTOSUM

EMT
18
GOBP_CARDIAC_EPITHELIAL_TO_MESENCHYMAL_TRANSITION
GOBP_EPITHELIAL_TO_MESENCHYMAL_TRANSITION
GOBP_MESENCHYMAL_CELL_DIFFERENTIATION
GOBP_MESENCHYME_DEVELOPMENT
GOBP_NEGATIVE_REGULATION_OF_EPITHELIAL_TO_MESENCHYMAL_TRANSITION
GOBP_POSITIVE_REGULATION_OF_EPITHELIAL_TO_MESENCHYMAL_TRANSITION
GOBP_REGULATION_OF_EPITHELIAL_TO_MESENCHYMAL_TRANSITION

Platelets
22
HP_EPISTAXIS
HP_IMPAIRED_PLATELET_AGGREGATION
HP_MENORRHAGIA
HP_PROLONGED_BLEEDING_FOLLOWING_PROCEDURE
HP_SPONTANEOUS_HEMATOMAS

Antioxidant activity
26
GOBP_HYDROGEN_PEROXIDE_CATABOLIC_PROCESS
GOBP_HYDROGEN_PEROXIDE_METABOLIC_PROCESS
GOBP_RESPONSE_TO_TOXIC_SUBSTANCE
GOMF_ANTIOXIDANT_ACTIVITY
GOMF_OXIDOREDUCTASE_ACTIVITY_ACTING_ON_PEROXIDE_AS_ACCEPTOR

Lactic acid
41
HP_ABNORMAL_CIRCULATING_PROTEINOGENIC_AMINO_ACID_DERIVATIVE_CONCENTRATION
HP_INCREASED_SERUM_LACTATE
HP_LACTIC_ACIDOSIS

Growth factors
28
GOMF_GROWTH_FACTOR_ACTIVITY
GOMF_HORMONE_ACTIVITY
GOMF_SIGNALING_RECEPTOR_REGULATOR_ACTIVITY
WP_PLURIPOTENT_STEM_CELL_DIFFERENTIATION_PATHWAY

Glucocorticoids

34

KEGG_MEDICUS_ENV_FACTOR_TCDD_TO_AHR_SIGNALING_PATHWAY
REACTOME_GLUTATHIONE_CONJUGATION
WP_GLUCOCORTICOID_RECEPTOR_PATHWAY
WP_NUCLEAR_RECEPTORS_META_PATHWAY

Anti-viral response

35

GOBP_ANTIVIRAL_INNATE_IMMUNE_RESPONSE
GOBP_DEFENSE_RESPONSE_TO_SYMBIONT
GOBP_NEGATIVE_REGULATION_OF_VIRAL_GENOME_REPLICATION
GOBP_NEGATIVE_REGULATION_OF_VIRAL_PROCESS

T cells

39

HP_ABNORMAL_T_CELL_MORPHOLOGY
HP_AUTOIMMUNE_HEMOLYTIC_ANEMIA
HP_T_LYMPHOCYTOPENIA

Transcription

40

REACTOME_NGF_STIMULATED_TRANSCRIPTION
REACTOME_NUCLEAR_EVENTS_KINASE_AND_TRANSCRIPTION_FACTOR_ACTIVATION
REACTOME_SIGNALING_BY_NTRKS

43

GOBP_POSITIVE_REGULATION_OF_MIRNA_METABOLIC_PROCESS
GOBP_POSITIVE_REGULATION_OF_MIRNA_TRANSCRIPTION
GOBP_REGULATION_OF_MIRNA_TRANSCRIPTION

Response to cAMP

42

GOBP_RESPONSE_TO_CAMP
GOBP_RESPONSE_TO_ORGANOPHOSPHORUS
GOBP_RESPONSE_TO_PURINE_CONTAINING_COMPOUND

CHAPTER 6

DISCUSSION

In this final chapter, the core concepts presented throughout the thesis will be articulated. The results and implications for each chapter have been comprehensively discussed in each of the respective chapter sections. Chapter 6 will consolidate this in context of the thesis as a whole, and illustrate the synergistic interplay of the findings between the chapters, as well as intertwine opportunities for future research. Additionally, the relationship of these findings to the current understanding and paradigms in the literature will be discussed, as well as the implications of the knowledge gained through the work completed in this thesis.

Cumulative Interplay and Significance of Findings

The principal objective of this thesis was to investigate the aberrant mechanisms governing the profibrotic activation of macrophages in the context of pulmonary fibrosis, and ultimately interfere with their programming to hamper fibrogenesis in the lung. Fibrosis and aberrant wound healing are implicated in the pathogenesis of a multitude of conditions across various organ systems in the body, including cancer, COVID-19 infection, endometriosis, inflammatory bowel disease, and fibrotic disease (including in the kidney, heart, lung, skin, tendons, and bone marrow). Fibrosis is a detrimental disease process and the involvement of extensive scarring can severely impair organ function, with approximately 45% of all deaths in the developed world being attributed to fibroproliferative disorders [1]. It is believed that similar cellular and molecular mechanisms mediate fibrosis across different organs [72], and so there is much to be learned by drawing inferences and applying knowledge from other fibrotic diseases. In Chapter 2, we focused on the fibrogenic mechanism of

macrophage-myofibroblast transition (MMT). MMT is a relatively new disease-contributing process being explored in fibrosis, with the term being officially coined in 2014 by Nikolic-Paterson et al. to explain the finding of monocyte-derived macrophages transitioning into myofibroblasts and promoting kidney fibrosis *in vivo* [35]. Majority of the evidence for MMT is in the kidney, however given the potential for overlap between fibrotic disorders, as well as the shared importance of macrophages and myofibroblasts in these diseases, we decided to explore this concept in the context of the lung in IPF. We investigated evidence for MMT in lung tissue from IPF patients. Through mining of a scRNAseq dataset of lung tissue explants from IPF patients and controls, we demonstrated that a subset of cells in the lung that have myofibroblast features co-express markers of monocytic origin ($ACTA2^{+}MAFB^{+}$). Further, using our curated surgical lung biopsy biobank of lung tissue from IPF patients, our assessments showed that MAFB, ACTA2, and CD68 transcripts were expressed in the same cells, as well as localization of α-SMA and CD68 proteins in similar areas. Although numerous studies have reported critical evidence for macrophage myofibroblast crosstalk in the pathogenesis of lung fibrosis [29,73–76], there is little known about direct transition of monocytes/macrophages to myofibroblasts in lung fibrosis. To the best of our knowledge, this was the first report of MMT-specific investigation in human-derived samples in IPF. However, it is likely that evidence for this may have existed before the official establishment of the MMT term in 2014. Evidence for circulating fibrocytes in IPF, defined as blood cells expressing CD45 and collagen-1, as well as association of these cells with poor

prognosis has been demonstrated [40]. Although pre-MMT establishment, it is plausible that these cells could represent a population of monocyte-derived mesenchymal-like cells undergoing MMT, further supporting the presence of this phenotype and its involvement in disease progression in IPF.

In Chapter 3, we aimed to develop a novel system that could be used for the translational evaluation of profibrotic macrophages in the lung. We established an *ex vivo* model for profibrotic programming of lung macrophages using precision-cut lung slices (PCLS), which offers the advantages of increased complexity, conservation of lung microenvironment and architecture, and moderate throughput of assessments – with the novel introduction of a quantitative histological approach for studying PCLS using FFPE tissue microarrays. Although previous studies have demonstrated successful modelling of fibrosis using PCLS [70], as well as conserved presence of macrophages in the slices [77], such a system had not been established for the specific evaluation of profibrotic macrophages. In our work, we show that multiple measurable features of profibrotic macrophage programming, including arginase enzyme activity, protein expression, soluble secretions, and histological markers, were induced with treatment of our polarization cocktail. Further substantiating the fibrotic properties of this model, we demonstrate upregulation of features related to fibrosis, including α-SMA expression, soluble collagen secretion, and ECM gene expression. Furthermore, through the development and optimization of a protocol for high-content immunostaining and cellular phenotyping using IBEX, which we describe in detail in Chapter 4, we show the ability to determine specific macrophage phenotype in our

PCLS. Using a variety of markers, we determine that both alveolar and interstitial macrophages undergo profibrotic polarization in our system. Perhaps most notably, through high-content phenotyping we also show that there is an increase in our model of α-SMA$^+$ cells that co-express the panel of markers we used to define profibrotic macrophages (CD45$^+$CD68$^+$CD11c$^+$Arg1$^+$CD206$^+$). In connection with Chapter 2, this finding suggests that our PCLS system may also be a suitable model for studying features and mechanisms of MMT in the lung. Further investigation is required to examine the properties and behaviours of these cells. Overall, this model provides a suitable screening tool for a variety of compounds and mechanisms of interest related to profibrotic macrophages in the lung, including MMT.

In Chapter 5, we uncover differential transcriptomic features of monocytes in IPF, as well as potential association of monocytic attributes with features related to disease severity. Specifically, we identified an aberrant metabolic profile in IPF characterized by decreased mitochondrial function and OXPHOS. We then applied this information to delve into mechanistic studies on the contribution of the identified aberrant features to profibrotic macrophage polarization, using macrophage cultures and our developed PCLS polarization system. Coincidentally, some of the first organ slice studies reported in the 1920's were conducted by Warburg (who discovered the Warburg effect) to study metabolism [87]. These findings set the stage for further metabolic studies on IPF monocytes, especially assessment of metabolic function using extracellular flux analysis. In our study we also performed cluster analysis, and show that cluster composition is seemingly related to severity of lung function. Interestingly,

when examining the differences of IPF patients between clusters with a GSEA network, we see that a number of features are upregulated in the more severe clusters. Expectedly, we observed traits for monocyte activation, including monocyte infiltration and differentiation and immune response. Furthermore, we see upregulation of fibrosis-related features including wound healing response and remodelling of collagen and ECM, and interestingly, in the system development module, we see upregulation of nodes "actin mediated cell contraction", "smooth muscle contraction" and "mesenchymal cell differentiation". This could signify potential MMT in these cells, as a cornerstone functional trait of true α-SMA^{+} myofibroblasts is the ability to contract [78]. This is a prospective area of interest for future studies, where functional assessments can be conducted to ultimately determine the presence of MMT in these cells. Nonetheless, these findings support a profibrotic phenotype of monocytes in IPF.

A Constellation for Biologically-Translational Research

One of the mainstays of this thesis was implementing a workflow that could be used for translational research in IPF. Given the progressive, fatal, and incurable nature of IPF, novel advancements in disease research are urgently required. It is critical that researchers continue to implement innovative strategies and explore novel avenues, contributing to the discovery of promising disease targets and therapies for treatment of IPF. However, the study of IPF presents several challenges. The observed complexity and heterogeneity of the disease have led clinicians and researchers to believe that IPF may constitute a group of disorders, which may contribute to the

explanation of the prevalence of failed clinical trials for treatment of IPF [79]. This also significantly adds to the challenge of modelling pulmonary fibrosis in research settings, as the drastic heterogeneity observed in patients and overall lack of understanding about the disease means that research models likely only encapsulate a limited fraction of the true disease manifestation. Compounding this, the lung is one of the body's most complex organs [69], and so modelling and investigating pulmonary disorders in ways that are physiologically accurate can be highly cumbersome.

In attempt to navigate these challenges in the context of studying profibrotic macrophage polarization in lung fibrosis, this PhD thesis implemented the following four components: 1. Development of a novel *ex vivo* model with increased biological relevance (PCLS model for macrophage polarization); 2. Patient-derived signatures (IPF monocyte transcriptomic study); 3. Insight into targets (identification of aberrant metabolic function in IPF monocytes); and 4. Mechanistic studies (effects of modulating these metabolic processes on macrophage polarization). This constellation allowed us to approach the investigation of profibrotic macrophage polarization in lung fibrosis from multiple angles. To maximize translational capacity of our research, we implemented a human-first approach where we collected and assessed samples from patients with IPF, and used these patient signatures to guide our discovery of potential targets of interest. After uncovering human-informed targets, we then conducted mechanistic studies using macrophage polarization models, including the novel complex PCLS model we developed, to assess potential disease-modifying

potential. This overall allowed us to identify and assess the implications of modulating processes that are shown to be present in true human disease, and are associated with patient clinical features.

Hypoxia and Metabolic Perturbation – A Potential Source of Self-Perpetuation of Disease in IPF

Hypoxia is a prominent feature in tissue fibrosis [80]. This is even more pronounced in fibrotic lung diseases, as scarring of the lung tissue impairs breathing and impedes oxygen diffusion. In the setting of low oxygen levels, normal homeostatic mechanisms cause cells to prioritize glycolysis as it is an anaerobic process of ATP production [81]. One of the mediating transcription factors of this switch is hypoxia-inducible factor-1 (HIF-1), which is directly upstream of PDK, thus leading to PDK activation and inhibition of OXPHOS [80,82]. In IPF, it has been found that the increased lactate levels from glycolytic flux lower pH in the tissue, which results in increased TGF-β activation, HIF-1 stabilization, and increased lactate dehydrogenase 5 (LDH5), thus promoting fibroblast-to-myofibroblast differentiation [42]. This may establish a self-perpetuating process of disease, as myofibroblasts are known to secrete ECM components and contribute to scarring in the lung, thus overall leading to decreased capacity for diffusion of oxygen. Lactate is also a known promoter of M2-like macrophage polarization, which may further contribute to this landscape [83]. Although it is believed that the Warburg effect, which involves a switch from OXPHOS to glycolysis even in the presence of adequate oxygen supply, drives metabolic dysregulation, hypoxic environments also naturally contribute to a

metabolic shift. Synergy of these processes may promote pathologic adaptation of cells to survive in hypoxic environments, effectuating a positive feedback loop that leads to a sustained suppression of OXPHOS in fibrotic lung disease.

Metabolically-Driven Expansion of Monocytes

Several studies, including our own, have exhibited that monocyte count is increased in IPF [31–34]. However, reasons for this expansion are unknown and although monocyte count predicts poor disease outcomes, it is not clear how the increased quantity is related to pathologic processes. Apoptosis is a programmed cell death process that eliminates cells to maintain homeostasis. It is known that abnormal cell survival can lead to pathologic states that drive various diseases [84]. Mitochondrial dysfunction and high rates of glycolysis promote apoptosis resistance through hyperpolarization of the inner mitochondrial membrane and inhibition of apoptotic factor release [85]. PDK4 has also been demonstrated to be required for the NF-kB-mediated pro-survival functions of TNF-α [44]. Adding to the propensity for expanded cell populations, it is known that cancer cells resort to the Warburg effect and increased glycolysis to allow for hyperproliferation [81]. Therefore, metabolism-mediated apoptotic resistance and hyperproliferation may contribute to the increased levels of monocytes observed in IPF.

Clinical Implications

The future of preclinical investigations in IPF calls for novel strategies, patient-centric approaches, and overall increase in translatability for ongoing research [86]. The establishment of our PCLS *ex vivo* system fits into this vision, as it provides a novel

strategy for testing the implications of experimental compounds and modulation of mechanisms on macrophages in a profibrotic lung environment in a moderate-throughput manner. The model can also be extended to human tissue, and is tunable based on desired outcome, such as through addition of further cytokines for stimulation.

Additionally, the results of our monocyte study in IPF patients provide evidence that monocytes exhibit characteristics of disease at the transcriptomic level. Our cluster analysis also showed that these characteristics may be related to disease severity. This suggests that monocytes in IPF hold potentially relevant clinical information, and in addition to the published findings on monocyte count as a biomarker in IPF [31–34], examining the profile of these monocytes may provide even more clinically relevant insight for prognostication in IPF. This is in accordance with the published study on outcome prediction in IPF using PBMC [12], supporting the application of circulating cells as suitable and accessible biomarkers in IPF. Further investigation is required to elucidate such biomarker potential, including validation cohort studies and association of monocyte characteristics with a multimodal assessment of disease severity in IPF, including radiographic imaging and symptoms. Assessing the relationship of monocytic traits to disease progression through longitudinal studies would also be beneficial.

Concluding Statement

The findings presented in this thesis contribute to the field by providing novel insight on the underlying processes governing profibrotic macrophage programming in the

lung, the establishment of a novel biologically-relevant approach to investigate these macrophages, discovery of a patient-derived signature in IPF monocytes, and evidence for mechanistic involvement of this signature in macrophage polarization. Overall, this work supports the pursuit of knowledge to better understand the profibrotic contribution of macrophages and monocytes in IPF, and offer insights for novel mechanistic avenues and potential therapeutic interventions in fibrosis.

REFERENCES (Chapters 1 and 6)

[1] T. Wynn, Cellular and molecular mechanisms of fibrosis, The Journal of Pathology 214 (2008) 199–210. https://doi.org/10.1002/path.2277.

[2] S.A. Antar, N.A. Ashour, M.E. Marawan, A.A. Al-Karmalawy, Fibrosis: Types, Effects, Markers, Mechanisms for Disease Progression, and Its Relation with Oxidative Stress, Immunity, and Inflammation, International Journal of Molecular Sciences 24 (2023) 4004. https://doi.org/10.3390/ijms24044004.

[3] N.N. Alrajhi, Post-COVID-19 pulmonary fibrosis: An ongoing concern, Ann Thorac Med 18 (2023) 173–181. https://doi.org/10.4103/atm.atm_7_23.

[4] R. Najjar-Debbiny, O. Barnett-Griness, J. Khoury, N. Gronich, G. Weber, Y. Adir, M. Shteinberg, S. Shneir, L. Sharma, W. Saliba, Association Between COVID-19 Infection and Pulmonary Fibrosis: A Nested Case-Control Study, The American Journal of Medicine 136 (2023) 1087-1093.e2. https://doi.org/10.1016/j.amjmed.2023.07.020.

[5] K.M. Antoniou, G.A. Margaritopoulos, S. Tomassetti, F. Bonella, U. Costabel, V. Poletti, Interstitial lung disease, European Respiratory Review 23 (2014) 40–54. https://doi.org/10.1183/09059180.00009113.

[6] P. Janowiak, A. Szymanowska-Narloch, A. Siemińska, IPF Respiratory Symptoms Management — Current Evidence, Front Med (Lausanne) 9 (2022) 917973. https://doi.org/10.3389/fmed.2022.917973.

[7] E. Fernández Fabrellas, R. Peris Sánchez, C. Sabater Abad, G. Juan Samper, Prognosis and Follow-Up of Idiopathic Pulmonary Fibrosis, Med Sci (Basel) 6 (2018) 51. https://doi.org/10.3390/medsci6020051.

[8] J.E. Michalski, D.A. Schwartz, Genetic Risk Factors for Idiopathic Pulmonary Fibrosis: Insights into Immunopathogenesis, J Inflamm Res 13 (2021) 1305–1318. https://doi.org/10.2147/JIR.S280958.

[9] V.S. Taskar, D.B. Coultas, Is idiopathic pulmonary fibrosis an environmental disease?, Proc Am Thorac Soc 3 (2006) 293–298. https://doi.org/10.1513/pats.200512-131TK.

[10] K. Boon, N.W. Bailey, J. Yang, M.P. Steel, S. Groshong, D. Kervitsky, K.K. Brown, M.I. Schwarz, D.A. Schwartz, Molecular Phenotypes Distinguish Patients with Relatively Stable from Progressive Idiopathic Pulmonary Fibrosis (IPF), PLoS One 4 (2009) e5134. https://doi.org/10.1371/journal.pone.0005134.

[11] D.J. DePianto, S. Chandriani, A.R. Abbas, G. Jia, E.N. N'Diaye, P. Caplazi, S.E. Kauder, S. Biswas, S.K. Karnik, C. Ha, Z. Modrusan, M.A. Matthay, J. Kukreja, H.R. Collard, J.G. Egen, P.J. Wolters, J.R. Arron, Heterogeneous gene expression signatures correspond to distinct lung pathologies and biomarkers of disease severity in idiopathic pulmonary fibrosis, Thorax 70 (2015) 48–56. https://doi.org/10.1136/thoraxjnl-2013-204596.

[12] J.D. Herazo-Maya, J. Sun, P.L. Molyneaux, Q. Li, J.A. Villalba, A. Tzouvelekis, H. Lynn, B.M. Juan-Guardela, C. Risquez, J.C. Osorio, X. Yan, G. Michel, N. Aurelien, K.O. Lindell, M.J. Klesen, M.F. Moffatt, W.O. Cookson, Y. Zhang, J.G. Garcia, I. Noth, A. Prasse, Z. Bar-Joseph, K.F. Gibson, H. Zhao, E.L. Herzog, I.O. Rosas, T.M.

Maher, N. Kaminski, Validating a 52-gene risk profile for outcome prediction in Idiopathic Pulmonary Fibrosis: an international multicentre cohort study, Lancet Respir Med 5 (2017) 857–868. https://doi.org/10.1016/S2213-2600(17)30349-1.

[13] M.J. Schafer, T.A. White, K. Iijima, A.J. Haak, G. Ligresti, E.J. Atkinson, A.L. Oberg, J. Birch, H. Salmonowicz, Y. Zhu, D.L. Mazula, R.W. Brooks, H. Fuhrmann-Stroissnigg, T. Pirtskhalava, Y.S. Prakash, T. Tchkonia, P.D. Robbins, M.C. Aubry, J.F. Passos, J.L. Kirkland, D.J. Tschumperlin, H. Kita, N.K. LeBrasseur, Cellular senescence mediates fibrotic pulmonary disease, Nat Commun 8 (2017) 14532. https://doi.org/10.1038/ncomms14532.

[14] I.V. Yang, C.D. Coldren, S.M. Leach, M.A. Seibold, E. Murphy, J. Lin, R. Rosen, A.J. Neidermyer, D.F. McKean, S.D. Groshong, C. Cool, G.P. Cosgrove, D.A. Lynch, K.K. Brown, M.I. Schwarz, T.E. Fingerlin, D.A. Schwartz, Expression of cilium-associated genes defines novel molecular subtypes of idiopathic pulmonary fibrosis, Thorax 68 (2013) 1114–1121. https://doi.org/10.1136/thoraxjnl-2012-202943.

[15] W.S. Bowman, C.A. Newton, A.L. Linderholm, M.L. Neely, J.V. Pugashetti, B. Kaul, V. Vo, G.A. Echt, W. Leon, R.J. Shah, Y. Huang, C.K. Garcia, P.J. Wolters, J.M. Oldham, Proteomic biomarkers of progressive fibrosing interstitial lung disease: a multicentre cohort analysis, Lancet Respir Med 10 (2022) 593–602. https://doi.org/10.1016/S2213-2600(21)00503-8.

[16] J.M. Oldham, Y. Huang, S. Bose, S.-F. Ma, J.S. Kim, A. Schwab, C. Ting, K. Mou, C.T. Lee, A. Adegunsoye, S. Ghodrati, J. Vu Pugashetti, N. Nazemi, M.E. Strek, A.L. Linderholm, C.-H. Chen, S. Murray, R.L. Zemans, K.R. Flaherty, F.J. Martinez, I.

Noth, Proteomic Biomarkers of Survival in Idiopathic Pulmonary Fibrosis, Am J Respir Crit Care Med (2023). https://doi.org/10.1164/rccm.202301-0117OC.

[17] R.K. Man, A. Gogikar, A. Nanda, L.S.N. Janga, H.G. Sambe, M. Yasir, S. Ramphall, A Comparison of the Effectiveness of Nintedanib and Pirfenidone in Treating Idiopathic Pulmonary Fibrosis: A Systematic Review, Cureus 16 (2024) e54268. https://doi.org/10.7759/cureus.54268.

[18] Y. Hu, X. Shao, L. Xing, X. Li, G.M. Nonis, G.J. Koelwyn, X. Zhang, D.D. Sin, Single-Cell Sequencing of Lung Macrophages and Monocytes Reveals Novel Therapeutic Targets in COPD, Cells 12 (2023) 2771. https://doi.org/10.3390/cells12242771.

[19] C.Y. Perrot, T. Karampitsakos, J.D. Herazo-Maya, Monocytes and macrophages: emerging mechanisms and novel therapeutic targets in pulmonary fibrosis, American Journal of Physiology-Cell Physiology 325 (2023) C1046–C1057. https://doi.org/10.1152/ajpcell.00302.2023.

[20] P.J. Murray, J.E. Allen, S.K. Biswas, E.A. Fisher, D.W. Gilroy, S. Goerdt, S. Gordon, J.A. Hamilton, L.B. Ivashkiv, T. Lawrence, M. Locati, A. Mantovani, F.O. Martinez, J.-L. Mege, D.M. Mosser, G. Natoli, J.P. Saeij, J.L. Schultze, K.A. Shirey, A. Sica, J. Suttles, I. Udalova, J.A. van Ginderachter, S.N. Vogel, T.A. Wynn, Macrophage activation and polarization: nomenclature and experimental guidelines, Immunity 41 (2014) 14–20. https://doi.org/10.1016/j.immuni.2014.06.008.

[21] I.E. Fernandez, O. Eickelberg, The impact of TGF-β on lung fibrosis: from targeting to biomarkers, Proc Am Thorac Soc 9 (2012) 111–116. https://doi.org/10.1513/pats.201203-023AW.

[22] Y. Gu, T. Lawrence, R. Mohamed, Y. Liang, B.H. Yahaya, The emerging roles of interstitial macrophages in pulmonary fibrosis: A perspective from scRNA-seq analyses, Front Immunol 13 (2022) 923235. https://doi.org/10.3389/fimmu.2022.923235.

[23] F. Zhang, E.A. Ayaub, B. Wang, E. Puchulu-Campanella, Y. Li, S.U. Hettiarachchi, S.D. Lindeman, Q. Luo, S. Rout, M. Srinivasarao, A. Cox, K. Tsoyi, C. Nickerson-Nutter, I.O. Rosas, P.S. Low, Reprogramming of profibrotic macrophages for treatment of bleomycin-induced pulmonary fibrosis, EMBO Molecular Medicine 12 (2020) e12034. https://doi.org/10.15252/emmm.202012034.

[24] A. Bhattacharyya, K. Boostanpour, M. Bouzidi, L. Magee, T.Y. Chen, R. Wolters, P. Torre, S.K. Pillai, M. Bhattacharya, IL10 trains macrophage profibrotic function after lung injury, American Journal of Physiology-Lung Cellular and Molecular Physiology 322 (2022) L495–L502. https://doi.org/10.1152/ajplung.00458.2021.

[25] R. Zou, X. Gui, J. Zhang, Y. Tian, X. Liu, M. Tian, T. Chen, H. Wu, J. Chen, J. Dai, H. Cai, Association of serum macrophage-mannose receptor CD206 with mortality in idiopathic pulmonary fibrosis, Int Immunopharmacol 86 (2020) 106732. https://doi.org/10.1016/j.intimp.2020.106732.

[26] A. Prasse, C. Probst, E. Bargagli, G. Zissel, G.B. Toews, K.R. Flaherty, M. Olschewski, P. Rottoli, J. Müller-Quernheim, Serum CC-chemokine ligand 18

concentration predicts outcome in idiopathic pulmonary fibrosis, Am J Respir Crit Care Med 179 (2009) 717–723. https://doi.org/10.1164/rccm.200808-1201OC.

[27] E. Tsitoura, E. Vasarmidi, E. Bibaki, A. Trachalaki, C. Koutoulaki, G. Papastratigakis, S. Papadogiorgaki, G. Chalepakis, N. Tzanakis, K.M. Antoniou, Accumulation of damaged mitochondria in alveolar macrophages with reduced OXPHOS related gene expression in IPF, Respiratory Research 20 (2019) 264. https://doi.org/10.1186/s12931-019-1196-6.

[28] M.A. Gibbons, A.C. MacKinnon, P. Ramachandran, K. Dhaliwal, R. Duffin, A.T. Phythian-Adams, N. van Rooijen, C. Haslett, S.E. Howie, A.J. Simpson, N. Hirani, J. Gauldie, J.P. Iredale, T. Sethi, S.J. Forbes, Ly6Chi Monocytes Direct Alternatively Activated Profibrotic Macrophage Regulation of Lung Fibrosis, Am J Respir Crit Care Med 184 (2011) 569–581. https://doi.org/10.1164/rccm.201010-1719OC.

[29] L. Zhang, Y. Wang, G. Wu, W. Xiong, W. Gu, C.-Y. Wang, Macrophages: friend or foe in idiopathic pulmonary fibrosis?, Respiratory Research 19 (2018) 170. https://doi.org/10.1186/s12931-018-0864-2.

[30] B.B. Moore, R. Paine, P.J. Christensen, T.A. Moore, S. Sitterding, R. Ngan, C.A. Wilke, W.A. Kuziel, G.B. Toews, Protection from pulmonary fibrosis in the absence of CCR2 signaling, J Immunol 167 (2001) 4368–4377. https://doi.org/10.4049/jimmunol.167.8.4368.

[31] M.K.D. Scott, K. Quinn, Q. Li, R. Carroll, H. Warsinske, F. Vallania, S. Chen, M.A. Carns, K. Aren, J. Sun, K. Koloms, J. Lee, J. Baral, J. Kropski, H. Zhao, E. Herzog, F.J. Martinez, B.B. Moore, M. Hinchcliff, J. Denny, N. Kaminski, J.D. Herazo-Maya,

N.H. Shah, P. Khatri, Increased monocyte count as a cellular biomarker for poor outcomes in fibrotic diseases: a retrospective, multicentre cohort study, Lancet Respir Med 7 (2019) 497–508. https://doi.org/10.1016/S2213-2600(18)30508-3.

[32] A.K.Y. Teoh, H.E. Jo, D.C. Chambers, K. Symons, E.H. Walters, N.S. Goh, I. Glaspole, W. Cooper, P. Reynolds, Y. Moodley, T.J. Corte, Blood monocyte counts as a potential prognostic marker for idiopathic pulmonary fibrosis: analysis from the Australian IPF registry, Eur Respir J 55 (2020) 1901855. https://doi.org/10.1183/13993003.01855-2019.

[33] M. Kreuter, S.J. Bradley, J.S. Lee, A. Tzouvelekis, J.M. Oldham, P.L. Molyneaux, D. Weycker, M. Atwood, K.-U. Kirchgaessler, T.M. Maher, Monocyte Count as a Prognostic Biomarker in Patients with Idiopathic Pulmonary Fibrosis, Am J Respir Crit Care Med (2021). https://doi.org/10.1164/rccm.202003-0669OC.

[34] K. Kawamura, K. Ichikado, K. Anan, Y. Yasuda, Y. Sekido, M. Suga, H. Ichiyasu, T. Sakagami, Monocyte count and the risk for acute exacerbation of fibrosing interstitial lung disease: A retrospective cohort study, Chron Respir Dis 17 (2020) 1479973120909840. https://doi.org/10.1177/1479973120909840.

[35] D.J. Nikolic-Paterson, S. Wang, H.Y. Lan, Macrophages promote renal fibrosis through direct and indirect mechanisms, Kidney Int Suppl (2011) 4 (2014) 34–38. https://doi.org/10.1038/kisup.2014.7.

[36] M. Kuwana, Y. Okazaki, H. Kodama, K. Izumi, H. Yasuoka, Y. Ogawa, Y. Kawakami, Y. Ikeda, Human circulating CD14+ monocytes as a source of progenitors

that exhibit mesenchymal cell differentiation, Journal of Leukocyte Biology 74 (2003) 833–845. https://doi.org/10.1189/jlb.0403170.

[37] M. Vierhout, A. Ayoub, S. Naiel, P. Yazdanshenas, S.D. Revill, A. Reihani, A. Dvorkin-Gheva, W. Shi, K. Ask, Monocyte and macrophage derived myofibroblasts: Is it fate? A review of the current evidence, Wound Repair and Regeneration 29 (2021) 548–562. https://doi.org/10.1111/wrr.12946.

[38] M.-P.D. Campli, A. Azouz, A. Assabban, J. Scaillet, M. Splittgerber, A.V. Keymeulen, F. Libert, M. Remmelink, A.L. Moine, P. Lemaitre, S. Goriely, The mononuclear phagocyte system contributes to fibrosis in post-transplant obliterans bronchiolitis, European Respiratory Journal 57 (2021). https://doi.org/10.1183/13993003.00344-2020.

[39] F. Geng, J. Xu, X. Ren, Y. Zhao, Y. Cai, Y. Li, F. Jin, T. Li, X. Gao, W. Cai, H. Xu, Z. Wei, N. Mao, Y. Sun, F. Yang, Effect of macrophage-to-myofibroblast transition on silicosis, Animal Models and Experimental Medicine n/a (n.d.). https://doi.org/10.1002/ame2.12470.

[40] A. Moeller, S.E. Gilpin, K. Ask, G. Cox, D. Cook, J. Gauldie, P.J. Margetts, L. Farkas, J. Dobranowski, C. Boylan, P.M. O'Byrne, R.M. Strieter, M. Kolb, Circulating fibrocytes are an indicator of poor prognosis in idiopathic pulmonary fibrosis, Am J Respir Crit Care Med 179 (2009) 588–594. https://doi.org/10.1164/rccm.200810-1534OC.

[41] M. Riou, A. Alfatni, A.-L. Charles, E. Andrès, C. Pistea, A. Charloux, B. Geny, New Insights into the Implication of Mitochondrial Dysfunction in Tissue, Peripheral

Blood Mononuclear Cells, and Platelets during Lung Diseases, Journal of Clinical Medicine 9 (2020) 1253. https://doi.org/10.3390/jcm9051253.

[42] D.C. Zank, M. Bueno, A.L. Mora, M. Rojas, Idiopathic Pulmonary Fibrosis: Aging, Mitochondrial Dysfunction, and Cellular Bioenergetics, Frontiers in Medicine 5 (2018). https://www.frontiersin.org/articles/10.3389/fmed.2018.00010 (accessed October 18, 2023).

[43] J. ZHENG, Energy metabolism of cancer: Glycolysis versus oxidative phosphorylation (Review), Oncol Lett 4 (2012) 1151–1157. https://doi.org/10.3892/ol.2012.928.

[44] E. Atas, M. Oberhuber, L. Kenner, The Implications of PDK1–4 on Tumor Energy Metabolism, Aggressiveness and Therapy Resistance, Front Oncol 10 (2020) 583217. https://doi.org/10.3389/fonc.2020.583217.

[45] T.M. Ashton, W.G. McKenna, L.A. Kunz-Schughart, G.S. Higgins, Oxidative Phosphorylation as an Emerging Target in Cancer Therapy, Clinical Cancer Research 24 (2018) 2482–2490. https://doi.org/10.1158/1078-0432.CCR-17-3070.

[46] L. Wang, M. Zhu, Y. Li, P. Yan, Z. Li, X. Chen, J. Yang, X. Pan, H. Zhao, S. Wang, H. Yuan, M. Zhao, X. Sun, R. Wan, F. Li, X. Wang, H. Yu, I. Rosas, C. Ding, G. Yu, Serum Proteomics Identifies Biomarkers Associated With the Pathogenesis of Idiopathic Pulmonary Fibrosis, Molecular & Cellular Proteomics 22 (2023) 100524. https://doi.org/10.1016/j.mcpro.2023.100524.

[47] N. Xie, Z. Tan, S. Banerjee, H. Cui, J. Ge, R.-M. Liu, K. Bernard, V.J. Thannickal, G. Liu, Glycolytic Reprogramming in Myofibroblast Differentiation and Lung

Fibrosis, Am J Respir Crit Care Med 192 (2015) 1462–1474. https://doi.org/10.1164/rccm.201504-0780OC.

[48] R.M. Kottmann, A.A. Kulkarni, K.A. Smolnycki, E. Lyda, T. Dahanayake, R. Salibi, S. Honnons, C. Jones, N.G. Isern, J.Z. Hu, S.D. Nathan, G. Grant, R.P. Phipps, P.J. Sime, Lactic Acid Is Elevated in Idiopathic Pulmonary Fibrosis and Induces Myofibroblast Differentiation via pH-Dependent Activation of Transforming Growth Factor-β, Am J Respir Crit Care Med 186 (2012) 740–751. https://doi.org/10.1164/rccm.201201-0084OC.

[49] T.M. Maher, Aerobic Glycolysis and the Warburg Effect. An Unexplored Realm in the Search for Fibrosis Therapies?, Am J Respir Crit Care Med 192 (2015) 1407–1409. https://doi.org/10.1164/rccm.201508-1699ED.

[50] J. Li, X. Zhai, X. Sun, S. Cao, Q. Yuan, J. Wang, Metabolic reprogramming of pulmonary fibrosis, Frontiers in Pharmacology 13 (2022). https://www.frontiersin.org/articles/10.3389/fphar.2022.1031890 (accessed October 15, 2023).

[51] N. Xie, H. Cui, J. Ge, S. Banerjee, S. Guo, S. Dubey, E. Abraham, R.-M. Liu, G. Liu, Metabolic characterization and RNA profiling reveal glycolytic dependence of profibrotic phenotype of alveolar macrophages in lung fibrosis, American Journal of Physiology-Lung Cellular and Molecular Physiology 313 (2017) L834–L844. https://doi.org/10.1152/ajplung.00235.2017.

[52] J. Talreja, P. Farshi, A. Alazizi, F. Luca, R. Pique-Regi, L. Samavati, RNA-sequencing Identifies Novel Pathways in Sarcoidosis Monocytes, Scientific Reports 7 (2017). https://doi.org/10.1038/s41598-017-02941-4.

[53] E. Leonova, S.L. Barratt, M.A. Lindsay, M.A. Gibbons, M. Whiteman, C.J. Scotton, Targeting pro-inflammatory and pro-fibrotic monocyte phenotype using novel mitochondria-targeted hydrogen sulfide delivery, European Respiratory Journal 62 (2023). https://doi.org/10.1183/13993003.congress-2023.OA4200.

[54] G. Sutendra, E. Michelakis, Pyruvate dehydrogenase kinase as a novel therapeutic target in oncology, Frontiers in Oncology 3 (2013). https://www.frontiersin.org/articles/10.3389/fonc.2013.00038 (accessed November 3, 2023).

[55] M.J. Buck, T.L. Squire, M.T. Andrews, Coordinate expression of the PDK4 gene: a means of regulating fuel selection in a hibernating mammal, Physiological Genomics 8 (2002) 5–13. https://doi.org/10.1152/physiolgenomics.00076.2001.

[56] R.A. Harris, B. Huang, P. Wu, Control of pyruvate dehydrogenase kinase gene expression, Advances in Enzyme Regulation 41 (2001) 269–288. https://doi.org/10.1016/S0065-2571(00)00020-0.

[57] M.K. Jha, S. Jeon, K. Suk, Pyruvate Dehydrogenase Kinases in the Nervous System: Their Principal Functions in Neuronal-glial Metabolic Interaction and Neuro-metabolic Disorders, Curr Neuropharmacol 10 (2012) 393–403. https://doi.org/10.2174/157015912804143586.

[58] J.-H. Jeon, T. Thoudam, E.J. Choi, M.-J. Kim, R.A. Harris, I.-K. Lee, Loss of metabolic flexibility as a result of overexpression of pyruvate dehydrogenase kinases in muscle, liver and the immune system: Therapeutic targets in metabolic diseases, Journal of Diabetes Investigation 12 (2021) 21–31. https://doi.org/10.1111/jdi.13345.

[59] X.-L. Duan, C.-C. Ma, J. Hua, T.-W. Xiao, J. Luan, Benzyl butyl phthalate (BBP) triggers the malignancy of acute myeloid leukemia cells via upregulation of PDK4, Toxicol In Vitro 62 (2020) 104693. https://doi.org/10.1016/j.tiv.2019.104693.

[60] T. Chen, L. Ye, J. Zhu, B. Tan, Q. Yi, Y. Sun, Q. Xie, H. Xiang, R. Wang, J. Tian, H. Xu, Inhibition of Pyruvate Dehydrogenase Kinase 4 Attenuates Myocardial and Mitochondrial Injury in Sepsis-Induced Cardiomyopathy, The Journal of Infectious Diseases (2023) jiad365. https://doi.org/10.1093/infdis/jiad365.

[61] K. Yuan, N.-Y. Shao, J.K. Hennigs, M. Discipulo, M.E. Orcholski, E. Shamskhou, A. Richter, X. Hu, J.C. Wu, V.A. de Jesus Perez, Increased Pyruvate Dehydrogenase Kinase 4 Expression in Lung Pericytes Is Associated with Reduced Endothelial-Pericyte Interactions and Small Vessel Loss in Pulmonary Arterial Hypertension, Am J Pathol 186 (2016) 2500–2514. https://doi.org/10.1016/j.ajpath.2016.05.016.

[62] Z. Zhang, S. Han, S. Ouyang, Z. Zeng, Z. Liu, J. Sun, W. Kang, PDK4 Constitutes a Novel Prognostic Biomarker and Therapeutic Target in Gastric Cancer, Diagnostics (Basel) 12 (2022) 1101. https://doi.org/10.3390/diagnostics12051101.

[63] P. Du, R. Guo, K. Gao, S. Yang, B. Yao, H. Cui, M. Zhao, S. Jia, Identification of differentially expressed genes and the role of PDK4 in CD14+ monocytes of coronary

artery disease, Bioscience Reports 41 (2021) BSR20204124. https://doi.org/10.1042/BSR20204124.

[64] Y. Jiang, B.R. Rosborough, J. Chen, S. Das, G.D. Kitsios, B.J. McVerry, R.K. Mallampalli, J.S. Lee, A. Ray, W. Chen, P. Ray, Single cell RNA sequencing identifies an early monocyte gene signature in acute respiratory distress syndrome, JCI Insight 5 (2020). https://doi.org/10.1172/jci.insight.135678.

[65] J. Goodwin, H. Choi, M. Hsieh, M.L. Neugent, J.-M. Ahn, H.N. Hayenga, P.K. Singh, D.B. Shackelford, I.-K. Lee, V. Shulaev, S. Dhar, N. Takeda, J. Kim, Targeting Hypoxia-Inducible Factor-1α/Pyruvate Dehydrogenase Kinase 1 Axis by Dichloroacetate Suppresses Bleomycin-induced Pulmonary Fibrosis, Am J Respir Cell Mol Biol 58 (2018) 216–231. https://doi.org/10.1165/rcmb.2016-0186OC.

[66] C.L.R. van Doorn, G.K. Schouten, S. van Veen, K.V. Walburg, J.J. Esselink, M.T. Heemskerk, F. Vrieling, T.H.M. Ottenhoff, Pyruvate Dehydrogenase Kinase Inhibitor Dichloroacetate Improves Host Control of Salmonella enterica Serovar Typhimurium Infection in Human Macrophages, Front Immunol 12 (2021) 739938. https://doi.org/10.3389/fimmu.2021.739938.

[67] E.M. Dunbar, B.S. Coats, A.L. Shroads, T. Langaee, A. Lew, J.R. Forder, J.J. Shuster, D.A. Wagner, P.W. Stacpoole, Phase 1 trial of dichloroacetate (DCA) in adults with recurrent malignant brain tumors, Invest New Drugs 32 (2014) 452–464. https://doi.org/10.1007/s10637-013-0047-4.

[68] A. Khan, D. Andrews, A.C. Blackburn, Long-term stabilization of stage 4 colon cancer using sodium dichloroacetate therapy, World J Clin Cases 4 (2016) 336–343. https://doi.org/10.12998/wjcc.v4.i10.336.

[69] J.A. Whitsett, T.V. Kalin, Y. Xu, V.V. Kalinichenko, Building and Regenerating the Lung Cell by Cell, Physiological Reviews 99 (2019) 513–554. https://doi.org/10.1152/physrev.00001.2018.

[70] H.N. Alsafadi, C.A. Staab-Weijnitz, M. Lehmann, M. Lindner, B. Peschel, M. Königshoff, D.E. Wagner, An ex vivo model to induce early fibrosis-like changes in human precision-cut lung slices, American Journal of Physiology-Lung Cellular and Molecular Physiology 312 (2017) L896–L902. https://doi.org/10.1152/ajplung.00084.2017.

[71] N.I. Winters, C.J. Taylor, C.S. Jetter, J.E. Camarata, A.J. Gutierrez, L.T. Bui, J.J. Gokey, M. Bacchetta, N.E. Banovich, J.M.S. Sucre, J.A. Kropski, Single-cell transcriptomic assessment of cellular phenotype stability in human precision-cut lung slices, (2021) 2021.08.19.457016. https://doi.org/10.1101/2021.08.19.457016.

[72] H. Miao, X.-Q. Wu, D.-D. Zhang, Y.-N. Wang, Y. Guo, P. Li, Q. Xiong, Y.-Y. Zhao, Deciphering the cellular mechanisms underlying fibrosis-associated diseases and therapeutic avenues, Pharmacological Research 163 (2021) 105316. https://doi.org/10.1016/j.phrs.2020.105316.

[73] H. Cui, N. Xie, S. Banerjee, J. Ge, D. Jiang, T. Dey, Q.L. Matthews, R.-M. Liu, G. Liu, Lung Myofibroblasts Promote Macrophage Profibrotic Activity through Lactate-

induced Histone Lactylation, Am J Respir Cell Mol Biol 64 (2021) 115–125. https://doi.org/10.1165/rcmb.2020-0360OC.

[74] C. Morse, T. Tabib, J. Sembrat, K.L. Buschur, H.T. Bittar, E. Valenzi, Y. Jiang, D.J. Kass, K. Gibson, W. Chen, A. Mora, P.V. Benos, M. Rojas, R. Lafyatis, Proliferating SPP1/MERTK-expressing macrophages in idiopathic pulmonary fibrosis, European Respiratory Journal 54 (2019). https://doi.org/10.1183/13993003.02441-2018.

[75] S.-Y. Hong, Y.-T. Lu, S.-Y. Chen, C.-F. Hsu, Y.-C. Lu, C.-Y. Wang, K.-L. Huang, Targeting pathogenic macrophages by the application of SHP-1 agonists reduces inflammation and alleviates pulmonary fibrosis, Cell Death Dis 14 (2023) 1–12. https://doi.org/10.1038/s41419-023-05876-z.

[76] A. Kishore, M. Petrek, Roles of Macrophage Polarization and Macrophage-Derived miRNAs in Pulmonary Fibrosis, Frontiers in Immunology 12 (2021). https://www.frontiersin.org/articles/10.3389/fimmu.2021.678457 (accessed January 10, 2024).

[77] N.J. Lang, J. Gote-Schniering, D. Porras-Gonzalez, L. Yang, L.J. De Sadeleer, R.C. Jentzsch, V.A. Shitov, S. Zhou, M. Ansari, A. Agami, C.H. Mayr, B. Hooshiar Kashani, Y. Chen, L. Heumos, J.C. Pestoni, E.S. Molnar, E. Geeraerts, V. Anquetil, L. Saniere, M. Wögrath, M. Gerckens, M. Lehmann, A.Ö. Yildirim, R. Hatz, N. Kneidinger, J. Behr, W.A. Wuyts, M.-G. Stoleriu, M.D. Luecken, F.J. Theis, G. Burgstaller, H.B. Schiller, Ex vivo tissue perturbations coupled to single-cell RNA-seq reveal multilineage cell circuit dynamics in human lung fibrogenesis, Science

Translational Medicine 15 (2023) eadh0908. https://doi.org/10.1126/scitranslmed.adh0908.

[78] R.T. Chitturi, A.M. Balasubramaniam, R.A. Parameswar, G. Kesavan, K.T.M. Haris, K. Mohideen, The Role of Myofibroblasts in Wound Healing, Contraction and its Clinical Implications in Cleft Palate Repair, J Int Oral Health 7 (2015) 75–80.

[79] A.C. Zamora, V.E. Ortega, E.M. Carmona, When the Third Time Is Not the Charm—Trial Outcomes in Idiopathic Pulmonary Fibrosis, JAMA (2024). https://doi.org/10.1001/jama.2024.8776.

[80] D.F. Higgins, K. Kimura, M. Iwano, V.H. Haase, Hypoxia-inducible factor signaling in the development of tissue fibrosis, Cell Cycle 7 (2008) 1128–1132.

[81] I.F. Robey, A.D. Lien, S.J. Welsh, B.K. Baggett, R.J. Gillies, Hypoxia-Inducible Factor-1α and the Glycolytic Phenotype in Tumors, Neoplasia 7 (2005) 324–330.

[82] J. Kim, I. Tchernyshyov, G.L. Semenza, C.V. Dang, HIF-1-mediated expression of pyruvate dehydrogenase kinase: A metabolic switch required for cellular adaptation to hypoxia, Cell Metabolism 3 (2006) 177–185. https://doi.org/10.1016/j.cmet.2006.02.002.

[83] A. Zhang, Y. Xu, H. Xu, J. Ren, T. Meng, Y. Ni, Q. Zhu, W.-B. Zhang, Y.-B. Pan, J. Jin, Y. Bi, Z.B. Wu, S. Lin, M. Lou, Lactate-induced M2 polarization of tumor-associated macrophages promotes the invasion of pituitary adenoma by secreting CCL17, Theranostics 11 (2021) 3839–3852. https://doi.org/10.7150/thno.53749.

[84] R. Singh, A. Letai, K. Sarosiek, Regulation of apoptosis in health and disease: the balancing act of BCL-2 family proteins, Nat Rev Mol Cell Biol 20 (2019) 175–193. https://doi.org/10.1038/s41580-018-0089-8.

[85] B. Liu, Y. Zhang, J. Suo, Increased Expression of PDK4 Was Displayed in Gastric Cancer and Exhibited an Association With Glucose Metabolism, Frontiers in Genetics 12 (2021). https://www.frontiersin.org/articles/10.3389/fgene.2021.689585 (accessed October 15, 2023).

[86] T.H. Mai, L.W. Han, J.C. Hsu, N. Kamath, L. Pan, Idiopathic pulmonary fibrosis therapy development: a clinical pharmacology perspective, Ther Adv Respir Dis 17 (2023) 17534666231181537. https://doi.org/10.1177/17534666231181537.

[87] E.B. Preuß, S. Schubert, C. Werlein, H. Stark, P. Braubach, A. Höfer, E.K.J. Plucinski, H.R. Shah, R. Geffers, K. Sewald, A. Braun, D.D. Jonigk, M.P. Kühnel, The Challenge of Long-Term Cultivation of Human Precision-Cut Lung Slices, Am J Pathol 192 (2022) 239–253. https://doi.org/10.1016/j.ajpath.2021.10.020.

[88] E. Fraser, L. Denney, A. Antanaviciute, K. Blirando, C. Vuppusetty, Y. Zheng, E. Repapi, V. Iotchkova, S. Taylor, N. Ashley, V. St Noble, R. Benamore, R. Hoyles, C. Clelland, J.M.D. Rastrick, C.S. Hardman, N.K. Alham, R.E. Rigby, A. Simmons, J. Rehwinkel, L.-P. Ho, Multi-Modal Characterization of Monocytes in Idiopathic Pulmonary Fibrosis Reveals a Primed Type I Interferon Immune Phenotype, Front Immunol 12 (2021) 623430. https://doi.org/10.3389/fimmu.2021.623430.

APPENDIX

Copyright Information: Reprint reproduced with publisher's permission (Chapter 2)

JOHN WILEY AND SONS LICENSE
TERMS AND CONDITIONS

May 28, 2024

This Agreement between Ms. Megan Vierhout ("You") and John Wiley and Sons ("John Wiley and Sons") consists of your license details and the terms and conditions provided by John Wiley and Sons and Copyright Clearance Center.

License Number	5797470561861
License date	May 28, 2024
Licensed Content Publisher	John Wiley and Sons
Licensed Content Publication	Wound Repair and Regeneration
Licensed Content Title	Monocyte and macrophage derived myofibroblasts: Is it fate? A review of the current evidence
Licensed Content Author	Megan Vierhout, Anmar Ayoub, Safaa Naiel, et al
Licensed Content Date	Jun 9, 2021
Licensed Content Volume	29
Licensed Content Issue	4
Licensed Content Pages	15
Type of use	Dissertation/Thesis
Requestor type	Author of this Wiley article

Format	Print and electronic
Portion	Full article
Will you be translating?	No
Title of new work	Investigating Monocytes and Macrophages as Profibrotic Contributors in Pulmonary Fibrosis
Institution name	McMaster University
Expected presentation date	Aug 2024
Requestor Location	Ms. Megan Vierhout 1280 Main Street West Hamilton, ON L8S4L8 Canada Attn: Ms. Megan Vierhout
Publisher Tax ID	EU826007151
Billing Type	Invoice
Billing Address	Ms. Megan Vierhout 1280 Main Street West Hamilton, ON L8S4L8 Canada Attn: Ms. Megan Vierhout
Total	0.00 CAD
Terms and Conditions	

TERMS AND CONDITIONS

no right, title or interest in or to the Wiley Materials or any of the intellectual property rights therein. You shall have no rights hereunder other than the license as provided for above in Section 2. No right, license or interest to any trademark, trade name, service mark or other branding ("Marks") of WILEY or its licensors is granted hereunder, and you agree that you shall not assert any such right, license or interest with respect thereto

- NEITHER WILEY NOR ITS LICENSORS MAKES ANY WARRANTY OR REPRESENTATION OF ANY KIND TO YOU OR ANY THIRD PARTY, EXPRESS, IMPLIED OR STATUTORY, WITH RESPECT TO THE MATERIALS OR THE ACCURACY OF ANY INFORMATION CONTAINED IN THE MATERIALS, INCLUDING, WITHOUT LIMITATION, ANY IMPLIED WARRANTY OF MERCHANTABILITY, ACCURACY, SATISFACTORY QUALITY, FITNESS FOR A PARTICULAR PURPOSE, USABILITY, INTEGRATION OR NON-INFRINGEMENT AND ALL SUCH WARRANTIES ARE HEREBY EXCLUDED BY WILEY AND ITS LICENSORS AND WAIVED BY YOU.

- WILEY shall have the right to terminate this Agreement immediately upon breach of this Agreement by you.

- You shall indemnify, defend and hold harmless WILEY, its Licensors and their respective directors, officers, agents and employees, from and against any actual or threatened claims, demands, causes of action or proceedings arising from any breach of this Agreement by you.

- IN NO EVENT SHALL WILEY OR ITS LICENSORS BE LIABLE TO YOU OR ANY OTHER PARTY OR ANY OTHER PERSON OR ENTITY FOR ANY SPECIAL, CONSEQUENTIAL, INCIDENTAL, INDIRECT, EXEMPLARY OR PUNITIVE DAMAGES, HOWEVER CAUSED, ARISING OUT OF OR IN CONNECTION WITH THE DOWNLOADING, PROVISIONING, VIEWING OR USE OF THE MATERIALS REGARDLESS OF THE FORM OF ACTION, WHETHER FOR BREACH OF CONTRACT, BREACH OF WARRANTY, TORT, NEGLIGENCE, INFRINGEMENT OR OTHERWISE (INCLUDING, WITHOUT LIMITATION, DAMAGES BASED ON LOSS OF PROFITS, DATA, FILES, USE, BUSINESS OPPORTUNITY OR CLAIMS OF THIRD PARTIES), AND WHETHER OR NOT THE PARTY HAS BEEN ADVISED OF THE POSSIBILITY OF SUCH DAMAGES. THIS LIMITATION SHALL APPLY NOTWITHSTANDING ANY FAILURE OF ESSENTIAL PURPOSE OF ANY LIMITED REMEDY PROVIDED HEREIN.

- Should any provision of this Agreement be held by a court of competent jurisdiction to be illegal, invalid, or unenforceable, that provision shall be deemed amended to achieve as nearly as possible the same economic effect as the original provision, and the legality, validity and enforceability of the remaining provisions of this Agreement shall not be affected or impaired thereby.

- The failure of either party to enforce any term or condition of this Agreement shall not constitute a waiver of either party's right to enforce each and every term and condition of this Agreement. No breach under this agreement shall be deemed waived or excused by either party unless such waiver or consent is in writing signed by the party granting such waiver or consent. The waiver by or consent of a party to a breach of any provision of this Agreement shall not operate or be construed as a

waiver of or consent to any other or subsequent breach by such other party.

- This Agreement may not be assigned (including by operation of law or otherwise) by you without WILEY's prior written consent.
- Any fee required for this permission shall be non-refundable after thirty (30) days from receipt by the CCC.
- These terms and conditions together with CCC's Billing and Payment terms and conditions (which are incorporated herein) form the entire agreement between you and WILEY concerning this licensing transaction and (in the absence of fraud) supersedes all prior agreements and representations of the parties, oral or written. This Agreement may not be amended except in writing signed by both parties. This Agreement shall be binding upon and inure to the benefit of the parties' successors, legal representatives, and authorized assigns.
- In the event of any conflict between your obligations established by these terms and conditions and those established by CCC's Billing and Payment terms and conditions, these terms and conditions shall prevail.
- WILEY expressly reserves all rights not specifically granted in the combination of (i) the license details provided by you and accepted in the course of this licensing transaction, (ii) these terms and conditions and (iii) CCC's Billing and Payment terms and conditions.
- This Agreement will be void if the Type of Use, Format, Circulation, or Requestor Type was misrepresented during the licensing process.
- This Agreement shall be governed by and construed in accordance with the laws of the State of New York, USA, without regards to such state's conflict of law rules. Any legal action, suit or proceeding arising out of or relating to these Terms and Conditions or the breach thereof shall be instituted in a court of competent jurisdiction in New York County in the State of New York in the United States of America and each party hereby consents and submits to the personal jurisdiction of such court, waives any objection to venue in such court and consents to service of process by registered or certified mail, return receipt requested, at the last known address of such party.

WILEY OPEN ACCESS TERMS AND CONDITIONS

Wiley Publishes Open Access Articles in fully Open Access Journals and in Subscription journals offering Online Open. Although most of the fully Open Access journals publish open access articles under the terms of the Creative Commons Attribution (CC BY) License only, the subscription journals and a few of the Open Access Journals offer a choice of Creative Commons Licenses. The license type is clearly identified on the article.

The Creative Commons Attribution License

The Creative Commons Attribution License (CC-BY) allows users to copy, distribute and transmit an article, adapt the article and make commercial use of the article. The CC-BY license permits commercial and non-

Creative Commons Attribution Non-Commercial License